UNIVERSITY OF SOUTHAMPTON

FACULTY OF MEDICINE

CANCER SCIENCE

SIP1/ZEB2-induced epithelial mesenchymal transition promotes metastasis and alters chemokine (C-C motif) ligand 5 expression to modulate the tumour microenvironment in colorectal cancer

by

HAJIR AL SAIHATI

Thesis for the degree of philosophy of doctorate

July 2016

UNIVERSITY OF SOUTHAMPTON

ABSTRACT

FACULTY OF MEDICINE

Cancer Sciences

Thesis for the degree of Doctor of Philosophy

SIP1/ZEB2-INDUCED EPITHELIAL MESENCHYMAL TRANSITION PROMOTES METASTASIS AND ALTERS CHEMOKINE (C-C MOTIF) LIGAND 5 EXPRESSION TO MODULATE THE TUMOUR MICROENVIRONMENT IN COLORECTAL CANCER

Hajir Ali Al Saihati

Epithelial mesenchymal transition (EMT) is a critical trans-differentiation program driving cancer metastasis. Patients showing signs of invasive cancer or the presence of distant metastasis have a poor prognosis. Another well-known feature of decreased cancer-associated survival is the lack of anti-cancer immune responses. Thus I hypothesized that the EMT and anti-tumor response could be linked via altered secretion of soluble factors by metastatic cells.

Colorectal cancer (CRC) cell lines and SIP1-inducible DLD cells were grown in DMEM. The induction of the *SIP1* gene was carried out using doxycycline for 3 days. The EMT status of the CRC cell lines were assessed by preforming western blotting, immunofluorescence and RT-PCR for EMT biomarkers. Cytokine/chemokine expression in SIP1 inducible DLD cells was analyzed using commercially-available antibody arrays. Validation of the selected chemokine (CCL5) was carried out using sandwich ELISA as well as RT-PCR, with the CCL5 expression level analysed in a panel of CRC cell lines using the same techniques. The *CCL5* promoter was then cloned into pGL3. The mechanism of action of ZEB1/2 on the *CCL5* promoter was studied by luciferace assay and chromatin immunoprecipitation (ChIP). CCL5 coding region was cloned into pcDNA3.1 and stably transfected into DLD-1 cells. DLD-1 cells over-expressing CCL5/RANTES were injected orthotopically into SCID mice, and metastasis was investigated by immunohistochemistry (IHC). The relationship between infiltrating T lymphocytes (TILs) and the expression of both CCL5/RANTES and SIP1 was studied in 75 CRC patients by IHC and tissue micrroarray.

The results of evaluating EMT status categorised 13 CRC cell lines as epithelial, intermediate epithelial, intermediate mesechymal and mesenchymal. Cytokine/chemokine antibody arrays showed a significant increase in CCL5/RANTES in induced DLD-SIP1 cells. ELISA, multiplex assays and RT-PCR confirmed the increased secretion of CCL5/RANTES in the induced DLD-SIP1 cells. The CRC cell line panel showed that the average level of secreted CCL5/RANTES from mesenchymal CRC cells was significantly more than in epithelial cells (639.7 ± 175 vs 107.6 ± 30 pg/ml, respectively; p=0.0075). mRNA expression profiling confirmed this finding from the CRC panel. Promoter studies showed that ZEB1/2 bind to *CCL5* promoter, thus activating *CCL5* gene expression. No metastatic spread for of DLD-1 cells overexpressing CCL5/RANTES was observed when orthotopically injected into SCID mice.

Our data shows that CCL5/RANTES is up-regulated by EMT-inducing transcription factor SIP1, and mesenchymal (metastatic) CRC cells secrete significantly more CCL5/RANTES compared to epithelial (non-metastatic) cells. Furthermore, abundant secretion of CCL5/RANTES might be a crucial regulator of immune infiltration in CRC, but not a direct inducer of metastasis, and that needs to be futher investigated. Inhibiting CCL5 activity in metastatic CRC may have a therapeutic potential.

Table of Contents

Table of Contents ..... **i**
List of Tables ..... **vii**
List of Figures ..... **ix**
DECLARATION OF AUTHORSHIP ..... **xv**
Acknowledgements ..... **xvii**
Abbreviations ..... **xix**
Chapter 1: Main Introduction **1**
1.1 Cancer 1
1.1.1 Common signalling pathways in cancer 1
1.1.2 Colorectal cancer 7
1.1.3 Cancer metastasis 13
1.2 Epithelial mesenchymal transition (EMT) 14
1.2.1 Phenotype of epithelial and mesenchymal and metastable cells in EMT 15
1.2.2 EMT biomarkers 18
1.2.3 Crosstalk between the EMT transcription factors 24
1.2.4 EMT subtypes 25
1.3 The tumour microenvironment 29
1.3.1 Cancer-associated fibroblasts 30
1.3.2 Mesenchymal stem cells 31
1.3.3 Endothelial cells of blood and lymphatic vessels 31
1.3.4 Immune cells 32
1.3.5 Chemokines as TME soluble factors 35
1.4 Chemokine superfamily 36
1.4.1 Chemokine ligand and receptor structure, classification and nomenclature 36
1.5 Hypothesis and the aims of the project 44
1.5.1 Hypothesis 44
1.5.2 Aims of the Project 44
Chapter 2: Materials and Methods **47**
2.1 Tissue culture 47

2.1.1 General principle 47
2.1.2 Cell lines 47
2.1.3 Cell counting and viability 47
2.1.4 SIP1 induction in DLD-SIP1 and A431-SIP1 EMT models 48
2.1.5 Cell propagation, and collection of cells and conditioned medium 48
2.1.6 Freezing cells for long term storage 48
2.1.7 Defrosting Cells 49
2.2 Western blotting 49
2.2.1 Main Principle 49
2.2.2 Preparation of cell lysate 50
2.2.3 Protein quantification 50
2.2.4 Gel preparation 51
2.2.5 Protein loading and gel electrophoresis 55
2.2.6 Protein transfer 55
2.2.7 Protein identification 55
2.3 Gene expression analysis 59
2.3.1 Total RNA extraction 59
2.3.2 cDNA Synthesis 60
2.3.3 RT-PCR 61
2.4 Immunofluorescence 65
2.4.1 Growing cell lines on coverslips 66
2.4.2 Indirect IF procedure 66
2.5 Human Chemokine and Cytokine Antibody Arrays 67
2.5.1 Assay principle 67
2.5.2 Proteomic array procedure 68
2.6 Multiplex detection immunoassay 69
2.6.1 Main principle 69
2.6.2 25- Multiplex detection immunoassay 70
2.7 Quantitative enzyme immunoassay 70
2.7.1 General principle 70
2.7.2 Human CCL5/RANTES ELISA 71
2.8 DNA cloning and recombinant DNA technology. 72

2.8.1 DNA Amplification 72
2.8.2 Gel extraction 73
2.8.3 DNA Ligation into the vector 74
2.8.4 Plasmid transformation 76
2.8.5 Plasmid DNA purification 76
2.8.6 Plasmid maxi-prep it 77
2.9 Transfection 78
2.9.1 Lipofectamine® 3000 Protocol 79
2.10 Flow cytometry 80
2.10.1 Preparation of samples for FACS 81
2.10.2 FACS analysis 82
2.11 Transwell migration assay 82
2.12 Site-directed mutagenesis 84
2.12.1 Primer design guidelines for SDM 85
2.12.2 Sample Reaction and Transformation 86
2.13 Promoter reporter assay 87
2.13.1 Main principle 87
2.13.2 Protocol of the luciferase reporter assay 88
2.14 Chromatin Immunoprecipitation (ChIP) 89
2.14.1 Optimising the shearing condition for DLD-SIP1 cells 90
2.14.2 Cell fixation to optimise shearing conditions 90
2.14.3 DNA clean up to assess shearing efficiency and DNA concentration 92
2.14.4 Active Motif's ChIP-IT® High Sensitivity kit 92
2.14.5 Fixation of cultured cells 93
2.14.6 Chromatin sonication 94
2.14.7 Input preparation 94
2.14.8 Examining the size of sheared chromatin 95
2.14.9 Chromatin immunoprecipitation 95
2.14.10 Reversal of cross-links and DNA purifications 97
2.14.11 Semi-qualitative PCR for ChIP analysis 97
2.15 Immunohistochemistry (IHC) 99
2.15.1 Tissue microarray (TMA) 99

2.15.2 Production of tissue microarrays, immunohistochemistry staining and digitalisation 100
2.16 Generating stably transfected cell lines 101
2.16.1 Preparation of pcDNA3.1 CCL5 plasmid stock 102
2.16.2 Neomycin kill curve and cell transfection 102
2.16.3 Transfection of DLD-1 cells with pcDNA3.1-CCL5 plasmid 102
2.16.4 Selection and expansion of stable polyclonal colonies 103
2.16.5 Identification and expansion of single monoclonal clones 103
2.16.6 Examination of CCL5 expression 103
2.16.7 Expansion and freezing of single clones with high CCL5 expressing .. 103
2.17 Animal experiments 103
2.18 Statistical analysis 104
Chapter 3: EMT Status in CRC 105
3.1 Introduction 105
3.2 The aim 105
3.2.1 Results 106
3.2.2 EMT Status of CRC panel cell lines and EMT-CRC model 106
3.2.3 Qualitative assessment of EMT markers 116
3.4 Discussion 124
3.4.1 EMT status of the 12 CRC cell lines in relation to their morphological appearance 124
3.2.4 Further investigation of intermediate cells by IF 131
3.2.5 EMT status of the DLD-SIP1 CRC EMT model in relation to its morphological appearance 134
Chapter 4: EMT Driven Cytokine/Chemokine Expression in CRC 137
5.1 Introduction 137
4.1 The aims 137
4.2 Results 138
4.2.1 Human chemokine and cytokine arrays for DLD-SIP1 CRC-EMT model 138
4.2.2 Criteria to limit the number of soluble factors for further investigation 140
4.2.3 Validation of CCL5, IL-8, MDK and CXCL5 141

4.2.4 The final candidate 149
4.3 Discussion 149
Chapter 5: The Mechanistic Role of ZEB1/2 EMT in Activating CCL5 in CRC 155
5.1 Introduction 155
5.1.1 C-C chemokine ligand 5 (CCL5) in cancer 155
5.2 The aim 160
5.3 Results 160
5.3.1 Analysing and cloning the *CCL5* promoter 160
5.3.2 Luciferase assay for the *CCL5* Promoter 163
5.3.3 ChIP analysis 169
5.4 Discussion 172
Chapter 6: The Molecular Basis of Immune Infiltration as a Result of a Metastasis Program in CRC 177
6.1 Introduction 177
6.2 The aims 177
6.3 Results 178
6.3.1 Generating CCL5 over-expressing DLD-1 cells 178
6.3.2 Validation of CCL5 produced by DLD-1-stably transfected cells 183
6.3.3 *In vivo* studies 187
6.3.4 SIP1 expression linked with immune infiltrate 190
6.4 Discussion 193
Chapter 7: Conclusion and Future Directions 197
7.1 Study objective and aims 197
7.2 Summary of the project findings 197
7.3 Future directions: 200
Appendices 203
List of References 209

List of Tables

Table 1: Pathological classification of CRC. 9

Table 2: Functional classification of the human chemokine family. 39

Table 3: List of in house buffers used in the project. 52

Table 4: List of the antibodies used for WB (Western blot). 57

Table 5: List of the primers used in RT-PCR. 63

Table 6: List of the primers used for SDM (Site-Directed Mutagenesis). 86

Table 7: List of the antibodies used for ChIP (Chromatin Immunoprecipitation). 96

Table 8: The primers used to preform PCR for ChIP assay. 98

Table 9: List of the antibodies used in the TMA (Tissue Microarray). 101

Table 10: The biological characteristics and supplier of the CRC cell lines analysed. . 107

Table 11: A summary of the obtained results from the human chemokine and cytokine arrays (R&D systems) 140

Table 12: The list of chemokines in the R&D chemokine array. 203

Table 13 The list of cytokines in the R&D systems cytokines array. 204

List of Figures

Figure 1: Hallmarks of cancer. 1

Figure 2: The TGF-β signalling pathway in cancer. 3

Figure 3: Receptor tyrosine kinase pathways (RTKs) in cancer. 5

Figure 4: Wnt/β-catenin signalling pathway in cancer. 6

Figure 5: P53-regulated pathways in cancer. 7

Figure 6: CRC Adenoma- Carcinoma Sequence and the main genetic alterations throughout the process. 8

Figure 7: The Invasion-Metastasis cascade. 14

Figure 8: Epithelial Mesenchymal Transition. 15

Figure 9: A summary of various junctions in the epithelial cell. 17

Figure 10: Crosstalk between SNAIL, TWIST, and ZEB1/2 and LEF-1 transcription factors (TFs) in EMT. 25

Figure 11: EMT in embryo development. 27

Figure 12: EMT in wound healing, tissue regeneration and organ fibrosis. 28

Figure 13: EMT in cancer. 29

Figure 14: The primary tumour microenvironment (TME). 30

Figure 15: Typical structure of chemokine ligands. 37

Figure 16: Structural classification of the chemokine family. 38

Figure 17: A representative structure of G protein-coupled chemokine receptors (GPCRs). 41

Figure 18: General principle of the Western blotting method. 50

Figure 19: General principle of immunofluorescence. 65

Figure 20: General principle of proteome profiler antibody arrays (R&D systems). 68

Figure 21: The general principle of multiplex beads immune-assay. 69

Figure 22: General principle of sandwich ELISA that was used in the project to determine the expression of CCL5. 71

Figure 23: The pcDNA3.1D/V5-His-TOPO® vector that was used to clone the *CCL5* coding region..... 75

Figure 24: pGL3 basic vector that was used to clone the *CCL5* promoter. 75

Figure 25: Lipid-mediated transfection of eukaryotic cells with plasmid DNA..... 79

Figure 26: General principle of flow cytometry. 81

Figure 27: General illustration of Transwell migration assay..... 83

Figure 28: A flow chart for the migration assay protocol that used in this project..... 84

Figure 29: A flow chart for site-directed mutagenesis..... 85

Figure 30: General principle of the Luciferase assay. 88

Figure 31: The Luciferase protocol for a 96-well plate. 89

Figure 32: A flow chart showing the main steps in chromatin immunoprecipitation (ChIP). 90

Figure 33 A flow chart illustrating the process of TMA (Tissue Microarray). 101

Figure 34: Morphology of AAC1/82 cells using a 10X objective..... 109

Figure 35: Morphology of CT26 cells using a 10X objective. 110

Figure 36: Morphology of Caco2 cells using a 10X objective. 110

Figure 37: Morphology of Colo205 cells using a 10X objective..... 111

Figure 38: Morphology of DLD-1 cells using a 10X objective..... 112

Figure 39: Morphology of HCT116 cells using a 10X objective. 112

Figure 40: Morphology of HT29 cells using a 10X objective. 113

Figure 41: Morphology of LoVo cells using a 10X objective. 113

Figure 42: Morphology of RKO cells using a 10X objective. 114

Figure 43: Morphology of SW48 cells using a 10X objective. 114

Figure 44: Comparing the morphology of SW480 and SW620 cells using a 10X objective. 115

Figure 45: EMT status for DLD-SIP1 and A431-SIP1 models. 115

Figure 46: The protein expression of canonical EMT markers and EMT-inducing transcription factors in a panel of 12 CRC cell lines and the inducible CRC EMT model 117

Figure 47: RNA expression of selected EMT markers and EMT-inducing transcription factors in a panel of CRC cell lines and DLD-SIP-1 inducible CRC EMT model. 118

Figure 48: Spatial E-cadherin, vimentin and F-actin protein expression were analysed using immunofluorescence and confocal microscopy in the intermediate HCT116, LoVo and SW620 cells. 121

Figure 49: The spatial expression of E-cadherin, β-catenin, ZO-1, connexin 43, F-actin and SIP1 proteins was analysed using confocal microscopy in DLD SIP-1 CRC EMT model. 123

Figure 50: Protein expression of ZO-1 and SIP1 detected using confocal microscopy in the DLD SIP-1 CRC EMT model, without the DAPI overlay. 124

Figure 51: Investigating the expression of 31 chemokines and 36 cytokines in the CRC-EMT model. 139

Figure 52: Charts summarising the results obtained from R&D system human chemokine and cytokine arrays. 140

Figure 53: Expression of MDK and CXCL5 in the CRC panel and DLD SIP-1 inducible CRC EMT model.....143

Figure 54: Intracellular MDK expression was analysed using immunofluorescence and confocal microscopy in DLD SIP-1 CRC EMT model. 143

Figure 55: 25-Multiplex detection immunoassay for DLD SIP-1 stable inducible CRC-EMT model. 144

Figure 56: Multiplex detection immunoassay for A431 SIP-1 stable inducible squamous cell carcinoma EMT model. 145

Figure 57: Expression of CCL5 in a panel of CRC cell lines and the DLD SIP-1 inducible CRC EMT model.....146

Figure 58: Spatial intracellular CCL5 expression was analysed using immunofluorescence and confocal microscopy in DLD SIP-1 CRC EMT model. 147

Figure 59: Human CCL5 was detected by sandwich ELISA in the supernatant of DLD SIP-1 and A431-SIP1 cells. 148

Figure 60: Human CCL5 was detected by sandwich ELISA in the supernatants of five chosen epithelial or intermediate epithelial CRC cell lines and three mesenchymal CRC cell lines 149

Figure 61: A systematic review of EMT and CCL5 in cancer 159

Figure 62: The sequence of the cloned region of the *CCL5* promoter (including a part of the first exon). 161

Figure 63: Illustration of the steps used to clone the *CCL5* promoter into pGL3. 163

Figure 64: Relative luciferase activity of *CCL5* promoter in a panel of CRC cell lines. 164

Figure 65: An illustration of *CCL5* promoter with SIP1/ZEB2 motif sites with or without mutation. 165

Figure 66: The relative luciferase activity of the *CCL5* promoter with or without SIP1/ZEB1motif sites mutations in DLD-SIP1 CRC EMT model. 166

Figure 67: The relative luciferase activity of the *CCL5* promoter with or without SIP1/ZEB1motif sites mutations in A431-SIP1 squamous cell carcinoma EMT model. 167

Figure 68: The Relative luciferase activity of the *CCL5* promoter with or without SIP1/ZEB1motif sites mutations in SW620 and SW480 cells. 168

Figure 69: Shearing size of DNA from DLD-SIP1 cells using a different number of pulses. 169

Figure 70: Further validation of chosen shearing condition (5 pulses) for DLD-SIP1 cells using PCR. 170

Figure 71: Validation of DLD-UI and DLD-I inputs before proceeding with immunoprecipitation (IP). 171

Figure 72: Validation of DLD-UI and DLD-I inputs before proceeding with immunoprecipitation (IP). 172

Figure 73: A) Steps of CCL5 cloning. 179

Figure 74: The abundance of secreted CCL5 in DLD-1 transfected cells with pcDNA3.1 or pcDNA3.1-CCL5 was detected using a human CCL5 sandwich ELISA. 180

Figure 75: ELISA screening for the secreted level of CCL5 in twenty-two DLD-CCL5 clones. 182

Figure 76: Validation of morphology and E-cadherin levels in the chosen DLD-CCL5 clones. 183

Figure 77: CCR5 expression in a panel of CRC cell lines and in the DLD-SIP1 CRC EMT model. 185

Figure 78: SW480 cells chosen to validate the functional activity of CCL5 obtained from the stably transfected DLD cells. 187

Figure 79: A bar chart illustrating the number of migrated SW480 cells in each individual condition. 187

Figure 80: Validation of clone 4 (high CCL5) and clone 17 (negative CCL5) before proceeding with the animal experiment. 188

Figure 81: Examining the presence of cancer formed by DLD cells expressing CCL5 or not in the Ceacum. 190

Figure 82: Haematoxylin and eosin (H&E) staining for the livers (potential site of metastases) from the orthothpically injected SCID mice with clone 4 or clone 17. 190

Figure 83: A representation of 3 different patterns of staining for each antibody used in this study 192

Figure 84: DNA sequence of the mutated CCL5 *promoter* ZEB2BOX2 (top line) aligned with wild-type *CCL5* promoter sequence (bottom line) using the BLAST program 205

Figure 85: DNA sequence of the mutated *CCL5* promoter ZEB2 BOX2 (top line) aligned with wild-type *CCL5* promoter sequence (bottom line) using the BLAST program 206

Figure 86: DNA sequence of the mutated *CCL5* promoter ZEB2BOX1 and ZEB2BOX2 (top line) aligned with wild-type *CCL5* promoter sequence (bottom line) using the BLAST program. 207

DECLARATION OF AUTHORSHIP

I, Hajir Al Saihati

Declare that this thesis and the work presented in it are my own and has been generated by me as the result of my own original research.

SIP1-induced epithelial mesenchymal transition promotes metastasis and alters chemokine (C-C motif) ligand 5 expression to modulate the tumour microenvironment in colorectal cancer

I confirm that:

1. This work was done wholly or mainly while in candidature for a research degree at this University;
2. Where any part of this thesis has previously been submitted for a degree or any other qualification at this University or any other institution, this has been clearly stated;
3. Where I have consulted the published work of others, this is always clearly attributed;
4. Where I have quoted from the work of others, the source is always given. With the exception of such quotations, this thesis is entirely my own work;
5. I have acknowledged all main sources of help;
6. Where the thesis is based on work done by myself jointly with others, I have made clear exactly what was done by others and what I have contributed myself;
7. None of this work has been published before submission.

Signed: .....

Date: .....

Acknowledgements

I would like to express my special appreciation and thanks to my supervisors Dr. Emre Sayan, Professor Graham Packham and Dr. Anthony Williams, who have been tremendous advisors for me. I would like to thank you for encouraging my research and for allowing me to grow as a research scientist.

Thank you to Mr. Alex Mirnezami for examining me in my transfer viva, and for his amazing calmness throughout the exam period. I would also like to thank my work colleague Dr. Rahul Sreekumar, for helping me retrieve the human CRC blocks for my Ph.D. thesis; Dr. David Johnson for helping me image my immunofluorescent slides using confocal microscopy; and Dr. Yifang Gao for helping me produce the lovely finding from the multiplex immunoassay. Many thanks as well to Dr. Karwan Moutasim and the histopathology department for helping me producing my tissue microarrays and immunohistochemistry staining.

With permission from my main supervisor, editorial advice has been sought. No changes of intellectual content were made as a result of this advice. Special thanks to Dr. Karen Pickard, Dr. Rahul Bhome, Andrew Irvine and Mr. Jonathan Lightfoot (IT Training & Development at University of Southampton) for editing my thesis.

Thanks to Dr. Patrick Duriez, Miss. Nasia Kontouli, Mr. Leon Douglas, Dr. Edwin Garcia, Dr. Denise Boulanger, Dr. Rachel Carter, Dr. Veronika Jenei and Mrs. Sophie Trudel for answering my scientific questions and supporting my research.

I am so grateful for my sponsored body, the Saudi Ministry of higher education under a unique scholar program that was conducted by King Abdullah bin Abdul-Aziz “May Allah bless his soul”.

A special thanks to my family. Words cannot express how grateful I am to my precious mother and my gorgeous sisters for all of the sacrifices that they’ve made on my behalf. Your prayer for me was what sustained me thus far. Endless thanks to my lovely friend Ola who helped me produce the amazing pictures for my thesis, and for encouraging me to strive towards my goal. At the end I would like to express my special appreciation to my husband Khalid who suffered more than anyone else through all my PhD period: thanks for being faithful and for your amazing support. Warm thanks to my big boy Ali and my lovely daughter Raneem for being well-behaved, hard-workers at school and patience with me during my busy period; my love for you darling is all things and forever.

Thank you all for your faith in me. It is a great pleasure to express my warm appreciation to all of you by introducing this work as a gift.

Abbreviations

5-FU	5-Fluorouracil
A431-I	A431–SIP1 cells induced
A431-UI	A431–SIP1 cells un-induced
AJCC	American Joint Committee on Cancer
ANGPTL1	Angiogenesis regulator protein
AP	Alkaline phosphatase
AP1	Activator protein 1
APC	Adenomatous polyposis coli
APCs	Antigen presenting cells
ATCC	American Type Culture Collections
ATM	Ataxia-Telangiectasia-mutated
ATR	Ataxia-Telangiectasia-related
BEC	Blood endothelial cells
bHLH	Basic/helix-loop-helix
BMP-RII	BMP type II receptor
BMP	Bone morphogenetic protein
BSA	Bovine serum albumin
BVs	Blood vessels
CAFs	Cancer associated fibroblasts
CBP	CREB binding protein
CC	Cell count
CCL5	C-C chemokine ligand 5
CCX-CKR	ChemoCentryx Chemokine Receptor
CDH1	E-cadherin gene/promoter
CEA	Carcinoemboryonic antigen
Chk1	Checkpoint kinase 1
Chk2	Checkpoint kinase 2
ChIP	Chromatin immunoprecipitation
CIN	Chromosomal instability
c-JNK	c-Jun N-terminal kinase
CRC	Colorectal cancers

CSF	Colony stimulating factor
CSLCs	Cancer stem like cells
CTLs or CD8+	Cytotoxic T cells
CXCL8	CXC chemokine ligand 8. Alternative name for IL-8
DARC	Duffy Antigen Receptor for Chemokines
DCs	Dendritic cells
DLD-I	DLD-SIP1 induced
DLD-UI	DLD-SIP1 un-induced
DMEM	Dulbecco's Modified Eagle's Medium
DMSO	Dimethyl sulphoxide
DRY	Aspartate-Arginine-Tyrosine
Dvl	Dishevelled
E	Epithelial
E1m	ZEB1/2 E-box1 mutated
E1m	ZEB1/2 E-box2 mutated
E1m+E2m	ZEB1/2 E-box1 and Ebox2 mutated
ECLs	Extracellular loops
ECM	Extracellular matrix
ECs	Endothelial cells
EDTA	Ethylenediaminetetraacetic acid
EGF	Epidermal growth factor
EGFR	Epidermal growth factor receptor
ELISA	Enzyme-linked immunosorbent assay
ELR	Glutamate-Leucine-Arginine
EMT	Epithelial mesenchymal transition
ERK	Extracellular signal–regulated kinase
F-actin	Filamentous actin
FAP	Familial adenomatous polyposis
FBS	Fetal bovine serum
FF	*Firefly*
FGF	Fibroblast growth factor
FOBT	Faecal Occult Blood test.

FSC	Forward scatter
FSP1	Fibroblast specific protein 1. Also called S100A4
Fz	Frizzled receptor
G-actin	Globular (monomeric) actin
GAGs	Glycosaminoglycans
GFP	Green fluorescent protein
GFs	Growth factors
GPCRs	G protein-coupled receptors
GRB2	Growth factor receptor–bound 2
GRB2	growth factor receptor–bound 2
GTPase	Guanosine Triphosphatase
H & E	Haematoxylin and eosin
HGF	Hepatocellular growth factor
HIF-1	Hypoxia inducible factors 1
HIF-2	Hypoxia inducible factors 2
HIV	Human immunodeficiency virus
HNPCC	Hereditary Non-Polyposis Colorectal Cancer
HRP	Horseradish peroxidase
IFN-γ	Interferon gamma
IGF	Insulin like growth factor
IHC	Immunohistochemistry
IL-1α	Interleukin-1 alpha
IL-6	Interleukin-6
IL-8	Interleukin-8. Alterative name for CXCL8
IP	Immun0precipitation
K-RAS	Kirstein rat sarcoma
Ks	Cytokeratins
LAS	Assay Substrate (LAS)
LB	Luria Bertani
LEC	Lymphatic endothelial cells
LEF-1	Lymphoid enhancer-binding factor
LRP6	Lipoprotein receptor-related protein 6

LVs	Lymphatic vessels
M	Mesenchymal
M1	M1 macrophage
M2	M2 macrophage
MAGUK	Membrane-associated guanylate kinase
MALAT-1	Metastasis-Associated Lung Adenocarcinoma Transcript 1
MAP	Mitogen-activated protein
MMX	Master mix
MDK	Midkine
MDSCs	Myeloid-derived suppressor cells
MET	Mesenchymal-epithelial transition
Metastable	ME
MFI	Mean Fluorescence intensity
MIS	Microsatellite instability
MMPs	Matrix metalloproteinases
MMR	Mismatch repair genes
MSCs	Mesenchymal stem cells
MSS	Microsatellite stable
mTOR1	Mammalian Target of Rapamycin Complex 1
mTOR2	Mammalian Target of Rapamycin Complex 2
N1	N1 neutrophil
N2	N2 neutrophil
NF- κB	Nuclear Factor –κB
NKG2D	Natural killer group 2 member D
NKs	Natural Killer cells
NMR	Nuclear magnetic resonance
Non-CSLC	Non-CSLC Non-cancer stem like cells
NOD/SCID	Non-obese diabetic mice SCID mice
PBS	Phosphate Buffer Saline
PCR	Polymerase chain reaction
PDGF	Platelet-derived growth factor
PDGFR	Platelet-derived growth factor receptor

PDK1	Phosphoinositide-dependent kinase 1
PI3K-AKT	Phosphatidylinositol-3-Kinase and Protein Kinase B
PIC	Protease Inhibitor Cocktail
PIP2	Phosphatidylinositol 4, 5-bisphosphate
PIP3	Phosphatidylinositol 3, 4, 5- triphosphate
PKP	Plakophilin
PLB	Passive Lysis Buffer
PMSF	Phenylmethylsulfonyl fluoride
PMTs	Photomultiplier tubes
PTEN	Phosphatase and tensin homolog
RANTES	Regulated on Activation, Normal T Expressed and Secreted. (It is an alternative name for CCL5).
RN	Renilla
ROS	Reactive oxygen species
RPE	R-Phycoerythrin
RT	Room temperature
RTKs	Receptor tyrosine kinases
RT-PCR	Reverse transcriptase PCR
SDF-1 or CXCL12	Stromal cell-derived factor-1
SDM	Site directed mutagenesis
SDS-PAGE	SDS-polyacrylamide gel electrophoresis
SGH	Southampton general hospital
SGS	Stop & Glo® Substrate
Shc	Src homology 2 domain–containing transforming protein
SIP1	Smad interacting protein 1
SOS1	Son of sevenless homolog 1
SSC	Side scatter
Streptavidin-RPE	Streptavidin conjugated to R-Phycoerythrin
TADCs	Tumour-associated dendritic cells
TAE	Tris acetate EDTA buffer

TAK1	TGF-β–activated kinase 1
TAMs	Tumour-associated macrophages
TBS-T	Tris buffered saline with Tween
TCF	T cell factor
TE	Tris EDTA
TFs	Transcription factors
TGB	Tris/glycine/SDS buffer
TGF-β	Transforming growth factor β
TGF-βRI	TGF-β receptor type I
TGF-βRII	TGF-β receptor type II
TGM	Tris/Glycine/methanol buffer
Th	Helper T cells
Th1	T helper-1
Th17	T helper 17
TME	Tumour microenvironment
TNF-α	Tumour necrosis factor alpha
TNM	Tumour, Node, Metastasis staging system
TNM7	7th edition TNM
TP53	Tumour protein-53
Treg cells	Regulatory T cells
UICC	International Union Against Cancer
VEGF	Vascular endothelial growth factor
VEGF-A	vascular endothelial growth factor A
VEGFRII-mAb	VEGF receptor 2 blocking monoclonal antibody
WB	Western blot
ZO-1	Zonula occludens protein 1
ZO-3	Zonula occludens protein 3
α-SMA	Alpha-smooth muscle actin

Chapter 1: Main Introduction

1.1 Cancer

Cancer is a disease in which an individual mutant cell acquires selective biological properties, allowing it to grow and divide more vigorously and survive more readily than its neighbouring cells. The selective biological properties include sustaining proliferative signalling, evading growth suppressors, resisting cell death, enabling replicative immortality, inducing angiogenesis and activating invasion and metastasis [1]. During the last decade, scientists have focused on two additional biological properties of cancer cells: the ability to reprogram energy metabolism and evade immune destruction [2]; **see figure 1**. The ability of cancer cells to activate invasion and metastasis and to evade immune destruction will be the main focus of this project.

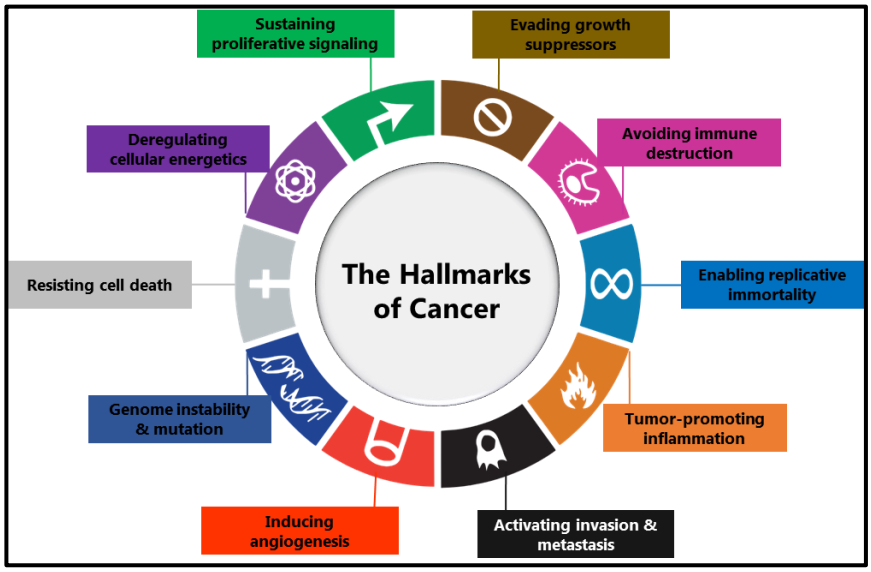

Figure 1: Hallmarks of cancer.
Adapted from [2].

1.1.1 Common signalling pathways in cancer

A number of molecular pathways play a significant role in promoting the hallmarks of cancer (see **Hallmarks of Cancer figure1**), including the transforming growth factor β (TGF-β), Wnt–β catenin, receptor tyrosine kinases (RTKs) and p53 signalling pathways.

These pathways are regulated by various stimuli such as growth factors, chemokines, cytokines, hypoxia and cell-cell or cell-extracellular matrix (ECM) engagement [3-11]. These pathways were reviewed in detail elsewhere [12], although a brief summary of each pathway is detailed below in order to have a better understanding of their contribution throughout the thesis.

1.1.1.1 TGF-β BMP signalling pathway

The TGF-β signalling pathway is activated via several ligands of the TGF-β superfamily including TGF-β 1-3, and BMP2-BMP7. These ligands bind to a heterotetrameric receptor complex combining TGF-β receptor type I and II (TGF-βRI and TGF-βRII). In mammalian systems, there are seven isoforms of the type I receptor and five isoforms of the type II receptor [13]. Upon ligand binding, TGF-βRII phosphorylates TGF-βRI, resulting in the activation of various intracellular signalling pathways including those mediated by SMAD2/3, RAS and PI3K. Activated SMAD2/3 complexes bind further to co-activator SMAD4, with the whole complex then translocating into the nucleus. In the nucleus, the SMAD complex binds to DNA regulatory elements where it can drive or repress the transcription of target genes. The TGF-β-SMAD pathway can be inhibited by post-translational or proteasome-mediated degradation of SMADs via Smurf1 and Smurf 2 [14] or it can be suppressed via SMAD6 and SMAD7 proteins which bind to TGF-βRI and prevent formation of the SMAD2/3/4 complex [13, 15]; **see figure 2.**

In addition, TGF-β signalling can mediate activation of various receptor tyrosine kinase pathways including Phosphatidylinositol-3-Kinase (PI3) and Protein Kinase B (otherwise known as AKT) and extracellular signal–regulated kinase (ERK). These pathways will be summarised later in this section; **see figure 2.**

The BMP signalling pathway bears similarities to TGF-β signalling although the receptor is a specific BMP type II receptor (BMP-RII) [16] and a SMAD 1/5/8 complex takes the place of SMAD2/3 [17].

Both TGF-β and BMP pathways have multiple functions in adult tissue, controlling cell proliferation, differentiation, survival and angiogenesis [18]. In cancer, TGF-β has a dual role. It acts as a tumour suppressor in the early stages of tumour progression by inducing cell cycle arrest, although in later stages the growth inhibitory function is selectively lost, and TGF-β induces un-controlled cell growth, invasion and metastasis [19, 20].

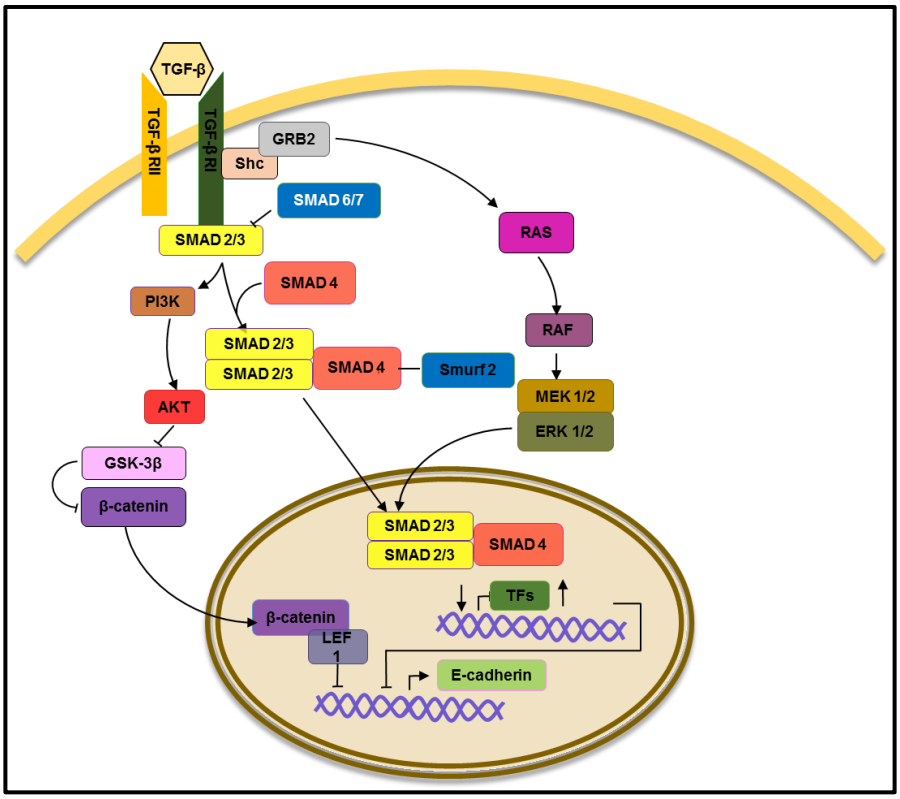

Figure 2: The TGF-β signalling pathway in cancer.

The TGF-β pathway can activate various signalling pathways that are either SMAD2/3-dependent or SMAD2/3-independent e.g. RAS and PI3K. The pathways activate transcription factors that induce the expression of various genes involved in enhancing cell proliferation and survival as well as invasion and metastasis. Inhibition of the SMAD-dependant pathway is mediated by SMAD6/7 and Smurf2. Adapted from [12]

1.1.1.2 Receptor tyrosine kinase signalling pathways

RTKs are activated via their respected ligand binding such as epithelial growth factor (EGF)-EGFR, fibroblast growth factor (FGF)-FGFR, insulin growth factor (IGF)-IGFR, and Platelet-derived growth factor (PDGF)-PDGFR [21-23]. Binding of these factors to their respective RTK leads to receptor dimerisation/tetramerisation and phosphorylation of intracellular domains resulting in the activation of downstream signalling pathways such as PI3K-AKT, ERK, c-Jun N-terminal kinase (JNK) and MAPK [24]; **see figure 3.**

1.1.1.2.1 PI3K –AKT signalling pathway

In the PI3K-AKT intracellular cascade, PI3K is first activated by receptor tyrosine kinases, which induces phosphorylation of the inositol ring of phosphoinositol diphosphate (PIP2) leading to phosphoinositol triphosphate (PIP3). Accumulated PIP3 induces 1) binding of AKT to PIP3 which facilitates membrane localisation and 2) activation of phosphoinositide-dependent kinase 1 (PDK1) that leads to phosphorylation of AKT at

Threonine 308. AKT can also be phosphorylated by the TORC2 complex or PDK2 at Serine 473 [25]. Phosphorylation of AKT activates the mammalian Target of Rapamycin Complex 1 (mTORC1) and mTORC2, which provide a check point for cell growth and proliferation, survival, motility and metabolism [26, 27]. Inhibition of PIP2 phosphorylation can be mediated through the phosphatase and tensin homolog (PTEN) which is rarely mutated or repressed in metastatic cancers [28]. Thus, PI3K-Akt-mTORC cascade is hyper- activated in cancer which may lead to increased cell survival, proliferation, migration and glycolytic metabolism [29, 30]; **see figure 3.**

1.1.1.2.2 RAS-MEK-ERK signalling pathway

RAS, the oncogenic Guanosine Triphosphatase (GTPase), is one of the most studied oncogenes. The importance of Ras comes from its ability to relay messages from RTKs to the ERK pathway. Upon ligand binding, RTKs become active and phosphorylated. The phosphorylated RTKs serve as docking stations for the GRB-SOS complex that removes the GDP from RAS. As a result GTP can bind and activate RAS binding to the Raf family of kinases. Upon activation Raf initiates the MEK/ERK signalling pathway [31, 32]. The RAS-MEK-ERK signalling pathway contributes to many cellular events including cell proliferation, differentiation and cell cycle progression [33]. In many cancers, the RAS-RAF-MEK-ERK signalling pathway is hyper-activated as a result of mutations in *KRAS, NRAS* and *BRAF* genes [34]; **see figure 3.**

1.1.1.2.3 JNK and p38 MAPK

The JNK and p38 MAPK cascades are activated upon RTK or Tumour Necrosis Factor Receptor (TNFR) binding. Consequently TRAF6, a E3 ubiquitin ligase, binds to the respected receptor leading to activation of TGF-β–activated kinase 1 (TAK1). TAK1 in turn activates p38 MAPK or JNK [35]. Activation of p38 MAPK or JNK promotes translocation of the Nuclear Factor–κB (NF-κB) family of transcription factors. Similar to other cellular pathways, JNK and p38 MAPK signalling controls many processes including inflammation and tissue homeostasis via altering cell proliferation, differentiation and survival [36]. In cancer, de-regulation of these cascades exacerbate metastasis [37-39]; **see figure 3.**

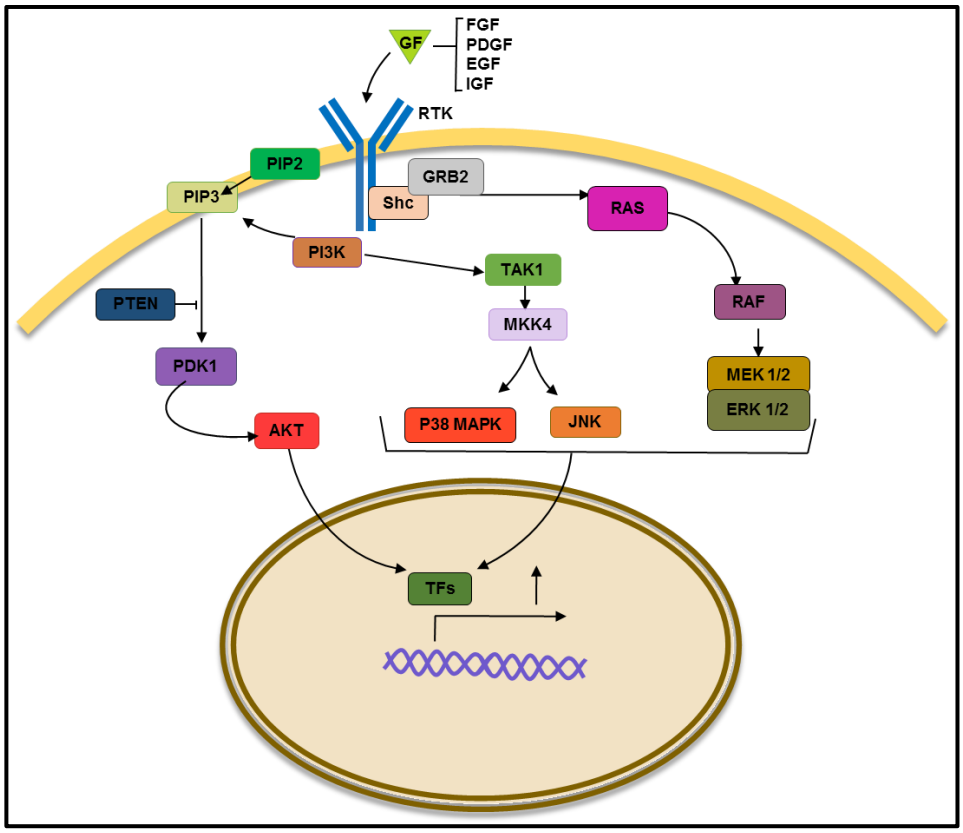

Figure 3: Receptor tyrosine kinase pathways (RTKs) in cancer.

Many growth factors (GFs) can activate RTKs, which in turn activate various cascades such as the RAS, PI3K, P38 MAPK, and JNK pathways. These signalling pathways trigger transcription factors to bind to various promoters to induce or repress genes involved in promoting cancer progression. PTEN is a critical phosphatase that can repress PI3K and Wnt signalling pathways in cancer. Adapted from [12]

1.1.1.3 **Wnt signalling pathway**

Wnt signalling is activated via binding of Wnt ligands to Frizzled receptors (Fz). In the absence of Wnt signalling, β-Catenin, which participates in cell-cell adhesion and cell signalling, is phosphorylated by the GSK-3β/Axin complex and the tumour suppressor Adenomatous Polyposis Coli (APC), and thus subject to proteasome degradation. However, Wnt signalling results in phosphorylation of low-density lipoprotein receptor-related protein 6 (LRP6) by GSK-3β and recruitment of Axin and Dishevelled (Dvl) to the cell membrane, thus inhibiting formation of the GSK-3β/Axin complex leading to accumulation of β-Catenin in the cytoplasm and subsequent translocation to the nucleus [40]. Aberrant regulation of Wnt signalling has been implicated in various types of cancer leading to increased cell proliferation and migration [41, 42]; **see figure 4.**

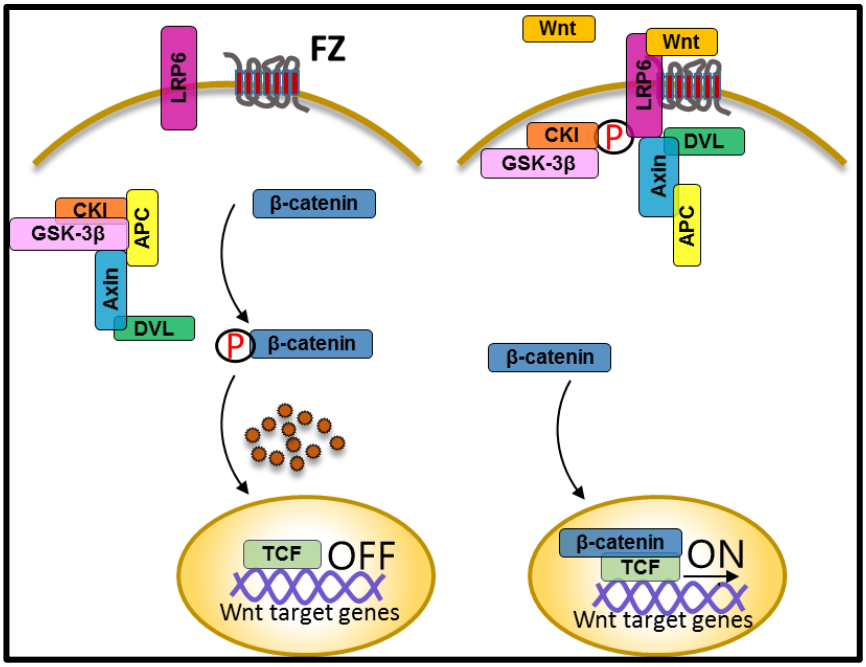

Figure 4: Wnt/β-catenin signalling pathway in cancer.

Wnt binds to the Frizzled (Fz) receptor and LRP6 as an accessory protein. As a result, β-catenin is not degraded but trans-locates to the nucleus and interacts with TCF/LEF-1 transcription factors which regulate the transcription of a number of genes involved in cancer development; adapted from [43].

1.1.1.4 **P53 signalling pathways**

Environmental hazards such as UV light, chemical agents as well as cellular stresses such as hypoxia can cause DNA damage and thus alter DNA structure and function. P53 (also known as the 'guardian of the genome') is a very important transcription factor in cancer biology that is involved in DNA repair and programmed cell death [44]. P53 is regulated by activation of specific pathways, including the Ataxia-Telangiectasia-mutated (ATM)-checkpoint kinase 2 (Chk2) pathway and the Ataxia-Telangiectasia-related (ATR)-Checkpoint kinase 1 (Chk1) pathway which are essential for DNA repair [45, 46]. Activated p53 regulates the transcription of a number of target genes implicated in cell cycle (e.g. *p21*), apoptosis (e.g. *bax* and *puma*), necrosis (e.g. *cathepsin Q*), autophagy (e.g. *dram* genes), angiogenesis (e.g. *thrombosondin1*) and senescence (e.g. *pai-1*) [46-48].

The E3 ubiquitin ligase Mdm2 is one of the most critical regulators of p53, which marks p53 for degradation by the proteasome [49, 50]. Mutations in the *TP53* tumour suppressor gene have been found in up to 50% of all human cancers [51, 52]; **see figure 5.**

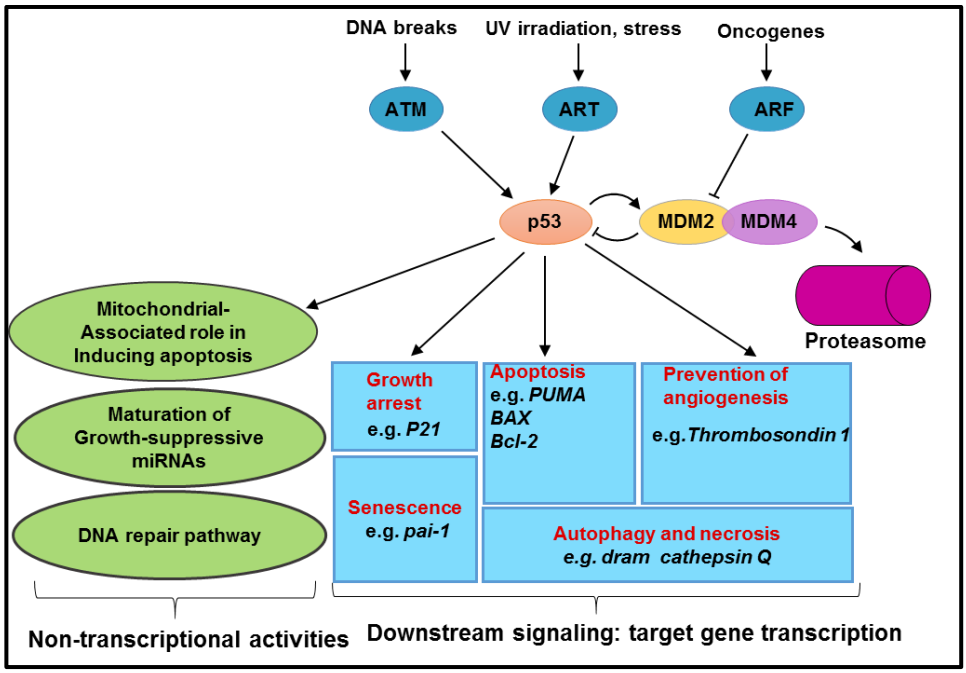

Figure 5: P53-regulated pathways in cancer.

P53 protein is activated upon recognition of cellular stress such as exposure to DNA damaging agents. It is implicated in various cellular pathways regulating cell cycle arrest, apoptosis, DNA repair, angiogenesis and senescence in order to maintain normal cellular function and genome stability. Mdm2 is one of the most critical regulators of p53; adapted from [53].

1.1.2 Colorectal cancer

Worldwide, 12.7 million new cancer cases and 7.6 million cancer-related deaths (around 13% of total deaths) were estimated to have occurred in 2008. The most commonly diagnosed cancers worldwide are lung (1.61 million, 12.7% of the total), breast (1.38 million, 10.9%) and colorectal cancers (CRC) (1.23 million, 9.7%). The most common cancer-related deaths are from lung cancer (1.38 million, 18.2% of the total), stomach cancer (738,000 deaths, 9.7%), liver cancer (696,000 deaths, 9.2%) and colorectal cancer (608,000 deaths, 8.0%) [54].

In the UK, CRC is the third most common cancer and the second most common cause of cancer-related mortality in both genders, with a male: female incidence ratio of 13:10. The incidence is strongly associated with ages ≥ 50. In 2011, 41,581 individuals were diagnosed with CRC, with 23,171 cases in men (54%) and 18,410 cases in women (44%); in 2012 around 16,200 people died which means more than 44 CRC patients died everyday [55].

1.1.2.1 The CRC adenoma-carcinoma sequence

Benign hyperplastic colorectal polyps are usually small in size (< 5mm) with normal surrounding mucosa, and are not considered a major precursor for developing CRC. Instead, adenomatous polyps are probably the important precursors of CRC. They arise from glandular epithelium and are characterised by a dysplastic morphology and the hyper-proliferation of epithelial cells [56]. Surgical removal of adenomas can decrease the risk of progression to CRC [57]. Despite the clinical relevance of polypectomy, only a fraction of adenomas progress to carcinoma in a process that may take years to decades. For example, adenomas ≤ 1 cm in size may have approximately a 10 to 15% chance of progressing to carcinoma over a 10-year period [58]; **see figure 6**.

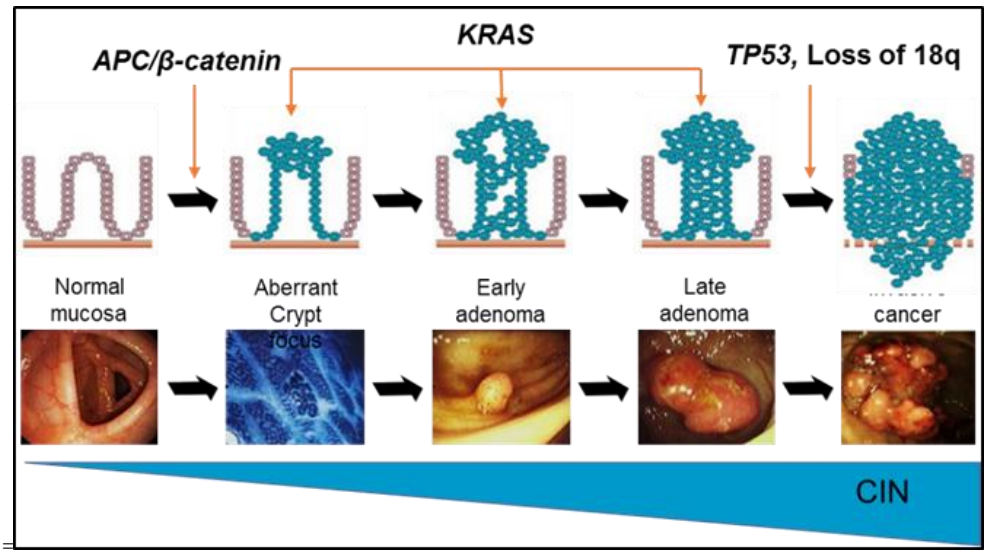

Figure 6: CRC Adenoma- Carcinoma Sequence and the main genetic alterations throughout the process.

CIN: Chromosomal instability. Adapted from [59, 60].

1.1.2.2 CRC classification

1.1.2.2.1 Pathological classification

Initially, CRC was classified into four stages (A, B, C, D) according to Dukes' staging system. Dukes' A indicates tumour infiltration into the bowel wall, Dukes' B specifies tumour infiltration through the bowel wall, Dukes' C indicates the presence or absence of lymph node metastasis, and Dukes' D classifies tumour infiltration with distant metastases [61]. This system has been completely replaced by the tumour, node, metastasis (TNM) staging system of the American Joint Committee on Cancer (AJCC) and the International Union Against Cancer (UICC), and has been revised several times. Now, the 7th edition

TNM (TNM7) is used as the standard for CRC staging and represents the primary tumour (T), regional lymph nodes (N) and distant metastases (M) followed by a number to indicate the severity of the tumour [62, 63], **see table 1**. In the UK, clinicians still use the 5th version of the TNM bowel cancer staging system.

Table 1: Pathological classification of CRC.
Adapted from [64].

Dukes	TNM stage	
-	TX	Primary tumour cannot be assessed
-	T0	No evidence of primary tumour
-	Tis	Carcinoma in situ: intraepithelial or invasion of laminaamna propria
A	T1	Tumour invades submucosa
A	T2	Tumour invades muscularis propria
B	T3	Tumour invades through the muscularis propria into pericolic tissues
B	T4a	Tumour penetrates to the surface of the visceral peritoneum
B	T4b	Tumour directly invades or is adherent to other organs or structures
-	NX	Regional lymph nodes cannot be assessed
B	N0	No regional lymph node metastasis
C	N1a	Metastasis in one regional lymph node
C	N1b	Metastasis in 2--3 regional lymph nodes
C	N1c	Tumour deposit(s) in the subserosa, mesentery or nonperitonealized pericolic or perirectal tissues without regional nodal metastasis
C	N2a	Metastasis in 4-6 regional lymph nodes
C	N2b	Metastasis in seven or more regional lymph nodes
C	M0	No distant metastasis
D	M1a	Metastasis confined to one organ or site (e.g. liver, lung, ovary, nonregional lymph node)
D	M1b	Metastasis in more than one organ/site or the peritoneum

1.1.2.2.2 Genetic classification

CRC is generally classified into three categories. The classification is based on hereditary influence, previous history of inflammatory bowel disease (Ulcerative colitis or Crohn's disease) and environmental risk factors such as the high consumption of red meat, a high-fat diet, inadequate intake of fibre, obesity, diabetes mellitus, smoking, and high

consumption of alcohol [65, 66]. The first group is sporadic CRC (60%) which includes patients with no notable family history and with no identifiable inherited gene mutation that accelerates cancer development. The second is familial CRC (30%) which refers to patients who have at least one relative with CRC or an adenoma, but with no specific germline mutation or clear pattern of inheritance. The third is hereditary CRC (10%) which results from the germline inheritance of mutations in highly penetrating cancer susceptibility genes [67].

Sporadic cancers are caused by the development of a series of genetic abnormalities in tumour suppressor genes and oncogenes that give cells selective advantages. One of the well-defined hereditary CRC syndromes is Hereditary Non-Polyposis Colorectal Cancer (HNPCC); also called Lynch syndrome. It accounts for 2-4% of all colorectal cancers and is inherited in an autosomal dominant fashion. Its clinical consequences develop from germline mutations in mismatch repair (*MMR*) genes. Lynch syndrome patients have an 80% risk of developing cancer during their lives. Familial Adenomatous Polyposis (FAP) is another common hereditary syndrome which accounts for approximately 1% of all colorectal cancers characterised by numerous adenomatous colorectal polyps. It is an autosomal dominant disorder caused by a germline mutation in the *APC* gene (adenomatous polyposis coli gene) [64, 67, 68].

1.1.2.2.3 Main genetic alterations in CRC

CRC is a heterogeneous disease that can arise as a consequence of genomic instability and the accumulation of genetic alterations resulting in dysregulation of molecular pathways controlling cell migration, differentiation, apoptosis and proliferation. Chromosomal instability (CIN) is the most common cause of CRC and is present in 60-70% of all cases. CIN involves genetic alterations in tumour suppressor genes and oncogenes which can inhibit the normal apoptotic process, over-activate cell proliferation or facilitate tumour progression through enhanced angiogenesis. [59].

The main genetic aberrations in CRC are mutations in *APC, K-RAS* (Kirstein rat sarcoma) and *TP53* (Tumour protein-53) genes, with frequent allelic loss at 17q and 18q [69]; **see figure 6**.

Mutation of *APC* is a common occurrence in the early development of all CRCs [68, 70, 71]. Germline mutations in *APC* underlie FAP or FAP variant syndromes. Somatic mutations in this gene are present in ~ 70-80% of sporadic CRC. In fact, APC plays a gatekeeper role in normal colorectal epithelial cells maintaining balanced cell proliferation

[72]. Consequently, *APC* mutagenesis is thought to have a potential effect in initiating CRC [73, 74].

K-RAS mutations have been found in 40% of CRC adenomas and 37% of CRC adenocarcinomas [75]. Mutations in *K-RAS* were proposed to follow *APC* mutations with advancing CRC progression. Evidence for this comes from the fact that mutations in both *APC* and *K-RAS* were found in only 20% of small adenomatous polyps, whereas they were present in approximately 50% of more advanced adenomas [76]. In fact, sequential alterations in *APC* and *K-RAS* have been shown to promote CRC progression from adenoma to carcinoma [73].

As mentioned previously, p53 has a function in promoting DNA repair via cell cycle arrest, regulation of metabolism or inducing permanent removal of damaged cells through activation of senescence and apoptosis [77]. Mutant *p53* can block these functions and acquire oncogenic properties that enable it to promote proliferation, survival, invasion and metastasis [78]. In CRC, *p53* mutations have been observed at later stages, which indicate that p53 may mediate the transition from adenoma to carcinoma [73, 79]. In addition to the frequent mutations of *APC, KRAS* and *p53* during CRC development, 85% of sporadic CRCs are also found to have chromosomal instability at several loci particularly 17p and 18q. The remaining 15% have a high-frequency microsatellite instability phenotype [64, 79, 80].

Microsatellites are short tandem repeat nucleotide sequences that are present throughout the genome. They are usually 1 to 10 nucleotides long. Microsatellite instability (MSI) is a measure of the DNA nucleotide mismatch repair system (MMR) to correct errors that often occur during DNA replication. The proteins involved in MMR and implicated in CRC include MLH1, MSH2, MSH6 and PMS2. Approximately 15% of CRC show MSI which occurs either by germline mutations in *MLH1, MSH2, MSH6* and *PMS2* or epigenetic silencing of *MLH1*. These germline mutations are responsible for genetic predisposition of HNPCC. On the other hand, somatic mutation of the *MLH1* gene is observed in approximately 15% of sporadic CRC cases [81].

1.1.2.2.4 Screening of CRC

Survival rates in patients with CRC have increased significantly in the last decade, mostly due to regular screening programmes and improved-targeted treatment options. The aim of screening is to detect malignant and pre-malignant lesions early in their course [64].

In the UK, Faecal Occult Blood testing (also called FOBT or FOB) with or without a colonoscopy are used to screen for bowel cancer in individuals between 60 and 74 years old or in younger people with certain high risk conditions such as FAP, HNPCC and ulcerative colitis. The FOBT test is used as a first line of CRC screening whereas colonoscopy is used as a second line when the FOBT gives an abnormal result [82].

The aforementioned tests have been clinically proven to reduce colorectal cancer-related mortality [83-85].Nonetheless, colonoscopy is associated with a risk of complications especially in elderly patients [64]. For that reason, DNA-based tests of blood or stool are being investigated and in progress [86].

1.1.2.2.5 Available treatments for CRC

Surgical resection of the primary colorectal tumour and any resectable metastases remains the principal treatment for CRC. However, recurrence following resection remains a considerable problem. A large study suggests a 12.8% local or 25.6% distant recurrence rate in patients five years after surgery [87]. Additionally, surgical resection of liver metastases can improve survival [88, 89], although the recurrence rate after surgery is high [90].

To reduce recurrence and to treat metastatic colonic cancer, patients often receive adjuvant chemotherapy. In rectal cancer neoadjuvant chemo-radiotherapy is used for the same effect. Commonly used chemotherapeutic agents include 5-Fluorouracil (5-FU) and Oxaliplatin. Other drugs such as Irinotecan are used in the advanced CRC setting. These drugs are sometimes given in combination with monoclonal antibody therapy such as Bevacizumab (a vascular endothelial growth factor A (VEGF-A) inhibitor) or epidermal growth factor receptor (EGFR) inhibitors cetuximab and panitumumab in advanced CRC treatment [91-93].

New drugs undergoing clinical trials include ramucirumab (VEGF receptor 2 blocking monoclonal antibody, VEGFRII-mAb) [94], AKT inhibitor MK-2206 and the MAPK kinase inhibitor selumetinib. These all target specific proteins involved in important signalling pathways in CRC [95].

Despite advances in surgical treatment and the continued discovery of chemotherapeutic and immunotherapeutic agents, the recurrence of CRC is still a clinical problem. The evidence for this problem has been reported by An *et.al.*,who found that the recurrence rate for 108 rectal cancer patients with liver metastases after receiving simultaneous surgical

resection and adjuvant chemotherapy or chemo-radiotherapy treatment was 71.3 and 68.8%, respectively, and that recurrence also occurred at distant organs [96]. It is therefore important to understand the mechanisms of CRC progression and metastasis, to find new therapeutic targets and develop new treatments.

1.1.3 Cancer metastasis

1.1.3.1 The invasion-metastasis cascade

The spread of cancer is a multistep process whereby epithelial cells from primary tumours first invade the local basement membrane, the surrounding extracellular matrix (ECM) and the stromal cell layers. They then intravasate into blood and lymphatic vessels, survive in the circulation, escape immune surveillance and populate secondary sites. Next, metastatic cells invade into the microenvironment of distant organs forming micro- metastases, and finally re-start their proliferative programs where they can be clinically detectable [97, 98]; **see figure 7**. Blockade of any of these steps could result in a complete failure of the whole metastatic process [99]. Cells from most types of carcinomas can detach from the primary tumour and migrate as a group of cells, termed ‘collective invasion’ or as individual cells. Invasion mechanisms include ‘mesenchymal invasion’ and ‘amoeboid invasion’ programs [100]. Although individual cell invasion is not compatible with epithelial tissue architecture due to strong cell-cell adhesion, an embryonic morphogenesis program known as ‘epithelial to mesenchymal transition’ (EMT) can help explain how cells from an epithelial origin are able to migrate individually [97]. In fact, EMT is believed to be an important process in the conversion of clustered tumour cells into single motile ones that are capable of initiating systemic metastasis [3, 101]. EMT in cancer will be discussed in detail later in this thesis.

1.1.3.2 CRC and metastasis

Although in many cases, tumour metastasis occur when the primary tumour is relatively large, metastasis has also observed when the tumour is relatively small or even undetectable [102, 103]. In CRC, 50–60% of all patients will develop metastases, and 20–30% of patients already have metastases at the time of diagnosis [91, 104]. The liver, followed by the lungs, are the commenest sites for CRC distant metastases with the majority of liver metastases being inoperable. Unfortunately, even when the surgical resection of hepatic metastases is possible, the recurrence rates are significantly high [90].

In fact, metastasis is responsible for more than 90% of cancer-associated mortality [105]; **see figure 7.**

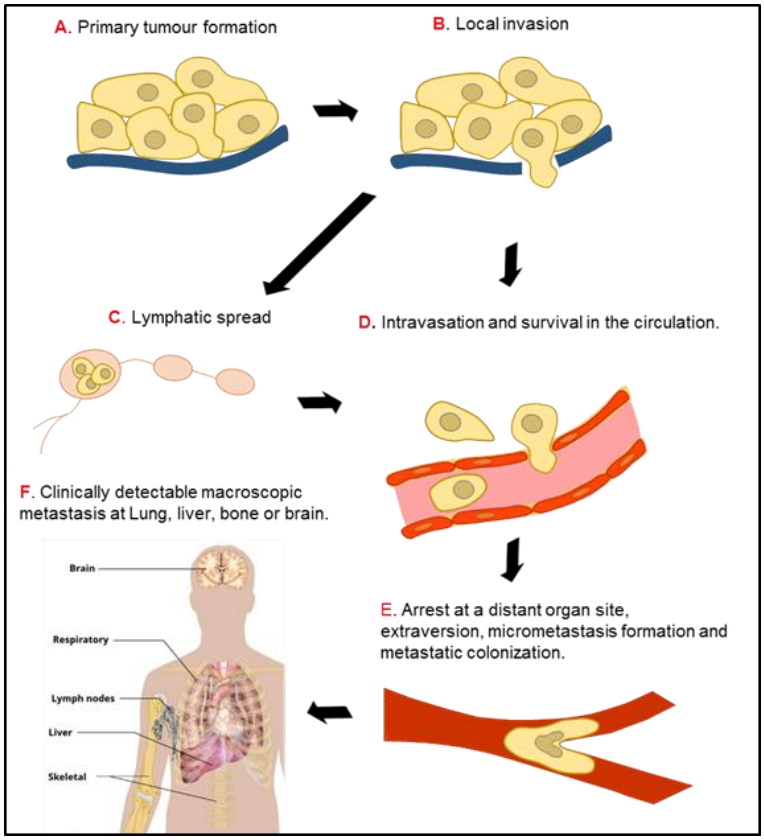

Figure 7: The Invasion-Metastasis cascade.

Blockade at any step could result in complete failure of the whole metastatic process; adapted from [97, 106].

1.2 Epithelial mesenchymal transition (EMT)

EMT is an epigenetic cellular trans-differentiation program that allows polarized, immotile epithelial cells to undergo numerous cellular and molecular changes to resemble elongated and bipolar motile mesenchymal cells [3, 101]. Prof. Elizabeth Hay pioneered the term ‘epithelial mesenchymal transformation’ following her observations from developmental studies [107-109]. The term ‘transformation’ was later replaced with ‘transition’ reflecting the plasticity of the process in converting cells from epithelial to mesenchymal and from mesenchymal to an epithelial morphology. Thus, the reversal of EMT is named ‘mesenchymal-epithelial transition’ (MET). These embryological EMT and MET programs can be also activated in association with tissue repair, fibrosis and cancer progression during adult life. The basic features of embryonic and adult EMT programs are

similar. Many of the signalling pathways and transcription factors which are important during physiological EMT process are also activated during pathological EMT [110]. However, EMT in these different biological settings may vary depending on the functional consequence and biological context [111]. For that, EMT has been classified into three different subtypes; developmental (Type I), fibrosis and wound healing (Type II), and cancer (Type III) [111]. However, before defining EMT subtypes, it is worth describing the main features of epithelial, mesenchymal and intermediate (metastable) cells, EMT biomarkers and signalling pathways. **See figure 8.**

1.2.1 Phenotype of epithelial and mesenchymal and metastable cells in EMT

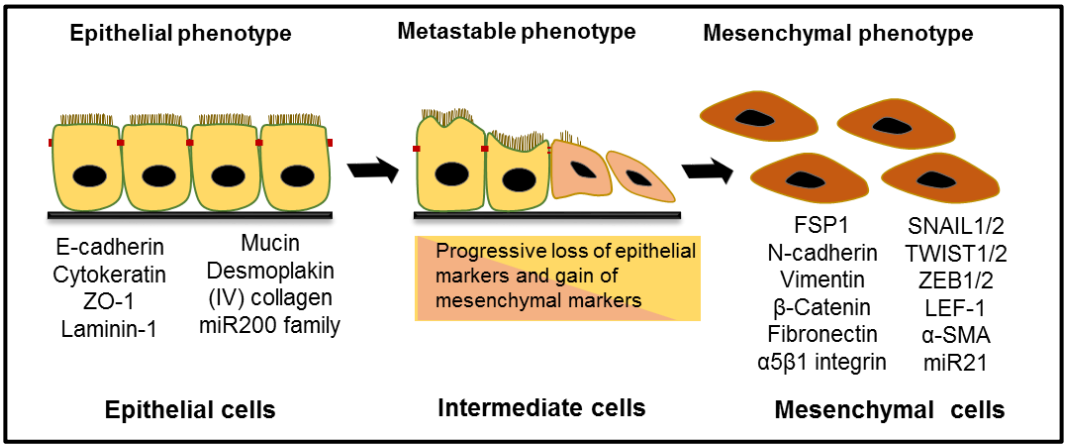

Figure 8: Epithelial Mesenchymal Transition.

EMT is a fundamental biological process, by which epithelial cells lose epithelial features and acquire features similar to mesenchymal cells. Not all cells undergo complete EMT, some cells can have both epithelial and mesenchymal features at the same time, and this is called partial EMT with an intermediate or metastable phenotype; adapted from [111].

1.2.1.1 Epithelial cell phenotype

The biological functions of epithelial tissues are 2 folds: 1) to aid as effective barriers against pathogens and 2) to specialise in secretion or absorption of macromolecules. These dynamic functions require tight associations between cells through the assembly of adhesion junctions that stabilise the integrity of the tissue. There are three main functional classes of cell junctions in metazoan tissues. They are anchoring junctions, occluding junctions and channel-forming junctions [112] **see figure 8 and figure 9.**

Anchoring junctions: Anchoring junctions include both cell-cell and cell-matrix junctions with cell-cell junctions further divided into adherent junctions and desmosomes.

Adherent junctions include classical trans-membrane cadherin linking two adjacent cells and they are supported by intracellular cytoskeletal actin filaments and intracellular anchor proteins such as β-catenin, α-catenin and p120-catenin. The three well-known classical cadherins are E-cadherin, which is present in many types of epithelial cells, N-cadherin that is present in nerve, muscle and lens cells, and P-cadherin which is present on cells in the placenta, epidermis and epithelium [112].

Desmosomes include non-classical cadherins such as desmoglein and desmocollin. They are connected to the other extracellular desmogleins and desmocollins of neighbouring cells by intracellular cytoskeletal intermediate filaments and intercellular anchor proteins such as plakophilin (PKP) and desmoplakin [112].

Cell-matrix junctions include actin-linked cell matrix adhesions and hemidesmosomes. Actin-linked cell-matrix adhesions couple trans-membrane integrins to the extracellular matrix and the extracellular proteins are bound by intracellular cytoskeletal actin filaments and intracellular anchor proteins such as paxillin and focal adhesion kinase (FAK). Hemidesmosomes bind trans-membrane integrin α6β4 and type XVII collagen to extracellular matrix proteins, which are held by intracellular cytoskeletal intermediate filaments and intracellular anchor proteins such as plectin and dystonin [112].

Occluding junctions: Squamous epithelial cells serve as selectively permeable barriers, separating the fluid that infuses the tissue on their basal side from fluid with a different chemical composition on their apical side. This barrier function requires that the space between adjacent cells be sealed together by occluding junctions (also called tight junctions or Zonula occludens), so that molecules cannot leak freely across the cell membrane. The major trans-membrane proteins forming occluding junctions are called claudins and occludin [113].

Channel-forming junctions: Channel-forming junctions or gap junctions create pathways linking the cytoplasm of adjacent cells. All epithelial and non-epithelial cells are joined by gap junctions. There are three distinct families of gap junctions including connexions, pannexins and innexins. These families are distinct in amino acid sequence but similar in shape and function. Cells connected by gap junctions share many of their inorganic ions and other small molecules which make the cells chemically and electrolytically joined [114].

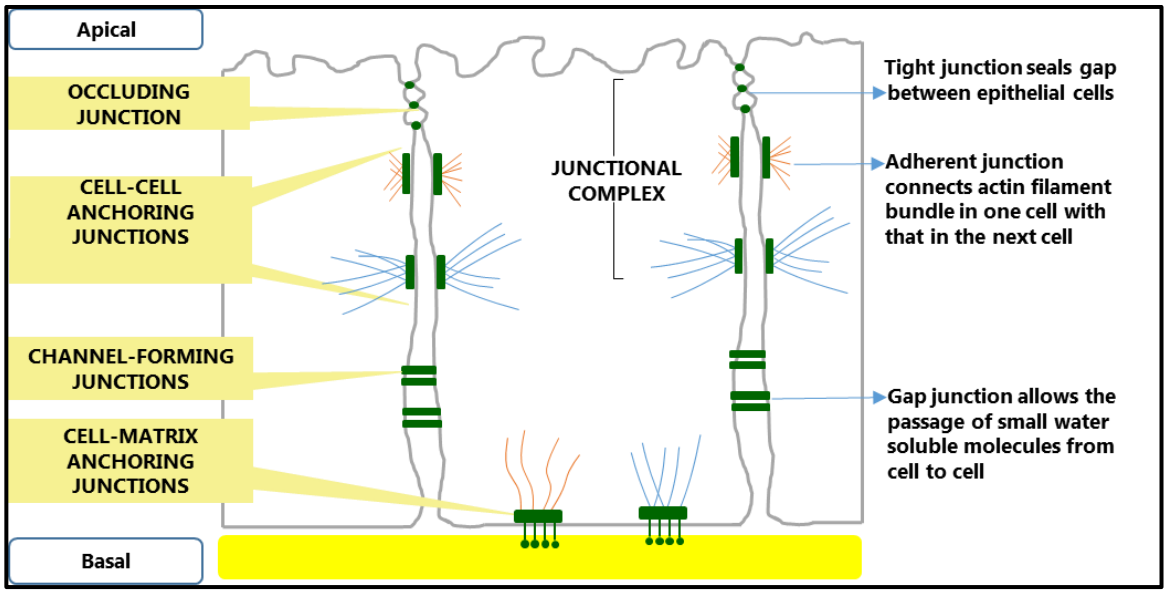

Figure 9: A summary of various junctions in the epithelial cell.
Adapted from [115].

1.2.1.2 Fibroblast and mesenchymal phenotype

Fibroblasts are non-vascular, non-epithelial and non-inflammatory cells within the ECM of the connective tissue. They are individual cells with a spindle-like shape [116, 117]. In healthy organs, fibroblasts have a dual role in maintaining fibrillar ECM homeostasis; they synthesise constituents of the ECM such as type I, III, IV and V collagens, fibronectin and laminin, as well as secreting ECM-degrading enzymes such as matrix metalloproteinases (MMPs) [118, 119]. They also play an important role in modulating the tissue immune response following an injury through the secretion of cytokines and chemokines [117].

Fibroblasts are involved in processes such as wound healing, scar formation, tissue fibrosis as well as tumour invasion and metastasis during cancer. Fibroblasts that are present in an inflamed tissue/cancer are called activated fibroblasts, reactive stromal fibroblasts or cancer-associated fibroblasts (CAFs). Activated fibroblasts secrete high levels of ECM-degrading proteases such as MMP2, MMP3 and MMP9 and abundant quantities of growth factors such as hepatocellular growth factor (HGF), insulin like growth factor (IGF) [117].

In culture, fibroblasts are often identified by their spindle-shaped morphology. Normal fibroblasts constitutively express vimentin and fibroblast specific protein 1 (FSP1) whilst activated fibroblasts, also known as myofibroblasts acquire expression of α-smooth muscle actin (α-SMA). However, the lack of additional fibroblast specific molecular markers has limited *in vivo* studies related to fibroblast biology [117].

Mesenchymal carcinoma cells resemble fibroblasts in their shape; elongated with filopodia and displaying a front-back polarity. In addition, they express fibroblasts markers such as vimentin and FSP1 [120]. Nevertheless, both mesenchymal cells and fibroblasts lack specific protein markers, and are considered the least understood cells at the molecular level [117, 121]; **see figure 8.**

1.2.1.3 The intermediate or metastable phenotype

EMT is a multistep program by which epithelial cells lose their epithelial junctions and acquire mesenchymal cell properties [3]. However, not all cells undergo complete EMT. Instead, some cells undergo partial EMT during development and cancer with cells maintaining an intermediate or a metastable phenotype, which is described by cells possessing some epithelial junctions but simultaneously exhibiting mesenchymal features including invasion, migration and stem-like properties [111, 122-127]. Huang et al. have classified the EMT status of 43 ovarian cancer cell lines into 4 groups including epithelial, intermediate epithelial, intermediate mesenchymal and mesenchymal [128]. The study characterised intermediate mesenchymal cells by their high expression of N-cadherin and ZEB1 and their low expression of E-cadherin and ERBB3/HER3 as well as their resistance to anoikis. However, until now, intermediate EMT states have not been well characterised, and there is no biomarker/s to specify them. It is proposed that the cells with partial EMT acquire some of the stem-cell like properties [123, 129], although further identifying this subpopulation in EMT would be beneficial. Recently, Ribeiro and Paredes [130] suggested that P-cadherin would be a promising future marker in breast cancer for identifying stem cell population within the intermediate phenotype. In fact, describing EMT with metastable states could imply a spectrum of heterogeneity instead of only presenting the two extreme ends of the EMT process, and could increase the advantage of more targeted therapies [128, 130]; **see figure 8.**

1.2.2 EMT biomarkers

As previously mentioned, during EMT, epithelial cells gain spindle shape morphology and lose polarity. Such cells also express mesenchymal/fibroblast cell markers and lose epithelial cell adhesion molecules and increase motility [3, 101]. The major EMT biomarkers *in vitro* include cell-surface proteins (E-cadherin, N-cadherin, ZO-1 and integrins), cytoskeletal proteins (α-SMA, vimentin, and β-catenin), extracellular matrix proteins (Collagens, Fibronectin, and Laminin), transcription factors (SNAIL1/2,

TWIST1/2, ZEB1/2 and LEF-1) and recently discovered microRNAs (miRNAs of 200 family). The main EMT biomarkers will be discussed in detail with a focus of their expression in cancer.

1.2.2.1 **Cell surface markers of EMT**

Down-regulation of E-cadherin is considered a typical marker for EMT in various types of cancers [131-136]. Altered expression of different cadherins (the cadherin switch), have been increasingly used to monitor EMT with N-cadherin and E-cadherin up- and down-regulated, respectively [3].

Zonula occludens (ZO) proteins, comprising ZO-1, -2 and -3, are peripheral proteins which localise at tight junctions of epithelial cells. They belong to the large family of membrane-associated guanylate kinase (MAGUK) proteins. ZO proteins have a scaffolding function providing the structural basis for various cell-cell junctions [137-139]. In fact, down-regulation of ZO proteins are reported during the invasion of many tumour types upon EMT activation [140-143].

Integrins are adhesion receptor molecules that mediate the attachment of cells to the ECM and upon ligand-binding trigger critical intracellular signalling pathways [144]. A switch in the expression of different integrins often reflects alterations in cell-ECM interactions. For example, in colon carcinoma, cancer cells that have undergone EMT express high levels of αVβ6 integrin compared to normal colon epithelium and non-invasive cancer cells [145, 146].

1.2.2.2 **Cytoskeletal markers of EMT**

FSP1 (fibroblast specific protein 1 (FSP1)) or S100A4 is a member of the family of calcium-binding, S100 proteins and is expressed in fibroblasts [147, 148]. It is believed that metastatic cells often express FSP1 [149, 150].

Vimentin is a major constituent protein of intermediate filaments, which is expressed widely in various cells such as normal fibroblasts, endothelial cells, neuronal precursors and cells of the hematopoietic lineage. It is known to maintain cellular integrity and provide resistance against mechanical stress [151-153]. Over-expression of vimentin in cancer correlates with increased tumour growth, invasion and poor prognosis [154] as

reported in gastrointestinal tumours, prostate, breast and lung cancers [155-158]. In fact, vimentin has gained significant importance as a marker for EMT [153, 159].

α-SMA is one of the six actin isoforms that is predominantly found in vascular smooth muscle cells and myoepithelial cells. It contributes to mechanical force contraction and mechanotransduction. α-SMA has also been found in myofibroblasts which are mainly present in healing wounds and fibrotic tissue [117, 160, 161]. In addition, α-SMA over-expression is associated with EMT in cancer [140, 162-167].

β-catenin is a cytoplasmic plaque protein which is mainly localised at the membrane of normal epithelial cells. β-catenin has structural and signalling functions; it serves as an integral structural component of cadherin-based cell–cell connections, and as a nuclear effector of canonical Wnt signalling which regulates cell fate; **see section 1.1.1.3 and figure 4**. The activity of β-catenin is regulated by controlling its protein abundance in the cytoplasm through either ubiquitination or recruitment to cadherin-binding partners. Loss of cell adhesion results in the dissociation of β-catenin away from the cell membrane and its accumulation in the cytoplasm, an event that occurs in association with E-cadherin down-regulation. In addition, accumulation of un-phosphorylated β-catenin, which escapes proteasome degradation as a result of activated Wnt signalling pathway, can result in nuclear translocation leading to altered gene expression; **see section 1.1.1.3** [168-170]. In fact, β-catenin has been used as a marker of EMT in various studies [171-175].

Cytokeratins (Ks) are intermediate filament proteins which interact with desmosomes and hemidesmosomes, thus providing mechanical stability and integrity of epithelial cells and tissues. They also collaborate in various cellular processes such as cellular polarity and migration [176, 177]. They are expressed in epithelial tissues, hair and skin [177, 178]. In humans, Ks originate from 54 unique genes and they are sub-classified into two types; Acidic type I (K 9-40) and basic or neutral type II (K 1-8 and keratin 71-86) [179] .These subfamilies heterodimerise in pairs consisting of a type I and type II subunit. The composition of the heterodimers helps to distinguish different epithelial cells, degree of differentiation and disease status. For example, basal epidermal keratinocytes express K5/K14, although during skin differentiation, this keratin pair is replaced by K1/K10 [180]. Moreover, the K7/K19 pair are markers for ductal and liver progenitor cells, and loss of K19 is an indication of primary biliary cirrhosis [181]. In addition, keratins play an active role in cancer progression. For instance, expression profile of cytokeratins K7/K20 has been shown to be a marker for CRC progression. The majority of CRC adenocarcinomas showed a K7-/K20+ profile [182-184]. Loss of keratin expression is

another marker of EMT. For example, the loss of K8/18, normally co-expressed in pre-invasive tumour epithelial cells, was found to activate EMT features of enhanced motility, invasion and chemo-resistance [185].

Microfilaments or actin filaments are highly abundant in the cytoplasm of many eukaryotic cells. Actin filaments have the ability to shift between monomeric (G-actin) and polymerised or filamentous (F-actin) under ATP hydrolysis, ion exchange and the interaction with large number of actin-binding proteins such as cofilin, profilin and the Arp2/3 complex. This makes actin filaments important in amoeboid cell movement and in maintaining cell shape and polarity [186]. In addition, F-actin can bind with other proteins in order to accomplish specific cellular functions, for example, interaction with myosin proteins resulting in dynamic muscle contraction [187]. Moreover, actin filaments are polymerised in response to appropriate cellular stimuli such as hydrolysis of phospholipids [188] or GTP-binding proteins including Cdc42, RhoA and RhoB which localise F-actin to the cell membrane thus contributing to cell movement and migration [189]. The importance of actin-binding proteins come from studies which show that alteration of actin regulators (e.g. cofilin, WAVE and Arp2/3 complex subunits) leads to increased cell migration and invasion via formation of lamellipodia, filopodia and invadopodia in normal and cancer cells [190-192]. On the other hand, an *in vivo* study showed that activation of Cofilin reduced both cancer cell motility and metastasis [193]. The actin cytoskeleton has been shown to be controlled during EMT [194]. For example, the actin-bundling protein fascin was found to be up regulated by SLUG during EMT, promoting cancer cell invasion, migration and metastatic potential in pancreatic cancer [195].

1.2.2.3 **Extracellular matrix proteins**

Numerous extracellular matrix proteins such as laminins, type I and IV collagens, tenascin and fibronectin are deregulated during EMT in cancer [166, 196-200]. Among them, laminins are considered the best extracellular protein biomarkers of the EMT process [110]. Laminins are heterotrimeric glycoproteins composed of α, β, and γ chains [201]. Laminin 332 (formerly laminin 5, α3βγ2) has been strongly associated with cancer invasion and its expression is linked with EMT in breast, hepatocellular and oral squamous carcinomas [202-207].

1.2.2.4 **Transcription Factors**

The full molecular reprogramming that occurs during EMT is mastered by the following major groups of transcriptional factors: ZEB1/2, SNAIL1/2, TWIST and lymphoid enhancer binding factor-1 (LEF-1) families. These factors do not only have the ability to directly repress E-cadherin but also to coordinate the whole EMT program by repressing and activating a large number of epithelial and mesenchymal genes, respectively [132, 208-211].

ZEB 1/2: the ZEB family consists of two members (ZEB1; also known as δEF1, and ZEB2; also known as smad-interacting protein 1 (SIP1)) which are highly conserved proteins across species [212]. Both ZEB1 (1124 amino acid) and SIP1 (1214 amino acid) proteins contain two clusters of zinc finger domains and one homeodomain. In human pathology, *SIP1* mutations are associated with *Hirschsprung* disease, a neurological syndrome, characterized by mental retardation and multiple congenital anomalies [213]. ZEB1 and ZEB2 trigger EMT by direct binding to E-boxes in the E-cadherin (*CDH1*) gene promoter through their zinc finger domains, and as a result repress E-cadherin expression [132, 214]. When EMT is induced, ZEB factors not only transcriptionally repress E-cadherin but also repress other epithelial markers and activate mesenchymal genes [211, 215-218]. Many extracellular and intracellular stimuli/factors can induce the activation of ZEB proteins, such as TGF-β, hypoxia, inflammatory cytokines, fibroblast growth factor (FGF) or insulin growth factor 1(IGF-1) [4, 5]. In addition, ZEB factors can be induced directly by downstream signals from RTKs such as RAS-ERK2-Fra1 and JAK/STAT3, which are frequently activated during carcinogenesis; see **section 1.1.1.2 and figure 3** [4]. Crucially, ZEB proteins are absent in normal gut epithelium as they are only present in tissue originating from ectoderm and mesoderm [219]. However, the high expression of these proteins has been found in a wide range of cancers including colorectal, breast, liver, gastric, prostate and pancreatic carcinomas which are associated with increased aggressiveness and metastatic capacity [4, 5, 220, 221]. In fact, ZEB factors have been shown to have an independent prognostic value for cancer dissemination, cancer-related survival and response to chemotherapy in many carcinomas including pancreatic, liver, bladder and gastric cancers [220-223].

SNAIL1/2: the SNAIL family comprises three members: SNAIL1 (originally known as SNAIL; 264 aa), SNAIL2 (SLUG; 268 aa), and SNAIL3 (Smuc; 292 aa). All of them share a common structure: a highly conserved C-terminal region, containing four to six zinc fingers and a highly conserved N-terminal SNAG domain region. SNAIL1/2 proteins

repress E-cadherin expression through binding to the E-boxes in the *CDH1* gene promoter which in turn promotes EMT [210, 224]. SNAIL1/2 also repress other epithelial genes and activate the expression of mesenchymal genes independently of their effect on E-cadherin. SNAIL2 is induced directly by β-catenin-mediated transcription, whereas SNAIL1 is induced indirectly upon Wnt stimulation by blocking GSK3β activity; GSK3β phosphorylates SNAIL1 and marks it for degradation [225, 226]. In addition, up-regulation of the E3 ubiquitin ligase, Mdm2 by the SMAD2/3/4 complex promotes degradation of p53, and loss of p53 function induces SNAIL which in turn mediates EMT via a microRNA-mediated mechanism [227]; **see figure 10**. SNAIL factors can also be activated by the upstream signalling of TGF-β, Notch, TNF-α, EGF, FGF, hypoxia, and oestrogen pathways [3]; **see section 1.1.1**. Similar to the ZEB family, SNAIL1 and 2 proteins are absent in normal epithelium and their presence is reported to be associated with aggressive disease and an independent prognostic factor of poor survival in many carcinomas such as breast, colon, liver, gastric, ovary, oesophagus and lung [4, 228-233] [234, 235].

TWIST 1/2: the TWIST family consists of TWIST1 (202 aa) and TWIST2 (160 aa) which share a basic/helix-loop-helix (bHLH) structure; two parallel α-helices joined by a loop required for dimerisation. TWIST proteins bind directly to conserved E-boxes on DNA, via their TWIST box at the C-terminal, and thus recruit proteins for both transcriptional activation and repression mechanisms [236]. For example, binding of TWIST proteins to the promoter of N-cadherin activates its transcription, whereas binding the promoter of *CDH1* represses its transcription [237]. Moreover, TWIST1 can also bind to the *SLUG* promoter and trigger its expression forcing EMT [238]. Thus, TWIST factors play a significant role in EMT during cancer metastasis [209, 237, 239]. TWIST factors are also up-regulated by classical EMT-inducing pathways such as TGF-β, Wnt, hypoxia, ligand binding activation of RTKs and inflammatory cytokines receptors [6, 236, 240]; **see section 1.1.1**. Like ZEB and SNAIL families, TWIST proteins are absent in normal epithelium but are induced in a number of human carcinomas such as breast, liver, prostate and ovarian cancers. TWIST factors are also reported to be independent prognostic factors associated with tumour aggressiveness, recurrence and poor patient survival [4, 241-246]. However, the upstream signalling pathways of TWIST1 and TWIST2 are less understood compared to ZEB and SNAIL family of EMT-inducers [4].

LEF-1: LEF-1 induces EMT as a result of *CDH1* down-regulation [247]. TGF-β signalling can directly increase LEF1 expression via SMADs. In addition, β-catenin accumulation in

the nucleus, as a result of Wnt signalling or PI3K-AKT activity, activates LEF-1 to induce EMT [171, 208, 247, 248]; **see section 1.1.1**

1.2.2.5 **MicroRNAs**

MicroRNAs (miRNAs) are short (20-25 nucleotides in length) non-coding RNAs. They suppress the expression of their target genes through mRNA destabilisation or inhibition of translation via binding to the 3' untranslated region of their target mRNAs. Recently, miRNAs have emerged as effective regulators of EMT/MET by targeting genes responsible for epithelial integrity or mesenchymal traits [249]. For instance, miRNAs regulate metastasis by targeting the translation of a large number of genes involved in EMT/MET including *TWIST*, *SNAIL* and *ZEB* genes.

A double negative feedback loop has been found between the miR-200 family (miR-200a/b/c, miR-141, and miR-429) and ZEB1/2. In other words, the miR-200 family can maintain epithelial status and prevent EMT or initiate MET through inhibition of ZEB factors. Reciprocally, the transcription of miR-200 members are repressed by ZEB1/2 which helps maintain the mesenchymal status of cells that have undergone EMT [250-252]. A similar double negative feedback loop also exists between SNAIL1/2 and miR-34a/b/c [251]. To date, few miRNAs have been linked to TWIST compared with SNAIL1/2 and ZEB1/2. TWIST1 is found to be inhibited by miR-29b, although it is not clear whether the down regulation is direct or a result of *SNAIL1* inhibition [253]. The emergence of such regulatory loops between miRNAs and the major EMT transcription factors provides evidence of the importance of miRNAs in enhancing cancer progression and the plasticity between EMT/MET during cancer metastasis [4].

1.2.3 Crosstalk between the EMT transcription factors

Recently, a crosstalk between SNAIL, TWIST and ZEB transcription factors in regulating cancer EMT has been discovered. This hierarchy also highlights the overlapping and distinct functions of these proteins [12, 254].

It was suggested that ZEB operates downstream of SNAIL and TWIST [255], and SNAIL regulates both TWIST and ZEB1 via direct binding to their promoter regions. From these studies, it became evident that SNAIL1 may be required to initiate EMT and TWIST and ZEB factors may be crucial in maintaining it [238, 241, 256, 257].

Understanding these signalling pathways in EMT will facilitate the therapeutic potential of targeting EMT, and thus promote controlled tissue regeneration, treat fibrosis, and prevent cancer metastasis; **see figure 10.**

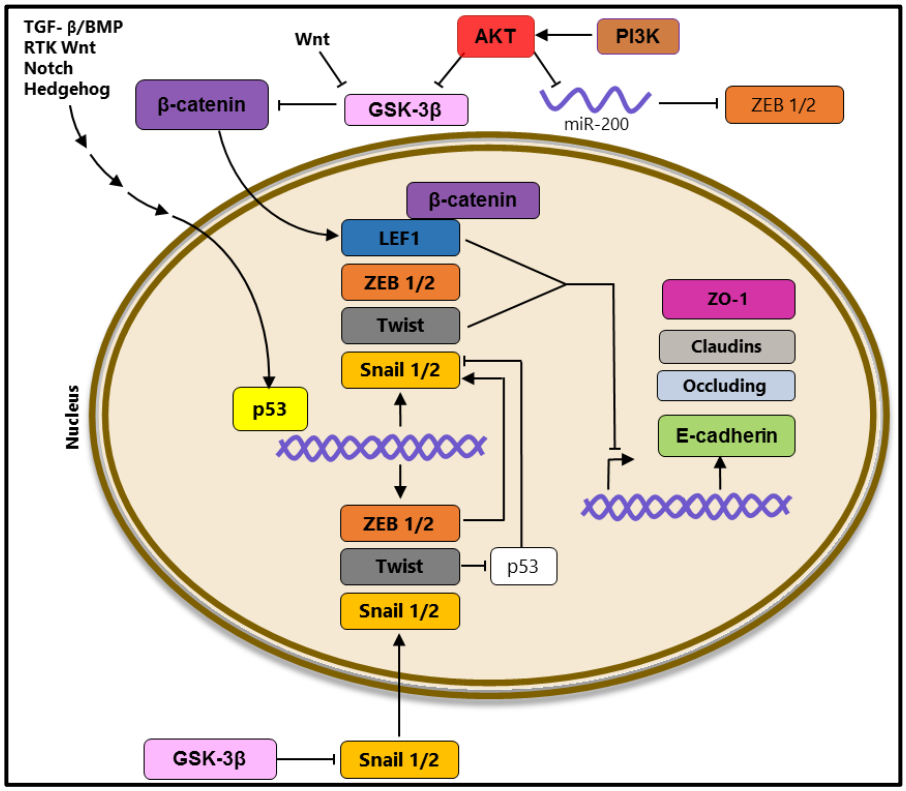

Figure 10: Crosstalk between SNAIL, TWIST, and ZEB1/2 and LEF-1 transcription factors (TFs) in EMT.

Various cancer cell-signalling pathways such as RAS, TGF-β, RAS, PI3K/AKT, Wnt/β-catenin can activate the EMT TFs. In the nucleus, they bind to DNA and regulate genes encoding cell-cell junction molecules, such as E-cadherin, ZO-1, claudins, and occludin facilitating the EMT process. The interaction between the TFs is not fully understood yet. However, SNAIL may be required to initiate EMT whereas TWIST and ZEB factors may be crucial in maintaining EMT. Many molecules are implicated in regulating the expression of the TFs. For example, GSK-3β can inhibit β-catenin from binding to LEF-1, and can inhibit SNAIL1/2 from trans-locating to the nucleus. The miR-200 family can inhibit the expression of ZEB1/2 [12].

1.2.4 EMT subtypes

1.2.4.1 Type 1 EMT: EMT associated with embryo formation and organ development

EMT and MET are evolutionarily conserved processes where cells of developing organs depend on the switch between epithelial and mesenchymal phenotypes. This type of EMT is well-defined and typically accompanied by a cell fate decision which neither causes fibrosis nor induces pathological invasiveness [111]; **figure 11, type1**. The main examples

illustrate the process of gastrulation [258], neural crest formation [259] and heart valve formation [260].

Gastrulation is an early embryonic event which gives rise to three primitive germ layers: the ectoderm, mesoderm and endoderm [258]. During gastrulation, the basement membrane underlying the epiblast breaks down leading to induction of EMT in the cells of the primitive streak by the action of FGF (fibroblast growth factor) resulting in up-regulation of SNAIL and repression of E-cadherin [261]. With complete EMT induction, the cells within the primitive streak undergo ingression and subsequently some either undergo MET and give rise to the endoderm or remain mesenchymal and give rise to the mesoderm [262].

Another example of EMT in vertebrate development is during neurulation. The cells near the junction of the neuroectoderm and the embryonic ectoderm undergo EMT, generating a migratory neural crest cell population. After delamination and migration throughout the developing embryo, these cells give rise to various cell types and tissue structures including facial and cervical structures, the neurons of the peripheral nervous system, pigment cells (melanocytes) and the cells of the adrenal medulla [259] . The migratory neural crest cells require SNAIL1/2 to undergo EMT [263]. Induction of SNAIL1/2 is likely controlled by Bone Morphogenetic Protein (BMP), Wnts and FGFs [264]. In fact, SNAIL1/2 deficiency causes congenital malformation in humans and animals such as *piebaldism* and *Waardenburg* syndrome [265-267].

In addition to gastrulation and neural crest formation, EMT is also critical in development of the cardiac valve. During heart development, endocardial cells activated by factors secreted by the adjacent myocardium undergo EMT and invade through the basement membrane and into the cardiac jelly. The cells remain as mesenchymal cells at the cardiac cushion and mediate development of the heart [260]. EMT-inducing factors such as BMPs [268], β-Catenin [269] and TGF-β [270] activate SNAIL2 [271] and regulate endocardial EMT.

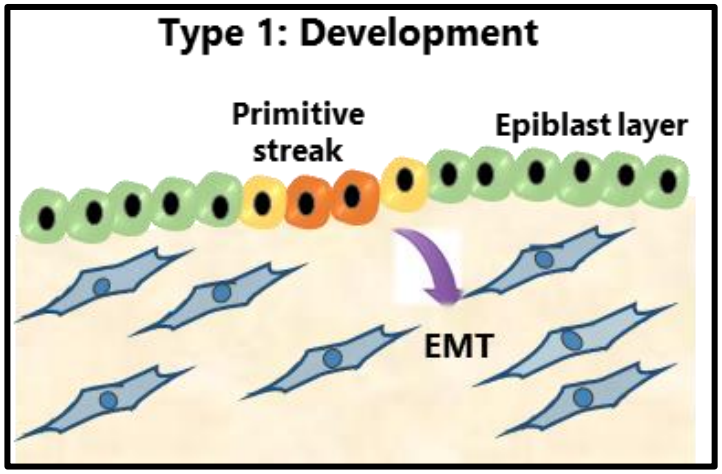

Figure 11: EMT in embryo development.

Successful and complete EMT and MET enable the development of the embryo and organs. It neither causes fibrosis nor induces a pathological invasive phenotype, adapted from [272].

1.2.4.2 Type 2 EMT: EMT associated with wound healing, tissue regeneration, and organ fibrosis

In type 2 EMT, the program is initiated as part of a repair process which leads to generation of fibroblasts and other cells in order to rebuild tissues following trauma and inflammatory injury. In contrast to type 1 EMT, type 2 EMT is associated with inflammation and terminates once inflammation ends. However, type 2 EMT resulting in organ fibrosis can continue to respond to ongoing inflammation, eventually leading to organ destruction. In fact, tissue fibrosis is considered as an undiminished form of wound healing due to persistent inflammation [111]; **figure 12, type 2 EMT**. Organ fibrosis is mediated by inflammatory cells such as macrophages and myofibroblasts that can trigger EMT through the release of growth factors, such as TGF-β, PDGF, EGF, and FGF [273, 274]. Activation of EMT via SNAIL leads to the acquisition of renal fibrosis and renal failure in transgenic mice [275]. High SNAIL expression and features of EMT have been also found in the kidneys of patients with renal fibrosis [275, 276]. Similarly, in patients with Crohn's disease, EMT was demonstrated in areas of fibrosis in the colon [277]. For that, developing novel therapeutics with a potential of reversing organ fibrosis via reversal of EMT is vital.

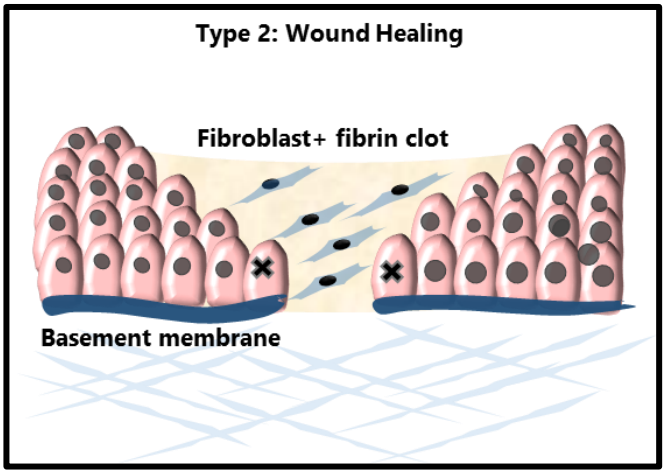

Figure 12: EMT in wound healing, tissue regeneration and organ fibrosis.

EMT of this type leads to the generation of mesenchymal or fibroblast-like cells that help in re-building damaged tissue. The process can be either terminated once the tissue is repaired or it can be continued to generate more fibroblast cells which lead to chronic inflammation and fibrosis; adapted from [272].

1.2.4.3 Type 3 EMT: EMT associated with cancer progression and metastasis

The EMT program has been widely documented to enhance cancer cell migration and invasion in many *in vitro* models. However, the *in vivo* significance of EMT during cancer progression has remained an area of debate until the last decade due to the lack of convincing evidence of EMT in clinical samples [3]. However, evidence has come from cancer cells at secondary sites which were found to resemble, at the histopathological level, the primary tumour indicating that these metastases colonise through activation of the reverse EMT process, MET [111]. Further evidence is the observation of small aggregates of tumour cells at invasive fronts detaching from the tumour mass into the adjacent stroma producing single migratory cells that lose E-cadherin expression [278]; **figure 13 type 3 EMT**. From such observations, the importance of the EMT/MET in cancer has been widely accepted and has been investigated further [279].

The signalling pathways that contribute to EMT in cancer are not completely clear yet. EMT can be triggered by various intrinsic signals as well as extrinsic signals [280]. It has been suggested that the tumour-associated stroma is the main origin of extrinsic signals. In many carcinomas, HGF, EGF, PDGF and TGF-β are the main factors secreted by stromal cells which activate intracellular signalling proteins such as ERK, MAPK, PI3K, AKT, SMADs, β-catenin and RAS**.** Upon activation of these signalling networks, SNAIL1/2 and ZEB1/2 orchestrate EMT [159, 281-283]; **see section 1.1.1** and **figure 2 and 3**. Activation of EMT programs is also facilitated by the disruption of cell-cell junctions and the cell-

ECM adhesions [280]. The main biomarkers implicated in inducing EMT in cancer have been discussed in **section1.2.2**

Importantly, EMT is not only involved in cancer metastasis, but also in other events highly relevant to tumour progression, including resistance to cell death, senescence, therapeutic resistance, de-differentiation and immunosuppression [3, 284, 285]. The main immune cells in the tumour microenvironment and the role of EMT in immunosuppression will be reviewed in detail in the next section as it the second aim of this project.

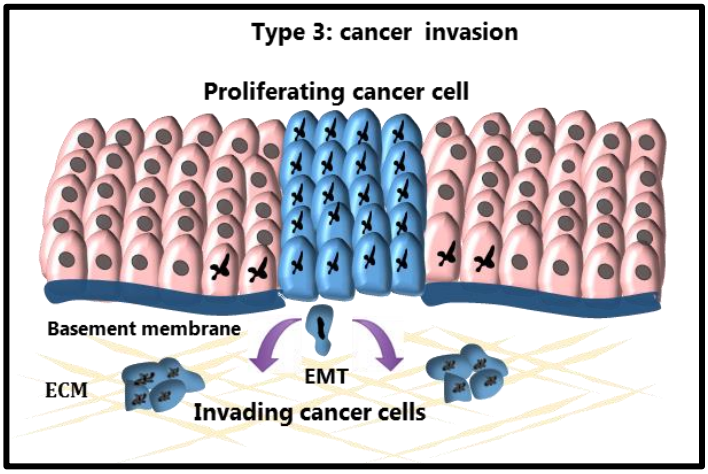

Figure 13: EMT in cancer.

EMT facilitates primary cancer cell proliferation, survival, migration, invasion, and metastasis, in which all lead to colonisation and formation of secondary tumours via MET, adapted from [272].

1.3 The tumour microenvironment

Recently, targeting cells in the tumour microenvironment (TME) has been identified as a potential way to treat cancer. Stromal cells residing in the TME significantly contribute to cancer progression via their crosstalk with cancer cells and ECM. The stromal cells include cancer-associated fibroblasts (CAFs), mesenchymal stem cells (MSC), immune cells and the surrounding blood vessels [286] [287]; **see figure 14.** Crosstalk between cancer and stroma has an influential role in promoting hallmarks of cancer including tumour growth [288], angiogenesis [289], invasion and metastasis [286, 290]. Additionally, cancer cells can gain stem cells properties by stromal influence [291] and develop resistance to chemotherapy [292] and the ability to evade host immunity. Indeed, targeting these stromal cells and the large quantity of factors they secrete may make a huge impact in cancer therapy [293].

In this section, I will introduce the TME briefly in respect to its non-cancer stromal cells as they are the main foucus of the project. In addition, I will introduce the role of chemokines (one of the soluble factors in TME) in promoting immunosuppression. For more details about the ECM, please refer to the review ‘A top-down view of the tumour microenvironment: structure, cells and signaling’ in which I am one of the authors [294].

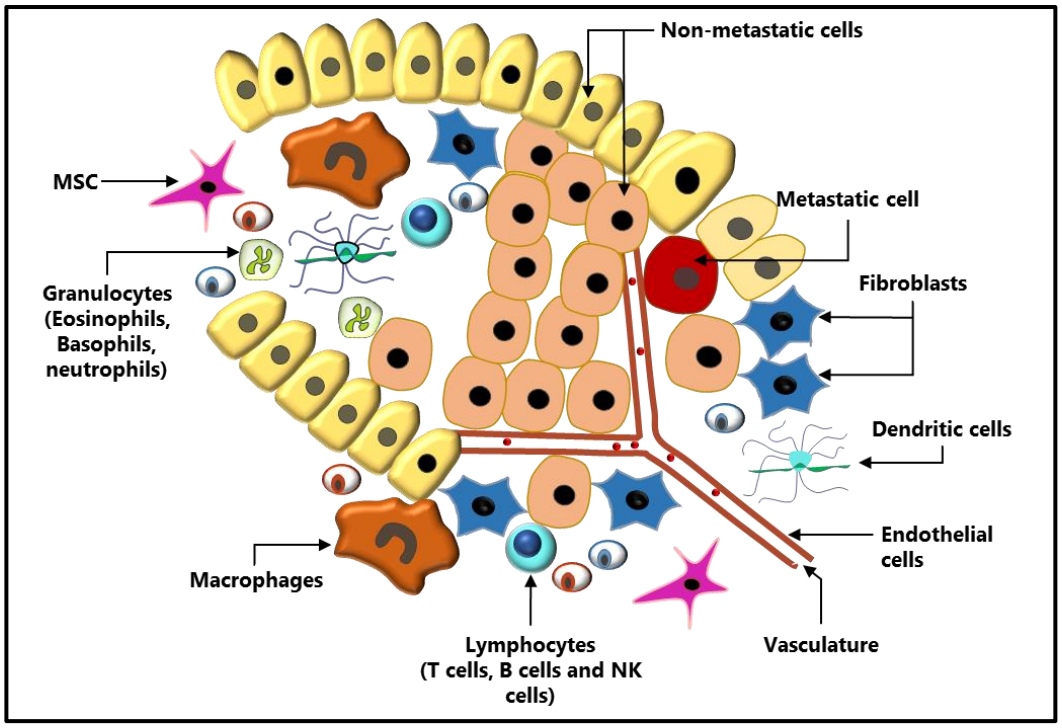

Figure 14: The primary tumour microenvironment (TME).

The tumour microenvironment is a heterogeneous mixture of stromal cells such as cancer-associated fibroblasts (CAFs) mesenchymal stem cells (MSCs), endothelial cells and immune cells, as well as the extracellular matrix molecules such as collagens and laminin. The interaction between the metastatic and non-metastatic cancer cells with stromal cells and the extracellular matrix can promote cancer cell proliferation, survival, invasion, and metastasis. The presence of various immune cells can have distinct functions. The presence of NK cells, T helper 1 cells, cytotoxic T cells, M1 macrophages and N1 neutrophils in TME can provide an anti-tumour response. However, the presence of myeloid-derived suppresser cells (MDSCs), M2 macrophages, T-helper 2 cells, T regs and N2 neutrophils in TME facilitates an immunosuppressive microenvironment, promoting the EMT process and thus metastasis; adapted from [295].

1.3.1 Cancer-associated fibroblasts

Cancer-associated fibroblasts (CAFs) are an active form of fibroblast which represents the most dominant cell type in the tumour stroma. The origin of CAFs are not well defined yet, although studies showed that they originate from various lines of cellular stroma including resident fibroblasts, smooth muscle cells, endothelial cells (ECs), tumour epithelial cells via EMT or bone marrow-derived cells such as MSCs [296]. CAFs contribute to tumour vascularisation and metastasis through expression of vascular endothelial growth factor

(VEGF), FGFs, HGF, TGF-β and stromal cell-derived factor-1 (SDF-1/CXCL12) [296, 297], and they are able to modulate the extracellular matrix [117] by expressing several proteins such as periostin [298] and tenascin-C [299]. Secretion of FGF-2 by CAFs has an important effect in promoting angiogenesis, and inhibition of FGF by Brivanib (a dual VEGF/ FGF tyrosine kinase inhibitor) has been shown to effectively block angiogenesis in pancreatic cancer [300]. CAFs are also associated with inducing EMT in breast, squamous cell and prostate cancers [301-303].

1.3.2 Mesenchymal stem cells

Mesenchymal stem cells (MSCs) are inflammatory cells that are phenotyped according to their surface markers (CD73, CD90, CD105) and their ability to adhere and differentiate [304]. MSCs are recruited from bone marrow to the tumour microenvironment via TGF-β and SDF-1 which are mainly expressed by CAFs [305]. As mentioned earlier, MSCs can differentiate into CAFs by stimuli from cancer cells [306]. The importance of MSCs was first evaluated by Karnoub et al., who observed that recruited MSCs secrete abundant levels of CCL5 and CCL5 enhances the metastatic potential of breast cancer cell lines [307]. The metastatic effect of MSC-derived CCL5 on cancer can be diminished through CCL5 knockdown in specific cell types [308]. MSCs have also been implicated in creating an immunosuppressive TME, thus enhancing breast cancer *in vivo* [309]. Moreover, MSCs can promote breast cancer metastasis by driving EMT through down-regulation of E-cadherin protein expression [310].

1.3.3 Endothelial cells of blood and lymphatic vessels

Blood vessels (BVs) and lymphatic vessels (LVs) consist of blood/lymphatic endothelial cells (BEC and LEC), respectively [311, 312]. Tumour BVs supply blood into the tumour, and therefore promote tumour growth and spread. LVs are more permeable compare to BVs, as they are only covered by pericytes and smooth muscle cells, and these cell types were shown to enhance cancer cell dissemination [311]. BVs and LVs provide a means of tumour cell movement but also allow secretion of soluble factors that mediate cancer cell proliferation, survival, angiogenesis, and thus invasion and metastasis [313, 314]. Angiogenesis is a process by which new BV or LV form from pre-existing endothelial structures in order to enhance primary tumour growth and tumour cell dissemination through blood stream or lymphatic drainage, respectively. Tumour BV angiogenesis is facilitated in hypoxic conditions by tumour cell secretion of high levels of Vascular

Endothelial Growth Factor Receptors (VEGFRs) in response to hypoxia through hypoxia inducible factors (HIF1 and HIF2) [315-317]. HIF-1 is associated with increased proliferation and migration of BECs [318], whereas HIF-2 promotes BECs maturation and quiescence [319]. Deletion of both *HIF-1* and *-2* suppresses primary tumour invasion, although HIF-1 deletion leads to reduced metastasis. Surprisingly, however, *HIF-2* deletion was associated with increased metastasis [320]. Additionally, activation of VEGFR-1 in breast cancer cells promotes migration and invasion through epithelial-mesenchymal transition [321].

High expression of epidermal growth factor (EGF) by endothelial cells themselves [322] enhances migration and invasion of breast and head and neck cancer cells through activating EMT. Tumour cells express and secrete PDGF which also enhances tumour spread via formation of new LVs [323, 324]. Indeed, LVs are considered the main reservoirs for TME inflammatory immune cells [293, 325]. Therefore, targeting cancer angiogenesis would be a beneficial cancer treatment.

1.3.4 Immune cells

In the early stages of cancer development, patients have an active immune response with various types of immune and inflammatory cells in the tumour stroma. The cells involved with tumour rejection are M1 macrophages, cytotoxic T cells, T helper-1 cells, myeloid-derived suppressor cells (MDSCs), antigen presenting cells (APCs) and natural killer cells (NKs). At later stages cancer cells develop mechanisms to escape immune surveillance either by inducing immune tolerance or by modifying their phenotype through immuno-editing. In contrast, M2 macrophages, regulatory T cells, and T helper-2 cells are the immune cells that support tumour progression [326-329]. In fact, avoidance of immune destruction has been defined as a hallmark of cancer [2].

1.3.4.1 **Macrophages**

Macrophages have a phagocytic function in innate and adaptive immunity. They are recruited from the blood to the sites of tumours which contribute in altering the TME and promote metastasis. At the tumour site, macrophages can differentiate into M1 or M2 variants depending on various signals generated from the tumour and stromal cells. M1 has a pro-inflammatory, and thus anti-tumorigenic function via expression of interleukin-1 and tumour necrosis factor alpha (TNF-α) [330]. On the other hand M2 has an anti-

inflammatory, and thus immunosuppressive, function through expression of interleukin-10 which promotes tumour development [331]. Indeed, M2 macrophages are also called tumour-associated macrophages (TAMs) because they are found in close proximity to tumour cells [332]. TAMs have been shown to be associated with metastasis in CRC [333] and renal cell carcinoma [334]. TAMs are also associated with tumour angiogenesis, through their ability to chemo-attract endothelial cells by releasing adrenomedullin [335]. Recently, TAMs were implicated in inducing EMT. Analysis of 491 patients with non-small cell lung cancer by immunohistochemistry showed a positive correlation between density of the TMA infiltration and the late stage of the tumour and EMT [336].

1.3.4.2 **Myeloid-derived suppressor cells**

MDSCs are characterized by the expression of CD11b and GR1 (comprised of LY6C and LY6G) and by the absence or low expression of mature myeloid cell surface markers [337]. Depending on the level of expression of LY6G, they are subdivided into monocytic MDSCs (CD11b+ LY6Chi LY6G low cells) and granulocytic MDSCs (CD11b+ LY6C low LY6Ghigh cells). MDSC-CD11b+GR1+ cells have been repeatedly reported to promote metastatic processes via immune-suppression. Indeed, MDSCs can functionally inhibit NK cells, B cells, dendritic cells, cytotoxic T cells, induce the recruitment of regulatory T cells (Tregs), and promote angiogenesis and cancer metastasis [338, 339]. Moreover, MDSCs in a spontaneous melanoma animal model can induce EMT via TGF-β and HGF signalling pathways [340]. Reciprocally, induction of EMT via SNAIL has been reported to activate multiple immunosuppression and immune-resistance mechanisms including activation of MDSCs [285].

1.3.4.3 **T-lymphocytes**

CD4+ cells or helper T cells (Th) have an effective function in innate and adaptive immunity. They help in protection against pathogens and malignancy by activating innate immunity inflammatory cells such as dendritic cells, macrophages, neutrophils, mast cells and eosinophils as well as activating cytotoxic T cells (CTLs) and B lymphocytes [341, 342]. The Th cells are sub-classified into several types, although Th1, Th2, Th17 and T reg cells are the main focus for research in cancer progression [341, 343].

Th1 cells can activate CTLs and TAMs which both take part in tumour rejection [344, 345]. Th2 function is not well defined although it has been implicated in recruiting

eosinophils which also have a role in the anti-tumour immune response. In a study of renal carcinoma, CD4+ cells from patients with stage I disease showed predominantly Th1-polarised responses to EphA2, whereas CD4+ cells from later stages showed progressively stronger Th2-polarised responses, with poorer prognoses [346]. From this study it can be suggested that Th2 has a dual function in tumorigenesis (immune surveillance during early tumour stages and immunosuppression at later stages).

Th17 cells are activated in response to TGF-β, IL-16 and IL-23 which are present in the TME. Th17 cells are the main producers of IL-17 and have been shown to promote tumour growth and angiogenesis with their presence a marker of poor prognosis [343, 347]. Indeed, blocking IL-17 in *APC* mutant mice showed a significant reduction in intestinal tumorigenesis [348].

CD25+ FOXP3+ regulatory T cells (Tregs) promote immune tolerance through release of cytokines that induce apoptosis of CD8+ cells and inhibit the activity of APCs, macrophages and NK cells [347, 349]. In fact, Tregs have been found to enhance metastasis in cancers including liver [350] and breast [351], lung ([352], melanoma [353] and colon [354]. Practically, a treatment that depletes Tregs and activates cytotoxic T cells may have a huge impact in advancing cancer treatment. Recently, Daclizumab (anti-CD25 monoclonal antibody) has shown a promising effect in cancer treatment which acts on depleting CD25-high Tregs and enhancing the IFN-γ-mediated CD4/CD8+ response in metastatic cancer [355, 356]. The role of Tregs in inducing EMT is not yet clear although, some evidence suggest that cancer EMT activates TME-resident Tregs [285, 357].

CTLs (CD8+ T cells) are a crucial component of the adaptive immune system. They have an important function in eliminating intracellular pathogens and promote cell destruction [358]. CTLs have a significant anti-tumorigenic impact by inducing apoptosis or controlling cancer cell proliferation through releasing interferon gamma (IFN-γ) [359, 360]. Recently, it has been observed that EMT induction impacts infiltration of CD4+ and CD8+ lymphocytes, with a high density of CD8+ cells correlating with chemotherapy response [361]. This has been suggested to be a prognostic factor in breast cancer and CRC [361-363]. A specific population of breast cancer cells undergoing EMT (stem like population; CD24-/CD44-/ALDH+) has been associated with inhibition of CTL-mediated cancer cell lysis [364], and thus EMT promotes immune-editing including suppressing CTLs and up-regulation of Tregs [285]. Growing lines of evidence have shown that activation of cytotoxic T-cells in cancer patients has an effective therapeutic potential [355, 356, 358].

1.3.4.4 **Dendritic cells**

APCs process and display antigens via MHC proteins to naïve T cells. MHC I-expressing cells stimulate CD8+ cells whereas MHC II-expressing cells stimulate CD4+ cells. In general, APCs are classified into professional and non-professional cells. The most important professional APCs are dendritic cells (DCs). Fibroblasts are an example of non-professional APCs which do not constitutively express MHC II but can stimulate T-cells by expressing IFN-γ [365]. DCs have an influential role in the TME in which they promote tumour rejection at early stages of cancer development. However, at later tumour stages, DCs fail due to lack of co-stimulatory factor B7 and the inability to stimulate CD8+ cells and evoke a significant immune response [366, 367]. In fact, EMT has been implicated in the abolition of DC function [285, 357]. In addition to that, differentiation of DCs from CD34+ to CD14+ progenitors can be impaired by the tumour cells expressing interleukin-6 (IL-6) and macrophage colony stimulating factor (MCSF) [368, 369], resulting in their differentiation into immature MDSCs [370] and TAMs [371]. Both MDSCs and TMAs have immuno-suppressive roles in the TME as discussed previously in this section.

1.3.4.5 **Natural killer cells**

NKs are innate lymphoid cells that have a function in eliminating pathogens and cancer cells. The vast majority of NK cells can be identified by surface markers such as CD3-CD56+ [372, 373]. NKs kill viruses or cancer cells [374] by synthesising cytotoxic granules containing perforin and granzymes [375] via plasma membrane receptor from natural killer group 2 member D (NKG2D) [376]. The important of NKs in eliminating tumour cells came from several human cancer studies, and the presence of NKs in the TME indicates a good prognosis for cancer patients [377-382]. However, at the late cancer stages, NKs can be functionally impaired by tumour cells themselves through cytokine secretion or upon EMT induction [285, 383, 384]. NK cell based adoptive cell immunotherapy provides a promising approach for cancer treatment [372, 385].

1.3.5 Chemokines as TME soluble factors

Activation of cytokines and chemokines is known to have an anti-tumour affect due to increased recruitment of effector immune cells to the TME. Nevertheless, growing evidence suggests that some chemokines and their receptors are directly or indirectly involved in reducing anti- tumour immune responses, enhancing tumour growth and

metastasis [386]. The next section of this introduction is to review the role of chemokines in cancer EMT.

1.4 Chemokine superfamily

1.4.1 Chemokine ligand and receptor structure, classification and nomenclature

1.4.1.1 Chemokine ligand structure and classification

Chemokines are a specific group of cytokines that were originally discovered as critical mediators of directional migration of immune cells to the site of inflammation and injury. Recently, chemokines have been found to be critical during microbial infection, organ development, lymphocyte maturation, angiogenesis, leukocyte trafficking and homing, tumorigenesis and metastasis [386-388]. The chemokine family consists of approximately 50 members of small molecular weight (8-14 KDa) proteins, most of which are secreted. Their structure has been determined by nuclear magnetic resonance (NMR) and/or X-ray crystallography. 3D images reveal that most chemokines have similar tertiary structure despite a relatively low level of sequence homology. For example, CCL5 was found to have a similar structure to CCL2, CCL11 and IL8 [389, 390]; **see figure 15**. They all consist of the N- terminus followed by a long loop (the N-loop) that ends in a 3_{10} helix, a three-stranded β-sheet and a C-terminal α-helix. Two disulphide bridges between the first and third, and the second and fourth cysteine residues at the N-terminus define and stabilise the three dimensional conformation [388, 391]; **see figure 15**. The N-terminus is the key signalling domain in all chemokines and any deletion or modification here results in altering function by directly affecting receptor binding. One of the factors that can modify chemokine function is the presence of various proteases at the inflammatory sites. For example, N-terminal truncation of CCL5 by CD26/dipeptidyl-peptidase IV protease results in CCL5 variants that display reduced effects on chemotaxis and changes in intracellular calcium mobilisation [392, 393].

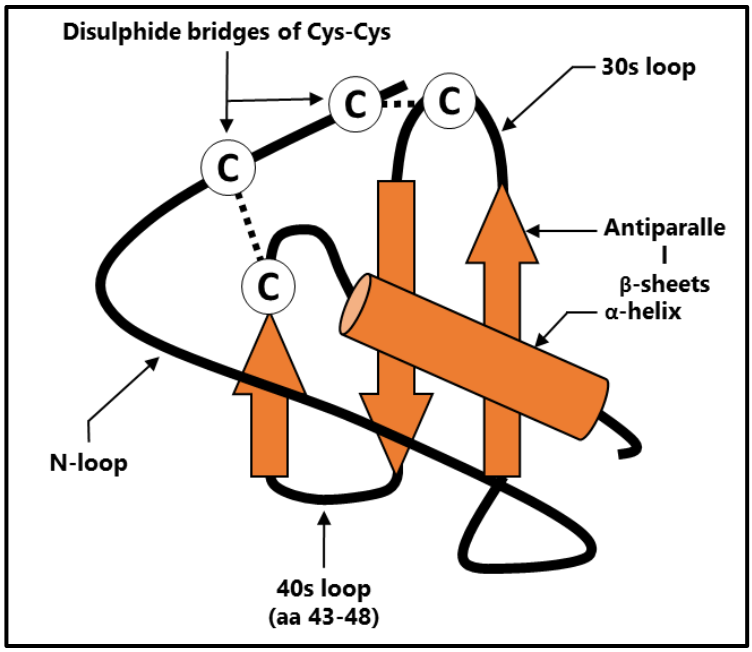

Figure 15: Typical structure of chemokine ligands.
Adapted from [394]

Upon secretion, chemokines accumulate on the cell surface and bind glycosaminoglycans (GAGs) such as heparin and heparin sulphate in the extracellular matrix, as a mechanism to provide directional signals for migrating cells and to prevent diffusion of chemokines away from their site of release, particularly under conditions of blood flow [395, 396]. Many chemokines form dimers upon binding to GAGs and these dimers fall into two general classes. The first class is CC chemokines, which form dimers through the formation of an antiparallel β-sheet with residues near their N-terminus surrounding the first two-cysteine residues. The second class is CXC chemokines that predominantly dimerise through residues in the first β strand [388, 397].

In addition to chemokine dimerisation, some chemokines form higher order oligomers upon binding GAGs. For example, CCL5 has the tendency to extensively aggregate into higher-order oligomeric structures in solution [398]. The physiological importance of oligomerisation and chemokine-GAG interactions is still not clear, because most chemokines interact with their receptors as monomers *in vivo*. Nevertheless, chemokine oligomersation may be essential for some chemokine physiological function. For example, CCL5, CCL4, and CCL2 require GAG interactions in order to bind to their receptors and thus induce some of their *in vivo* activities [399].

The disulphide bridges allow further classification of the superfamily into 4 distinct subfamilies (C, CC, CXC and CX3C), based on the relative location and presence of the

first two cysteine residues at the N-terminus. The first two-cysteine residues in CC chemokines are adjacent, whereas in CXC chemokines they are separated by one non-conserved amino acid. The XC chemokines lack the first cysteine, whereas in the single member of the CX3C subfamily (CX3CL1), the first two cysteine residues are separated by three non-conserved amino acids [391]; **see figure 16.**

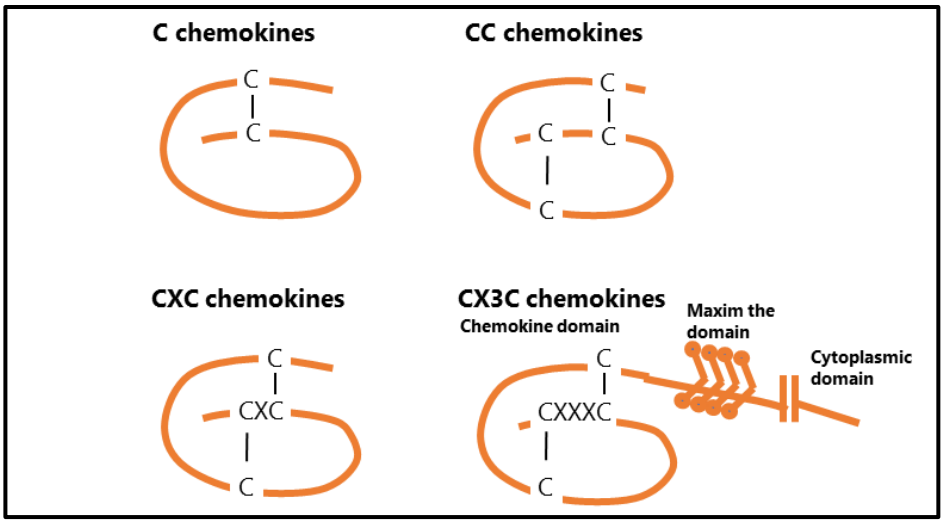

Figure 16: Structural classification of the chemokine family.

Besides the structural classification, chemokines can be further divided into two functional groups: inflammatory chemokines and homeostatic chemokines. The inflammatory chemokines are involved in the recruitment of leukocytes to the site of inflamed tissues whereas homeostatic chemokines are involved in the development and migration of normal leukocytes within secondary lymphoid organs. This classification has a limitation because some inflammatory chemokines may have homeostatic functions, and *vice versa*. For that, a third group has been established called dual-function chemokines [400]; **see Table 2.**

The difference between inflammatory and homeostatic chemokines lies in their evolutionary origin whereby inflammatory chemokines evolved rapidly compared to homeostatic ones. Inflammatory chemokines are clustered on chromosomes 4 and 17 whereas homeostatic chemokines are located separately or in mini-clusters on different chromosomes. Furthermore, inflammatory chemokines differ markedly in their function between species. In contrast, homeostatic chemokines are well conserved in terms of structure and function between species. Therefore, studies in genetically modified mice deficient for homeostatic chemokines are more likely to reflect the human physiology as compared to inflammatory chemokine mutant models [401].

Table 2: Functional classification of the human chemokine family.
Adapted from [400].

Inflammatory			Homeostatic			Dual-Function		
CXCL6[a,b] (GCP-2)[c]	CXCR1[d]	Innate immunity	CXCL12 (SDF-1)	CXCR4	Hematopoiesis	CXCL9 (Mig)	CXCR3	T lymphopoiesis
CXCL8 (IL-8)		(Granulocytes)			Homeostasis of leukocytes	CXCL10 (IP-10)		Adaptive immunity
CXCL1 (GRα)	CXCR2					CXCL11 (I-TAC)		(Th1 responses)
CXCL2 (GROβ)			CXCL13 (BCA-1)	CXCR5	Follicular activities	CCL17 (TARC)	CCR4	T lymphopoiesis
CXCL3 (GROγ)					B-cell responses	CCL22 (MDC)		Adaptive immunity
CXCL5 (ENA-78)			CXCL14 (BRAK)	ND	APC development			(Cutaneous T cells)
CXCL6 (GCP-2)						CCL20 (LARC)	CCR6	DC development
CXCL7 (NAP-2)			CCL19 (ELC)	CCR7	T lymphopoiesis			Adaptive immunity
CXCL8 (IL-8)			CCL21 (SLC)		Spleen-, LN-homing (T-cell area)			
						CCL1 (I-309)	CCR8	T lymphopoiesis
CX3CL1 (Fractalkine)	CX3CR1	Extravasation						Adaptive immunity
		(Inflammation)	CCL18 (DC-CK1)	n.d.	T-cell–DC interaction (Spleen, LN)			Th2 or Tr responses
CCL3 (MIP-1α)	CCR1	Innate and adaptive immunity				CCL25 (TECK)	CCR9	T lymphopoiesis
CCL5 (RANTES)								Adaptive immunity
CCL7 (MCP-3)								T- and B-cell traffic in small intestine
CCL8 (MCP-2)								
CCL13 (MCP-4)								
CCL14 (HCC-1)						CXCL16	CXCR6	T lymphopoiesis
CCL15 (HCC-2)								Extravasation
CCL2 (MCP-1)	CCR2							
CCL7 (MCP-3)								
CCL8 (MCP-2)								
CCL13 (MCP-4)								
CCL5 (RANTES)	CCR3							
CCL7 (MCP-3)								
CCL8 (MCP-2)								
CCL11 (Eotaxin)								
CCL13 (MCP-4)								
CCL15 (HCC-2)								
CCL24 (Eotaxin-2)								
CCL26 (Eotaxin-3)								
CCL3 (MIP-1α)	CCR5							
CCL4 (MIP-1β)								
CCL5 (RANTES)								
CCL8 (MCP-2)								
XCL1, XCL2/ Lymphotactin-α,β	XCR1							
CCL27 (CTACK)	CCR10							
CCL28 (MEC)	CCR3 CCR10							

[a]Abbreviations: APC, antigen-presenting cell; BCA-1, B-cell-attracting chemokine-1; BRAK, breast and kidney expressed chemokine; CTACK, cutaneous T-cell attracting chemokine; DC, dendritic cell; DC-CK1, DC-chemokine 1; ELC, EBI1 ligand chemokine; ENA-78, epithelial–neutrophil activating peptide-78; GCP-2, granulocyte chemotactic protein-2; GROα, melanoma growth-stimulating activity α; HCC-1, human CC chemokine-1; IL-8, interleukin-8; IP-10, IFN-γ-inducible protein-10; I-TAC, interferon-inducible T-cell α chemoattractant; LARC, liver- and activation-regulated chemokine; LN, lymph node; MCP-3, monocyte chemotactic protein-3; MDC, monocyte-derived chemokine; MEC, mucosae-associated epithelial chemokine; Mig, monokine induced by IFN-γ; MIP-1α, macrophage inflammatory protein-1α; NAP-2, neutrophil-activating peptide-2; ND, not determined; SDF-1, stromal cell-derived factor-1; SLC, secondary lymphoid tissue chemokine; TARC, thymus- and activation-regulated chemokine; TECK, thymus-expressed chemokine; Tr, T regulatory.
[b]Systematic nomenclature that combines structural motifs (CXC, CC, XC, CX3C) with L for ligand and the number of the respective gene (http://cytokine.medic.kumamoto-u.ac.jp gives access to recent updates) [6].
[c]Traditional abbreviations, such as IL-8 and MCP-1, dating back to the time of chemokine discovery.
[d]Chemokine receptors are designated according to the type of chemokine(s) they bind (CXC, CC, XC, CX3C), followed by R for receptor and a number indicating the order of discovery.

The CXC chemokines are further subdivided into ELR+ and ELR- groups based on the presence or absence of the Glutamate-Leucine-Arginine (ELR) motif preceding the CXC sequence. ELR+ chemokines are potent promoters of angiogenesis and include CXCL1, CXCL2, CXCL3, CXCL5, CXCL6, CXCL7 and CXCL8 (IL-8) whereas CXCL12 is the only ELR- chemokine with angiogenic properties [402].

1.4.1.2 Chemokine receptors: structure and classification

Chemokine receptors are a subfamily of G protein-coupled receptors (GPCRs), the largest family of cell surface receptors accounting for ~3% of the human genome regulating almost all physiological processes. Structural studies of GPCRs are extremely difficult because they are expressed in very small amounts in biological tissues which make them hard to purify in sufficient amounts. In addition, they are highly unstable when extracted from membranes and solubilized by detergents and are structurally destroyed during crystallisation [403]. In 2000, the first 3D structure of a GPCR was achieved using bovine rhodopsin [404] and in 2007 the structure of the first GPCR with diffusible ligand (β2-adrenergic receptor), was determined using advanced micro crystallisation [405]. More recently in 2010, the 3D structure of CXCR4 was resolved [406]. This was followed by CXCR1 [407], making CXCR4 and CXCR1 the only the chemokine receptors to be crystallised up till now.

All GPCRs including chemokine receptors share a common structure of seven trans-membrane α-helices connected by three extracellular loops (ECLs) and three intracellular loops (ICLs). The extracellular region includes the N-terminus and is responsible for ligand binding. The intracellular region interacts with G proteins, arrestins and other downstream effectors and includes a cytoplasmic helix VIII. The C-terminus contains multiple serine/threonine and tyrosine phosphorylated residues that provide sites for palmitoylation and other signalling sites. In addition to that, chemokine receptors have disulphide bridges in their extracellular domains which provide structure to the overall receptor. Generally, one disulphide bridge connects the N-terminus to the third ECL, while a second links the first and second ECL [408]. Most chemokine receptors are coupled to G-proteins through the conserved DRY (Asp-Arg-Tyr) motif in the second ICL [409]. Chemokine receptors are critical for triggering intracellular calcium signalling and regulating leukocyte chemotaxis in immune surveillance, inflammation, and development [410]; **see figure 17.**

Chemokine receptors are grouped into 4 subfamilies according to their major chemokine ligands e.g. CC chemokines bind to CCRs, CXC chemokines bind to CXCRs, XC chemokines bind to XCRs, and CX3CL1 is the ligand for the CX3CR1 receptor. The chemokine receptor genes are clustered on human chromosome 3 suggesting a rapid evolution through repeated gene duplications. However, compared to the ligands, chemokine receptors are relatively well conserved between species [412].

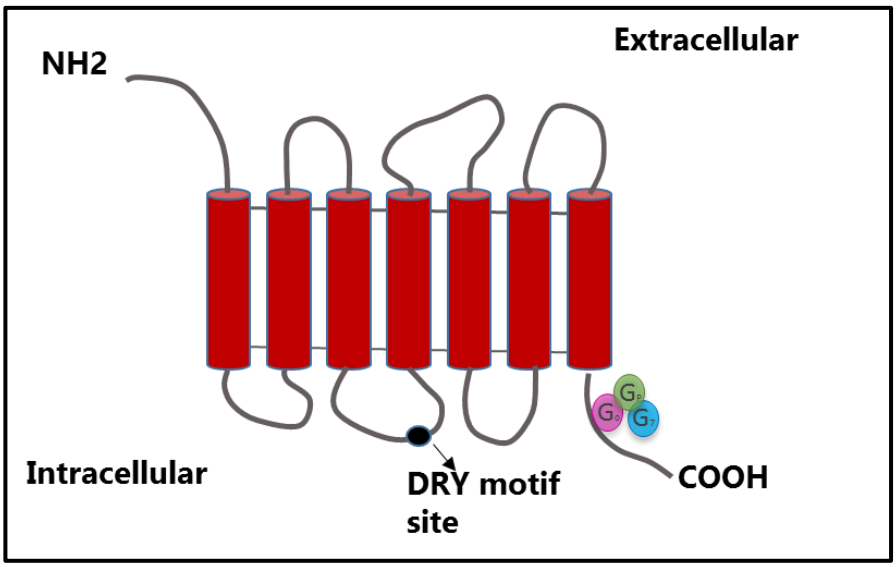

Figure 17: A representative structure of G protein-coupled chemokine receptors (GPCRs). Adapted from [411].

To date, 20 chemokine receptors with the standard Gαi-dependent chemotactic activity have been identified in humans and mice. In addition to the 20 chemokine receptors, 5 atypical chemokine receptors, also known as decoy or interceptors (internalising receptors), have been identified. Atypical and conventional chemokine receptors are similar in their structure but atypical ones do not transduce the full spectrum of signals that lead to chemotactic and other cellular responses. This is partly due to modification or lacking the typical DRY motif site in the second intracellular loop; DRY is known to be important for efficient coupling with the Gαi class G-proteins. Representative examples for atypical chemokine receptors are DARC (Duffy Antigen Receptor for Chemokines), D6 and CCX-CKR (ChemoCentryx Chemokine Receptor) [413].

Similar to chemokine receptors, chemokine receptors are expressed at the cell surface as either homo- or heterodimers or oligomers [414]. Several studies also report that certain GPCRs can function as monomers *in vitro* [415]. Having only 20 active chemokine receptors for about 50 chemokine ligands, could indicate a redundancy in ligand and receptor binding; many chemokine ligands bind to more than one receptor, and at the same time, most chemokine receptors have a number of high affinity ligands. For example, CCL5, CCL4 and CCL3 all have affinity to CCR5 whilst CCR5, CCR1 and CCR3 may all be bound by the aforementioned ligands [386, 416, 417].

1.4.1.3 Chemokine ligands and receptors nomenclature

In 2000, a chemokine ligand and receptor nomenclature system was introduced. Each ligand and its receptor are identified by their sub-family and given an identifying number. For example, SDF-1α (Stromal-Derived Factor 1α) is now known as CXCL12 for CXC chemokine ligand 12, and RANTES (Regulated on Activation Normal T cell expressed and secreted) is now known as CCL5 for CC chemokine ligand 5. Of note, human chemokines are designated capital letters with mouse chemokines in lowercase letters. For example, CCL2 is the human chemokine while Ccl2 is the mouse one [412, 418, 419]. The most recent nomenclature of chemokine ligands and their receptors will be used throughout the report.

1.4.1.4 Chemokine system in health and disease

Chemokines and their receptors have a major role in immune integrity of the host. Homeostatic chemokines recruit blood-borne cells into target tissues and regulate homeostasis through controlling the micro-environmental coordination of primary and secondary lymphoid organs. Inflammatory chemokines play a key role in stimulating immune responses against pathogens [420]. In addition, both haemostatic and inflammatory chemokines and their receptors are involved in cell polarisation and adhesion, gene expression, cell proliferation and survival [391, 421]. They are also involved in processes such as chronic inflammation [422, 423] and autoimmune diseases[421], HIV cell entry [424], development and reproduction [425], wound healing [426] and also tumorigenesis [386].

1.4.1.5 Chemokines in cancer

Chemokines play a key role in cancer, modulating the composition of immune cells within the tumour microenvironment. Inflammatory leukocytes migrating towards the tumour can have either an anti-tumour or a pro-malignant effect [427]. Nonetheless, some chemokines may display both activities. For example, CCL2 promotes anti-metastatic activity via the recruitment of CD4+ helper T cells and neutrophils [428, 429]; at the same time, CCL2 recruits inflammatory macrophages that release factors such as MMPs thus increasing invasiveness of cancers [430]. The current understanding of this dilemma is as follows: the anti-tumour activities of leukocytes are employed in the early stages of the process, but

when cancer cells escape immune surveillance and proliferate, they use the components of the immune system for their own benefit [329].

Chemokines may also mediate several key steps of metastasis such as homing of tumour cells to specific organs, angiogenesis and proliferation. In particular, inflammatory chemokines may be associated with later stages of tumorigenesis and poor patient survival [430-433].

The first chemokine implicated in tissue-specific metastasis is CXCL12. It is locally expressed by lung, lymph node, liver and bone marrow tissues attracting cancer cells expressing CXCR4 [434-437]. Also, CCL19 and CCL21 have been implicated in attracting melanoma cells expressing CCR7 towards lymph nodes [438, 439]. IL-8 is frequently reported to have an important role in tumour angiogenesis by triggering CXCR1 and CXCR2 positive cells to proliferate, survive and produce angiogenic factors such as MMPs and VEGF [440, 441]. CCL5/CCR5 are also reported to facilitate cancer metastasis and are predictors of poor patient survival [431, 433]. The importance of CCL5/CCR5 in cancer will be discussed further as they are pivotal to this project.

1.4.1.6 **Chemokines and cancer EMT**

Despite the fact that EMT is a fundamental process in cancer invasion and metastasis, very few reports have been published linking chemokines to EMT. However, Bates et al., showed that TGF-β-induced EMT leads to up-regulation of IL8 and its receptor CXCR1 [432]. More specifically, several lines of evidence have shown showed that SNAIL, TWIST and Brachyury, (EMT-inducing transcription factors), directly up-regulate IL-8 and its receptors (CXCR-1 and CXCR-2), resulting in activation and maintenance of EMT, induction of stem cell–like features, angiogenesis and enhancement of invasion and metastasis [442-445]. Palena *et.al.,* and Cheng *et al.,* found that IL8 alone is able to induce EMT and remodel the tumour microenvironment [446] via binding to CCL20 and activating PI3K/AKT-ERK1/2 and Wnt/β-catenin pathways [447, 448]. Similarly, the CXCL12/CXCR4 pair; a major mediator of tumour cell migration and survival, was repeatedly reported to be over-expressed upon EMT activation [449-451] in various types of cancers [452-454]. Recently CCL18, derived from TAMs, has been implicated in inducing EMT in lung and pancreatic cancer cells via SNAIL which leads to increased cell invasion, migration and chemo-resistance [455, 456]. CCL2, the main recruiter of TAMs, has been reported to be up regulated upon induction of EMT via TWIST, SNAIL and

ZEB2, and thus promote metastasis via immunosuppression and stimulating angiogenesis [357, 457, 458]. Taken together, an understanding of chemokine function in the context of EMT and metastasis may prove valuable in discovering more specific and targeted cancer therapy.

1.4.1.7 **Chemokines in cancer therapy**

To date, only 2 drugs targeting chemokine receptors have been approved for clinical use. One is Maraviroc, a CCR5 antagonist which is used to inhibit human immunodeficiency virus (HIV) entry into CCR5 positive cells [424]. The other drug is Plerixafor or AMD3100, a CXCR4 antagonist which has been approved to promote mobilisation of human hematopoietic progenitor and stem cells from bone marrow [459, 460]. In cancer however, despite chemokine systems inducing an anti-tumour immune response and blocking metastasis [433, 461-466], no clinical trials have been successful. This is could be due to the animal models used for evaluating the role of inflammatory chemokines not translating well to human disease [391]. Furthermore, chemokine systems are complex; considering multiple chemokine ligands bind to the same receptor whilst numerous chemokine receptors recognise the same ligand. In addition, a wide range of cell types express chemokine receptors, therefore inactivation or inhibition of such receptors may cause severe systemic complications. Also, impairing the function of specific chemokine-chemokine receptors may have a short-term action [467]. For that, it has been suggested that appropriate target selection, appropriate timing of the intervention and, most importantly, appropriate dosing would help in achieving successful clinical trials [468].

1.5 Hypothesis and the aims of the project

1.5.1 Hypothesis

EMT and anti-tumour responses are linked via the altered secretion of soluble factors by metastatic cells.

1.5.2 Aims of the Project

- Characterise the EMT status of a panel of CRC cell lines and the CRC-EMT model.

The biological characteristics of 12 CRC cell lines and CRC-EMT model (DLD SIP1) will be reviewed from the literature and comparisons of their morphological appearance will be carried out using a light microscope. In addition, various epithelial and mesenchymal markers will be used to assess the EMT status of the panel and CRC-EMT model. Western blot (WB), RT-PCR and immunofluorescence will be the main techniques used to obtain this goal.

- Perform a screen of human cytokines and chemokines and correlate their expression with the EMT status of CRC cells.

R&D systems chemokine and cytokine arrays will be used to screen large numbers of soluble factors of two cellular compartment of the DLD-SIP1 CRC-EMT model. Then, criteria will be established and used in order to choose the most significant chemokines altered during EMT. From there, one chemokine will be chosen to focus on further and correlate its expression with the EMT status of some mesenchymal and epithelial CRC cell lines.

- *In vivo* and *in vitro* studies to investigate the mechanism and the function of the chosen chemokine.

  The chosen chemokine gene will be subjected to *in silico* analysis to define if SIP1 can be directly involved to its transcriptional regulation. This will be confirmed by Chromatin Immunoprecipitation and promoter reporter assays. Finally, *in vivo* experiments will be conducted to question whether the altered expression of the chosen cyto/chemokine is an outcome or reason for SIP1-induced metastasis.

Chapter 2: Materials and Methods

2.1 Tissue culture

2.1.1 General principle

All tissue culture work was done in a laminar flow hood. Cells were grown at 37°C in a humidified 5% CO_2 incubator (Heraeus Hera Cell Incubator, Thermo scientific). All tissue culture reagents were stored in a dedicated 4°C refrigerator.

2.1.2 Cell lines

Thirteen CRC cell lines and two EMT models (DLD-SIP1 CRC-EMT model and A431-SIP1 squamous cell carcinoma EMT model) were used in this project. All cell lines were purchased from the American Type Culture Collections (ATCC) apart from AAC1/82, RKO and DLD-SIP1 and A431-SIP1 cells. AAC1/82 cells were a kind gift from Professor C. Parakeva (University of Bristol), RKO cells were provided by Professor Graham Packham (University of Southampton; CRUK), and DLD-SIP1 and A431-SIP1 cells were from Prof. Eugene Tulchinsky. All the cell lines are derived from human tissue with the exception of CT26 (mouse CRC).

Cell lines were tested for Mycoplasma contamination once defrosted. Only Mycoplasma-free cell lines were cultured and used. Cells were grown in Dulbecco's Modified Eagle's Medium (DMEM; Sigma) supplemented with 10% Fetal Bovine Serum (FBS; Sigma), 2 mM L-Glutamine (Sigma) and 1% of 100 X Penicillin/Streptomycin (Sigma). Of note, DMEM with the above mentioned supplemented reagents will be referred in the text as ‘Complete DMEM’.

2.1.3 Cell counting and viability

The cell count was performed using a haemocytometer. Only cells in the central 25 squares were counted, including the ones on left and bottom line whilst ignoring any cell at the right or upper edges.

The cell suspension was first diluted in10 ml DMEM. Then, 100 µl of the suspension was diluted further 1:2 with 0.2% Trypan Blue. Trypan blue is used to assess the viability of the

cells, where the dead cells will acquire the blue colour. 10 µl of the final dilution was introduced in each side of the counting chamber and the cells were counted using a light microscope with a 10X-objective. The final cell count and the viability were calculated as follows:

Number of cells in 25 squares x dilution factor Ψ x 10^4

Ψ the dilution factor used in the project was 20.

Viability= live cells/total cell count x 100

2.1.4 SIP1 induction in DLD-SIP1 and A431-SIP1 EMT models

The induction of the *SIP-1* gene in DLD-SIP1 and A431-SIP1 cells was carried out using 2µg/ml Doxycycline (Sigma; Stock concentration 50 mg/ml) treatment for three days.

2.1.5 Cell propagation, and collection of cells and conditioned medium

Cells were propagated 2-3 times a week. The growth rate was monitored by using an inverted microscope, and by cell count (CC). Where necessary, both the supernatant and cells were collected. The supernatants were collected at day 3 after centrifugation at 300 x g for 5 min to exclude any floating/dead cells. The supernatants were aliquoted and frozen at -20°C or used immediately. The adherent cells were trypsinised using 1X Trypsin-EDTA (Sigma), re-suspended in DMEM to inactivate trypsin and then centrifuged at 300 x g for 5 min, washed in 1 x phosphate buffer saline pH 7.0 (PBS), pelleted and frozen at -20C°.

2.1.6 Freezing cells for long term storage

Freezing media (73% complete DMEM, 20 % FCS and 7 % dimethyl sulphoxide (DMSO; Sigma) was prepared in advanced and kept on ice. Cells in a 175 cm^2 culture flask (Corning®) at 80-90% confluency were trypsinised in the same fashion as explained in section 1.1.5, collected in 15 ml sterile Falcon tube (BD), counted and centrifuged at 300 x g for 3 min. Pelleted cells were re-suspended in the prepared freezing medium. After that, ~1-2 million cells /ml were aliquoted into cryo-vials (Grenier Bio-one Ltd). The cryo-vial tubes were first placed at -80°C freezer in a NALGENE® Mr. Frosty container for 1-2 days and then transferred into a liquid nitrogen tank.

2.1.7 Defrosting Cells

The cells were taken from the liquid nitrogen (-180°C) and placed immediately on dry ice to avoid a sudden change in the temperature. Rapid thawing was then carried out at 37°C for 2 min in a water bath. Defrosted cell lines were mixed immediately with 10 ml warm complete DMEM and centrifuged at 300 x g for 5 min. After that, the supernatant containing DMSO was discarded and the pellets were re-suspendered in 1ml complete DMEM and transferred into a T75 flak (Corning® Incorporated) with 10 ml complete DMEM. A small aliquot is taken at this stage and the cells were counted manually by a haemocytometer to calculate the percentage of viability, and then placed in an incubator. The cell lines were allowed to recover from the effects of cryopreservation for at least 1 passage before being used in experiments.

2.2 Western blotting

2.2.1 Main Principle

Western blotting allows detection of a single protein among many using molecular weight based discrimination and antigen-antibody specificity. To achieve this aim, proteins separated by molecular weight (electroporation) are transferred to a solid support (nitrocellulose membrane) and marked by specific antibodies to allow detection. Appropriate enzyme-conjugated secondary antibodies to target primary antibodies are used followed by a chemo-luminescent substrate-based detection system. The light emitted from the reaction can be detected using photographic film or alternatively by a sensitive computer-linked digital camera; **see figure 18.**

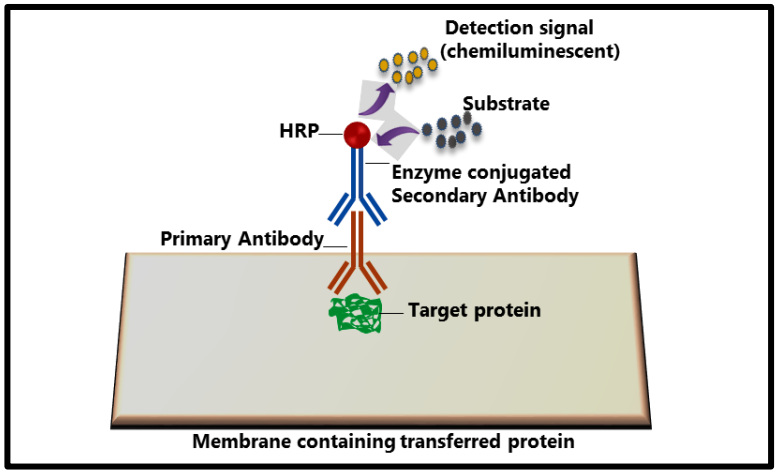

Figure 18: General principle of the Western blotting method.
Adapted from [469].

The Main steps of Western blotting (WB) are:

- Preparation of Cell Lysate
- Protein Quantification
- Gel Preparation
- Protein Loading and Gel Electrophoresis
- Transfer of proteins to solid support
- Protein Identification

Of note, the list of buffers used for this assay are summarised in **Table 3.**

2.2.2 Preparation of cell lysate

The frozen cell pellets were thawed on ice and then the proteins were extracted. The protein extraction was done in two steps. First, the cells were lysed with an appropriate volume of 2x SDS-PAGE loading (Laemmli) buffer. Secondly, in order to ensure proper cell lysis, the cells were sonicated at 1.5 m Watts for 15 seconds (BioLogics Company). The extracted proteins were then quantified using protein assay reagent (BCA; Thermo Scientific) as described in the next section.

2.2.3 Protein quantification

Working BCA mix was prepared (50 parts of reagent A with 1 part of reagent B) and 150 µl of the mixture was distributed in each well of a 96-well plate. The first well was left as blank and the next 9 wells were used for the standard curve (3 concentrations in triplicate).

Bovine Serum Albumin (BSA; Fisher; main stock 2 mg/ml) was used as standard and added at 2 µg, 10 µg and 25 µg to wells. Also 5 µl from each cell lysate (in triplicate) was added to individual wells and mixed by pipetting. Following that, the plate was incubated for 15 min at 37°C to allow colour development. The intensity of the colour was measured by a spectrophotometer device (Bio Rad) at 570 nm. The standard curve was drawn using excel and the protein concentration of samples were back-calculated using the equation obtained by the BSA curve.

2.2.4 Gel preparation

Sodium Dodecyl sulphate-polyacrylamide (SDS-PAGE) gels were made according to Dr. Emre Sayan Laboratory protocol that were adopted from Molecular Cloning book [470]. Please refer to **Table 3 for all buffers that were used in this project to prepare gels.**

Each SDS-PAGE gel was composed of two layers:

- Separating/running gel (lower part, 1.5M Tris: pH 8.8 is used); the density (percentage of acrylamide) of this part depends on the size of the protein of interest.
- Stacking gel (upper layer, 1M Tris: pH 6.8 is used): always 5%.

2.2.5 Protein loading and gel electrophoresis

After protein quantification and gel preparation, the lysates were supplemented with an appropriate volume of 5 x loading buffer. The samples, along with protein marker (Precision Plus Protein™ All Blue (10–250 KDa); Bio-Rad) were heated up at 95°C for 2 min to denature protein. After that, 5 µl of the protein ladder was loaded in the first well of the polyacrylamide gel. Along that, 30 µg of protein of each cell lysate was loaded in the subsequent wells. The gels were run at 180 V for 65 min using 1 x Tris/glycine/SDS buffer (TGS; Geneflow; Main stock 10 x).

Table 3: List of in house buffers used in the project.

Buffer Name	Buffer Components	Supplier
30% (w/v) 37.5:1 Acrylamide: Bis-acrylamide solution	37.5 g Acrylamide (Fisher) 1 g Bis-Acrylamide (Fisher) Dissolved in dH_2O to a final concentration of 30%	In house or Geneflow
30% (w/v) 29:1 Acrylamide : Bis-acrylamide solution	29.0 g Acrylamide (Fisher) 1 g Bis-Acrylamide (Fisher) Dissolved in dH_2O to a final concentration of 30%	Geneflow
1.5M Tris buffer (pH 8.0 and pH 8.8)	182.25g Tris (Fisher). dH_2O Adjust pH to 8.0, adjust volume to 1 litre Adjust pH to 8.8, adjust volume to 1 litre	In house
1M Tris buffer (pH 6.8)	121.1g Tris-base (Fisher) dH_2O Adjust pH to 6.8, adjust volume to 1 litre	In house
10% APS	1 g APS (Fisher) Adjust volume to 10 ml with dH_2O Store at 4ºC for several weeks	In house
10% SDS	1 g SDS (Fisher) Adjust volume to 10 ml with dH_2O Store at RT	In house
5 X SDS-PAGE buffer	dH_20 0.5 M Tris (pH 6.8) ----------12.5% Glycerol (Sigma)----------10% 10% SDS (w/v) ----------20%	In house
5 X SDS-PAGE Gel Loading buffer	dH_20 0.5 M Tris (pH 6.8) ----------12.5% glycerol----------10% 10% SDS (w/v)----------20% 2β- Me----------5% 0.05%(w/v) BPB----------5%	In house

Buffer Name	Buffer Components	Supplier
10 X Tris-Glycine-SDS (TGS)	0.25M Tris 1.92M Glycine 1% SDS dH_2O	Geneflow/In house
10 X Tris-Glycine-Methanol (TGM)	0.25M Tris 1.92M Glycine 20% Menthol (Fisher) dH_2O	Geneflow/ In house
10 X TBS	100 mM Tris (pH 8.0) 1.5 M NaCl dH_2O	In house
1 X TBS-T (1 litre)	100ml 10X TBS (Geneflow) 900ml dH_2O 0.1% Tween®20 (Sigma)	In house
4% Dried skimmed milk in TBS-T	2g dried skimmed milk (Marvel) 50 ml 1X TBS-T	In house
2.5% BSA in TBS-T	1.25g BSA (Fisher) 50 ml 1X TBS-T	In house
PBS	125mM NaCl (Fisher) 16mM $Na_2HPO_4.7H_20$ 10mM KH_2PO_4 HCL to Adjust pH 7.3-7.6	In house
PBS-T	1 x PBS buffer 0.1%-1.0% Tween-20	In house
Ponceau S	5 % (w/v) Ponceau S 10 % Glacial Acetic Acid (Sigma) dH_2O Store in dark at RT	
0.05 M EDTA (Di sodium Ethylenediaminetetraacetic acid)	8.61 g EDTA (Sigma) 80 ml dH_2O Adjust pH to 8.0, Adjust volume to 100 ml	In house

Buffer Name	Buffer Components	Supplier
TAE Electrophoresis buffer (50X stock solution)	242 g Tris-base 57.1 ml glacial acetic acid 100 ml 0.5 M EDTA (pH 8.0) Adjust volume to 1 litre	In house
1% agarose	1g agarose (Fisher) 100ml TAE buffer	In house
4% paraformaldehyde (v/v)	4ml paraformaldehyde (Fisher) 96 ml dH_2O	In house
0.2% Triton in PBS	98.8 ml 1 x PBS 200µl Triton	In house
Specific cell lysate for human chemokine and cytokine arrays	1% Igepal CA-630, 20 mM Tris-HCl (pH 8.0), 137 mM NaCl, 10% glycerol, 2 mM EDTA and tablet contains 10 µg/mL Aprotinin, 10 µg/mL Leupeptin, and 10 µg/mL Pepstatin.	In house
Luria Bertani (LB)	10g/L Tryptone, 5 g/L Yeast extract and 10 g/L NaCl	In house

2.2.6 Protein transfer

The separated proteins were then transferred onto nitro-cellulose membranes (Whatman Protran, GE healthcare). This was achieved by sandwiching the gel and the membrane in a transfer cassette (Bio-Rad) between 2 pieces of filter paper and 2 sponges, and placing the cassette in a transfer tank containing 1 x Tris/Glycine buffer with 20% methanol (TGM; Geneflow; main TG stock 10 x) at 4°C, 20 V overnight. Ponceau red staining was used to check equal loading and efficient transfer of bands. The Ponceau red was removed using Tris-buffered saline (pH 7.4) containing 0.01% Tween-20 (TBS-T).

2.2.7 Protein identification

After blotting, membranes were incubated in blocking solution (4% semi-skimmed milk in TBS-T) for 30 min at RT to block non-specific epitopes. Subsequently, the membranes

were incubated for 30 min-1 hour with appropriate primary antibodies (diluted in TBS-T with 2.5% BSA). After being washed three-times with 5 min interval incubation in TBS-T, the membranes were incubated with the appropriate type of horseradish peroxidase (HRP)-conjugated secondary antibodies (diluted in 4% semi skimmed milk in TBS-T) for 30 min at RT. After a further 3 washing steps, the antigen-antibody interactions were visualised by using 1:1 (v/v) supersignal®west Dura luminal/enhancer solution (Thermo Scientific), which was incubated with the blots for 5 min at RT. The enzymatic reaction and the band intensity were then detected by X-ray film and films developed using an autoradiography machine.

The primary antibodies used in this work and their corresponding secondary antibodies are summarised **in Table 4.**

Table 4: List of the antibodies used for WB (Western blot).

Primary antibody	Used as	Molecular Weight (KDa)	Catalog no.	Supplier
Human E-cadherin	Epithelial maker	135	610181, Mouse IgG	BD Transduction Laboratories™
Human cytokeratins	Epithelial maker	65-35	C5992, Mouse IgG mix	Sigma
Human ZO-1	Mesenchymal marker	220	BD610966 / Mouse IgG1	BD Transduction Laboratories™
Human Vimentin	Mesenchymal marker	57	C5741 / Rabbit mAb IgG	Cell Signalling
Human ZEB1	Mesenchymal marker	220	SC-25388 / Rabbit polyclonal IgG	Santa Cruz Biotechnology
Human SIP1	Mesenchymal marker	220	Rabbit polyclonal IgG	In House antibody (Sayan, Griffiths et al., 2009)
Human TWIST	Mesenchymal marker	28	Ab50887 / Mouse mAb IgG1	Abcam®
Human SLUG	Mesenchymal marker	30	C19G7 / Rabbit mAb IgG	Cell Signalling
Human SNAIL	Mesenchymal marker	29	C15D3 / Rabbit mAb IgG	Cell Signalling
Human N-cadherin	Mesenchymal marker	140	36/E-Cadherin/ Mouse IgG2a	BD Transduction Laboratories™
Human α-Smooth muscle actin	Mesenchymal marker	43	1A4 / Mouse IgG2a	Sigma
Human Actin	Equal loading marker	45	SC-1615/Goat IgG	Santa Cruz Biotechnology
Human CCL5	Chemokine	8	C6118/Rabbit IgG	Sigma

Primary antibody	Used as	Molecular Weight (KDa)	Catalog no.	Supplier
Human Midkine	Chemokine	16	Ab137793/Rabbit polyclonal IgG	Abcam®
Human CXCL5	Chemokine	8	C19 SC-1407/ Goat polyclonal IgG	Santa Cruz Biotechnology

2.3 Gene expression analysis

2.3.1 Total RNA extraction

TRIzol® Reagent is a monophasic solution, which contains phenol, guanidine isothiocyanate, and other proprietary components that facilitate simultaneous isolation of large and small molecular weight nucleic acids (DNA and/or RNA) and proteins. It disrupts cells and dissolves cell components. After homogenising the sample with TRIzol® reagent, chloroform is added to enhance the separation of the macromolecule-enriched liquid phases. The sample is then centrifuged at high speed to visualise the three-monophasic layers; the clear upper aqueous layer (RNA), a white interphase layer (DNA), and a red organic layer (proteins). The RNA is precipitated from the aqueous layer, washed to remove impurities and re-suspended in water to be used in downstream application e.g. RT-PCR, northern blot analysis, dot blot hybridization, ploy(A)+selection, *in vitro* translation or RNase protection assay.

To extract RNA with Trizol technique, frozen/fresh cell pellets (up to 10^7 cells) were defrosted on ice and suspended in 1 ml TRIzol. The lysate is incubated 5 minutes at RT to allow complete lysis. After that, 200 µl chloroform (per ml of Trizol used) was added to each sample, vortexed for 20 seconds and centrifuged at 10000 x g for 15 min at 4°C for phase formation. The clear upper aqueous layer containing RNA was collected. RNA is precipitated by adding 0.5 ml of 100% isopropanol (per ml of Trizol used). If necessary, the RNA: Isopropanol mixture can be incubated at -20°C, centrifuged at 13000 x g for 15 min in a 4°C centrifuge to increase yield. Subsequently, the precipitated RNA was washed with 1 ml 75% ethanol, incubated again at -20°C, centrifuged at 13000 x g for 15 min in a 4°C centrifuge. The extracted RNA pellets were air-dried for 10 min at room temperature (RT). Finally, the RNA pellets were re-suspended in 50-100µl RNase-free water by

vortexing and incubating at 55-60°C for 10 min. The total RNA yield was measured using a NanoDrop 1000 Spectrophotometer (Thermo Scientific). RNA purity was assessed using an A260/A280 ratio.

The extracted RNA was either used immediately to synthesise cDNA or frozen at -80°C.

2.3.2 cDNA Synthesis

RevertAid™ M-MuLV Reverse Transcriptase Kit (MBI Fermentas) was used in this project. The kit contains RevertAid™ M-MuLV Reverse Transcriptase, which is active at 42-50°C. In addition, the kit contains RiboLock™ RNase inhibitor, which protects RNA from degradation at temperatures up to 55°C. The kit also contains two types of primers; oligo (dT) and random hexamer. The oligo (dT) primer selectively anneals to the 3´end of poly(A) RNA therefore allows synthesis of complementary DNA (cDNA) derived from mRNA while the random hexamer primers bind to the RNA template at more random but frequent fashion to synthesise cDNA from all RNA populations. The final product, cDNA, can be used directly as a template in PCR, real-time PCR (RT-PCR) or as a probe in hybridisation experiments.

In this project cDNA was used as a template for RT-PCR. The cDNA synthesis reactions were performed in sterile, nuclease-free, PCR tubes as follows:

- 2.5 µg extracted total RNA (Template)
- 1 µl Oligo (dT) primer (stock conc. 0.5 µg/µl)
- Top the volume up to 12 µl with dH_2O

The reaction was then placed in a PCR machine to undergo the reverse transcription programme (70°C for 5 min, 37°C for 3 min, 42°C for 45 min, 70°C for 5 min, 4°C forever). Upon reaching the last minute of the 37°C, the programme was paused and 8µl Master Mix (MMX) was added to each reaction. The MMX contains the following:

- 4 µl of 5X Reaction Buffer (250 mM Tris-HCl (pH 8.3), 250 mM KCl, 20 mM $MgCl_2$, 50mM DTT)
- 2 µl 10 mM dNTP Mix
- 1 µl RiboLock™ RNase inhibitor (stock conc. 20 U/µl)
- 1 µl RevertAid™ M-MuLV Reverse Transcriptase (stock conc. 20 U/µl)
- 1 µl dH_2O

The final cDNA product was either used immediately for reverse transcriptase PCR (RT-PCR) or stored at -20°C.

2.3.3 RT-PCR

RT-PCR was performed using MyTaq™ Red Mix (BIOLINE). The mix contains all reagents needed for a PCR reaction (1.5 mM $MgCl_2$, 200µM dNTP mix, Taq polymerase and DNA loading dye) in 2x format. It only requires addition of template, primers and nuclease-free water to dilute the Red mix to 1x.

PCR reaction was made up to a total of 20 µl by adding the following components:

- 10 µl 2 x MyTaq™ Red Mix
- 6 µl dH20 water
- 1 µl forward primer (stock conc.10 pmol/µl)
- 1 µl reverse primer (stock conc.10 pmol/µl)
- 2 µl of cDNA

The PCR reaction was then placed in a PCR machine using an optimised programme. In general the programme was standardised at:

1- 95°C for 5 minutes (for DNA denaturation)

2- 94°C for 30 seconds (Denaturation step)

3- 55-70°C for 30 seconds for primers annealing*

4- 72°C for 20-45 seconds for DNA extension§ Steps 2-4 Repeat 25-40 cycles.

5- 72°C for 5 minutes (to complete extension)

6- 4°C forever (to stabilise the product)

*The exact temperature and cycles depend on the primers, complexity of the template and the purpose of use.

§ The extension time depends on the amplicon size. 200-1000 bp amplicon needs ≤ 30 seconds. ≥ 1000 bp amplicon needs ≥ 30 second/1000bp.

1% agarose gel prepared in 1 x Tris-acetate EDTA buffer (1 x TAE) and ethidium bromide was used to visualise the PCR product. 15 µl of each PCR product along with 5 µl DNA ladder marker (NORGEN) were loaded into the gel. The gel was run using 1 x TAE buffer at 140 V for 40 min. The amplified bands were visualised using a UVP machine (3UV™ Transilluminator; Thermo Scientific).

Of note, all primers were designed by me or other researchers in Dr. Sayan's lab.

2.3.3.1 **Primers used in RT-PCR**

The list of primers used in RT-PCR are displayed in **Table 5.**

Table 5: List of the primers used in RT-PCR.

Oligo Name	Sequence (5'-3')	Product Size	Purpose	Supplier
GAPDH Forward	CAAGGTCATCCATGACAACTTTG	496 bp	For equal loading	Sigma
GAPDH Reverse	GTCCACCACCCTGTTGCTGTAG			
E-cadherin Forward	CACCCGGGCTGAGCTGGACAGGG	619 bp	Epithelial Marker	Invitrogen
E-cadherin Reverse	CCGGGTGTCATCCTCTGGG			
SIP1 Forward	TCTGAGGAGCTCCAGGGTGA	1218 bp	Mesenchymal Marker	Invitrogen
SIP1 Reverse	CATGCCATCTTCCATATTG			
SLUG Forward	CACCATGCCGCGCTCCTTCCTGGTC	808 bp	Mesenchymal Marker	Sigma
SLUG Reverse	GTGTGCTACACAGCAGCCAGAT			
SNAIL Forward	CACCATGCCGCGCTCCTTCCTGGTGA	880 bp	Mesenchymal Marker	Sigma
SNAIL Forward	GGGGCCCGGGCAGCAGCCA			
TWIST Forward	CACCATGATGCAGGACGTGTCCAGCT	610 bp	Mesenchymal Marker	Sigma
TWIST Reverse	GTGGGACGCGGACATGGACC			
ZO-1 Forward	GGCCTACACTGATCAAGAACT		Mesenchymal Marker	Sigma
ZO-1 Reverse	GAGTTGGGGTTCATAGGTCAG			
Vimentin Forward	GAGCTCGAGCAGCTCAAGG	291 bp	Mesenchymal Marker	Sigma

Oligo Name	Sequence (5'-3')	Product Size	Purpose	Supplier
Vimentin Reverse	AAGGTCAAGACGTGCCAGAG			
CCL5 Forward	GGATCAAGACAGCACGTGGAC	227 bp	Chemokine	Invitrogen
CCL5 Reverse	GCTCATCTCCAAAGAGTTGATGTA			

2.4 Immunofluorescence

Immunofluorescence (IF) is a technique to detect specific target proteins with fluorescently-labelled antibodies which are then visualised using fluorescence microscopy. Indirect IF requires two incubation steps; the first with a primary antibody followed by a compatible secondary antibody. The secondary antibodies have the fluorescent dye (FITC, PE, Cy5, Alexa 488, 594, etc.) conjugated to them. In contrast, direct IF requires only one incubation step with a primary antibody with a fluorescent dye (FITC, PE, Cy5, Alexa 488, 594, etc.) conjugated to it. **See Figure 19.**

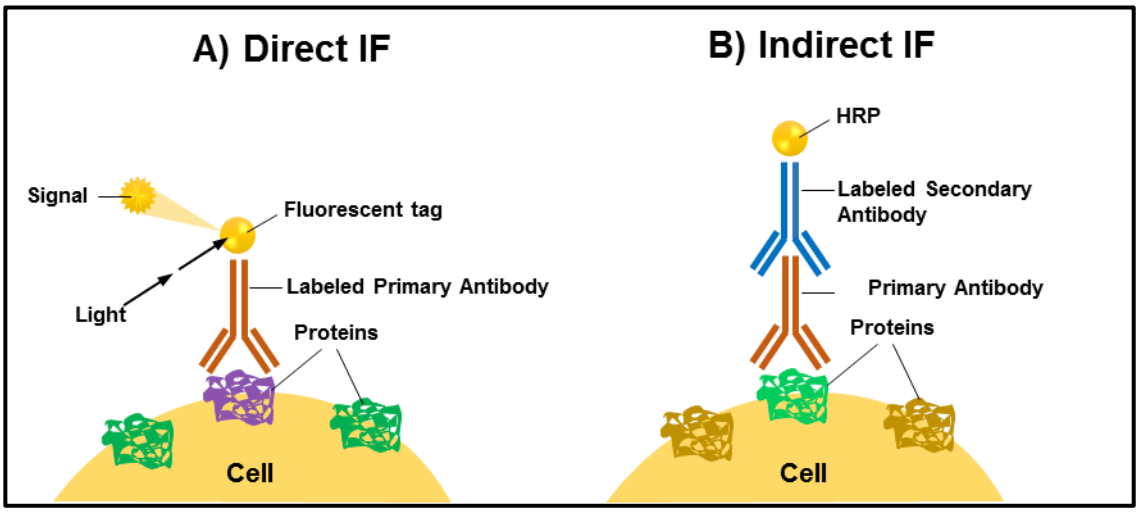

Figure 19: General principle of immunofluorescence.

Direct immunofluorescence (IF): one fluorophore-conjugated primary antibody is directed against the protein of interest.
Indirect immunofluorescence (IF): Two antibodies. An un-conjugated primary antibody which binds to the protein of interest is followed by a fluorophore-conjugated secondary antibody directed against the primary antibody; adapted from [471].

2.4.1 Growing cell lines on coverslips

Both IF techniques require growing cells on a substrate that is appropriate for light microscopy, such as glass coverslips. To do this, 2 ml of 1 x PBS was first put in each well of a 6-well plate. Round coverslips (2 mm; VWR international) were immersed in absolute ethanol to sterilise them, and then placed in one well to wet the coverslip. After a couple of minutes when the coverslip has settled to the bottom of the well, the PBS was removed and replaced with complete DMEM containing 35,000 cells (DLD-SIP1). Where necessary, cells were treated with 2 µg/ml doxycycline for three days in order to induce expression of the *SIP1* gene. On the third day, the IF procedure was carried out when cells had reached ~ 80% confluency.

2.4.2 Indirect IF procedure

In this project indirect IF was used. The main steps for the procedure are:

2.4.2.1 **Cell fixation**

The un-induced and induced DLD-SIP1 cells were first washed once with 1 x PBS to remove any growth media. After that, the cells were fixed with 4% paraformaldehyde (PFA) for 15 min, and the washed once PBS. At this stage cells can be kept at 4°C for future use (overnight) or used for immunostaining immediately.

2.4.2.2 **Cell permeabilisation**

Before proceeding with immune-detection, cells were permeabilised with 0.2% Triton-X (prepared in PBS) for 3 minutes, then immediately washed three times with PBS (5 min each).

2.4.2.3 **Immunostaining**

The cells were first incubated with a blocking solution (2.5% BSA in PBS or PBS-0.2%Triton X) to block non-specific antibody binding sites. Subsequently, an appropriate diluted primary antibody in 2.5 % BSA-PBS (1-10 µg / ml) was added, incubated for 30 min at RT, and the sample then washed three times with PBS (5 mins each). Following that, matched fluorescent-labelled conjugated secondary antibodies (1:500 Alexa 488 or 1:500 Alexa594 fluoro-chromes; Molecular Probes) were added and the sample incubated

in dark for 30 min at RT, and then washed again with PBS three-times (5 mins each). To stain each nuclei, DAPI (1:10 000 of stock concentration 1mg/ml, Vector Laboratories) was used (incubated for 5 min) and immediately rinsed twice with PBS. Finally the glass coverslips were inverted and transferred into a clean slide having a fine drop of a mounting media (Mowiol or antifade; provided by the Biomedical Imaging Unit, University of Southampton). The slides were then examined with help from Dr. Dave Johnston of the Biomedical Imaging Unit using either a dark field florescent microscope (Olympus IX8) or Leica SP5 Laser Scanning Confocal Microscope.

2.5 Human Chemokine and Cytokine Antibody Arrays

The Human Cytokine or Chemokine Arrays are fast, sensitive, and cost-effective tools to detect the difference between samples in the relative expression level of cytokines or chemokines. In addition, it is a time-effective tool, where the expression levels of numerous chemokines and cytokines can be determined without performing multiple immunoassays.

2.5.1 Assay principle

Cell culture supernatants, cell lysates, serum, or plasma are first diluted and mixed with a cocktail of biotinylated detection antibodies. The cytokines or chemokines first make a complex with their matching detection antibodies. The antigen/antibody complex then binds to the corresponding capture antibodies that are spotted by the manufacturer on nitrocellulose membranes. To determine the antigen/ antibodies binding affinity, Streptavidin-HRP and chemiluminescent detection reagents are used. The amount of light produced at each spot is in proportion to the amount of cytokine or chemokine in the sample. **See figure 20.**

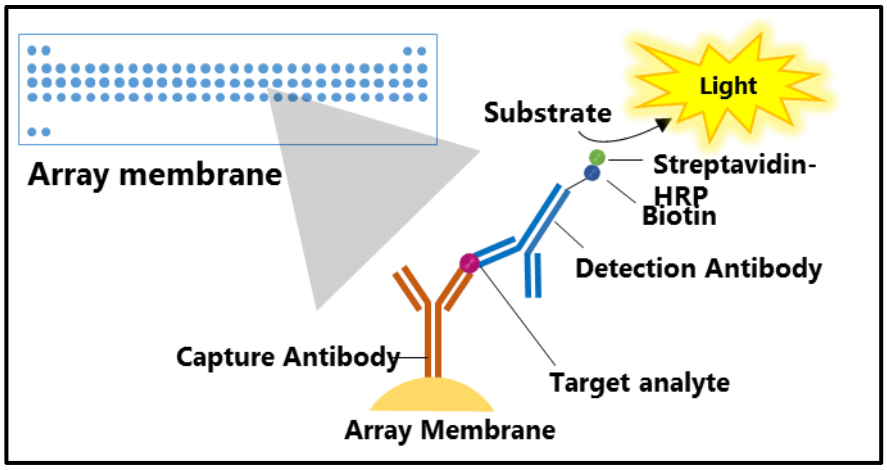

Figure 20: General principle of proteome profiler antibody arrays (R&D systems).

The arrays used in this project were for chemokines and cytokines. They were analysed in the DLD-SIP1 EMT CRC inducible model; adapted from [472].

2.5.2 Proteomic array procedure

The chemokine and cytokine arrays (R&D systems) consists of 3 sample control antibodies, 31 different capture chemokine antibodies or 36 capture cytokine antibodies. The antibodies are spotted in duplicate on nitrocellulose membranes; see **table 12 and 13 at the appendix section** for the list of the antibodies in the arrays. The non-specific binding sites of the captured antibodies were blocked using a blocking buffer (supplied with the kits) for 1 hour at room temperature. During the blocking time, 300 µg of un-induced and induced DLD-SIP1 cell lysates and 700 µl of the cells' supernatants were prepared according to the kit's instructions, mixed with a cocktail of biotinylated detection antibodies and incubated for 1 hour at room temperature. After that, the blocking buffer was aspirated and the mixture of cell lysate or supernatant with the cocktail detection antibodies were added, and incubated overnight at 4 °C on a rocking platform shaker. Next day, the membranes were washed three times with 1 x wash buffer (supplied with the kit) in order to remove any unbounded antibodies. After that, 1:100 streptavidin-HRP dilution (supplied with the kit) was added, incubated for 30 min at room temperature on a rocking platform shaker and washed three times. Chemiluminescent detection reagents 1 and 2 (supplied with the kit) were prepared (1:1) and applied to the membranes. Finally, the membranes were exposed to X-ray films for 1-10 mins. The signal produced from each captured spot corresponded to the amount of bound protein. The positive signals which are seen on the developed film were identified by placing the transparency overlay template on the array developed film and aligning it with the pairs of reference spots. Pixel densities on

developed X-ray film were analysed using a transmission mode scanner and Image J analysis software.

2.6 Multiplex detection immunoassay

2.6.1 Main principle

The multiplex immunoassay system is a multi-analyte profiling assay. It utilises numerous, beads of different colour and size which allows the analysis of up to 100 different analytes within a single sample. In general, a set of beads of the same colour is attached to one antibody that can recognise one specific analyte that can also be identified depending on bead size. The antigen/antibody complex is then detected by an analyte-matched secondary antibody attached to a fluorescent reporter dye label. Flow cytometer is used to determine the analytes concentration by measuring the fluorescent reporter dye label and size of beads. **See figure21.**

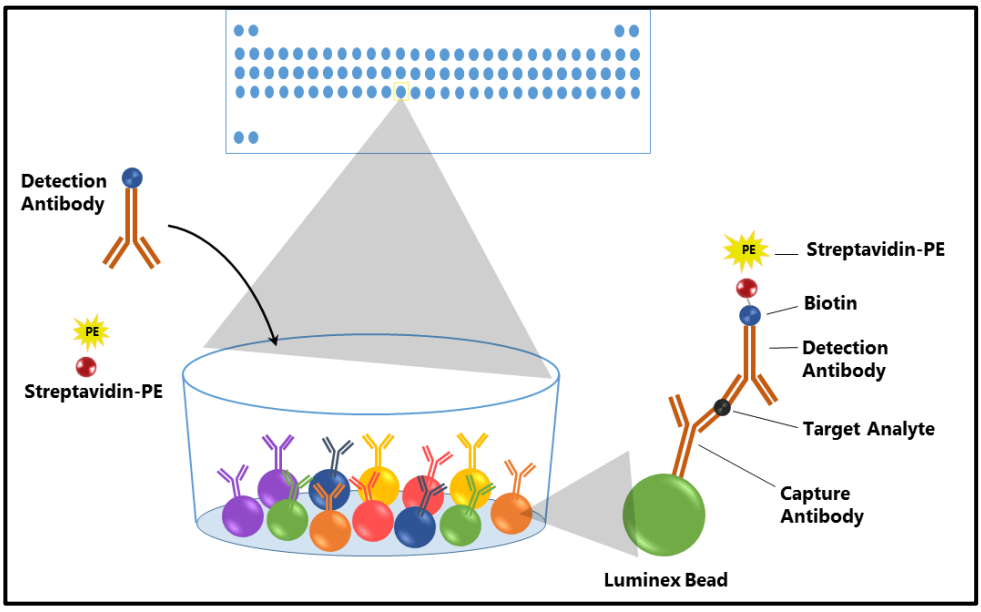

Figure 21: The general principle of multiplex beads immune-assay.
Adapted from[473]

This assay is efficient in analysing multiple proteins using a small quantity of sample (~ 50 µl) compared to ELISA which can only analyse a single protein. In addition, it is also time- and cost-effective compared to western blotting (WB) although each multiplex assay (of 100 analytes X10 reactions) can cost up to £5000.

2.6.2 25- Multiplex detection immunoassay

A 25- Multiplex detection immunoassay (Life Technology) was used for this project. This particular assay utilises 25 distinctly coloured beads which allows the analysis of up to 25 different analytes within a single sample. It was used as a confirmatory assay for the R&D systems cytokine and chemokine arrays. The procedure was performed by members of Dr. Williams's lab (Southampton University) and observed by me.

Briefly, specific antibodies for human IL-1β, IL-1RA, IL-2, IL-2R, IL-4, IL-5, IL-6, IL-7, IL-8, IL-10, IL-12p40/p70, IL-13, IL-15, IL-17, TNF-α, IFN-α, IFN-γ, GM-CSF, MIP-1α, MIP-1β, IP-10, MIG, Eotaxin, RANTES, and MCP-1were captured on 5.6 µm polystyrene beads. Test samples, control samples and standards were incubated with the beads for 2 hours at room temperature to facilitate the antigen-antibody interaction. At the end of the incubation, the excess antigens were washed and protein-specific biotinylated detector antibodies were added and incubated for 1 hour. During this incubation, the protein-specific biotinylated detector antibodies bind to the appropriate immobilised antigens. Similarly, the excess biotinylated detector antibodies were washed off and streptavidin conjugated, R-Phycoerythrin (Streptavidin-RPE) was added and incubated for 30 minutes. The Streptavidin-RPE binds to the biotinylated detector antibodies associated with the immune complexes on the beads. The unbound Streptavidin-RPE was washed off and the beads were analysed with the Luminex detection system. By monitoring the spectral properties of the beads and the amount of associated RPE fluorescence, the concentration of one or more proteins was determined.

2.7 Quantitative enzyme immunoassay

2.7.1 General principle

Enzyme-linked immunosorbent assay (ELISA) is designed to measure specific analytes in cell culture supernatants, serum, platelet-poor plasma, or urine. In sandwich form, a monoclonal antibody specific to the protein of interest is coated onto a solid substrate such as a microplate, and then the target antigen in the sample or standard is incubated with the pre-coated antibody. The antigen/antibody complex forms. Subsequently, enzyme-linked antibody specific for the target antigen is added, followed by enzyme specific substrate. The enzymatic reaction develops a colour that is in proportion to the amount of the antigen

of interest present in the sample or standard. The intensity of the developed colour is measured by a spectrophotometer device; **see figure 22.**

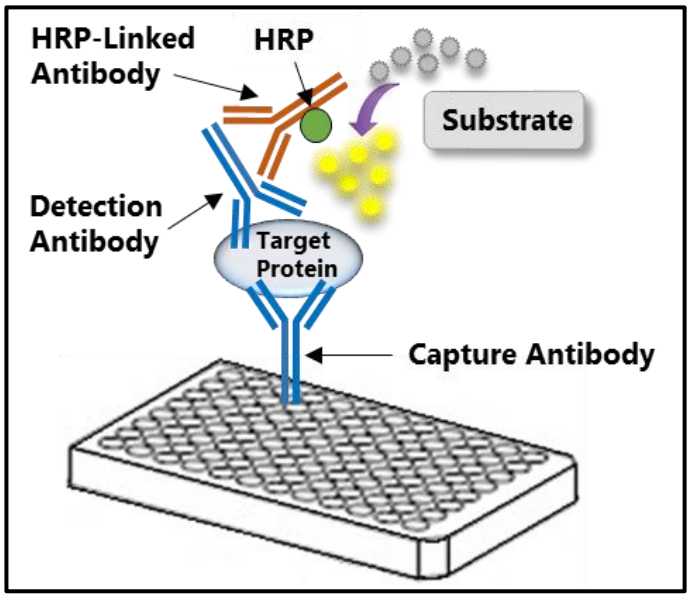

Figure 22: General principle of sandwich ELISA that was used in the project to determine the expression of CCL5.

Adapted from [474].

2.7.2 Human CCL5/RANTES ELISA

The level of CCL5 in the supernatant of five epithelial and three mesenchymal CRC cell lines was detected using an R&D system Duoset ® human CCL5 ELISA kit (Catalog number: DY278).

The ELISA plate was prepared for the assay as follows. The wells were coated overnight at room temperature with 100 µl of 1.0 µg/ml mouse anti-human RANTES capture antibody (stock concentration 180 µg/ml). Then, the wells were washed three times with ELISA wash buffer (PBS, pH 7.4). Next, 300 µl of a prepared blocking reagent (Reagent diluent; 1% BSA in PBS) was added to each well and incubated for 1 hour at room temperature to block non-specific antibody binding sites. After 1h, the wells were washed three times with PBS. It is critical to get rid of any excess wash buffer by inverting the plate and blotting it against clean paper towel.

Recombinant human RANTES (stock concentration 120 ng/ml) was used to prepare the assay standard. Three fold serial dilutions of 2000 pg/ml of the highest standard were prepared to create a six point-standard curve. The supernatants of the cultured cell lines

and the patient serum were diluted in the reagent diluent at the appropriate concentration prior to use.

One hundred µl of diluted samples or standards were added in each well with each sample or standard loaded in triplicate. The plate was then covered and incubated at room temperature for 2 hours. After the incubation period, the wells were washed three times with washing buffer (0.05% Tween®20 in PBS, pH 7.27.4), then 100 µl of 20 ng/ml detection antibody (which is supplied with the kit) were added in each well (stock concentration 3.6 µg/ml). Once more, the plate was covered, incubated at room temperature for 2 hours and then washed three times. After that, 100 µl of diluted streptavidin conjugated horseradish peroxidase (1:100) was added to each well, incubated for 20 min at room temperature and then washed off three times with the wash buffer. Finally, 100 µl of substrate solution (1:1 H_2O_2: Tetramethylbenzidine) was added to each well and the optical density was determined using a microplate reader set at 450 nm and 570 nm wavelength correction. The reading was taken at 5 min intervals for 40 mins.

2.8 DNA cloning and recombinant DNA technology.

DNA cloning is a genetic engineering approach to generate a large number of copies of a DNA fragment. This approach helps to study either a the expression of a gene, function of the gene, how mutations may affect the gene's function or make large quantities of the protein encoded by that gene [475]

The main milestones for DNA cloning are:

- DNA amplification
- DNA extraction
- DNA ligation into a plasmid
- Transformation of plasmid DNA
- Purification of plasmid DNA

2.8.1 DNA Amplification

Multiple copies of the *CCL5* coding region or the *CCL5* promoter were amplified from cDNA or genomic DNA, respectively, using KOD DNA polymerase (Novagen®). KOD polymerase is a thermo-stable polymerase that can amplify targeted DNA with greater accuracy and a higher yield compared to Taq polymerase.

Before proceeding with the PCR, special primers containing defined restriction enzymes were designed depending on the particular construct used. The CCL5 coding region was amplified using cDNA generated from the RKO cell line while the CCL5 promoter was amplified from human genomic DNA (obtained from Jon Strefford's group).

The CCL5 coding region was ligated into pcDNA 3.1 plasmid (5.5 kb; s**ee figure 23**).

In the case of CCL5 promoter, which was ligated into the PGL3 basic plasmid (4.8 kb; se**e figure2**4), the following primers were used:

CCL5 promoter forward primer with *Mlul* restriction site (Thermo scientific; Catalog no. ER0561): 5'AAA**ACGCGT** CCAATAATGATAGAGTATGCT 3'

CCL5 promoter reverse primer with *XhoI* restriction site (Thermo scientific; Catalog no. ER0691): 3'GGG**CTCGAG** CGGAGACCTTGATGGTACCTGT5'

The PCR reaction mixtures were then prepared as following:

- 10 µl 2 x KOD buffer-enzyme mix
- 6 µl nuclease-free water
- 1 µl (10 pmol) CCL5 promoter forward primer
- 1 µl (10 pmol) CCL5 promoter reverse primer
- 2 µl of cDNA or genomic DNA Total volume 20 µl

The reactions were amplified at a pre-optimised condition, mixed with DNA loading buffer, loaded in 1% agarose gel and run at 100 V for 40 minutes, **see section 2.3.3** for more details.

2.8.2 Gel extraction

QIAquick Gel Extraction kit using a micro-centrifuge (Qiagen, Catalog no. 28704) was used for gel extraction. Of note, all the buffers used in this protocol were already prepared with the kit. The composition of the buffers is not disclosed by the manufacturer.

The amplified DNA fragments for the *CCL5* gene promoter or *CCL5* coding region at the expected size were cut from the agarose gel using a clean scalpel. Excess agarose gel was removed to minimize the size of the gel. The gel slice was then weighed and ~300 µl of buffer QG was added to every 100 mg of gel slice. The gel was then dissolved completely

by incubating the tube at 50°C and vortexing every 2-3 min (the mixture colour should be yellow indicating a pH ≤7.5). To increase the yield of DNA fragments, 100 µl of isopropanol was added to every 100 mg DNA fragment. After that, the sample was applied to the QIAquick spin column and centrifuged for 1 min. The flow-through in the collection tube was discarded and the column was placed back in the same collection tube. To remove all traces of agarose, 0.5 ml of buffer QG was added to the column and centrifuged for 1 min at ≥10,000 x g. Next, the column was washed with 0.75ml of buffer PE, centrifuged again for 1 min at ≥10,000 x g and the flow-through was discarded. The column was then centrifuged for another 1 min to remove any residual ethanol (from buffer PE). Finally, the retained DNA in the column was eluted by placing the column into a clean 1.5 ml micro-centrifuge tube, and adding 50 µl of deionised water at the centre of the column and centrifuged for 1 min at ≥10,000 x g. Typically, the elution volume should be no less than 90% of the volume of eluting solved added. To obtain a high elution efficiency, the pH of the water should be between pH 7-8.5. The collected DNA was used immediately or stored at -20°C to avoid DNA degradation.

2.8.3 DNA Ligation into the vector

2.8.3.1 **TOPO® cloning of *CCL5* cDNA**

PcDNA™3.1/V5-His TOPO® expression kit (Invitrogen) was used for direct insertion of the CCL5 coding region into the pcDNA™3.1/V5-His TOPO® plasmid vector (**see figure 23**). TOPO isomerisation is a highly efficient, quick, one-step cloning strategy; there is no need for ligase, post PCR procedures or PCR primers containing specific sequences.

A 6 µl of TOPO® cloning reaction was prepared as following:

- 1 µl of salt solution (supplemented with the kit).
- 1 µl TOPO® vector.
- 4 µl fresh CCL5 PCR extracted product.

The reaction was mixed gently and incubated for 5-15 mins at room temperature then transformed into an E-coli strain (JM109).

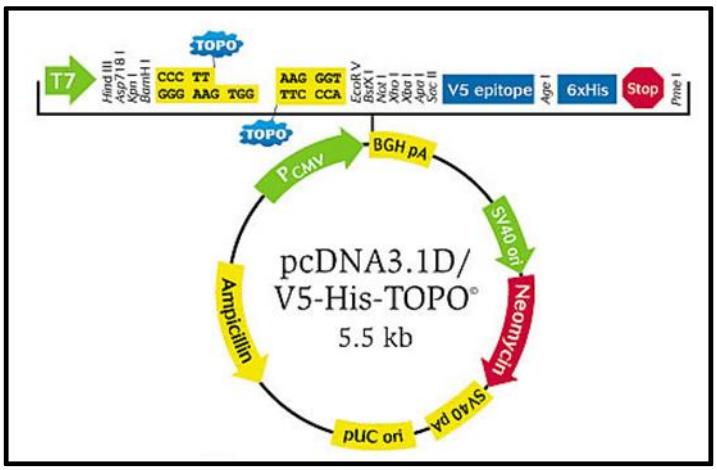

Figure 23: The pcDNA3.1D/V5-His-TOPO® vector that was used to clone the *CCL5* coding region.
Adapted from [476].

2.8.3.2 PGL3 Cloning for the *CCL5* Promoter

The extracted *CCL5* promoter was ligated into pGL3 basic vector (already present in Dr. Sayan's lab); **see figure 24**.

- A 10 µl cloning reaction was prepared as follows:
- 5 µl of 2 x ligation buffer (Takara, Clontech)
- 1 µl PGL3 vector
- 4 µl fresh CCL5 promoter extracted product Total volume: 20 µl

The reaction was mixed gently and incubated for 15 mins at room temperature then transformed into an E-coli strain.

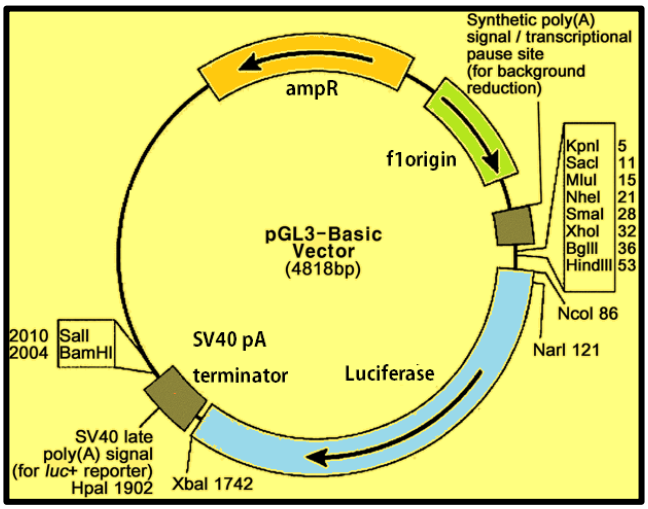

Figure 24: pGL3 basic vector that was used to clone the *CCL5* promoter.
Adapted from [477].

2.8.4 Plasmid transformation

Chemically competent E.coli (JM109) cells were used to transform the pcDNA3.1-CCL5 or pGL3-CCL5 promoter plasmids. A total of 5 µl from the cloning reaction was mixed gently with 50 µl of JM109 and incubated on ice for 30 min. After that, the cells were exposed to a heat shock for 30 seconds at 42°C and placed immediately on ice for 2 minutes. The entire transformed amount was then added into a tube containing 400 µl of SOC medium. The tube was placed horizontally into a shaker at 200 rpm, 37°C for 1 hour. At the end of the 1 hour, the tube was centrifuged at 13,000 rpm. The supernatant was then discarded and the pellet was dissolved in 50µl Luria Bertani (LB; 10 g/L Tryptone, 5 g/L Yeast extract and 10 g/L NaCl) and spread onto LB-Agar (LB+20g/L agar) containing 100 µg/ ml ampicillin. The plate was incubated overnight at a 37°C. Five colonies were picked up and the inserted DNA fragment was amplified and analysed by performing PCR with the specific designed primers for the *CCL5* gene promoter or *CCL5* coding region.

2.8.5 Plasmid DNA purification

2.8.5.1.1 Small Scale Plasmid DNA Purification

A QIAGEN Plasmid mini Kit (Catalog no. 2123) was used to harvest the successfully ligated and transformed plasmid from the bacteria. Of note, all the buffers used in this protocol are ready to use. The composition of the buffers is not disclosed by the manufacturer.

The colony with the pcDNA3.1-CCL5 or PGL3-CCL5 promoter plasmids were cultured overnight in 5 ml LB medium containing 100 µg/ml ampicillin and incubated for 12-16 hours at 37°C with vigorous shaking. The next day, 1.5 ml of the bacterial culture (~ 15 µg of high-copy plasmid DNA) was harvested at ≥10,000 x g for 10 min at 4°C. The supernatant was then removed. The bacterial pellet was re-suspended in 250 µl buffer P1 in the presence of an appropriate volume of RNase A solution and LyseBlue reagent to ensure complete elimination of RNA and complete dissolving of the pellet, respectively. After the bacteria were suspended completely by vortexing and pipetting, 250 µl of lysis buffer (P2) was added and mixed gently by inverting the tube 4-6 times without vigorous mixing to avoid shearing of genomic DNA. Of note, after adding buffer P2, the colour of the cell suspension should turn blue, which indicates complete cell lysis On the top of buffers P1 and P2, 350 µl of neutralising buffer N3 was added, mixed immediately and gently by inverting the tube until the blue colour diminishes. The homogenous, colourless suspension

indicates that the SDS is effectively precipitated and the lysate is neutralised and adjusted to high-salt binding conditions. The tube was then centrifuged at ≥ 10,000 x g for 10 min which creates a compact, white pellet with a colourless supernatant. The white pellet contains denatured proteins, chromosomal DNA, cellular debris and SDS while the aqueous solution contains the denatured plasmid DNA.

The aqueous solution was applied into the QIAprep spin column, centrifuged for 1 min at ≥ 10,000 x g and the flow-through discarded. To remove the high level of endonuclease activity in the JM109 cells (E coli, endA+ strain), the column was washed by adding 500 µl PB buffer, centrifuged for 1 min and the flow-through discarded. Another wash was done by adding 750 µl buffer PE to the column, which was then centrifuge for 1 min and the flow-through discarded. To ensure that all residual ethanol from the wash buffer was removed, another spin was performed for 1 min. Finally, the column with retained DNA was placed in a clean 1.5 ml tube, and eluted with 50 µl dH_2O. The column was incubated at room temperature for 1 min and the eluate removed by centrifugation at ≥ 10,000 x g for 1 min.

Before sending 5-10 µl of the collected plasmids for sequencing (Source Bioscience) the direction of cloned fragment was checked by either using a restriction enzyme e.g. (BgIII) or doing a PCR with V5 reverse primer and the specific CCL5 forward primer.

2.8.6 Plasmid maxi-prep it

The bacteria containing the pcDNA3.1-CCL5 or pGL3-CCL5 promoter plasmids were cultured overnight in 125 ml LB with 100 µg/ml Ampicillin at 37 °C in order to obtain large quantities of the plasmids. QIAGEN Plasmid Maxi Kit (Catalog no. 12162) was used for this purpose. Of note, all the buffers used in this protocol are ready to use. Buffer compositions are not disclosed by the manufacturer.

The plasmid was purified using the same procedure of the mini prep that was explained in detail in the previous section, but on a large scale “Maxi prep”. In brief, the procedure is based on alkaline lysis of bacterial cells, followed by adsorption of DNA onto a silica membrane in the presence of a high-salt buffer and elution of the plasmid DNA in a low-salt buffer or dH_2O.

The collected plasmid was either used immediately for transfection or stored at -20 °C for later use.

2.9 Transfection

Transfection is the process by which nucleic acids are introduced into eukaryotic host cells, for stable integration into the host genome (stable transfection), or temporary expression (transient transfection). There are different methods of transfection:

1- Calcium Phosphate transfection

This is a chemical transfection method which depends on DNA condensation by Calcium phosphate co-precipitation. The calcium phosphate co-precipitation agent is generated by mixing DNA with calcium chloride in buffered saline/phosphate. The reaction mixture is then dispensed into cultured cells, and the DNA enters cells via endocytosis. This method is labour, time and cost effective, and suitable for many and difficult types of cultured cells. However, it is cytotoxic to a lot of cells and the procedure is dependent on pH, temperature, and buffer salt concentrations.

2- Electroporation

This is physical transfection method which aims to create pores in cell membrane by electronic pulses that facilitates the transfer of nucleic acids into cells. Although this method is easy, rapid and effective, it has a major drawback which is the high percentage of cell death due to high voltage pulses.

3- Lipid-mediated transfection:

The principle of this transfection technique relies on the positive surface charge of liposomes interacting with negatively charged nucleic acids (phosphate backbone of DNA, RNA or siRNA). The liposome/nucleic acid complex fuses into cells through direct interaction with the negatively charged cell membrane and endocytosis. Once the transfected nucleic acids get inside the cells, they diffuse through the cytoplasm and are either expressed temporarily or integrate to the genome for stable gene expression; **see figure 25.**

It is a fast, simple, non-toxic and reproducible transfection method. It is a very suitable technique for many types of cells including adherent, suspension, and insect cells, as well as primary cultures.

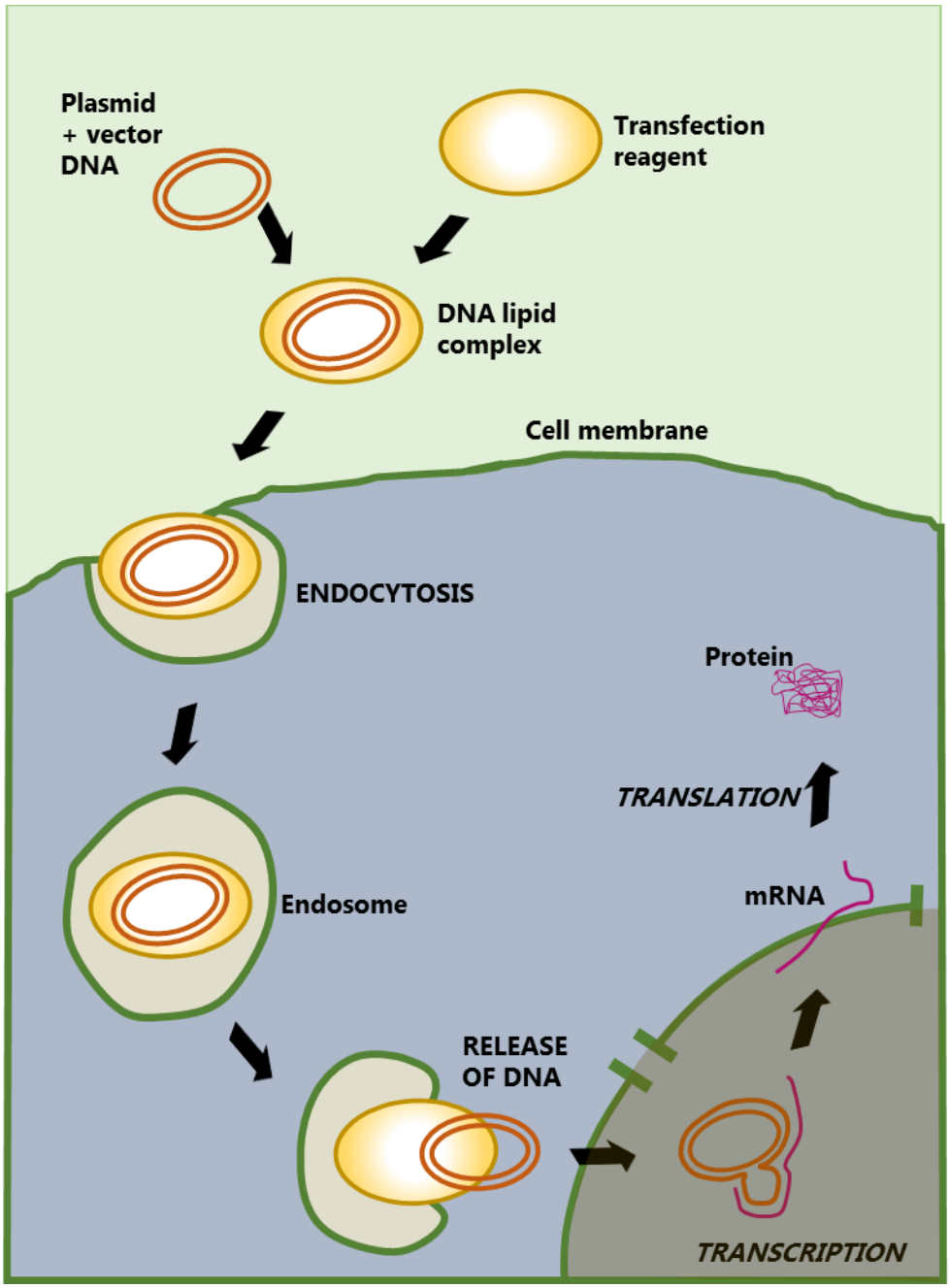

Figure 25: Lipid-mediated transfection of eukaryotic cells with plasmid DNA.

This is the main transfection method used in the project using Lipofectamine® protocol; adapted from [478].

2.9.1 Lipofectamine® 3000 Protocol

Lipofectamine®3000 (Thermo Scientific; Catalog no. L3000001) were used to transfect our constructed DNA into CRC cells. This reagent gives 10-times higher efficiency into a broad spectrum of difficult-to-transfect cells as compared to other Lipofectamine reagents.

First, the appropriate numbers of cells were seeded in in 6- or 96-well plates in an appropriate volume of complete DMEM. The transfection is performed when the cells reached 60-80 % confluency.

The kit has two lipid reagents: Lipofectamine 3000 reagent and P3000 reagent. Following the assay procedure, the appropriate quantity of the reagents and DNA are added. In general the main steps of transfection are:

- Dilute Lipofectamine 3000 reagent in Opti-MEM®, vortex for 3 second and keep aside at RT until required.
- Dilute Plasmid-DNA or transfection efficiency control plasmid (such as pEGFP or Renilla luciferase plasmids) in Opti-MEM® and then add an appropriate volume of P3000 reagent.
- After that, mix the two mixtures and incubate at RT for 5 min.
- Finally, add the DNA-lipids mixture to the cells drop by drop. Mix gently by rocking the plate back and forth and incubate at 37°C.
- Change the media after 6 hours and replace it with Opti-MEM® or complete DMEM.
- 1-2 days post-transfection, the up-stream and/or the down-stream effect of the transfected nucleic acid can then be assessed using an appropriate assay.
- If a pEGFP plasmid is used, assessment of transfection efficiency can be performed using a fluorescent microscope. If the Renilla luciferase plasmid was used, the Renilla enzyme substrate could be added to lysed cells and light emission measured using a luminometer device.

2.10 **Flow cytometry**

The fundamental aim of flow cytometry is to detect single cells in a liquid stream under the action of pressure. As a laser passes through the cell, it creates light scattering in all directions. The forward scatter (FSC) detects the size of the cell, while the side scatter (SSC) at 90 degrees determines the morphology (e.g. granularity) of the cell. The FSC and SSC are converted to voltage pulses that are proportional to the particle size and the granularity, respectively. In addition, flow cytometry enables detection of light emitted from an antibody conjugated to a fluorophore or dye due to absorbing energy from a laser set at a specific wavelength, which passes through filters and mirrors to capture light at specific wavelengths. The photons of the light are converted by a photomultiplier tube

(PMTs) into electrical impulses, which are translated into a numerical signal. The intensity of the colour is then recorded by a computer system as a histogram [479]; **see figure 26**.

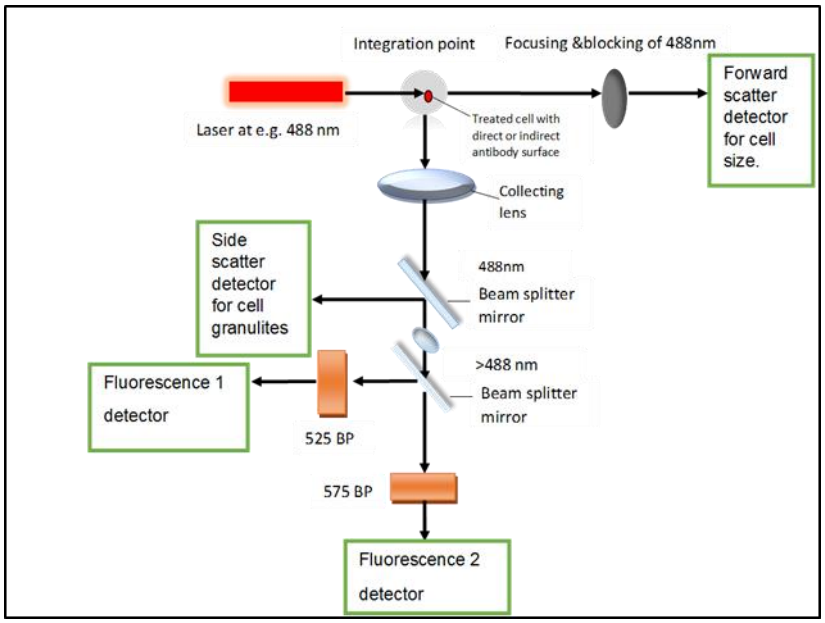

Figure 26: General principle of flow cytometry.
Adapted from [479].

2.10.1 Preparation of samples for FACS

Around 2 million cells of induced or induced DLD-SIP1, SW480, SW620, HCT116 and DLD-1 were collected, washed once with FACS Buffer (1 x PBS + 2.5 % BSA), and centrifuged at 1250 x g for 3 min. The supernatants were discarded and the cells re-suspended in 150 µl FACS Buffer. Then, cells of each cell line were then distributed equally in four tubes. Following that, each tube was then treated with primary conjugated antibodies against CCR5 as detailed:

- 2 µl of Isotype IgG negative control (Stock concentration)
- 2 µl of CCR5 APC (stock concentration)

All tubes were incubated for 30 min on ice in the dark. The reactions were then washed with 1 ml FACS Buffer, centrifuged at 1250 x g for 3 min, the supernatants were carefully discarded and the pellets were re-suspended in 300 µl FACS buffer and analysed immediately. Alternatively the reaction can be fixed with formaldehyde and analysed the next day.

2.10.2 FACS analysis

Prior to running the samples, the Becton Dickinson FACS calibur machine was prepared and operated by following the department's standard operating procedure. Emission spectra of various flourochromes were checked using Flow-Check™ Flurospheres (Beckmann coulter, Ireland, UK).

All samples were analysed by a Becton Dickinson FACS calibur flow-cytometry with an argon laser (488nm) for FL2 and Red Diode laser (635 nm) for FL4. Gate A was drawn around the visible cell population using the FSC versus SSC plot and, and when possible, 10,000 events were collected to give a statistically significant number of CRC5 or CCR3 in each sample. The fluorescent colours emitted from CCR3 PE and CCR5 APC antibodies were detected in FL2 and FL4 channels, respectively. The results were displayed on a logarithmic scale in a histogram. After this, the percentage of CCR5 or CCR3 cells was determined from the gate using FSC vs. FL2 or FSC vs. FL4 histograms. The positive and negative peaks were defined by comparisons to the isotype negative control.

2.11 Transwell migration assay

Cell migration assays were preformed over 24 hours using polycarbonate invasion chambers with 8 µm pore size (BD). The top and the lower chambers were first wetted with DMEM for 10 min. In the meantime, SW480 cells, which were found by us to have high expression of CCR5, were trypsinised, counted, re-suspended in DMEM with 10% serum and seeded at a density of 3.0 x10^5 cells/well in the top chambers. The cells were left to attach for 2-3 hours, after which the medium in the top chamber was changed to serum-free DMEM. At the same time, 800 µl DMEM was added to the lower chambers containing chemo-attractant or anti-chemo-attractant agents in the following order:

- DMEM with 10% FCS serum
- DLD-1 supernatant from negative CCL5 clone (0.2ng/ml)
- DLD-1 supernatant from positive CCL5 over-expression clone (8ng/ml)
- DLD-1 supernatant from positive CCL5 over-expression clone + 0.12 µg /ml of Monoclonal Mouse IgG CCL5 neutralising antibody (R&D system; stock conc. 0.698 mg/ml); to have 50% neutralization dose (ND50) in the presence of 10 ng/ml human CCL5.

- DMEM with 10% FCS serum + 5 ng/ml of human Recombinant CCL5 (R&D systems; stock conc. 100 µg/ml); to have 50% effective dose (ED50).

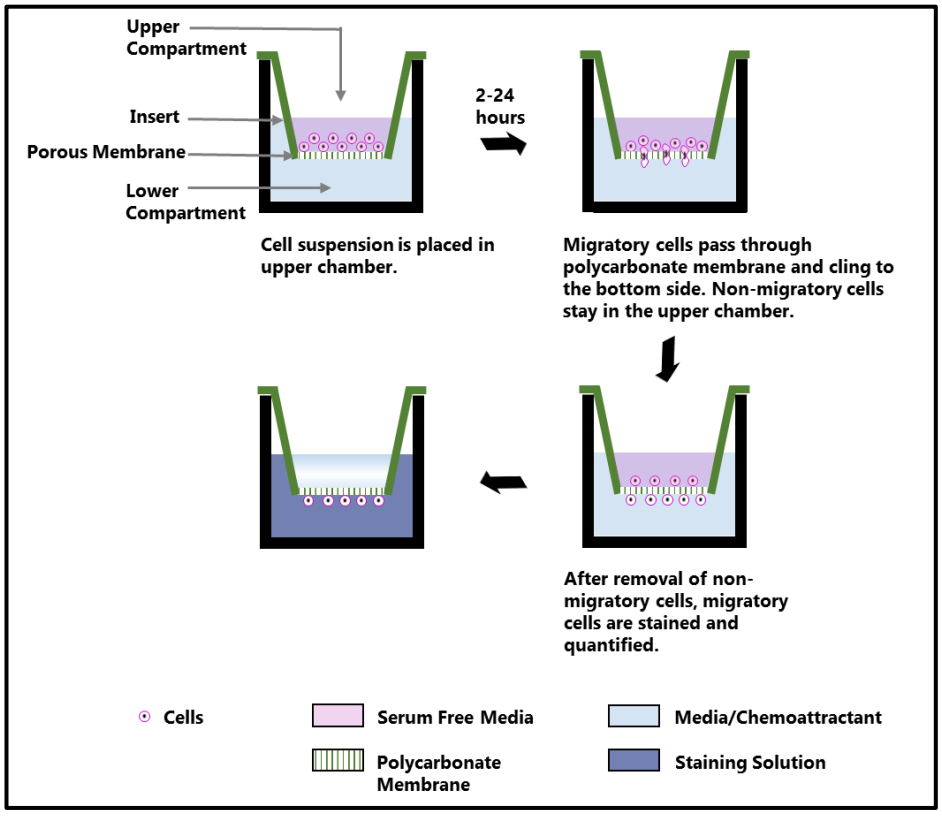

Figure 27: General illustration of Transwell migration assay.
SW480 cells were seeded in the upper chamber. Migration through the polycarbonate membrane (pore size 0.8 mm) towards different chemo-attractants was assessed. The migrated cells were stained by DAPI, and examined by fluorescent microscopy under UV light. The number of cells for each condition was scanned using image J. Adapted from [480].

Of note, each condition was repeated 3 times to calculate the standard error. After 24 hours, the cells on the top and the bottom chambers were washed with 1x PBS, fixed with ice-cold Acetone-Methanol (50%:50%) and washed again with 1x PBS. Next, the top chambers were stained with Eosin and the lower chambers were stained with 1:5000 diluted DAPI in 1x PBS for 5-10 min. After that, both compartments were washed with 1x PBS and the cells stained with Eosin were removed from the top chamber using a wet cotton swab to avoid any interference with DAPI stain.

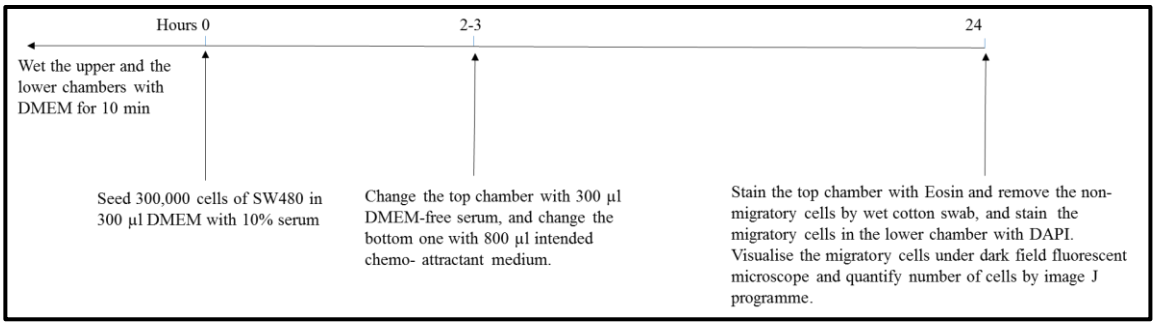

Figure 28: A flow chart for the migration assay protocol that used in this project.

2.12 **Site-directed mutagenesis**

The Quick Change II Site-Directed Mutagenesis kit (Agilent Technologies; Catalog #200523) [481] was used for Site-Directed Mutagenesis (SMD). SDM is a useful technique to introduce nucleotide changes to double stranded DNA (dsDNA) for studying complex relationships between protein structure and function, and for gene expression elements. It requires a double-stranded plasmid (supercoiled double-stranded DNA) with the insert of interest, PfuUltra high-fidelity DNA polymerase which amplifies DNA with less replication errors and specific primers containing the desired mutation (which can either be amino acid substitution, deletions or insertions). The process is a quick and rapid technique that only requires three main steps:

1- PCR reaction: *PfuUltra* HF DNA polymerase extends the oligonucleotide mutated primers at a specific temperature, generating a new mutated plasmid at the point of interest.
2- *Dpn I* endonuclease treatment of the PCR product digests (dam+) methylated and hemi-methylated parental DNA template.
3- Transformation of the new plasmid containing the desired mutation. **See figure 29.**

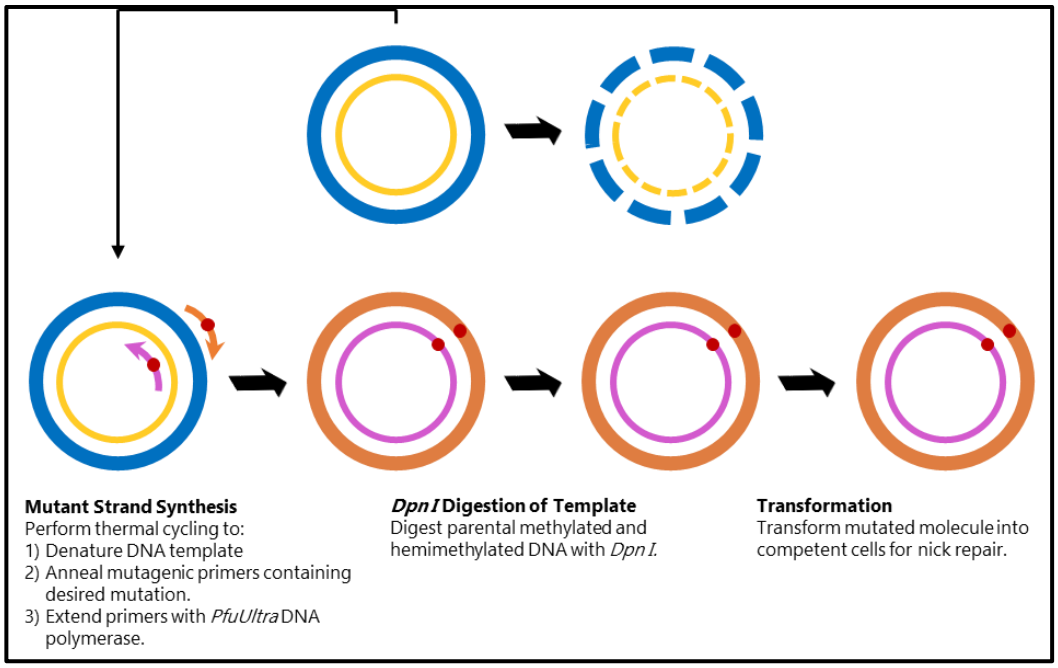

Figure 29: A flow chart for site-directed mutagenesis.
Adapted from [481].

2.12.1 Primer design guidelines for SDM

The list of the primers used is summarised in **Table 6**. The mutagenic oligonucleotide primers was designed individually using primer design software for Quick-change SDM and following the protocol's primer design guidelines:

1- Primers should be between 25 and 45 bases in length, have ≥ 40 % GC content, and a melting temperature (Tm) of ≥ 78°C. Tm does not include the substituted, inserted or deleted bases.
2- The desired mutation should be in the middle of the two complementary oligonucleotide primers, with ~10–15 correct oligonucleotide sequence at each side. It is preferable that the primers terminate with one or more C or G bases to increase the chance of annealing.

The human *CCL5* promoter was analysed by TFBIND software for ZEB2 (SIP1) binding sites. Two ZEB2 binding sites (GCTCACCTCC and GCACGTGGA) were found **(see figure 62 and 65).** From there, *CCL5* promoter ZEB2BOX1 and - *CCL5* promoter ZEB2BOX1 2 primers were designed for the SDM study by substituting the middle four bases with adenine bases to observe the maximum effect of mutation as previously determined by[482].

Table 6: List of the primers used for SDM (Site-Directed Mutagenesis).

Primer	Mutated Sequence (5'-3')	Supplier
CCL5 Promoter ZEB2BOX1-SDM- Forward	AGTGTGAGTGTGCTAAAATCCTTTGGGGACTG	Sigma
CCL5 Promoter ZEB2BOX1-SDM- Reverse	CAGTCCCCAAAGGATTTTAGCACACTCACACT	
CCL5 Promoter ZEB2BOX2-SDM- Forward	GGATCAAGACAGAAAAAGGACCTCGCACAG	Sigma
CCL5 Promoter ZEB2BOX2-SDM- Reverse	CTGTGCGAGGTCCTTTTTCTGTCTTGATCC	

2.12.2 Sample Reaction and Transformation

Two sample reactions for *CCL5* promoter ZEB2BOX1 and *CCL5* promoter ZEB2BOX2 were prepared to study the mechanistic effect of SIP1 protein on the *CCL5* promoter.

The components of the reactions were added in order as follows:

- 5 µl of 10× reaction buffer
- 50 ng of PGL3 *CCL5* promoter plasmid + dH_2O to a final volume of 50 µl.
- 125 ng of oligonucleotide forward primer + 1 µl of *PfuUltra* HF DNA polymerase (2.5 U/µl).
- 125 ng of oligonucleotide reverse primer
- 1 µl of dNTP mix

The reactions were then placed in a PCR thermocycler Cycle at the following condition:

1- 95°C for 5 min

2- 95°C for 30 sec Step 2-4 repeat 12 cycles

3- 55°C for 1 min

4- 68°C for 7 min*

*The time depends on plasmid length (1 min/Kb). In our case pGL3 vector + insert= 6.5 Kb.

After the amplification, the reactions were placed on ice for 2 min to cool the reaction. Then, 1 µl *DpnI* enzyme (10 U/µl) was added to each tube, mixed well, and incubated at 37°C for 1 hour to degrade the parental supercoiled plasmid. Finally, 1 µl of the *Dpn I* treated DNA from each sample reaction was transformed using the same protocol that was explained previously in **section 2.8.4.**

2.13 Promoter reporter assay

2.13.1 Main principle

The primary objective of the promoter reporter assay is to quantify the strength of promoter activity by measuring light output from a reporter that is translated under a particular promoter. The luciferase gene is one of the commonly used reporter genes which is isolated from the *firefly* "*Photinus pyralis*". The luciferase enzyme encoded by this gene oxidises D-luciferin in the presence of ATP, O_2 and Mg^{2+}. This reaction yields a light that is proportional to the amount of steady-state luciferase enzyme protein levels within a transfected cell population. As a reference for normalising gene expression in transfected cells, the Renilla luciferase reporter plasmid can be used. Renilla luciferase is an enzyme obtained from *Renilla reniformis*, and it oxidises the coelenterazine substrate and as a result, light is emitted. The ratio of Firefly Luciferase: Renilla Luciferase is then calculated which represents the precise activity of the promoter of interest [483, 484]; **see figure 30.**

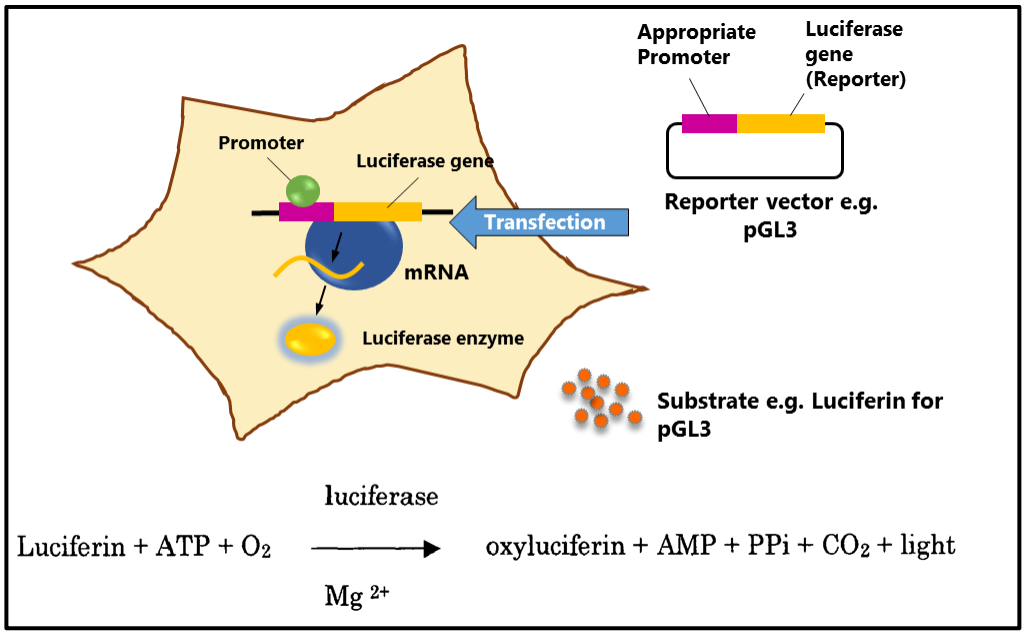

Figure 30: General principle of the Luciferase assay.
Adapted from [485].

2.13.2 Protocol of the luciferase reporter assay

The dual-Luciferase® reporter assay system (Promega; catalogue no: E1910) was used to measure *CCL5* promoter activity in un-induced and induced DLD-SIP1 or A431-SIP1 cells, as well as SW620 and SW480 cells under steady state conditions. Briefly, ~ 10,000-20,000 cells were seeded in each well of a 96-well plate. Of note, the *SIP1* gene in DLD-SIP-1 and A431-SIP1 cells were induced for three days before used. Next day, the cells were transfected with either pGL3, pGL3-CCL5 promoter, pGL3-CCL5 promoter ZEB2EBOX 1, PGL3-CCL5 promoter ZEB2EBOX 2, PGL3-CCL5 promoter SDM-ZEB2EBOX 1 or PGL3-CCL5 promoter SDM-ZEB2EBOX 2 (100 ng /well) using Lipofectamine 3000 reagent; please refer to **section 2.9.1** for the transfection protocol. To account for any variability in transfection between wells, 2-5 ng Renilla Luciferase Reporter plasmid was also transfected in each well. The day after the transfection, *CCL5* promoter activity was detected. Before starting the protocol, all luciferase reagents supplied by the kit including 5 x Passive Lysis Buffer (PLB), Luciferase Assay Substrate (LAS) and 1X Stop & Glo® Substrate (SGS) were prepared as recommended by the manufacturer. Subsequently, the growth media from cells was removed and the transfected cells were rinsed once with 1 x PBS. The transfected cells were lysed using 40 µl of 1 x PLB and gently shaken for 15 min at RT. Immediately, 60 µl of luciferase LAS was dispensed to each well using a multichannel pipette and the Firefly luciferase enzyme activity was measured within 1 min using a luminometer (Thermo Scientific). Following

that, 60 µl of SGS was dispensed to each well and Renilla luciferase activity was measured using the same luminometer device.

The ratio of Firefly: Renilla luciferase activities were then analysed using Microsoft Excel. The percentage of increase of *CCL5* promoter activity in SIP1 induced cells and SW480 were calculated and compared to un-induced cells and SW620, respectively.

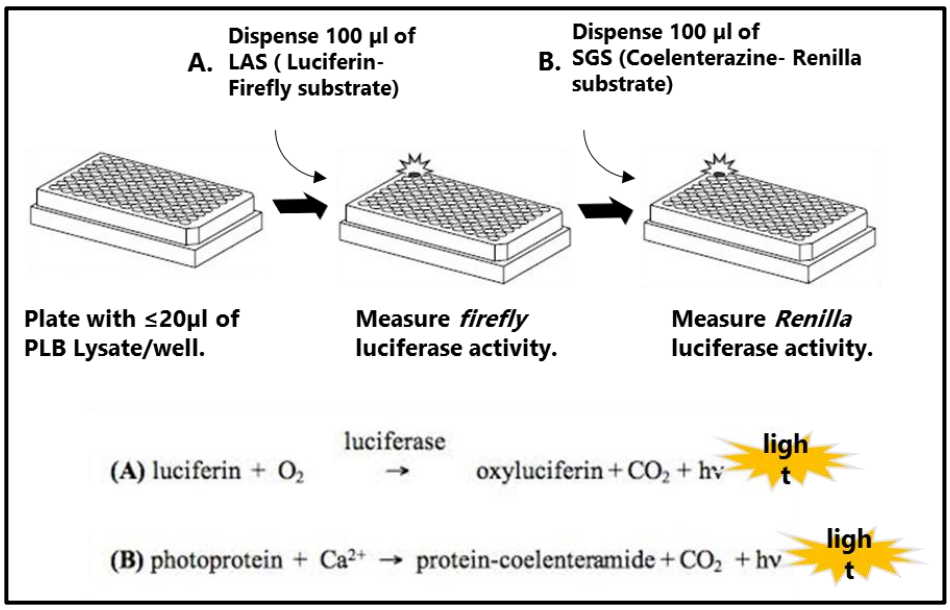

Figure 31: The Luciferase protocol for a 96-well plate.

First, the transfected cells harbouring pGL3 or Renilla reporter plasmids are lysed with PLB (passive lysis buffer). Next, A) the firefly (FF) luciferase activity is measured by adding luciferase assay substrate (LAS). The emitted light is detected using a luminometer device within 1 min. After that, B) the Renilla (RN) luciferase activity is measured immediately by adding Stop & Glo® Substrate (SGS). The emitted light is detected using the same luminometer device within 1 min. The final result is calculated as a ratio of FF: RN. Adapted from the Promega product manual [486].

2.14 Chromatin Immunoprecipitation (ChIP)

ChIP is a demanding but useful technique to investigate the localisation of proteins bound to specific DNA loci, including transcription factors and co-regulatory proteins. The protein/DNA interactions are first stabilised and preserved by cross-linking using formaldehyde fixative solution. The DNA is then sheared into small and uniform fragments by either sonication or enzymatic digestion. Following that, the fragments containing the specific protein/DNA complexes are immune-precipitated using high quality antibodies directed against the target-bound proteins of interest, efficient precipitation reagents (usually protein A or G beads), specialised buffers, inhibitor cocktails and blocking reagents to reduce both non-specific binding and protein

degradation. After immunoprecipitation, the cross linking between DNA and protein is reversed. The proteins are then degraded using Proteinase K and the DNA fragments analysed by PCR (**see figure 32).**

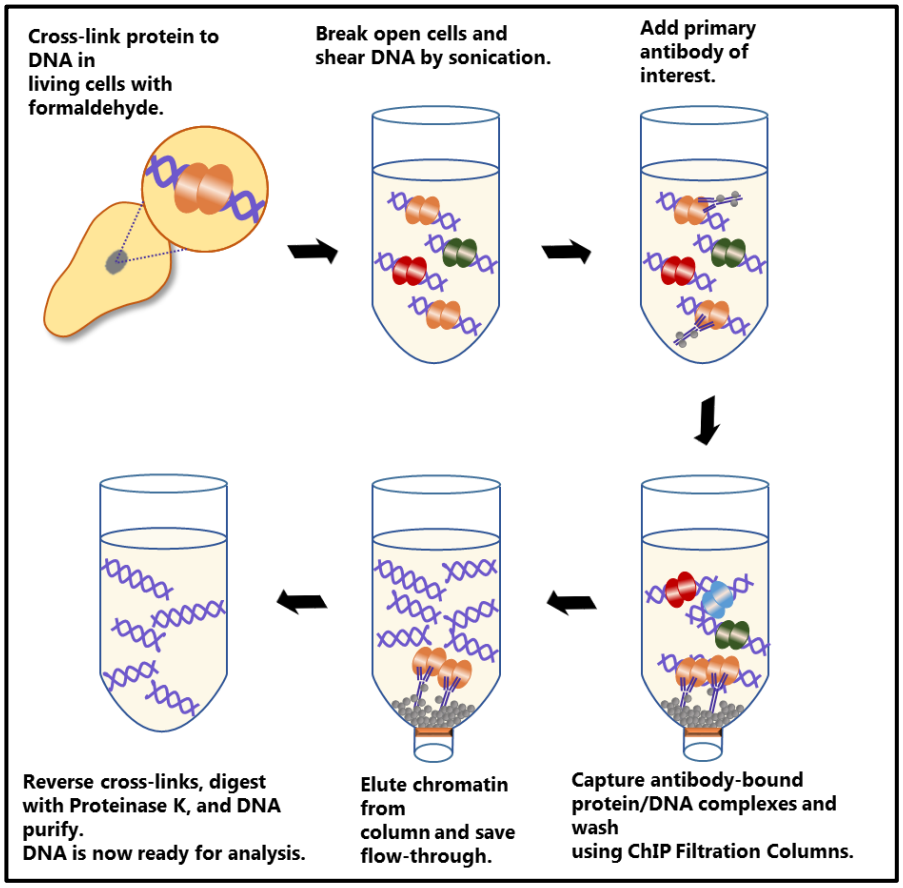

Figure 32: A flow chart showing the main steps in chromatin immunoprecipitation (ChIP). Adapted from [487]

2.14.1 Optimising the shearing condition for DLD-SIP1 cells

Optimisation of sonication for DLD-SIP1 cells had been validated before proceeding the with ChIP assay.

The optimisation was done following the steps in appendix section A, B and C of the ChIP-IT Express Kit (catalogue no. 53008).

2.14.2 Cell fixation to optimise shearing conditions

The SIP1 protein in DLD-SIP cells was induced for 3 days using 2 µg/ml doxycycline. Three 10 cm dishes for both induced and un-induced cells were grown to 80-90% confluency. The growth medium was then removed and 8 ml of fresh Fixation Solution

(1.62 ml of 37% formaldehyde to 60 ml minimal cell culture medium) was added and agitated gently at room temperature for 15 min. After that, the fixation solution was removed and the excess was washed off by adding 10 ml ice-cold 1x PBS. Following that, the fixation reaction was stopped by adding 5 ml Glycine Stop-Fix Solution (mixture of 3 ml of 10x Glycine buffer (5M, pH 8.0), 3 ml 10x PBS and 24 ml dH_2O). After mixing well and 5 min incubation at RT, the Glycine Stop-Fix Solution was discarded and the plates were washed with 10 ml ice-cold PBS. The cells were then scraped with a rubber policeman after removing the PBS and adding 2ml ice-cold Cell Scraping Solution (1.8 ml 10x PBS to 16.2 ml dH_2O), supplemented with 40 µl 100 mM PMSF. The cells from all the 3 plates of un-induced or induced DLD-SIP1 cells were pooled in one 50 ml conical tube and pelleted down by centrifugation at 2400 x g at 4ºC for 3 min. The supernatants were discarded and the pellets were re-suspended in 2 ml ice-cold lysis buffer supplemented with 15 µl Protease Inhibitor Cocktail (PIC, supplied with the kit) and 15 µl 100 mM Phenylmethylsulfonyl fluoride (PMSF), mixed gently, incubated on ice for 30 min, transferred into an ice-cold dounce homogenizer (tight fitting pestle) and homogenised with 30 strokes to aid nuclei release. The homogenised cells were then collected in 1.5 ml Eppendorf tubes and centrifuged at 2,400 x g at 4ºC for 10 min to pellet the nuclei. The supernatants were carefully removed and the pellets were re-suspended in 1.5 ml shearing buffer supplemented with 15 µl PIC and 15 µl 100 mM PMSF, mixed gently by pipetting up and down and aliquoted into equal volumes of 250 µl. Six aliquots of un-induced or induced DLD-SIP1 cells were sheared using a sonication device under the following conditions:

- One pulse of 20 seconds, with a 30 second rest on ice at 1.0 output.
- Two pulses of 20 second each, with a 30 second rest on ice between each pulse at 1.0 output.
- Three pulses of 20 second each, with a 30 second rest on ice between each pulse at 1.0 output.
- Five pulses of 20 second each, with a 30 second rest on ice between each pulse at 1.0 output.

- Eight pulses of 20 second each, with a 30 second rest on ice between each pulse at 1.0 output.
- Ten pulses of 20 second each, with a 30 second rest on ice between each pulse at 1.0 output.

The sheared chromatin was then centrifuged for 10 min at 18,000 x g in a 4°C centrifuge, and 50 µl of each sheared chromatin supernatant was aliquoted into 1.5 ml Eppendorf tubes. These were used to determine the shearing efficiency using different number of pulses. All remaining optimal preparations were frozen at -80°C for future use after adding 15 µl PIC and 15 µl 100 mM PMSF.

2.14.3 DNA clean up to assess shearing efficiency and DNA concentration

The saved 50 µl aliquots of each sheared chromatin samples were mixed with 150 µl dH_2O and 10 µl NaCl, and placed in a thermocycler at 65°C overnight to reverse the DNA-protein cross linking. The next day, 1 µl RNase A was added to each sample and incubated at 37°C for 15 min to digest the RNA. Following that, 10 µl of 0.5µg/µl Proteinase K was added and the samples were incubated for 2 hours at 42 °C to digest proteins. To clean up the DNA, 200 µl of phenol/chloroform (TE saturated, pH 8) was added to each sample, vortexed to mix completely and centrifuged at the maximum speed for 10 min. The aqueous layer containing the DNA was transferred into a new 1.5 Eppendorf tube, 20 µl of 3M sodium acetate pH 5.2 and 500 µl absolute ethanol were added immediately, mixed well and placed at -20°C overnight to aid DNA precipitation. After the overnight incubation, the samples were centrifuged in a 4°C centrifuge at 13,000 rpm for 10 min to pellet the DNA. Carefully, the supernatants were discarded and the pellets were washed with 500 µl 70% ethanol. The mixture was then spun at the maximum speed at 4°C for 5 min, supernatants were removed and the pellets were air dried and re-suspended in 30µl water. Finally, 16 µl of each sheared DNA sample was mixed with 4 µl of 6x DNA loading buffer and, from that, a 5 µl or 10 µl mixture was analysed using agarose gel electrophoresis (1 % gel).

2.14.4 Active Motif's ChIP-IT® High Sensitivity kit

Active Motif's ChIP-IT® High Sensitivity kit (catalogue no. 53040) was chosen to preform ChIP because it provides the highest quality ChIP-enriched DNA, and it is ideal to detect specific binding with even a low abundance transcription factor or when using low-

affinity antibodies. In addition, it gives reproducible results with multiple sample types and can be performed from as little as 100 cells. The immune reaction is precipitated using Protein G agarose beads which are then filtered through a specific column. This is an advance way which makes the procedure easier and consistent compared to the ChIP-IT® express kit that contains Protein G magnetic beads.

Of note, most of the components and buffers are supplied by the company and they are ready to use except Complete Cell Fixation Solution (For 2.5 ml: add 180 µl fixation buffer+1.57 ml dH_2O+ 750 µl 37% formaldehyde solution containing 10% methyl alcohol).

In general, the procedure is divided into 5 sections:

- Cell fixation
- Chromatin sonication
- Input preparation and chromatin size validation
- Immunoprecipitation
- Reverse cross-linking
- Semi-qualitative PCR

2.14.5 Fixation of cultured cells

The SIP1 protein in DLD-SIP stable inducible model was induced for 3 days using 2 µg/ml doxycycline. Three 10 cm^2 dishes for each induced and un-induced cells were grown to 80-90%. Each plate was fixed with 1ml freshly prepared Complete Cell Fixation Solution (1/10th of growth medium volume) and agitated gently at room temperature for 15 min. The fixation solution was stopped by adding 550 µl of Stop Solution (1/20th of growth medium volume) and shaken gently at RT for 5 min. Following the incubation, the cells of the 3 plates for each single cell type were scraped using a rubber scraper and collected into pre-chilled 50 ml conical falcon tubes. The cells were then pelleted by centrifugation at 1250 x g at 4ºC for 3 min. The supernatants were discarded and the pellets were washed twice with 15 ml ice-cold PBS, re-suspended by pipetting up and down, centrifuged at 1250 x g at 4ºC for 3 min. Finally, each pellet were re-suspended in 15 ml Chromatin prep buffer supplemented with 15 µl Protease Inhibitor Cocktail (PIC) and 15 µl 100 mM Phenylmethylsulfonyl fluoride (PMSF), mixed gently and incubated on ice for 10 mins. Each 5 ml of 15 ml re-suspended pellets of either induced or un-induced cells were transferred into a chilled dounce homogenizer (tight fitting pestle), homogenized with 30

strokes, collected into new 15 ml conical tubes and centrifuged at 1250 x g at 4ºC for 3 mins. To ensure cell lysis is complete, 10 µl of the cell lysate was inspected using a haemocytometer and a phase contrast microscope.

Following the centrifugation, the supernatants were discarded and the pellets were re-suspended in 1.5 ml ChIP buffer supplemented with 15 µl PIC and 15 µl 100 mM PMSF, mixed gently by pipetting up and down and incubated on ice for 10 min before proceeding to chromatin sonication.

2.14.6 Chromatin sonication

After optimising the conditions for DLD-SIP1 cells that was achieved **in section 2.14.1,** aliquots of 250 µl of fixed un-induced and induced DLD-SIP1 nuclei that were collected from **2.14.6** were sonicated at 1.0 output with 3 pulses of 20 second each, with a 30 second rest on ice between each pulse. To pellet the cellular debris, the sonicated samples were centrifuged at 4°C and 18,000 x g for 2 min. From that, 25 µl of each sample was set aside in a chilled 250 µl PCR tube to be processed as input, and the remaining sheared chromatin was stored at -80°C for chromatin immunoprecipitation.

2.14.7 Input preparation

To each 25 µl, that was saved **in section 2.14.7,** 175 µl of TE buffer (10 mM Tris-HCl, 1 mM disodium EDTA, pH 8.0) and 1 µl of RNase A were added, mixed well and incubated at 37°C for 30 min. After that, 2 µl Proteinase K was added, mixed well and incubated in a thermocycler at 55°C for 30 min where the enzyme can degrade proteins and then inactivated at 80°C for 2 hours. Following that, to enhance DNA precipitation, 83 µl Precipitation buffer (supplied with the kit), 2 µl carrier (supplied with the kit) and 750 µl 100% ethanol were added, vortexed and placed at -80°C overnight. Next day, the samples were pelleted by centrifugation at 18,000 x g for 15 min at 4°C. Without disturbing the pellets, supernatants were removed and the pellets were washed with 500 µl 70% ethanol, spun in a 4°C centrifuge at 18,000 x g for 5 min. The supernatants were then discarded whilst any residual ethanol was removed by a pipette tip leaving the tubes uncapped to air-dry the pellets for 15-30 min.

When the pellets dried and all residual ethanol had completely evaporated, they were re-suspended in 25 µl DNA Purification Elution buffer (Supplied with the Kit), incubated at RT for 10 min and mixed well. This suspension contains the input DNA. The DNA

concentration of each input was measured by a NanoDrop device at 260 nm and stored at -20°C until required.

2.14.8 Examining the size of sheared chromatin

To further check, 500 ng of the inputs were mixed with 1 µl of 500 mM NaCl, made up to 10 µl with dH_2O and boiled at 100°C for 20 mins followed by gradually decreasing the temperature to 50°C. Finally, the samples were incubated at RT for 5 min and then loaded on a 1.5% agarose gel including the DNA ladder. DNA should appear as a smear between 200-1200 bp. If the size of the input preparations were successful, the stored aliquoted chromatins at -80°C from **section 2.14.7** can be used to perform immunoprecipitation reactions.

2.14.9 Chromatin immunoprecipitation

First, the sonicated chromatins containing correct size DNA fragments (200-1200 bp.) were thawed on ice, spun at 4°C at 18,000 x g for 2 min and then ChIP reaction set up in a 1.5 ml Eppendorf by adding the components in the following order:

- 10-30 µg Sheared chromatin
- Top up to 200 µl ChIP buffer
- 1 µl Protease Inhibitor Cocktail (PIC)
- 4 µg Antibody*
- 5 µl Blocker mix Total Volume 240 µl

* To enhance the antibody affinity, add 2 µg from the main antibody + 2µg mouse IgG bridging antibody.

The antibodies used in this project, their purpose and suppliers are summarized in **Table 7.**

Table 7: List of the antibodies used for ChIP (Chromatin Immunoprecipitation).

ChIP antibody	Concentration used	Purpose	Supplier
Human anti-mouse IgG (Stock conc.0.2 µg/µl)	4 µg	Negative control	Active Motif. ChIP-IT® Control kit catalogue no. 53010
Bridging antibody anti-mouse (stock conc. 1.0 µg/µl)	2 µg	To improve the binding of protein G beads to mouse IgG primary antibodies.	Active Motif. ChIP-IT® Control kit catalogue no. 53010
RNA Pol II human anti-mouse monoclonal (Stock conc. 0.2 µg/µl)	2 µg + 2 µg anti-mouse Bridging antibody	Positive control	Active Motif. ChIP-IT® Control kit catalogue no. 53010
Human anti-mouse monoclonal c-MYC (Stock conc.)	2 µg + 2 µg anti-mouse bridging antibody	SIP1 targeted antibody (tagged domain)	Sigma
Human anti-mouse polyclonal SIP1 antibody	2 µg + 2 µg anti-mouse bridging antibody	SIP1 targeted antibody	In house

The ChIP reaction was incubated overnight on an end-to end rotator at 4°C. Next day and before proceeding to the next step, Protein G agarose beads were washed twice with TE buffer pH 8.0, as instructed by the manufacturer. Then, 30 µl of the washed beads were added to each reaction tube and incubated again on an end-to-end rotator at 4°C for at least 3 hours.

In the meantime, ChIP filtration columns were labelled and placed in an empty 1 ml pipette tip box as a holder. After that, the ChIP reactions were placed on ice and 600 µl ChIP buffer were added, mixed well, loaded onto the columns and allowed to flow by gravity. The columns were then washed five times with 900 µl wash buffer (AM1, supplied with the kit). Once the flow through had passed, the column was rested for 3 mins before adding the next wash. At the final wash, each column was placed in a new 1.5 ml Eppendorf tube and centrifuged at 1250 x g for 3 min to remove residual Wash Buffer. Following centrifugation, the columns were placed in new 1.5 ml tubes, and the ChIP DNA were eluted with 100 µl pre-warmed (37°C) Elution Buffer (AM4 ,Supplied with the kit), spun in a RT centrifuge at 1250 x g for 3 min. At this point, the eluted chromatin was placed on ice to proceed with reverse cross-linking and DNA purification steps.

2.14.10 Reversal of cross-links and DNA purifications

Each eluted ChIP chromatin was transferred into 250 µl PCR tubes, and 2 µl Proteinase K was added, mixed and incubated at 55°C for 30 min to degrade the proteins followed by another incubation at 80°C for 2 hours to inactivate it. After that, 500 µl of DNA Purification Buffer was added in the tubes, mixed well and the pH was adjusted to be acidic addition of 3M sodium acetate. The mixture of each reaction was then added in its own labelled DNA Purification column, capped and centrifuged at 14,000 x g for 1 min. The flow-through was discarded, and the columns were washed once with 750 µl DNA Purification Wash Buffer containing 70% absolute ethanol. The columns were spun twice at 14,000 x g for 1 min to remove any residual alcohol. Finally, the columns were transferred into new 1.5 ml collection tubes and the DNA was eluted by adding 100 µl of DNA Purification Elution Buffer and centrifuging at 14,000 x g for 1 min. This step is repeated to have ~200 µl as a total elution volume. Eluted DNA can be stored at -20°C or used immediately for downstream applications such as quantitative, qualitative PCR, ChIP-Seq or ChIP-on-chip analysis.

2.14.11 Semi-qualitative PCR for ChIP analysis

2.14.11.1 **Primers Used**

The PCR primers used in this study are summarized in in **Table 8.**

The PCR was performed in the same manner that was previously explained **in section no. 2.3.3**.

Table 8: The primers used to preform PCR for ChIP assay.

Oligo Name	Sequence (5'-3')	PCR condition	Product Size	Purpose	Supplier
GAPDH Promoter Forward	Information Disclosed by the supplier	94°C for 30 second 59°C for 30 second 72°C for 30 second For 40 cycles	180 bp	Positive ChIP control primer for RNA Pol II binding site	Active Motif. ChIP-IT® Control kit catalogue no. 53010
GAPDH Promoter Reverse	Information Disclosed by the supplier				
E-cadherin Promoter Forward	GGCCGGCAGGTGAAC	94°C for 30 second 55°C for 30 second 72°C for 10 second For 40 cycles	147 bp	Positive product for SIP1 protein binding site	Sigma
E-cadherin Promoter Reverse	GGGCTGGAGTCTGAAGTGAC				
PKP Promoter Forward	GCGACAAAGCCTGACTAACCA	94°C for 30 second 55°C for 30 second 72°C for 30 second For 40 cycles	138 bp	Positive product for SIP1 binding site	Sigma
PKP Promoter Reverse	GGATGGATTTCCGCTCGAT				
CCL5 E-BOX1 Forward	GGGCCAGCCTGAGCTGCA	94°C for 30 second 55°C for 30 second 72°C for 10 second For 40 cycles	178 bp	To examine SIP1 protein bind to CCL5 promoter	Sigma
CCL5 E-BOX1 R Reverse	GGTGGTCAAGACCAGGACT				
CCL5 E-BOX2 Forward	CTATGCTGCTTCATGGCAG	94°C for 30 second 55°C for 30 second 72°C for 30 second For 40 cycles	169 bp	To examine SIP1 protein bind to CCL5 promoter	Sigma
CCL5 E-BOX2 Reverse	CTGCTGACAGGCATGAGTC				

2.15 **Immunohistochemistry (IHC)**

IHC is a technique for signifying the presence and location of proteins in tissue or cellular specimens. It helps in recognising the target protein by a highly specific antibody. The antibody-protein interaction is then visualised by a secondary antibody conjugated to an enzyme (e.g. usually horseradish peroxidase (HRP) or alkaline phosphatase (AP)) or a fluorescent dye.

Briefly, the basic steps of IHC are as follows:

- Specimen fixation and embedding into wax.
- Cutting the block into thin (1-10 µm) sections.
- Dehydrating, deparaffinising and rehydrating.
- Antigen retrieval to expose epitopes masked by fixation (by enzyme or heat).
- Section immunostaining.
- Nuclei staining by Mayers Haematoxylin counterstain.
- Mounting.
- Analysing the stained section for the expression of desired proteins using a microscope.

All IHC was done at the Histochemistry Research Unit, University Hospital Southampton. Human Specimens were collected from patients who had undergone surgery for CRC at University Hospital Southampton. Approval from the Ethics Committee and Trust Research and Development were obtained from patients in the form of written consent for each case.

Mice Specimens were collected from mice that had undergone orthotropic CRC surgery. All animal procedures were performed by Mr. Rahul Sreekumar, a clinical academic doing his PhD. with my supervisor, in parallel with his experiments. All protocols and procedures were covered by Mr. Sreekumar's personal license and the project license (owner Mr. Alex Mirnezami).

2.15.1 Tissue microarray (TMA)

TMA is a useful and rapid tool for high-throughput analysis of multiple specimens. It is possible to obtain large amounts of data without experimental variability from a single

immunostaining protocol. It also saves on reagent cost and laboratory processing time [488]

2.15.2 Production of tissue microarrays, immunohistochemistry staining and digitalisation

TMA production was purchased as a service from the Histochemistry Research Unit, University Hospital Southampton under the supervision of Dr. Emre Sayan and Dr. Karwan Moutasim.

The TMA was prepared to compare tumour infiltrated lymphocyte (TILs) (including T-helper, T-cytotoxic and T-regulatory cells) between two groups with previously known SIP1 status by our research group.

Seventy five consecutive CRC Tumour Specimens (stage IV) were selected and then blocks with known SIP1 status were selected as categories in two groups: 25 blocks with SIP1-negative group and 25 blocks with SIP1-highly positive group and the remaining 25 as mixed SIP1 status.

Whole sections from each Stage IV adenocarcinoma CRC block were stained with Haematoxylin and Eosin (H&E), and reviewed by a pathologist to select invasive areas. Subsequently, the TMA was prepared by punching and assembling the blocks using a semiautomatic array machine (ALPHELYS MiniCore 3, Plaisir, France) with 1 mm punch core at the pre-selected regions representing the core and invasive front of each tumour.

TMA sections were then immunostained by a histostaining instrument (Autostainer XL, Leica) using primary antibodies for different T-cell subpopulations (CD3, CD4, CD8 and FOXP3 cells), which were validated by the cellular pathology group at the hospital for use in immunohistochemistry (**see table 9**). This was followed labelling with a horse radish peroxidase-polymer secondary antibody and, finally counterstained with Mayers Haematoxylin stain. The TMA slides then mounted on a coverslip using an automated system (Automated glass coverslipper CV5030, Leica).

Finally, the slides were scanned by an automated scanner system Aperio XT (Aperio Technologies). CD3, CD4, CD8 and FOXP3 expression was subsequently scored by two independent pathologists blinded to the SIP1 status. Each stained core was scored semi-quantitatively as following: Absent ≤ 25%; Low intensity 25-50%; Medium intensity 50-75%; High intensity ≥ 75%; **see figure 33.**

Table 9: List of the antibodies used in the TMA (Tissue Microarray).

IHC Primary antibody	Purpose of use	Supplier
CD3	T-cells pan marker	Dako
CD4	T-helper cell marker	Dako
CD8	Cytotoxic T-cell marker	Dako
FOXP3	Regulatory T-cell marker	Dako
CCL5	Chemoattractant agent for T-cells	R&D systems.

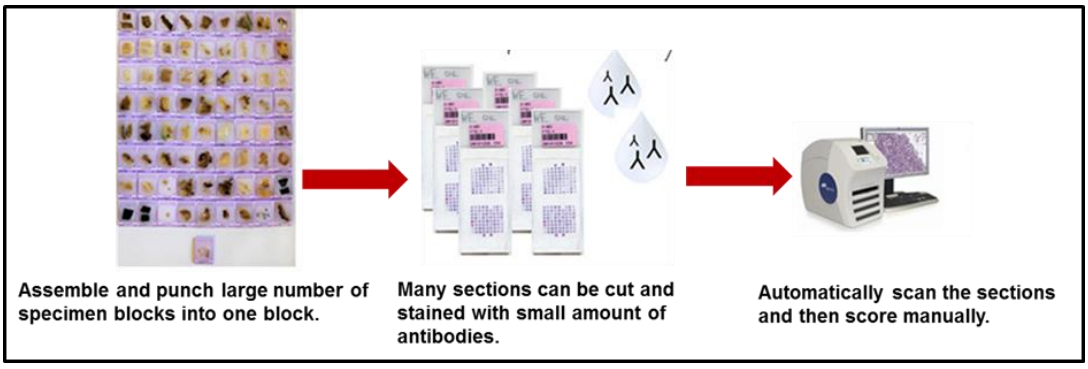

Figure 33 A flow chart illustrating the process of TMA (Tissue Microarray).
Adapted from:[489].

2.16 Generating stably transfected cell lines

Generating stably transfected cell lines enables cells to be generated which express the protein of interest for a longer period of time in comparison to transient transfection where maximal gene expression is observed for only 24-96 hours. This technology can be achieved by using eukaryotic antibiotic selection such as neomycin, zeocin or blasticidin. The selection of antibiotic depends on either the plasmid construct containing the gene of interest (in cis) or on a separate plasmid co-transfected with the plasmid containing the gene of interest (*in Trans*). The cis approach is usually easier and has a higher probability for the positive selection of clones (ref- Mirus Generation of Stable Cell Lines protocol online).

In general, the protocol requires the flowing steps:

- Preparation of plasmid containing the desired gene of interest.
- Antibiotic kill curve to identify the optimum antibiotic concentration to achieve maximum death of un-transfected cells.
- Cell transfection with the plasmid containing the desired gene.
- Selection and expansion of stable polyclonal colonies.
- Identification and expansion of single clones.
- Validation of gene expression.
- Expansion and freezing down the single clones with high gene expression.

In this project, the DLD-1 cell line was chosen to create a DLD-1 stably-transfected CCL5 using pcDNA3.1 CCL5 plasmid. The details of this experiment are explained below.

2.16.1 Preparation of pcDNA3.1 CCL5 plasmid stock

As previously explained in **section 2.8.**

2.16.2 Neomycin kill curve and cell transfection

It is a critical step to determine the optimal antibiotic dose required to kill cells which have not received the resistance plasmid.

In our case, 0.5 x 10^6 DLD-1 cells were seeded in each well of a 12-well plate until at ~60-80% confluency. After that, increasing concentrations of neomycin at 100, 200, 300, 400, 500 µg/ml were added to duplicate wells, leaving 2 wells with no Neomycin as a control. Neomycin was used because the pcDNA3.1-CCL5 construct contains the neomycin resistance gene see **figure 23.** Every day for maximum of one week, the cells were inspected for visual toxicity and the optimal dose was chosen.

2.16.3 Transfection of DLD-1 cells with pcDNA3.1-CCL5 plasmid

The cells were seeded in a 10 cm dish at ~ 60% confluency. They were then transfected with 5 µg/ml pcDNA3.1 CCL5 (main stock 0.9 µg/µl) by Lipofectamine 3000 reagent in the same way that was previously explained in section 2.9.1. Two days after transfection, the optimal dose of neomycin, 200 µg/ml (Sigma, Stock concentration 50 mg/ml), was added. The cells were checked daily to examine toxicity. Obviously, the cells that had not

integrated the CCL5 plasmid will die and the cells that incorporated the plasmid into their genome will survive for more than 7 days post-transfection.

2.16.4 Selection and expansion of stable polyclonal colonies

Survived cells were left for 2 weeks to expand, and during this period, the media was changed twice a week with media containing 200 µg/ml neomycin. Following this, stable clones with polyclonal cells were diluted further in order to obtain single cell clones.

2.16.5 Identification and expansion of single monoclonal clones

The polyclonal cells were further cultured at a density of 0.8 cells/well in a 96-well plate in media supplemented with 100 µg/ml neomycin. By doing this, there will be a high probability that some wells will only contain one cell whilst the remaining are empty. The wells containing 1 cell were then maintained and monitored for 2 weeks until they reached high confluency. The clones were then further expanded into 24-well plates and 6-well plates as they reached confluency.

2.16.6 Examination of CCL5 expression

Supernatants from the clones, which were growing in the 6-well plate at this stage, were collected from each well to assess the extracellular expression of CCL5 protein using the ELISA technique; for ELISA details please refer to **section 2.7.2.**

2.16.7 Expansion and freezing of single clones with high CCL5 expressing

After analysing CCL5 expression, single clones of DLD cells with high -CCL5 expression were expanded in a T75 flasks with low dose of antibiotic e.g. 50 µg/ml until they reached high cell densities. Once the clones were confluent, they were frozen in media lacking neomycin. For more details about freezing adherent cells please refer to **section 2.1.6.**

2.17 Animal experiments

All animal work has been carried out by Mr. Rahul Sreekumar, a PhD student supervised by Dr Emre Sayan. I acted as an observer for all procedures because I do not hold a personal license.

The DLD-1 CCL5 clone 4 and 16 were chosen for *in vivo* work. Five animals were used for each group. We chose the immune-deficient NOD/SCID strain of mice because we wanted to exclude the contribution of TILs to the metastasis of DLD cells. Two million cells/animal were prepared (trypsinised, counted and pelleted) for the day of injection, washed with PBS, re-suspended in100 µl PBS and placed on ice. The cells were mixed with an equal volume of Matrigel (BD biosciences) and kept on ice till injection.

The animals were operated on in a dedicated, sterile laminair hood. Isofluorane (2-4%) was used to induce and maintain anaesthesia. The animals were placed on a flat surface and limbs were immobilized by adhesive tape. The caecum was injected with 200 µl of cell/Matrigel mix and the surgical wound was closed by stitching. The animals were then left to recover in a heated resuscitation chamber and then placed back into their respective cages. After surgery, the welfare of animals was followed daily by Mr. Sreekumar and the Biomedical Research Facility staff. Fourteen weeks later, the animals were euthanized by excessive CO_2 inhalation and the caecum and livers harvested. The tissues were immediately passed to the histopathology unit of SGH and embedded in paraffin. Finally, multiple sections, potentially covering most of the organs were stained with an H/E and microscopically analysed by me, my supervisor and Mr. Sreekumar for the presence of primary and metastatic CRC.

2.18 **Statistical analysis**

A student's T-test was used to compare the two groups of results with equal variance that was obtained from CCL5 ELISA expression to calculate the *p* value and standard error.

Chapter 3: EMT Status in CRC

3.1 Introduction

EMT is a conserved and fundamental biological programme that contributes to development, tissue regeneration and cancer. EMT is described as a multistep program in which epithelial cells lose their close association and acquire phenotypic characteristics similar to mesenchymal cells [3]. During the EMT process, epithelial cells down-regulate proteins which are involved in tight junctions, adherent junctions, desmosomes and epithelial intermediate filaments such as cadherins, ZO1, integrins and cytokeratins. Destruction of these junctions leads to redistribution of other molecules at the cell surface and reorganisation of cell cytoskeleton proteins and up-regulation of ECM components [121, 280, 490]. For example, down regulation of E-cadherin, which is considered a hallmark of EMT in cancer metastasis [132, 159, 214, 491], causes the translocation of β-catenin from the cytoplasm to the nucleus which can then activate several EMT-inducing transcription factors [169]. The main transcription factors involved in regulating EMT are ZEB1/2, SNAIL1/2, TWIST1/2 and LEF-1. They are all implicated in facilitating suppression of epithelial gene expression and activating mesenchymal genes [108, 132, 209, 228, 247, 492, 493]. Mesenchymal cells are defined as single cells with a spindle shape having a front-back-end polarity and expressing mesenchymal protein such as vimentin and FSP-1. They are highly motile and invasive [149, 153]. Interestingly, not all cells undergo complete EMT. Instead, some cells undergo partial EMT with an intermediate or metastable phenotype. The intermediate phenotype is characterised by cells retaining some epithelial junctions and showing some of the mesenchymal features at the same time [111, 122-127].

3.2 The aim

In order to identify chemokines or cytokines that change because of EMT and to study the function of the selected molecules, correctly identifying the EMT status of a panel of CRC cell lines is necessary. Therefore, the aims of this chapter are:

1- Review the biological characteristics of 12 CRC cell lines (AAC1/82, CT26, Caco-2, Colo205, DLD-1, HCT116, HT29, LoVo, RKO, SW48, SW480, and SW620) and the

DLD-SIP1CRC-EMT model, and compare the morphological appearances as observed with a light microscope.

2- Identify the EMT status of the CRC panel and the CRC EMT model using mesenchymal and epithelial biomarkers, and a set of EMT-inducing transcription factors using Western blotting, IF and RT-PCR.

3.2.1 Results

3.2.2 EMT Status of CRC panel cell lines and EMT-CRC model

3.2.2.1 **Morphological appearance**

Pictures of the twelve cell lines and DLD-SIP1 CRC EMT were taken with a light microscope at 10X and 40X microscope objectives, and descriptions of the phenotype of each noted.

3.2.2.2 **Phenotype of the CRC panel cell lines**

The origin, morphology, oncogene expression, and supplier of the 12 CRC cell lines (AAC1/82, CT26, Caco-2, Colo205, DLD-1, HCT116, HT29, LoVo, RKO, SW48, SW480, and SW620) were reviewed from the literature and are summarised in **Table 10.**

Table 10: The biological characteristics and supplier of the CRC cell lines analysed.

Cell line	Organism	Source	Morphology	Oncogene	Depositors	Supplier
AAC1/82	*Homo sapiens*	From PC/colonic Adenoma cell line	Epithelial/ mixed, adherent and suspension	Not known	[494]	Gift-University of Bristol
CT26	*Mus musculus*	Undifferentiated colon carcinoma (BALB/c mouse)	Fibroblast/adherent	Not known	[495]	ATCC® CCL2638™
Caco-2	*Homo sapiens*	Colorectal adenocarcinoma (Dukes' type ND[α])	Epithelial /adherent	c-myc+; ras+; myb+; fos+; sis+; p53+abl- ; ros-; src-	[496, 497]	ATCC® HTB -37™
COLO205	*Homo sapiens*	Colorectal adenocarcinoma (Dukes' type D)	Epithelial mixed, adherent and suspension	c-myc+; ras+; myb+; fos+; sis+; p53+abl- ; ros-; src-	[497, 498]	ATCC® CCL 222™
DLD-1	*Homo sapiens*	Colorectal adenocarcinoma (Dukes' type C).	Epithelial/ adherent	c-myc+; ras+; myb+; fos+; sis+; p53+abl- ; ros-; src-	[497, 499, 500]	ATCC® CCL 221™
HCT116	*Homo sapiens*	Colorectal carcinoma	Epithelial with very few scattered mesenchymal cells/adherent	c-myc+; ras+; myb+; fos+; sis+; p53+abl- ; ros-; src- TGFβ1 and TGFβ2 Positive	[501]	ATCC® CCL -247™
HT29	*Homo sapiens*	Colorectal adenocarcinoma (Dukes' stage ND)	Epithelial / adherent	c-myc+; ras+; myb+; fos+; sis+; p53+abl- ; ros-; src-	[496, 497]1	ATCC® CCL -38™
LoVo	*Homo sapiens*	Colorectal adenocarcinoma Derived from a metastatic site (left supraclavicular region-Dukes' type ND)	Epithelial with many scattered mesenchymal cells/adherent	c-myc+; ras+; myb+; fos+; sis+; p53+abl- ; ros-; src-	[502]	ATCC® CCL229™
RKO	*Homo sapiens*	Poorly differentiated primary Colon carcinoma	Mesenchymal phenotype/ adherent	p53+	[503]	Packham Laboratory, University of Southampton-ATCC® CCL2577™

Cell line	Organism	Source	Morphology	Oncogene	Depositors	Supplier
SW48	*Homo sapiens*	Colorectal adenocarcinoma (Dukes' type C, grade IV)	Epithelial / adherent	c-myc+; ras+; myb+; fos+; sis+; p53+abl- ; ros-; src	[496, 497, 504]	ATCC® CCL 231™
SW480	*Homo sapiens*	Colorectal adenocarcinoma (Dukes' type B).	Mesenchymal	c-myc+; ras+; myb+; fos+; sis+; p53+abl- ; ros-; src	[496, 497] [505]	Not known
SW620	*Homo sapiens*	Colorectal adenocarcinoma Derived from a metastatic site (lymph node). The line was derived from the same tissue as SW480 (Dukes' type ND)	Epithelial with some scattered mesenchymal cells /adherent	c-myc+; ras+; myb+; fos+; sis+; p53+abl- ; ros-; src-	[496] [497, 505]	ATCC® CCL 227™

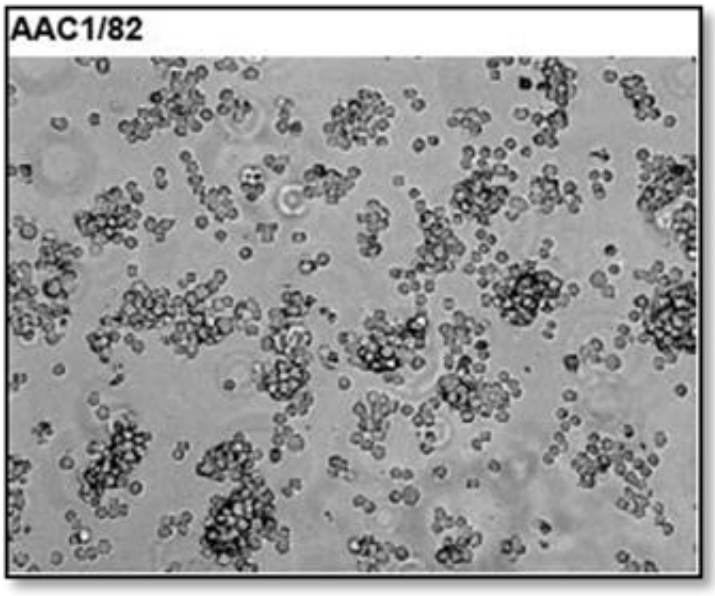

Figure 34: Morphology of AAC1/82 cells using a 10X objective.

ACC1/82 cells grow as a mixture of attached and floating cells. The attached cells are very small, round in shape and group in small epithelial islands. These cells had a very slow

growth rate; when the cells were seeded at 20% confluency it takes more than a week to reach 80% confluency; see **figure 34**.

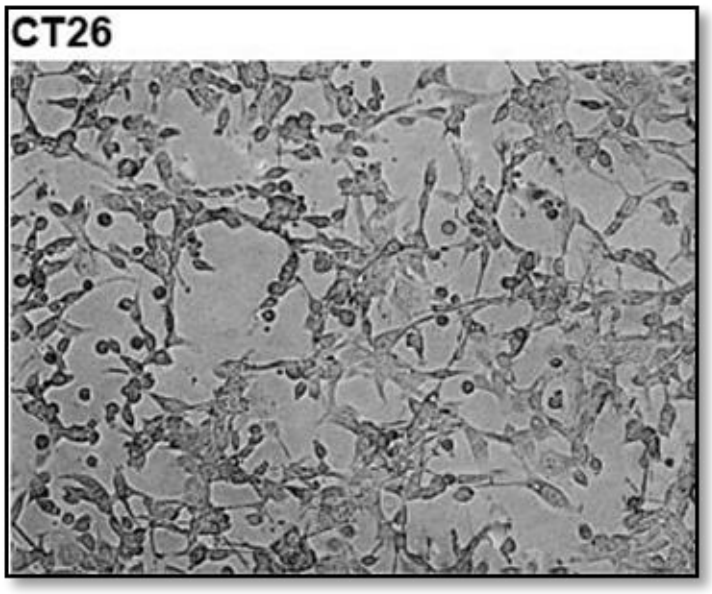

Figure 35: Morphology of CT26 cells using a 10X objective.

CT26 is a BALB/c mouse CRC cell line that was originated from a poorly differentiated cancer; **see table 10**. The cells are adherent, uniform, spindle and very elongated in shape resembling that of fibroblasts; **see figure 35.**

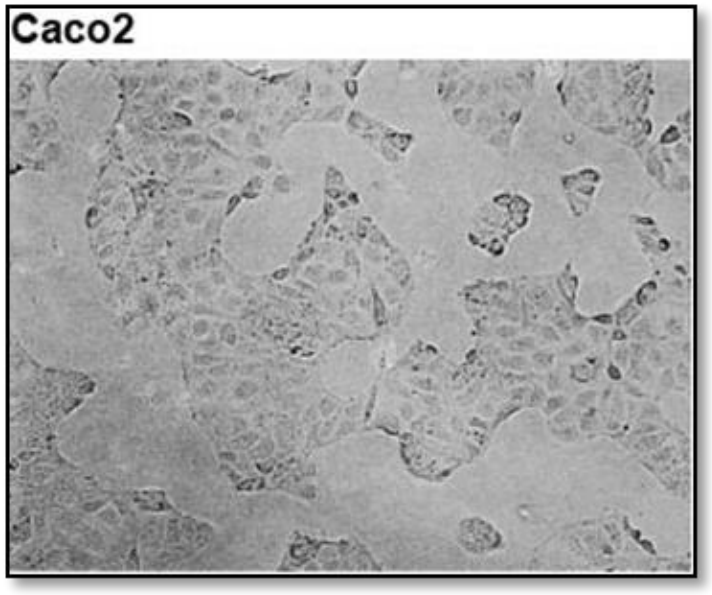

Figure 36: Morphology of Caco2 cells using a 10X objective.

Caco-2 is a human colorectal adenocarcinoma cell line; **see table 10.** The cells are adherent, and they grow as polarized tightly packed epithelial islands. The growth rate is

more than 24h/division and it forms a monolayer when it reaches 90% confluency; **see figure 36.**

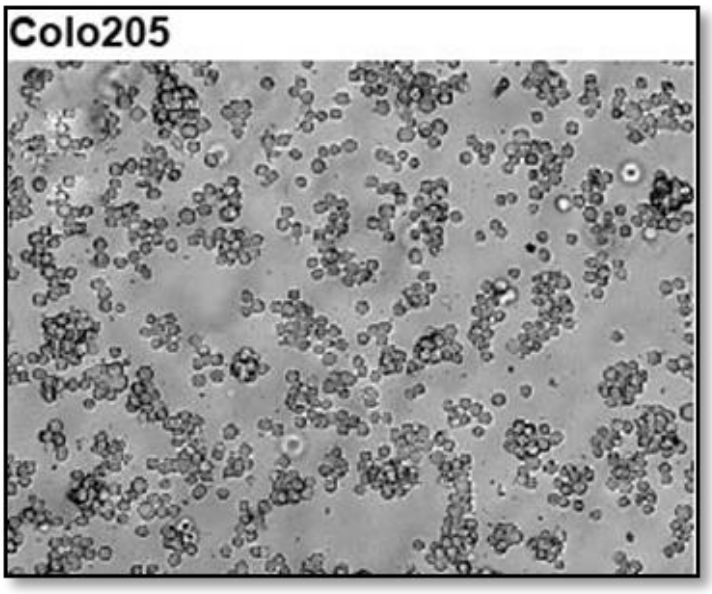

Figure 37: Morphology of Colo205 cells using a 10X objective.

The Colo205 cell line was derived from ascites fluid obtained from a male patient with colon adenocarcinoma of Dukes D stage; **see table 10**. This cell line looks similar to AAC1; small round cells proliferating slowly as a mixture of loosely attached epithelial islands and free-floating cells. Similarly, the growth rate was very slow and it took a week to become fully confluent; **see figure 37.**

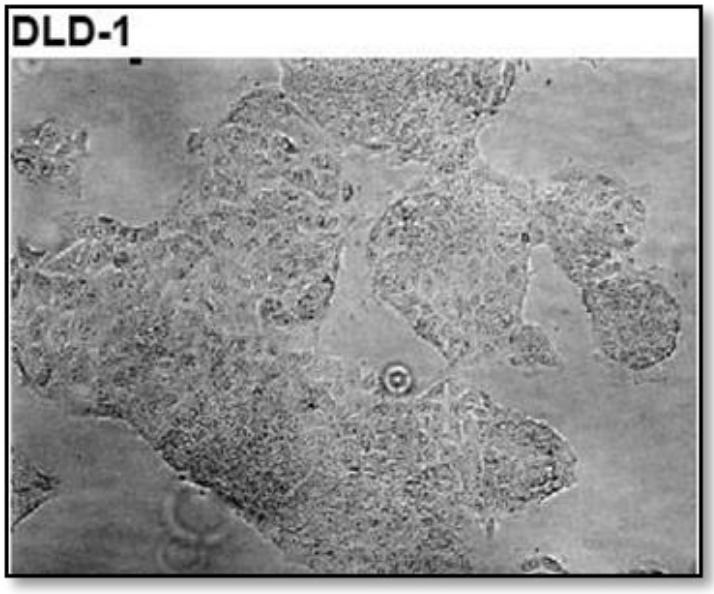

Figure 38: Morphology of DLD-1 cells using a 10X objective.

DLD-1 was established from a primary colon cancer; **see table 10.** The cells grow in large tightly packed epithelial islands. The population doubling time was ~ 24h; **see figure 38.**

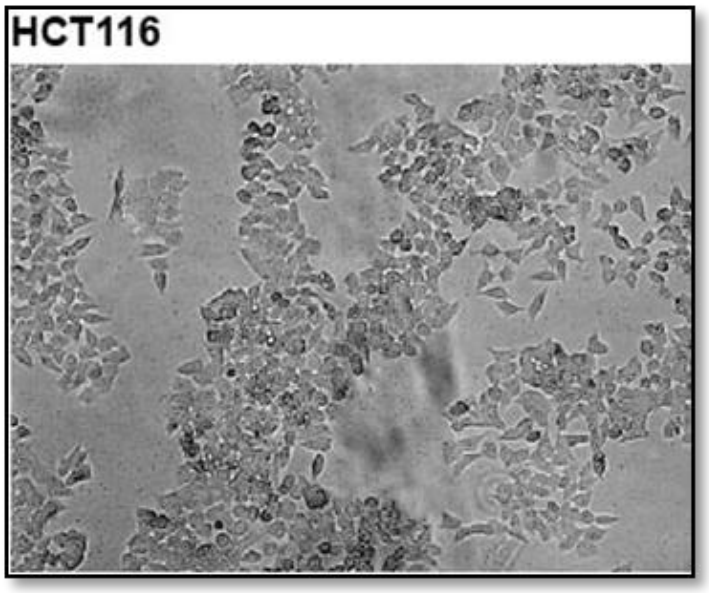

Figure 39: Morphology of HCT116 cells using a 10X objective.

HCT116 cell line was obtained from a primary colon carcinoma; **see table 10**. The cells are polygonal in shape and form tightly packed islands. In addition to the formed islands, few small fibroblast-like cells grew at the borders of the islands, which indicate the presence of two cell populations. The doubling rate was ~24 h**; see figure 39.**

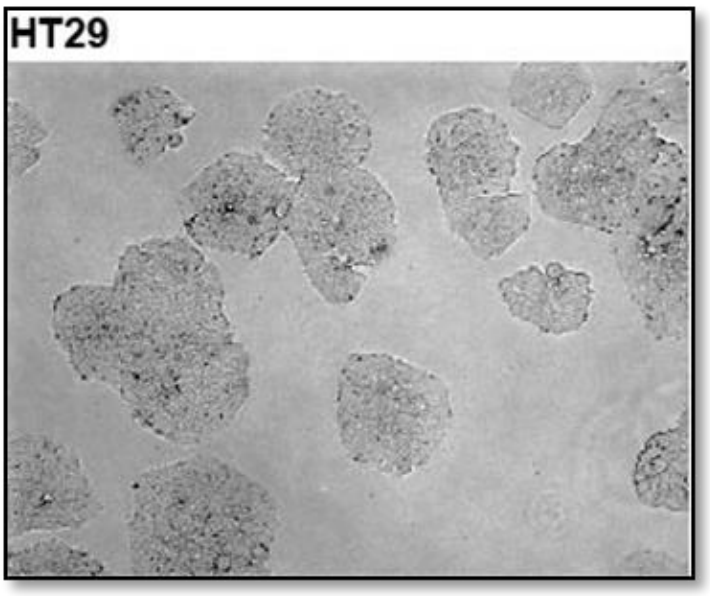

Figure 40: Morphology of HT29 cells using a 10X objective.

HT29 is a well differentiated primary colon cancer cell line; **see table 10**. The cells are polygonal in shape and form tightly packed islands with visible sharp edges. The epithelial islands are intermediate in size and this cell line barely forms a monolayer. The growth rate is more than 24h/division; **see figure 40.**

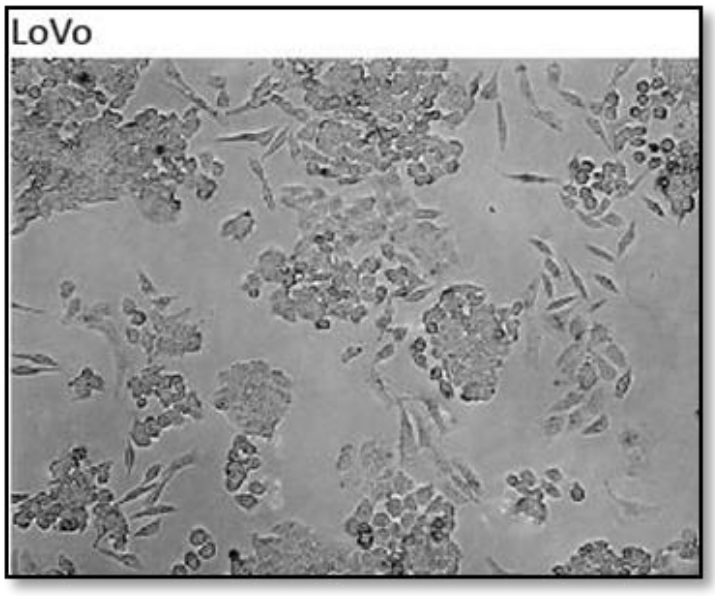

Figure 41: Morphology of LoVo cells using a 10X objective.

The LoVo cell line was derived from a supraclavicular metastatic site of a patient with colorectal adenocarcinoma; **see table 10.** Microscopically, the cell line displays two populations, one group of polygonal unpacked cells and the other one is with many single bipolar fibroblast-like cells. The population doubling time was ~ 24h; **see figure 41.**

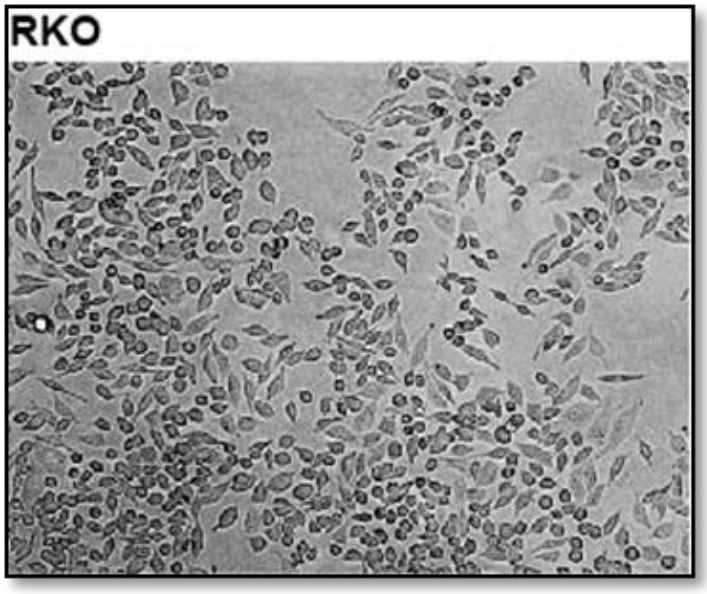

Figure 42: Morphology of RKO cells using a 10X objective.

The RKO cell line originates from a poorly differentiated primary colon cancer; see table 10. The cells grow as uniform individual bipolar fibroblast-like cells. At 100% confluence, the cells covered the entire growth surface. The growth rate was ~24h/cell division; see **figure 42**.

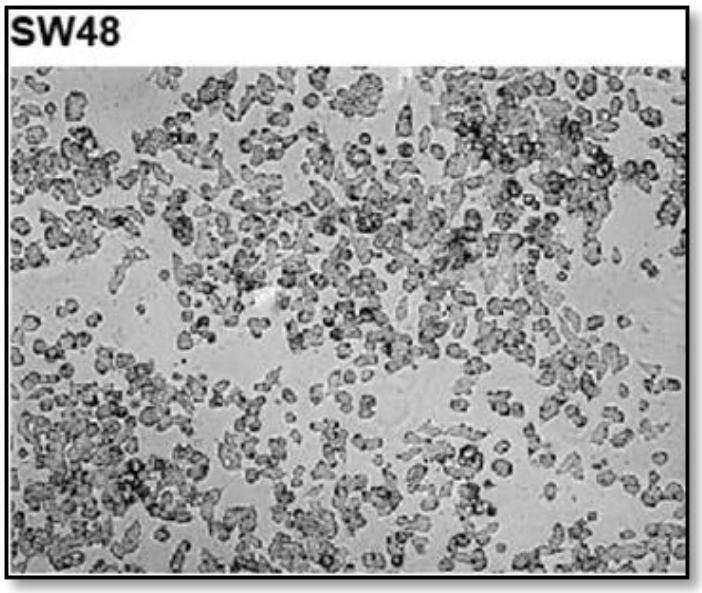

Figure 43: Morphology of SW48 cells using a 10X objective.

The SW48 cell line was established from a Duke C primary colon cancer [287, 288]. This cell line is difficult to grow. The cells are adherent and round in shape and they form tightly unpacked epithelial islands with no visible boundaries. They do not form a

monolayer and the growth is very slow; it took more than a week to reach 80% confluency. The cells also appear to grow on top of each other; **see figure 43.**

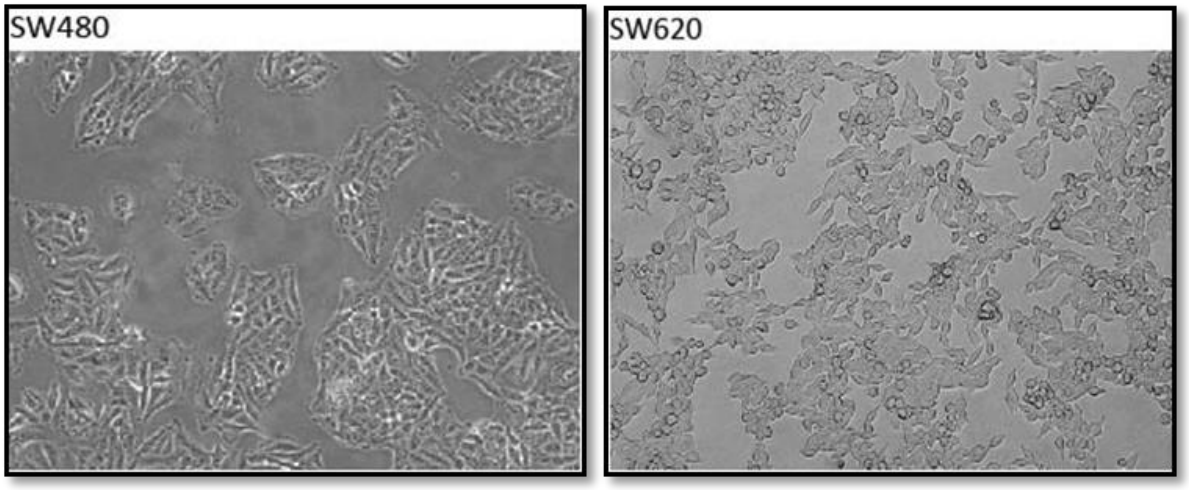

Figure 44: Comparing the morphology of SW480 and SW620 cells using a 10X objective.

SW480 and SW620 cells were isolated from the same patient. SW480 was isolated from primary colon adenocarcinoma, whereas SW620 was isolated from a metastatic region in a lymph node. SW480 cells grow as bipolar elongated fibroblast-like cells. On the other hand, SW620 cells grow as a mixture of small individual sphere-shaped cells, which are clustered in unpacked epithelial islands, and small bipolar individual fibroblast-like cells. The growth rate for both cell lines was ~ 24h/division; **see figure 44.**

3.2.2.3 **Phenotype of the EMT-CRC model**

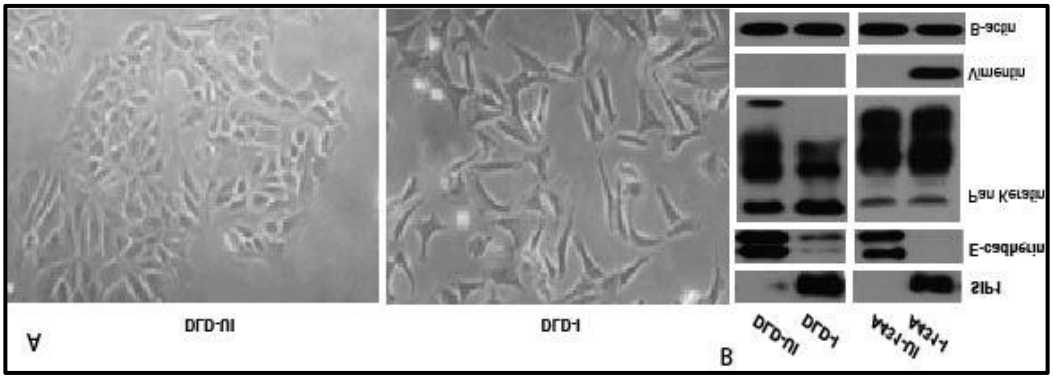

Figure 45: EMT status for DLD-SIP1 and A431-SIP1 models.

A) The morphological appearance of the DLD-SIP1 CRC EMT inducible model (40X objective). The un-induced DLD-SIP1 cells (DLD-UI) were firmly attached to each other forming islands. After 3 days of induction of SIP1 gene (DLD-I) using 2 µg/ml doxycycline, the formerly polarised islands dissociate to leave individual cells resembling fibroblasts.

B) Detection of various EMT-related proteins before and after SIP1 induction in DLD-SIP1 CRC EMT model and the A431 squamous cell carcinoma EMT model. A431-UI (Un-induced A431-SIP1 cells); A431-I (Induced A431-SIP1 cells).

DLD-SIP1 cells were used as a CRC-EMT model in this project. Un-induced DLD cells grow in epithelial islands. When the *SIP1* gene is induced using 2 µg/ml doxycycline, the formerly polarised epithelial islands dissociate and become individual elongated cells resembling the phenotype of mesenchymal cells and fibroblasts**; see figure 45.**

3.2.3 Qualitative assessment of EMT markers

3.2.3.1 **Western blotting and RT-PCR results of the 12 CRC cell lines**

The EMT status of the 12 cell lines was identified using EMT biochemical markers (E-cadherin, ZO-1, Keratin expression highlights epithelial status whereas vimentin, N-cadherin and α-SMA are used as mesenchymal markers). In addition to these, the expression of five EMT-inducing transcription factors (SIP-1, ZEB1, TWIST1, SLUG and SNAIL1) was studied. Most of the markers were detected at protein and RNA levels using western blotting and RT-PCR techniques, respectively; **see figure 46 and 47.**

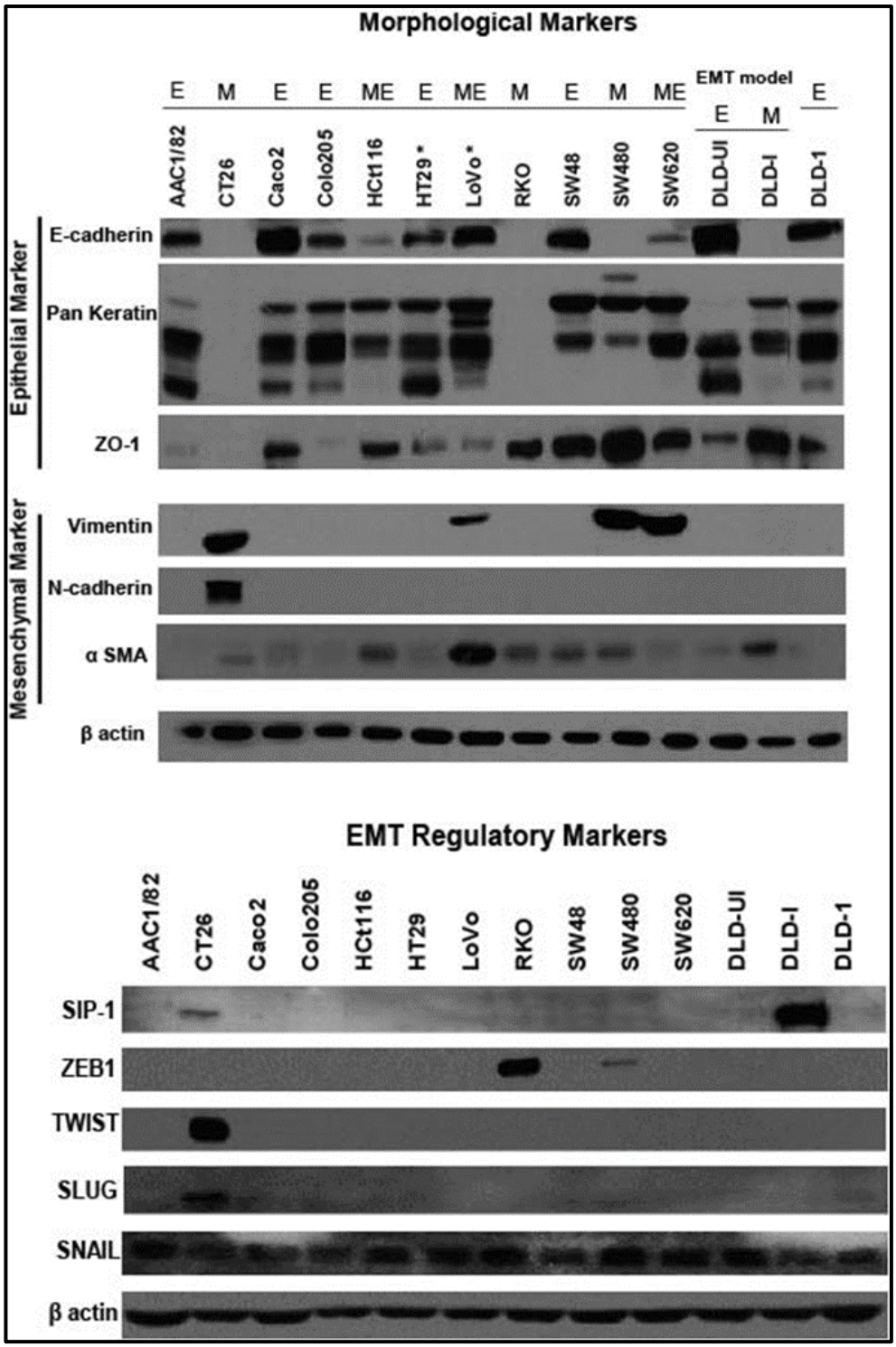

Figure 46: The protein expression of canonical EMT markers and EMT-inducing transcription factors in a panel of 12 CRC cell lines and the inducible CRC EMT model
β-actin was used as an equal loading marker. 20-30 µg of total protein was loaded. The figure is a representative demonstration of at least 3 independent results. E (epithelial), M (mesenchymal), ME (metastable), ZO-1 (zonula occludens protein 1), α-SMA (smooth muscle actin). * HT29 and LoVo were miss-loaded when identifying E-cadherin; HT29 cells have more E-cadherin than LoVo cells.

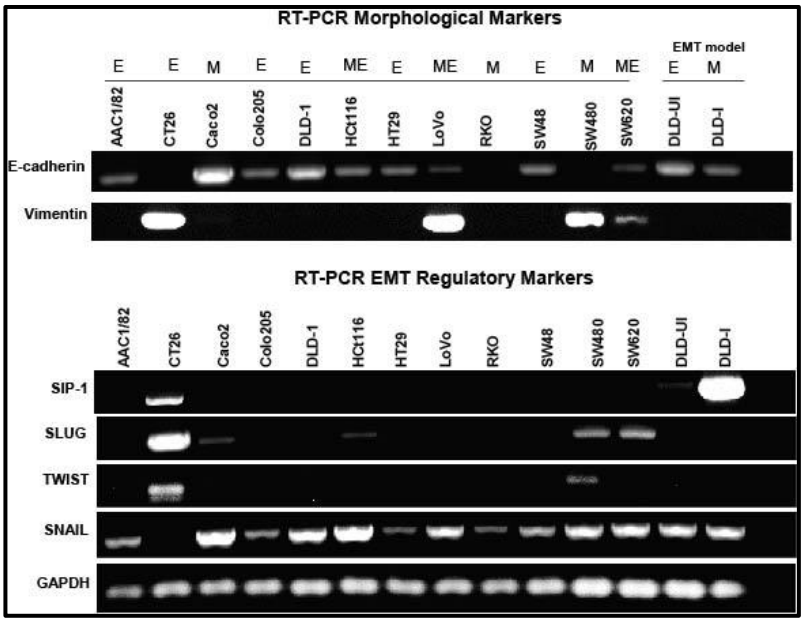

Figure 47: RNA expression of selected EMT markers and EMT-inducing transcription factors in a panel of CRC cell lines and DLD-SIP-1 inducible CRC EMT model.

The figure is a representative demonstration of at least 3 independent results. (Epithelial), M (Mesenchymal), ME (Metastable).

3.2.3.1.1 Morphological markers

The E-cadherin protein was found abundantly expressed in Caco2 cells and at moderate level in AAC1, Colo205, DLD-1 HT29, LoVo and SW48 cells. On the other hand, a low level of E-cadherin was observed in HCT116 and SW620 cells, whilst no E-cadherin was seen in CT26, RKO or SW480 cells. Similar results were confirmed by RT-PCR apart from HCT116 which was found to have more E-cadherin mRNA compared to its protein level.

At the protein level, ZO-1 was abundantly expressed in SW480 and un-induced DLD-SIP1 cells compared to SW620 and induced DLD-SIP1 cells, respectively. On the other hand, it was found at a moderate level in Caco2, DLD-1, HCT116, RKO and SW48 cells, and at a low level in HT29, LoVo, AAC1 and Colo205 cells, but barely detected in the CT26 cell line. Although ZO-1 is an epithelial marker, its detection in cells with no or a low level of E-cadherin may indicate that it is expressed in the cytoplasm and therefore non-functional protein.

Intermediate epithelial filament proteins (cytokeratins) were detected abundantly and at similar amounts in AAC1, Caco2, Colo205, DLD-1, HT29 cells, although cytokeratins were seen less and at varying amounts in the other cell lines. Significantly, CT26 and RKO showed no expression of cytokeratins at all, whilst SW480 and HCT116 cells showed

similar amounts of cytokeratin. On the other hand, LoVo and SW620 exhibited more filaments compared to HCT116 and SW480 cells.

N-cadherin was not found in any of the CRC cell lines except CT26. Vimentin expression was detected in CT26, LoVo, SW480, and SW620 cells at both the protein and RNA levels. Of note, SW480 and SW620 have an equal amount of vimentin at the protein level but different amounts of mRNA; SW480 has more vimentin compared to SW620.

The mesenchymal marker α-SMA was found abundantly expressed in LoVo cells but barely detectable in most of the other cell lines. However, it was more heavily expressed in SW480 cells compared to SW620 cells.

3.2.3.1.2 EMT regulatory markers

SIP1 (ZEB2) was seen only in CT26 at both the protein and RNA levels. However, ZEB1 was abundantly expressed in RKO cells and moderately expressed in the SW480 cell line, but not in any other CRC cell lines.

Apart from CT26, SNAIL1 was found in an equal amount in all CRC cell lines at both protein and mRNA levels. TWIST was detected only in CT26 at the protein and RNA levels, and only on the RNA level in SW480 cells. SLUG mRNA, but not protein, was found at a low level in Colo205 andHCT116 cells and in equal amount in SW480 and SW620 cells.

The results of GAPDH and β-actin indicated that there was an equal loading of the cDNA and the proteins in all the 12 CRC cell lines for RT-PCR and Western blotting detection techniques, respectively; see figure 46 and 47.

3.2.3.2 Immunofluorescence (IF) analysis of cell lines with an intermediate phenotype

Certain cell lines were found to express both epithelial and mesenchymal proteins, therefore, were chose to further analyse these by IF; **see figure 48.** This is for investigating whether a stem cell-like sub population (mesenchymal) exists or certain cell lines acquired a plastic (exhibiting both epithelial and mesenchymal properties at the same time) state [2].

The HCT116 cell line was seen to have two populations of cells comprised of epithelial (clustering) and mesenchymal (single cell) cells, and expressed E-cadherin and α-SMA proteins **(see figure 39 and figure 46).** LoVo cells also showed two populations of

epithelial and mesenchymal cells, with expression of E-cadherin, Vimentin and α-SMA (**see figure 41 and figure 46).** SW620 showed a homogenous morphology of small fibroblast-like cells, although it expressed E-cadherin and vimentin (**see figure 44 and figure 46).** Based on this, HCT116, LoVo and SW620 cells were considered as borderline cell lines. E-cadherin, vimentin and phalloidin were the markers chosen to further analyse these cells. DLD-1 cells were used as an internal positive control for E-cadherin and SW480 cells were chosen as an internal positive control for vimentin; **see figure 48.**

The IF staining showed that these cells do express E-cadherin but at a lower level compared to DLD-1 cells. However, SW620 cells showed stronger E-cadherin staining compared to SW480 cells. Of note, SW480 cells have undetectable levels of E-Cadherin according to Western blotting.

Similar to the observation by WB, both SW480 and SW620 showed vimentin expression, but the staining was stronger with SW620 cells compared to SW480 cells. None of the other cell lines showed vimentin staining.

Phalloidin, which is a dye that stains actin filaments and helps to define the cell morphology, was observed at the cell-cell junctions of DLD-1 and HCT116 cells. LoVo cells showed both cell to cell and filamentous staining and stress-like fibers in the cytoplasm of single cells. On the other hand, SW480 and SW620 showed an obvious staining of stress-like fibers all over their cytoplasm and at the edge of their membranes. However, the fibers were more stretched in SW480 cells compared to SW620 cells.

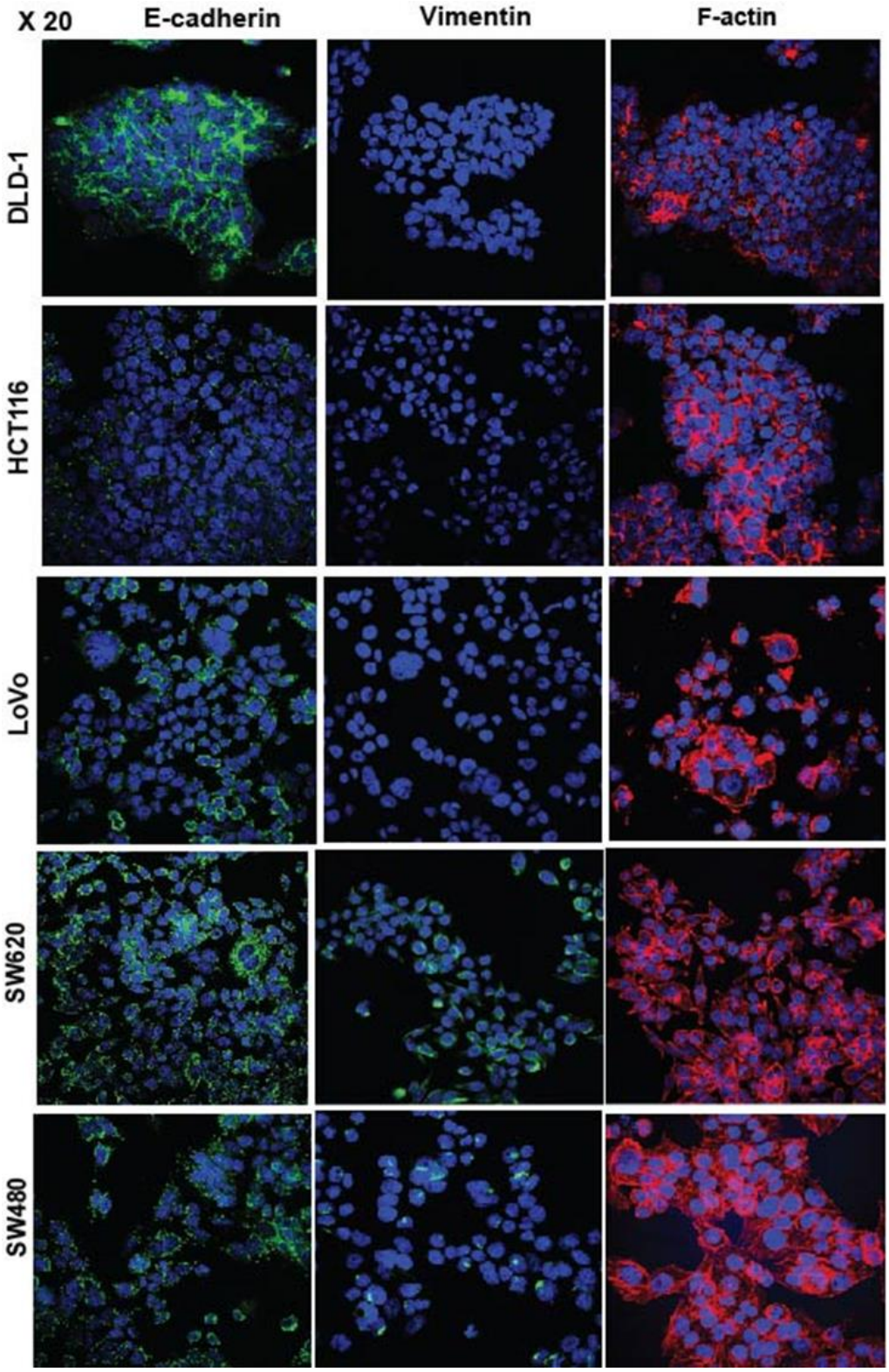

Figure 48: Spatial E-cadherin, vimentin and F-actin protein expression were analysed using immunofluorescence and confocal microscopy in the intermediate HCT116, LoVo and SW620 cells.

The cells exhibited expression of both epithelial and mesenchymal proteins or RNA by WB (western blot) and RT-PCR, respectively. E-cadherin and vimentin were detected using specific antibodies followed by green (Alexa 488)-conjugated secondary antibodies. F-actin was stained using phalloidin dye. DAPI counterstain was used to stain the nucleus.

3.2.3.3 Western blotting, IF and RT-PCR results for the DLD-SIP CRC-EMT model

The epithelial and mesenchymal markers, that were used to assess EMT status in the 12 CRC cell lines at the protein and RNA levels, were also used to check the EMT status of the DLD-SIP1 CRC-EMT model; see **figure 46 and figure 47**. In addition to that, E-cadherin, ZO-1, β-Catenin, Connexin 43, actin cytoskeleton (phalloidin) and SIP1 proteins were checked by IF in order to confirm the EMT status of this model.

WB results showed that un-induced DLD-SIP1 has more E-cadherin, more intermediate filaments or cytokeratins compared to the induced DLD-SIP1 cells. On the contrary, the ZO-1 tight junction protein was seen more in the induced DLD- SIP1 cells compared to un-induced ones. No mesenchymal markers were detected in this model apart from the obvious morphological changes, and increased α-SMA which was expressed in the induced cells; **see figure 46 and 47**

Similarly, RT-PCR also showed that this model expressed no Vimentin, and the transcription of *the CDH1* gene was down-regulated when the expression of the SIP1 protein is induced in DLD-SIP1 cells.

Likewise, IF staining showed a down-regulation of E-cadherin and cadherin associated protein (β-catenin) in the induced cells compared to the strong membranous staining in the un-induced cells. In contrast, ZO-1 protein, which was observed more in the induced DLD-SIP1 cells by WB, was seen clearly at cell-cell junctions, and the staining reduced significantly after the induction of SIP1; see **figure 48** and also **figure 49** which shows ZO-1 staining without the DAPI overlay. Instead, cytoplasmic ZO-1 was observed in SIP1-induced cells. Connexin 43, a gap junction protein, was also expressed "as a dot shape" compared to the induced ones. Phalloidin, a high affinity filamentous actin (F-actin) dye, strongly stained the cytoskeleton and the margins between the epithelial cells in DLD-UI. EMT-related changes of the filaments were observed as stress fiber formation all over the cytoplasm and the cell membranes in induced cells; **see figure 49.and 50.**

None of the EMT regulatory markers were detected in this model except endogenous SNAIL1 and exogenous SIP1. Similar to the CRC panel, SNAIL protein and RNA were seen in DLD-SIP1 cells without a change between DLD-UI and DLD-I cells. In fact, SIP1 was the only differentiated EMT regulator marker for this model where it was found more

in the induced compared to un-induced cells at both protein and RNA Levels. IF also confirmed the SIP1 protein level. The nuclear SIP1 was seen clearly in the induced DLD-SIP1 cells and it was absent or very faint in the un-induced DLD-SIP1 cells**; see figure 50,** which shows SIP1 staining without the DAPI overlay.

In general, WB, IF and RT-PCR results all confirmed that the un-induced DLD-SIP1 cells expressed most of the examined epithelial markers and little or none of the mesenchymal ones. However, when the *SIP1* gene was induced, the epithelial markers were switched off and the mesenchymal ones switched on.

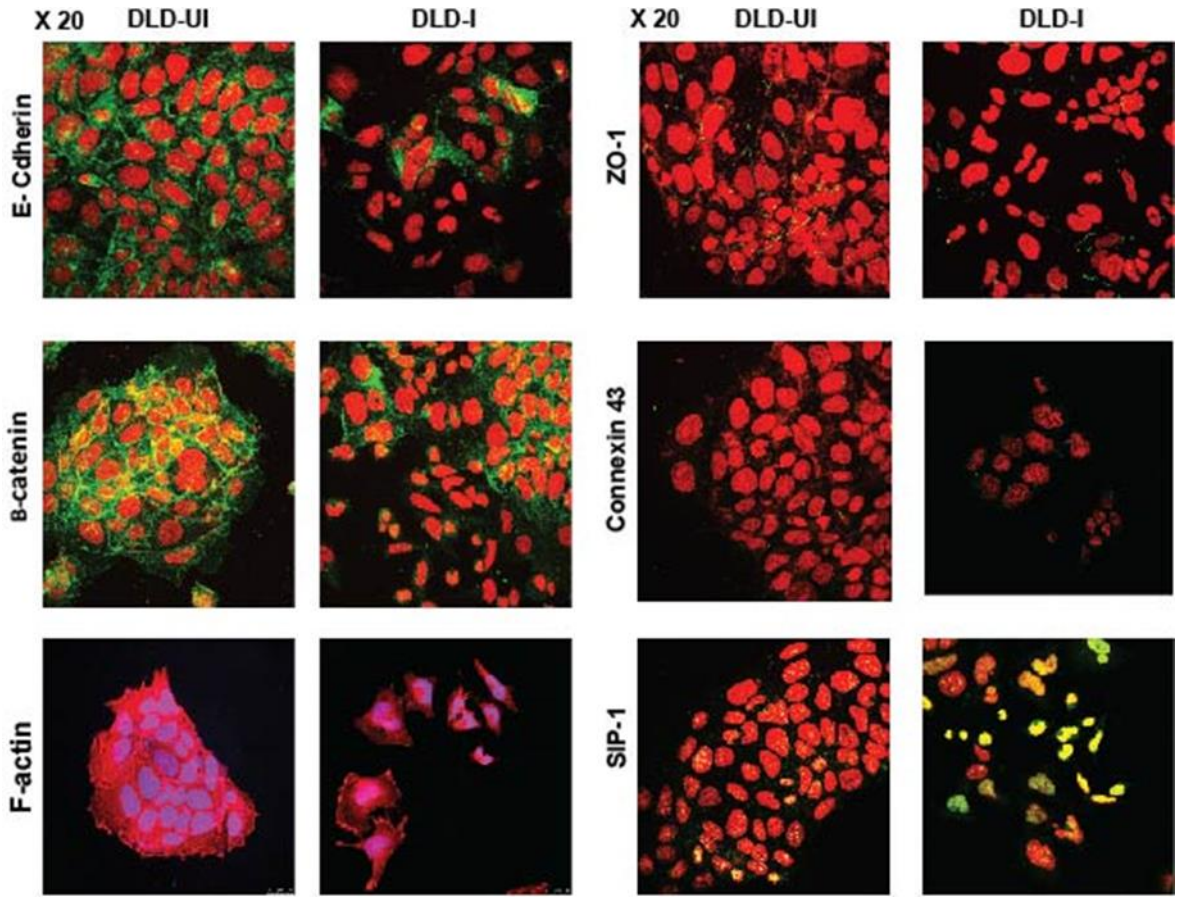

Figure 49: The spatial expression of E-cadherin, β-catenin, ZO-1, connexin 43, F-actin and SIP1 proteins was analysed using confocal microscopy in DLD SIP-1 CRC EMT model.

DLD-SIP1 cells were induced for 3 days with 2µg/ml doxycycline. Induced DLD-SIP1 cells scattered and showed stress fibres as well as reduced expression of E-cadherin, β-catenin, ZO-1 and connexin 43 as compared to the un-induced ones. All proteins apart from F-actin were detected using specific antibodies followed by green (Alexa 488)-conjugated secondary antibody. Phalloidin dye was used to stain F-actin. DAPI counterstain was used to detect the nucleus. DLD-UI (un-induced DLD-SIP1 cells) DLD-I (induced DLD-SIP1 cells).

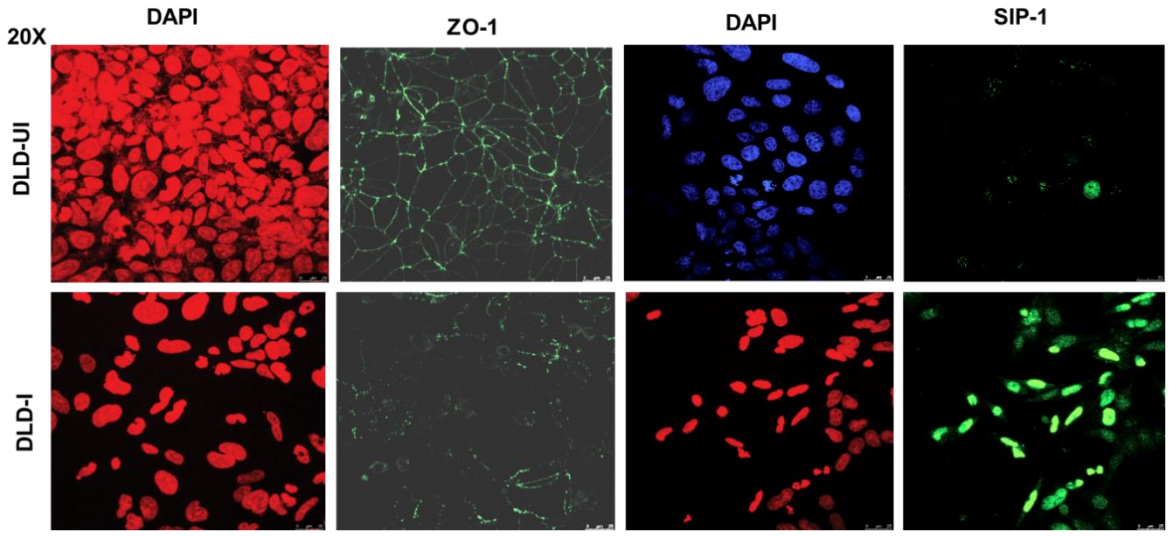

Figure 50: Protein expression of ZO-1 and SIP1 detected using confocal microscopy in the DLD SIP-1 CRC EMT model, without the DAPI overlay.

In order to visualise the expression of ZO-1 and SIP-1 in DLD-SIP1 CRC EMT model, DAPI overlay was avoided. A sharp expression of ZO-1 at cell-cell junctions was observed in the DLD-UI, but the expression reduced significantly in DLD-I cells. On the other hand, SIP1 is clearly over-expressed in the nucleus (green). DLD-UI (un-induced DLD-SIP1 cells) DLD-I (induced DLD-SIP1 cells).

3.4 Discussion

3.4.1 EMT status of the 12 CRC cell lines in relation to their morphological appearance

The aim of this chapter was to analyse the EMT status in a panel of CRC cell lines and relate this to their morphological appearance and biological characteristics. To attain this goal, 12 CRC cell lines (AAC1, CT26, Caco2, Colo205, DLD-wt, HCT116, HT29, LoVo, RKO, SW48, SW480 and SW620) were chosen. All the cell lines are human cell lines except CT26 which is obtained from the BALB/c mouse. EMT status was identified by western blotting, IF and RT-PCR using various EMT markers such as E-cadherin, ZO-1, cytokeratins, F-actin as epithelial markers and vimentin, N-cadherin, α-SMA as mesenchymal markers. Moreover, SIP1, ZEB1, TWIST1, SLUG and SNAIL1as EMT transcription factors were included in the analysis. β-actin and GAPDH were used as equal loading markers for western blotting and RT-PCR techniques, respectively. To our knowledge, this is the first study that includes such a large collection of CRC cell lines and EMT markers to study EMT in CRC; see figure **46, 47, 48. 49** and **50**.

Based on our findings from the western blotting, the RT-PCR and the light microscopy, it has been decided to categorise the CRC cell line panel into three distinct groups. The groups are:

A- An epithelial phenotype category, which includes cell lines having epithelial cell, shapes and moderate to high levels of E-cadherin, with no expression of mesenchymal markers or EMT regulators.
B- A mesenchymal phenotype category which includes cell lines expressing no E-cadherin, but with mesenchymal morphological appearances.
C- An intermediate phenotype category, which includes cell lines with low levels of E-cadherin and one or more mesenchymal markers or EMT regulator markers. In addition, they have a mixed population of both epithelial and mesenchymal cells.

Of note, SNAIL1 and ZO-1 results were not considered in the evaluation of EMT status of the CRC cell line panel. Although up-regulation of SNAIL1 in cancer has frequently been reported and associated with invasiveness, metastases, poor prognosis and induction of EMT [506], SNAIL1 was seen widely expressed in epithelial and mesenchymal CRC cell lines at both the protein and mRNA levels without any clear differentiation. SNAIL1 could be stabilised via inhibition of GSK3 [143] or by macrophage-secreted factors such as TNF-α and IL-1β [507, 508]. However, stabilisation of SNAIL1 could not justify our finding because our culture medium did not intentionally contain any IL-1β and TNF-α. Recently, a study done by Hsu and colleagues suggested that acetylation of SNAIL via the CREB-binding protein can mediate transactivation of several genes involved in promoting an immunosuppressive microenvironment, thus leading to metastasis. This means activation by acetylation, rather than expression, is critical for SNAIL function. This could be another reason for our findings that SNAIL is widely expressed in epithelial and mesenchymal CRC cells [509].

ZO-1, which was intended as an epithelial marker of cells, was also detected in the mesenchymal cell lines C26, RKO, SW480 and induced DLD-SIP1 cells. Actually, this is not an unusual finding. ZO-1 has previously been reported in fibroblasts at adherens-like junctions, with N-cadherin, Cadherin 11, and junction Adhesion Molecule-C and localised to the nucleus of primary fibroblast cells and proliferating epithelial cells. These findings suggested that ZO-1 could have additional roles in cellular processes beside tight-junction formation [510-514]. However, for an epithelial morphology proper, ZO-1 has to be expressed on the surface and at cell junctions. Detection of ZO-1 by immunofluorescence is a better way to conclude the EMT status than simply analysing ZO-1 expression. From

this, I suggest that studying the role of cytoplasmic nuclear ZO-1 in EMT could be of interest.

Looking into the details of the EMT status of each cell line, I found that the AAC1 cell line, which was derived from PC/AA human colonic adenoma cell line, showed keratins and a moderate amount of E-cadherin at both the protein and mRNA levels but did not express any of the mesenchymal markers or the EMT transcriptional factors. Morphologically, these cells grow as a mixture of adherent and floating cells where the adherent cells form very small epithelial islands. In the literature, it has been described as a glandular organisation of goblet-like cells, which produce mucin [494]. These characterisations could classify this cell line as epithelial. Up to our knowledge there is no previous study showing the EMT status of this cell line.

CT26, the murine CRC cell line, is the most similar one to fibroblast cells, and it expresses most of the mesenchymal markers and most of the EMT transcription factors that were studied in this project; Vimentin, N-cadherin and α-SMA and SIP-1, TWIST and SLUG. Furthermore, it does not express any E-cadherin or cytokeratins. This cell line is described as being aggressive, highly metastatic and poorly differentiated [515, 516], and this could be due to the expression of multiple mesenchymal and EMT regulators. From the above description, CT26 can be grouped under the mesenchymal category.

Caco2 cells showed an abundant level of cytokeratins and E-cadherin at both the protein and mRNA levels with no expression of any mesenchymal markers. In addition, none of the investigated EMT transcriptional markers were detected at the protein or RNA level except SLUG mRNA. Expression of the SLUG mRNA but not the SLUG protein could be because the translation of mRNA is inhibited by miRNAs such as mir-1 and mir-200 [517]. On top of the abundant level of E-cadherin and cytokeratins, other epithelial markers such as villin, occludin, claudin1, microvilli and, desmosomes have been reported as well. Morphologically, the cell line was described as a polarised epithelial cell monolayer that provides a good model to study the physical and the biochemical properties of epithelial barriers for the passage of small molecules [496, 497, 518, 519]. The reported formation of monolayer matches our observations by light microscopy. It is also known that these cells are non-invasive or non-metastatic [520, 521]. For all of the aforementioned results, Caco2 can be placed with the epithelial category and it can be considered as a highly epithelial CRC cell line.

The Colo205 cell line had a similar morphological appearance to AAC1 cells with a mixture of both adherent and floating cells. The same morphology was described in the literature and some epithelial markers such as cytokeratins, microvilli, ZO-1, desmosomes were identified [497, 498]. In addition to these epithelial markers, we identified a moderate level of E-cadherin expression at both the protein and RNA level with an abundant expression of cytokeratins. Neither mesenchymal markers, nor EMT transcription factors markers were detected in this cell line except SNAIL. To our knowledge, only one study has investigated the EMT status in Colo205 cells, and it was done by quantitative RT-PCR. The study compared the EMT status of Colo205 sensitive (Colo205-S) and a Colo205-resistant clone (Colo205-R) to a drug (PEP005 drug; alternative name is Ingenol 3-angelate). The study found that Colo205-S ,which is similar to the Colo205 cell line used in this project, express more E-cadherin, claudin, mucin, and connexin-32 and undetectable levels of N-cadherin, Vimentin, fibronectin-1, ICAM-1 and MMP9, SNAIL, SLUG and TWIST compared to the Colo205-R clone [522]. Given this, Colo205 can be considered as an epithelial cell line and thus can be allocated with the epithelial group.

DLD-1 cells (DLD-wild type) has a plentiful amount of E-cadherin at protein and mRNA. In addition, cytokeratin expression is similar to the level of that found in the Caca2 or Colo205 epithelial cell lines. None of the mesenchymal markers or EMT inducing transcription factors were detected apart from SIP-1 mRNA. Expression of SIP-1 mRNA in DLD-1 cells was also seen in a previous study [523]. The study found that the translation of SIP-1 mRNA could be blocked by high levels of the miRNA-200 family which in turn could preserve the epithelial identity of this cell line [524]. In addition to E-cadherin expression and cytokeratins, microvilli, Zonula adherens, desmosomes, plakoglobin, and the membranous (γ-catenin) and β-catenin were also reported in this cell line [247, 497]. Morphologically, DLD1 cells present as tightly-packed islands which form a monolayer at a very high density. This can be linked to the high expression of E-cadherin and other epithelial markers. It is also reported that this cell line has a low level of carcinoemboryonic antigen (CEA); CEA is a marker for occult CRC which could classify the cell line as a non-metastatic cell line [497]. These data provide evidence that DLD-1 cell line is epithelial and should therefore be placed in the epithelial category.

HCT116 displays a low level of E-cadherin and few keratins compared to DLD-1 and Caco2 cells. Also no expression of N-cadherin or Vimentin was detected. However, it expresses a reasonable level of α-SMA protein and a low level of SLUG mRNA. The same observations were seen by other authors in addition to TWIST mRNA, although not at the

protein level [525]. SLUG protein could be impaired due to high expression of miR-1, miR-200 and miR124 [517, 526] or high expression of angiopoietin-like protein 1 (ANGPTL1; angiogenesis regulator protein) [527]. In fact, expressing both epithelial and mesenchymal markers at the same time may explain the growth pattern of this cell line in culture where two populations of un-tightly packed epithelial islands and fibroblast-like cells are seen. The same morphology had been described by the scientist who deposited this cell line to the ATCC [501]. It is also reported that this cell line has a degree of metastatic potential in mouse experiments [520, 528]. The metastatic potential could be due to the presence of fibroblast-like cells. These findings can categorise this cell line as either intermediate or metastable cells with partial EMT, although, more investigation is needed.

HT29 is a mucus-secreting human colonic cancer cell line which grows in culture as a tightly packed cluster of epithelial islands. Other authors reported similar growth descriptions [496, 529]. The epithelial morphology was confirmed by assaying some EMT markers. This cell line showed a moderate level of E-cadherin expression with a similar amount of cytokeratins in comparison to DLD-1 and Caco2 epithelial cells. No mesenchymal markers or any EMT regulators were detected. A controversial result was reported which found that HT29 cells have low levels of vimentin, ZEB1, SLUG and TWIST1 proteins [530, 531]. Nonetheless, I confirmed our results by two techniques and repeated them multiple times, and I believe that our results are more representable, whilst Celesti *et al*., also found similar findings as ours [525]. Moreover, desmosomes, cytokeratins, microvilli, zonula adherens and tight junctions were reported for HT29 cells [497, 532, 533]. Therefore, HT29 cells cannot be mesenchymal and can only be classified as epithelial.

LoVo is a highly metastatic CRC cell line that was originated from a metastatic site (left supraclavicular region) [502, 520, 534]. In culture, it displays a growth pattern of two populations; epithelial islands with “fuzzy borders” and abundant amount of fibroblast-like cells. This pattern was also previously reported [502]. The WB and RT-PCR results also confirmed the morphological appearance. The cell line showed a moderate level of E-cadherin whilst the expression of cytokeratins are different in their pattern and number than DLD-1, Caco2, Colo205 and HT29 epithelial cells. However, it also showed an abundant amount of Vimentin and α-SMA. The same results of Vimentin and E-cadherin had been found previously. However, the author reported that LoVo cells also express N-cadherin and ZEB1 [535]. Unfortunately, this study is the only report presenting the EMT

status of this cell line. For that, I repeated the finding more than three times, and I found no expression of either N-cadherin or ZEB1. By considering these findings, LoVo cells can be classified as an intermediate cell with partial EMT although more thorough characterisation of this cell line is likely required.

RKO cells express no E-cadherin or cytokeratins at all. This representative finding of E-cadherin is supported by a study by Breen *et al*., which found that RKO completely lack the E-cadherin/α-Catenin complex, explaining why it is so aggressive, poorly differentiated and highly invasive compared to the one transfected with E-cadherin [536]. Surprisingly, among all the mesenchymal and EMT transcriptional factors, ZEB1 was the only one expressed at a high level in this cell line. Morphologically, the cells grow as a uniform individual cells and look like small fibroblasts. To our knowledge, this the first study that identifies and validates the EMT status of RKO with a credible number of EMT markers. Taking together, RKO is classified as a mesenchymal cell line.

SW48 cell line has a very slow growth rate. To enhance the growth rate, the supplier (ATCC) recommended using a special medium containing Leibovitz L-15 medium with 10% fetal calf serum, insulin and cortisol. However, due to the unavailability of this medium, I used complete DMEM medium with 20% serum, non-essential amino acids and sodium pyruvate. When this cell line reaches 50% confluency, it forms loose grapelike clusters of epithelial islands. The same morphology has been described previously [537]. At both the protein and mRNA level, these cells showed a moderate amount of E-cadherin but less cytokeratins compared to other epithelial cell lines in the panel. This cell line was found to have a mutation in the *p120-catenin* gene which in turn causes reduced expression of the p120 cadherin anchoring protein, which could explain the expression level of E-cadherin and cytokeratins [538]. None of the mesenchymal markers or EMT regulators were seen except α-SMA. It is known that α-SMA is a sole marker for active fibroblasts [161]. Detecting the expression of this marker in epithelial cells is unusual, and there is no report in the literature showing α-SMA in non-fibroblast cells. For that, I went back and check if this cell line has any fibroblast cells in the culture. I found very few small fibroblast like cells that are randomly scattered around the epithelial islands. I was not sure if it was due to any technical problem during handing the cell line, or due to its origin. In fact, the depositor of this cell line mentioned that they observed some contaminated fibroblast grew readily and from fibroblast monolayer. They attempted to curb the fibroblast growth by adding 0.5 mg/ml collagenase to Leibovitz L-15 medium, and after 39 days the supernatant containing the free epithelial cells, which were disassociated from

fibroblast monolayer, were taken and transferred to another flask. From this, the expression of α-SMA might be due to contaminating fibroblasts [537]. The cell line is reported to be non-metastatic with a very low CEA (8 ng per million cells) [504], and it showed no liver metastasis in immune-deficient Non-obese diabetic mice (NOD-SCID) [520]. To our knowledge, this is the first time that the EMT status of this cell line has been investigated. From all the aforementioned data, I concluded that SW48 is non-metastatic epithelial cell line.

SW480 and SW620 colon cancer cell lines originated from the same patient, thus they have the same genetic background. SW480 was isolated from primary colon cancer and SW620 was isolated from a metastatic site in a lymph node [539]. In culture, we observed that SW480 has a different morphological appearance than SW620. SW480 cells grow as a mixture of small epithelial islands whereas SW620 cells grow as small individual spherical cells and elongated bipolar cells. An electron microscopy study of these two cell lines revealed that SW620 has fewer microvilli than SW480 which indicates that SW620 has undergone a dedifferentiation process [504]. Our data shows that SW620 cells express low levels of E-cadherin protein as well as mRNA, whereas SW480 cells do not show any expression of E-cadherin protein or RNA. In addition, SW480 has fewer and different number of cytokeratins, more vimentin and α-SMA in comparison to SW620. ZEB1 protein /mRNA and TWIST mRNA were seen only in SW480 cells, whereas SLUG mRNA was seen in both cell lines at an equal amount. Expression of TWIST and SLUG mRNA, but not the proteins could be due the presence of post-transcriptional TWIST1 and SLUG suppresser microRNAs [526, 527, 540]. The results of the very low or no E-cadherin expression, and the high expression of ZEB1 in SW480 cells were found previously [220, 247, 541]. However, contrary findings describing the EMT status of each cell line and metastatic potential have been reported. SW620 cells were seen to express mesenchymal markers including nuclear β-Catenin, Vimentin and fibronectin as well as EMT-inducing transcription factors such as ZEB1, SLUG and SNAIL1. On the other side, SW480 cells were shown to express epithelial markers such as E-cadherin, connexin43 and connexin 26 [516, 542-545]. Also, SW620 cells were showed to be more invasive by expressing more ROCK and less Cdc42 and Rac1 [546], and by over-expression of E-cadherin suppresser mRNA/proteins such as TCF12 [542], and down-regulation of microRNAs such as miR-200, miR-221 and miR-224, compared to SW480 cells [547, 548]. Moreover, *in vivo* experiments showed that SW620 cells, but not SW480, have a potential to metastasize to the liver and spleen [539, 548]. The controversial results of the two cell lines status lead me to search the literature for their depositors [496, 497, 504],

and we found that their differentiation of the cell lines are in agreement with our reproducible findings (*n*=4). In addition, many studies reveal that metastatic cells at distant metastatic tumours re-gain the expression of E-cadherin [131, 133-135, 549, 550], and this aligns with our E-cadherin findings. Indeed, many studies showed that SW480 cells are more invasive, migratory and metastatic compared to SW620 cells [551]. In fact, specific characterisation of keratins could be a useful tool to distinguish them and their degree of differentiation as well as the origin of the primary or secondary tumour. For example, the relative expression of K20 and K7 can be used to differentiate between epithelial tumours in which the majority of CRC adenocarcinomas showed a K7-/K20+ profile [182-184]. However, loss of keratin expression at late tumour stages and a gain in others at secondary sites could be used as an important marker of EMT and MET. For example, the loss of K8/18 expression, which are normally co-expressed in simple epithelial cells and are maintained during tumorigenesis until the tumour becomes invasive, was found to activate EMT features of cell motility, invasion and chemo- resistance [185, 552, 553]. From all of these biological data, SW480 is a mesenchymal cell line whereas SW620 could be classified as intermediate as cells have undergone a re-differentiation process or MET although, more thorough characterisation is needed. In fact, SW480 and SW620 cells can be considered as a suitable and validated model to study colon cancer progression with respect to EMT and MET.

3.2.4 Further investigation of intermediate cells by IF

The intermediate EMT or partial EMT status has not been well evaluated and elucidated in the medical research field, and there are no biomarkers to specify cells belonging to this category. Indeed, it has been suggested that detecting cells with a metastable status could imply a spectrum of heterogeneity instead of only presenting the two extreme ends of the EMT process, and could increase the potential for a more targeted therapy [128, 130]. The intermediate phenotype could be due to acquiring a plastic state exhibiting both epithelial and mesenchymal features or due to the presence of a stem cell-like subpopulation or both. Recently, P-cadherin was predicted to be a promising marker to identify a stem cell-like subpopulation within an intermediate or metastable subset of EMT cells in breast cancer [130]. Additionally, another study carried out by Huang *et al*, which defined the EMT status of 43 ovarian cancer cell lines, differentiated the intermediate phenotype into intermediate epithelial, and intermediate mesenchymal by identifying the expression of E-cadherin, cytokeratins, N-cadherin, vimentin and ZEB1 proteins [128]. Given this, we intended to further classify HCT116, LoVo, and SW620 intermediate cells by investigating

their expression for stem cell markers (P-cadherin) as well as by their expression of E-cadherin, vimentin and F-actin using IF; **see figure 48**. We included our WB findings for E-cadherin, cytokeratin, vimentin, N-cadherin and ZEB1 to reach a final conclusion for their EMT status. Unfortunately, P-cadherin was not included due to unavailability of a good P-cadherin antibody in our lab. Two P-cadherin antibodies from different companies were used to detect P-cadherin expression in the CRC panel, but none of them worked. DLD-1 cells were used to represent the abundance expression E-cadherin, whereas SW480 mesenchymal cells were used as an internal control for vimentin expression. Investigating F-actin would be a useful means to identify any morphological changes in cancer cells by observing the re-organisation of actin filaments with or without actin binding proteins at the cell membrane which cause invadopodia-, lamellipodia- and filopodia-dependent cell motility [194]. Indeed, actin cytoskeleton reorganisation is one of the major indications of invasion, migration, metastatic potential and thus EMT [554] [280] [555].

DLD-1 epithelial cells, the internal control for E-cadherin expression, showed high expression of E-cadherin at cell-cell junctions, and no vimentin by IF; **see figure 48.** These cells also exhibited a well organised and homogenous F-actin staining without any indication of a heterogeneous population or any membranous projections characteristic of invadopodia. On the other hand, SW480 mesenchymal cells showed much less E-cadherin compared to DLD-cells, but more vimentin and invasive re-organisation of the actin cytoskeleton. In fact, cooperation of actin, microtubules and vimentin intermediate filaments have been shown to facilitate the elongation of invadopodia [556]. Interestingly, vimentin was observed to be concentrated at the edges of the nuclear envelope, and not at the cytoplasmic membrane. There is no clear explanation for this result. I think it is an isolated finding, and the staining should be repeated potentially with a different antibody. However, due to restriction of the project time, the staining could not be repeated; **see figure 48.**

HCT116 cells showed no expression E-cadherin but not vimentin by IF although the level of E-cadherin level was less than DLD-1 cells. These findings are in agreement with our WB findings; see **figure 46.** The presence of the two populations: the epithelial islands and single fibroblast-like cells that we observed by light microscope see **figure 39** and [501]), was not shown with F-actin staining. F-actin staining showed that microfilaments are organised at the cell-cell junctions with no clear signs of invadopodia; **see figure 48**. This cell line also expresses less cytokeratins compared to DLD-1 cells, no N-cadherin and some expression of α-SMA. Due to our findings, it can be noted that this cell line

expresses more epithelial markers and less mesenchymal ones with a phenotype near to an epithelial morphology which classifies this cell line as an intermediate epithelial cell line.

LoVo cells, as observed by light microscopy, have two distinct populations of epithelial and mesenchymal like cells; **see figure 41** and [502]. They also showed a heterogeneous morphology with F-actin labelling. Some of the cells adhere together and some appear as single cells with invadopodia. The presence of some epithelial islands could explain the moderate expression of E-cadherin by IF and WB compared to DLD-1 cells (**see figure 46 and figure 48).** However, our observation of vimentin by both mRNA and WB was not in agreement with our IF result. There is no clear explanation for the lack of vimentin expression as detected by IF, and due to short time frame towards submission deadline, I was not able to validate this finding using another vimentin antibody. Despite vimentin IF finding, this cell line showed a moderate level of E-cadherin, vimentin and α-SMA by WB, and it was reported to express N-cadherin and ZEB1 [535]. In addition to this, it has frequently been characterised as a highly metastatic cell line [502, 520, 534], and this might be confirmed by the presence of mesenchymal-like cells. From all of these findings, it is clear that the LoVo cell line has more mesenchymal characteristics, and this could classify it as an intermediate mesenchymal cell line that is unable to undergo complete EMT.

SW620 and SW480 was obtained from the same colon cancer patient in which the former was taken from a metastatic site and the second one from the primary site [539]. Similar to observations of tumour material from metastatic sites, SW620 cells re-gained a reasonable level of E-cadherin by WB and IF [131, 133-135, 549, 550]. This could be a sign of SW620 cells re-differentiating and undergoing an MET process. SW620 cells also exhibited a moderate amount and a homogenous immune staining of vimentin as observed by WB. F-actin indicated a homogenous population of small fibroblast-like cells with microfilaments organised at the front of cells providing an invadopodia-like shape. Indeed, a recent study investigated the morphological features of SW620 and SW480 with respect to their cytoskeleton using different kinds of advanced light microscopy. They concluded that SW480 represents more lamellipodia and filopodia with a thin and extended cell membrane of actin filaments compared to SW620 which displayed a smoother surface with a lower filopodia density and lamellipodia area, and fewer number of actin protrusions [557]. Indeed, SW620 cells were reported to have less metastatic and migration potential compared to SW480 [551]. N-cadherin was not detected in SW620 cells and the amount of keratins was greater than in SW480 mesenchymal cells but less than DLD-1 epithelial

cells. ZEB1 and α-SMA proteins were seen in SW480, but they are much less or non-existent in SW620 cells. All of these findings could indicate that SW620 cells are intermediate cells with more epithelial morphology, perhaps representing a greater completion of the MET process.

From this discussion, it can be concluded that the 12 CRC cell line panels can be categorised into three groups depending on their EMT status and morphological appearance:

- Epithelial cell category, which includes: AAC1, Caco2, Colo205, DLD-1, HT29 and SW48.
- Mesenchymal cell category, which includes: CT26, RKO and SW480 cell lines.
- Intermediate cell category is sub-classified into
- Intermediate epithelial cells: HCT116 and SW620.
- Intermediate mesenchymal cells: LoVo.

3.2.5 EMT status of the DLD-SIP1 CRC EMT model in relation to its morphological appearance

DLD-1 cells used in this study were stably transfected with a doxycycline-inducible SIP-1 plasmid. SIP1 expression was achieved with 2µg/ml doxycycline. Morphologically, after 3 days of induction, DLD SIP-1 cells converted from clustered epithelial islands into single bipolar fibroblast-like cells. The remarkable plasticity of the DLD-SIP1 EMT CRC model as well as the A431-SIP1 squamous cancer EMT model were reported for the first time by Vandewalle and colleagues [216], who found that different mRNA and proteins that are related to tight junctions and desmosomes were down-regulated upon SIP1 induction in DLD-SIP1 cells. As the DLD-SIP1 EMT CRC model will be used during the entire project, checking the EMT status of the model before conducting any experiments was necessary. The EMT status of DLD-SIP1 model was analysed using WB, IF and mRNA profiling; see **figures 45, 46, 47, 49 and 50**. E-cadherin was radically reduced and SIP1 was remarkably up-regulated upon SIP1 induction in all the methods used. In addition, IF staining for ZO-1, β-catenin and connexin 43, revealed that these proteins were expressed at lower levels and trans-located from their integrated sites at the cell-cell membranes to cytoplasm; **see figure 49**. Moreover, WB for cytokeratins and α-SMA demonstrated that DLD-I cells has less keratins and more α-SMA than DLD-UI cells. In addition, F-actin was well organised at the cell-cell junction but it got oriented toward the cell membrane which led to an increase in the number of protrusions resembling invadopodia after SIP1

induction in the DLD-SIP1 cells. Based on these results, it can be concluded that the DLD-SIP1 CRC EMT model offered a suitable means of investigating our hypothesis established at the outset of this project.

Chapter 4: EMT Driven Cytokine/Chemokine Expression in CRC

5.1 Introduction

The presence of metastatic or invasive cancer cells has been proposed to predict poor patient outcome [90, 220, 230, 245]. Similarly, as mentioned in the main introduction, the presence of certain types of immune cells, infiltrating the primary cancer, are linked with patient survival and therefore metastasis [332, 354, 558, 559]. However, whether **1-** metastatic cells can alter the tumour microenvironment by secreting soluble factors that define immune infiltrate or **2-** certain immune cells infiltrate the primary tumour and induce EMT by secreting cytokines/chemokines and therefore induce metastasis, is not clearly understood. For the reason that metastatic cells can be detected very early during tumorigenesis, and even in some cases distant metastasis can occur without any sign of a primary tumour [102, 103], we reasoned that metastatic cells have a bigger influence on the immune filtrate. To address this question, we performed a screen to qualitatively investigate 67 chemokines and cytokines using the DLD-SIP1-inducible EMT model. We intended to validate our findings with multiple chemokine/cytokine detection techniques using the EMT status of CRC cell line panel as characterized in the previous **chapter (4).**

4.1 The aims

- Identify chemokines that are significantly up regulated during SIP1-induced EMT.
- Establish criteria to limit the number of soluble factors for further investigation
- Correlate the expression of the candidate soluble factors with the EMT status of CRC cell lines.
- Choose the most relevant soluble factor for mechanistic/functional studies.

4.2 Results

4.2.1 Human chemokine and cytokine arrays for DLD-SIP1 CRC-EMT model

Thirty-one chemokines and thirty-six cytokines spotted onto four nitrocellulose membranes were analysed using 300 µg cell lysates and 700 µl supernatants of the un-induced and induced DLD-SIP1 cells. See **Table 12** and **Table 13** in the appendix section for the list of the analysed chemokines and cytokines. The nitrocellulose membranes with chemokine and cytokine capture antibodies were incubated overnight with a mixture of biotinylated detection antibodies and the cell lysates or supernatants. The obtained results are summarised in **Table 9, figure 51** and **figure 52**.

The results were calculated by measuring the mean pixel density of the selected chemokines/ cytokines and then obtaining the percentage change in the induced DLD cells compared to the un-induced ones.

The total cell lysate (intracellular) and cell culture media supernatants (extracellular) were both used to assess the expression pattern of cytokines/chemokines. All the reference spot controls gave the same mean pixel density for both the samples, which means that the system was working efficiently.

CCL5 was repeatedly seen in the intracellular and extracellular chemokine and cytokine arrays with a remarkable increase; fold change of the average mean pixel density compared to the un-induced cells was 2.7- and 5–times increase, respectively. Additionally, CXCL8 (IL-8) was found decreased in both intracellular and extracellular chemokine and cytokine arrays with a fold change of the average mean pixel density of 11-14-times compared to the un-induced cells.

Midkine (MDK) and CXCL5 chemokines were found to increase sharply 10-times and decreased by 25-times in the induced cells compared to the un-induced ones, respectively. However, the radical change in the amount of MDK or CXCL5 was only seen in one compartment; MDK was seen in the extracellular compartment whereas CXCL5 was observed in the intracellular compartment. Moreover, CXCL4, CXCL7 chemokines and IL-α cytokine also gave important findings; they were all found to be decreased in both cellular compartments of the induced-DLD cells compared to the un-induced ones.

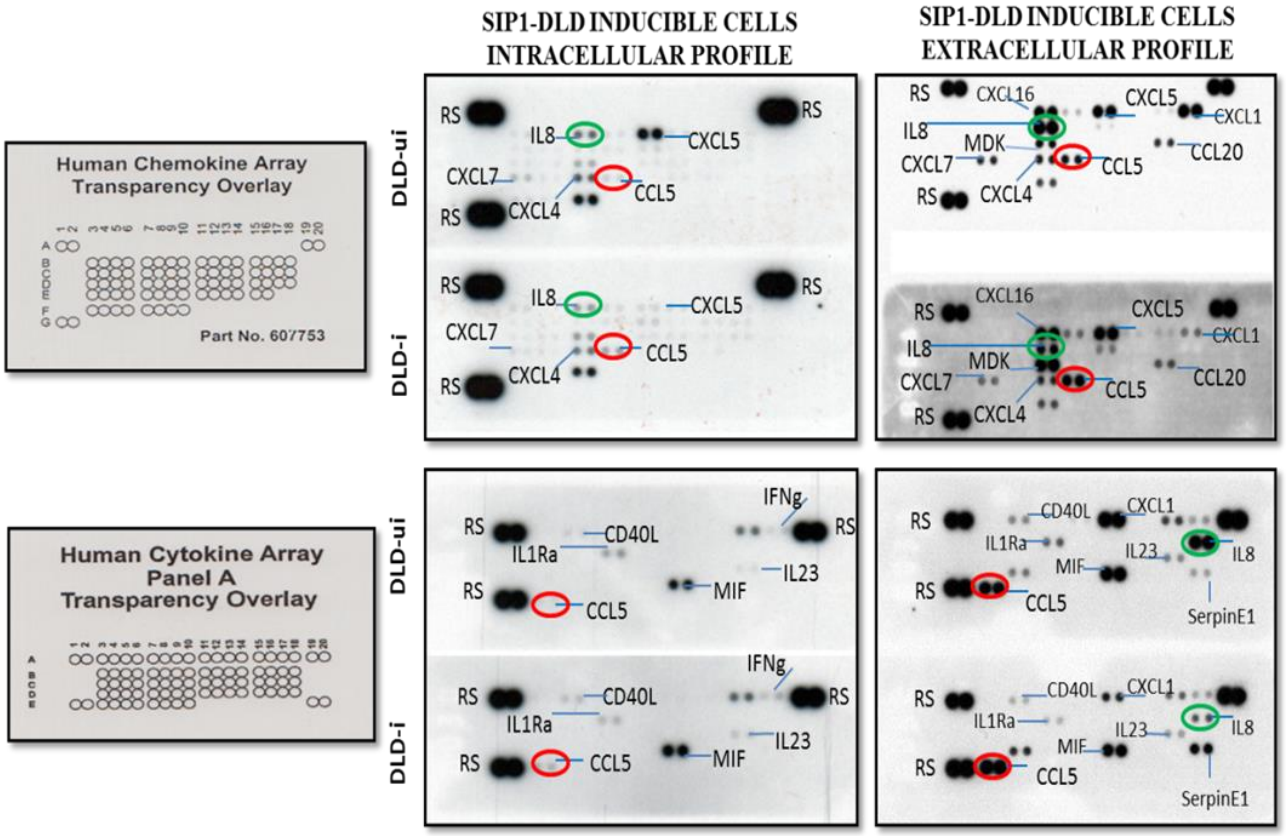

Figure 51: Investigating the expression of 31 chemokines and 36 cytokines in the CRC-EMT model.

DLD-SIP1 cells were treated with 2 µg/ml doxycycline for 3 days. 300 µg of cell lysate and 700 µl of cell culture supernatants of DLD-UI and DLD-I cells were mixed with a cocktail of biotinylated detection antibodies and incubated overnight with captured antibodies spotted onto nitrocellulose membranes. The reaction was visualised with ECL reagent and on X-ray films. The location of the controls and cytokines or chemokines was identified by aligning the membrane with transparency overlay template and following the pair reference numbers listed in the kit leaflet. Pixel densities on developed X-ray film were analysed using a transmission scanner and image analysis software. RS (reference spot). DLD-UI (un-induced).

Table 11: A summary of the obtained results from the human chemokine and cytokine arrays (R&D systems)

	Intracellular chemokine	Extracellular chemokine	Intracellular cytokine	Extracellular cytokine
↑	CCL5	CCL5 Midkine	CCL5 MIF CD40L IL23 IFN-δ CD54	CCL5 CXCL10 Serpin E1
↓	CXCL5 IL-8 CXCL4 CXCL7	CXCL-8 IL-8 CXCL1 CXCL4 CXCL7 CLL20 CXCL16	IL-1α	IL-1α CD40L CXCL1 CD54 IL-8 IL23 MIF GM-CSF

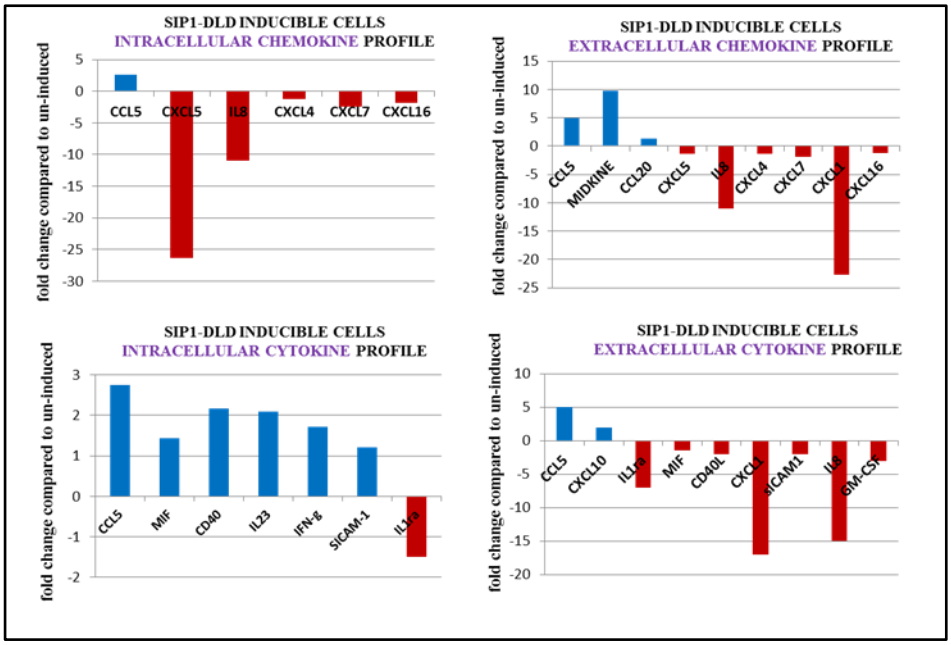

Figure 52: Charts summarising the results obtained from R&D system human chemokine and cytokine arrays.

4.2.2 Criteria to limit the number of soluble factors for further investigation

Briefly, our aim was to narrow down our findings from the R&D systems array to 4 soluble factors by setting up selective criteria. Only one out of 4 soluble factors will be selected on to address the hypothesis and to accomplish the main goals of my thesis; **see section 1.5.2** of the first chapter. The criteria were gradually moved from **Tier 1** to **Tier 2**.

Tier 1:

- Chemokines and cytokines will be equally assessed but chemokines will be given priority because they are less studied compared to cytokines. This is necessary for the novelty aspect of the project.
- They should be significantly increased or decreased, both in the cell and in the cell supernatant.
- There should be a significant correlation in the literature in relation to cancer/ metastasis with minimal mechanistic investigation.

Tier 2:

- The change in expression should be validated by more than one applicable technique (ELISA, multiplex, etc.) and give similar results.
- The expression change (increase/decrease) should be valid in the CRC panel of cell lines. The final candidate should have no conflicting results between mesenchymal and epithelial groups.

As a result, the following chemokines were chosen; CCL5, IL-8, MDK and CXCL5 as they fulfilled the tier1 criteria. Tier 2 will be assessed and discussed throughout the next sections.

4.2.3 Validation of CCL5, IL-8, MDK and CXCL5

4.2.3.1 Validating MDK and CXCL5 at the mRNA and protein levels in DLD SIP-1 CRC-EMT Model and the CRC Panel

MDK and CXCL5 were found by R&D arrays to be sharply increased and decreased, in the induced-DLD-SIP1 cells, respectively. RT-PCR and WB were the techniques used to validate their transcription and translation in the DLD-SIP1 CRC EMT model as well as in some randomly chosen CRC cell line with known EMT status.

MDK mRNA was found to be up-regulated in induced-DLD-SIP1 cells in comparison to un-induced-DLD-SIP1 cells. WB, showed a slight reduction of the intracellular MDK protein in the induced DLD-SIP1 cells and no detectable expression was found with the lysate of either DLD-SIP1 induced or un-induced cells; see **figure 53.** IF was used to further validate the intracellular MDK protein in this model. The staining confirmed that

MDK is a cytoplasmic protein expressed more in mesenchymal cells (DLD-I cells) than epithelial ones (DLD-I cells); see **figure 54.**

The randomly chosen CRC cell lines: CT26, SW480 mesenchymal cell lines, and Colo205, HT29 epithelial cell lines, and SW620 intermediate epithelial cell lines, were tested for their intracellular MDK level; see **figure 53.** No significant difference was observed between the mesenchymal and the epithelial cell lines for their MDK protein. Similarly, the whole CRC panel (12 cell lines) were analysed for the transcriptional level of MDK. Unfortunately, there was no conclusive result from analysing the mRNA level between the mesenchymal/intermediate mesenchymal and the epithelial/intermediate epithelial cell lines. MDK mRNA was found high in Caco2, Colo205, SW620 epithelial/intermediate epithelial as well as HCT116, RKO mesenchymal/ intermediate epithelial cells. MDK mRNA was not detectable in CT26 due to primers specifically amplifying only human MDK.

Interestingly, WB analysis agreed with the finding from R&D systems arrays for a sharp decrease in extracellular CXCL5 level in the DLD-SIP1 model. Clearly, the extracellular CXCL5 was down-regulated in the cell culture supernatant of DLD- SIP1 cells after SIP1 induction compared to its level without induction. However, the intracellular level was not detected at all by WB using the same model. mRNA was used to validate the transcriptional level of CXCL5. The result showed that the intracellular transcription level of CXCL5 mRNA was down-regulated in SIP1 induction. Also, the transcriptional level of mRNA CXCL5 was also investigated in the 12 CRC cell lines. No detectable amount was observed in any of the 12 CRC cell lines except DLD-1; see **figure 53**. From this, we think it might an isolated event specific for DLD-SIP1 cells.

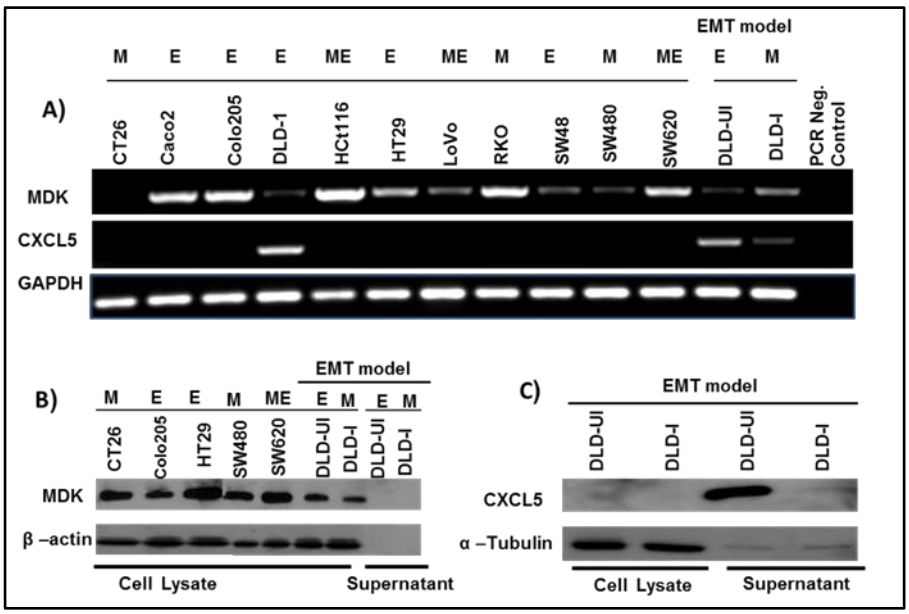

Figure 53: Expression of MDK and CXCL5 in the CRC panel and DLD SIP-1 inducible CRC EMT model

A) RT-PCR from MDK and CXCL5 cells in the CRC panel and DLD SIP-1 inducible CRC EMT model.
B) The intracellular and extracellular protein levels of MDK in a panel of CRC cells and in DLD SIP-1 stably induced CRC-EMT model by using WB.
C) The intracellular and the extracellular protein level of CXCL5 in DLD SIP-1 CRC-EMT model by using WB. The figures are a representative demonstration of at least 3 independent results. MDK (Midkine), DLD-UI (un-induced DLD-SIP1 cells), DLD-I (induced DLD-SIP1 cells), M (mesenchymal), E (epithelial), ME (metastable).

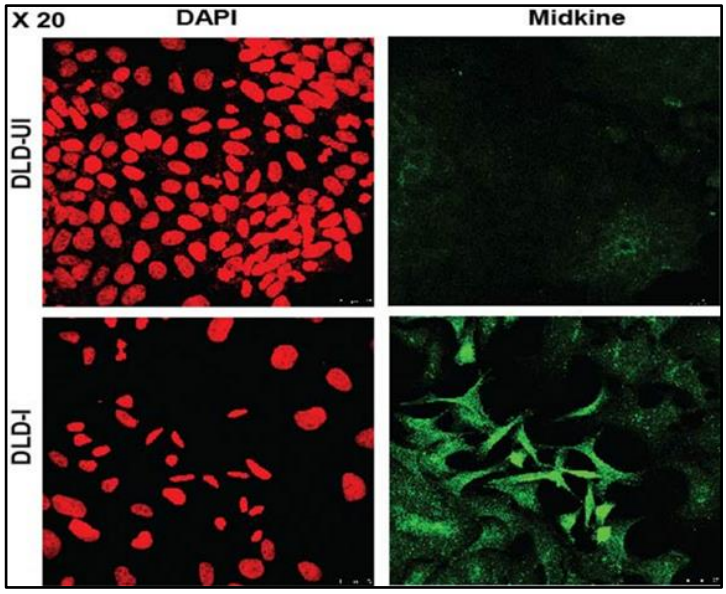

Figure 54: Intracellular MDK expression was analysed using immunofluorescence and confocal microscopy in DLD SIP-1 CRC EMT model.

DLD-SIP1 cells were induced for 3 days with 2 µg/ml doxycycline. DLD-I cells showed high MDK expression compared to the un-induced ones. MDK was detected using MDK antibody followed by a green- (Alexa 488) conjugated secondary antibody. The figure is a representative demonstration of at least 2 independent results. DLD-UI (un-induced DLD-SIP1 cells) DLD-I (induced DLD-SIP1 cells).

4.2.3.2 Validation of CCL5 and IL-8 findings by 25-Multiplex detection immunoassay in SIP1 EMT models

Our findings of CCL5 and IL-8 cytokines by R&D systems were validated further using a cytokine multiplex immunoassay that was provided by my third supervisor, Dr. Anthony Williams, who is specialist in clinical immunology and allergy. Supernatant from DLD-SIP1 cells before and after induction were used. Similarly, CCL5 sharply increased in the supernatants of the induced DLD cells to 2290 pg/ml compared to the un-induced cells (790 pg/ml). IL-8, which was found sharply decreased in the R&D systems array, was also seen to decrease to 1730 pg/ml in the supernatant of the induced DLD cells as compared to the un-induced DLD cells (29070 pg/ml); see **figure 55.** These results validated the changes observed for CCL5 and IL-8 by the R&D systems arrays.

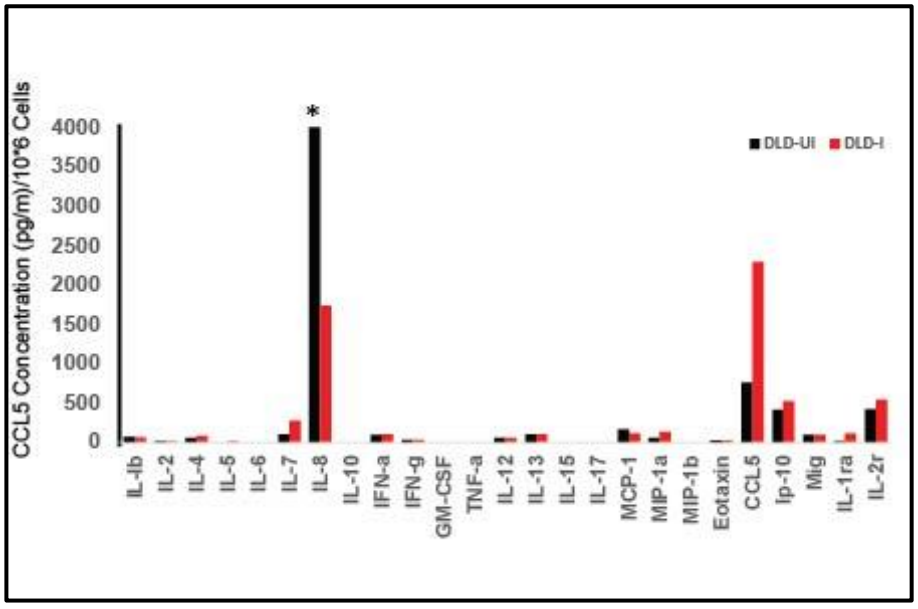

Figure 55: 25-Multiplex detection immunoassay for DLD SIP-1 stable inducible CRC-EMT model.

Equal number of cells were seeded and cultured for 3 days. The supernatants from DLD-UI and DLD-I cells were collected after 3 days. The test samples, control samples and standards were incubated with different beads attached to various capture antibodies overnight. The beads were analysed with a luminex detection system to measure the concentration of the soluble factors. DLD-UI (un-induced DLD-SIP1 cells) DLD-I (induced DLD-SIP1 cells). *more than 4000 pg/ml.

To generalise our findings, we used another SIP1 inducible model of EMT (A431-SIP1 cells) and performed the multiplex experiment. A431 cells are of epithelial carcinoma origin and they show all biochemical and morphological signs of EMT [216]. Cell culture supernatant from induced and un-induced A431-SIP1 cells was used. As observed before, CCL5 increased 4 folds in A431-I cells (460 pg/ml vs 1940 pg/ml). However, IL-8 was up-

regulated 2-times (8060 pg/ml) in A431-I as compared to A431-UI cells (3500 pg/ml); **see figure 56.**

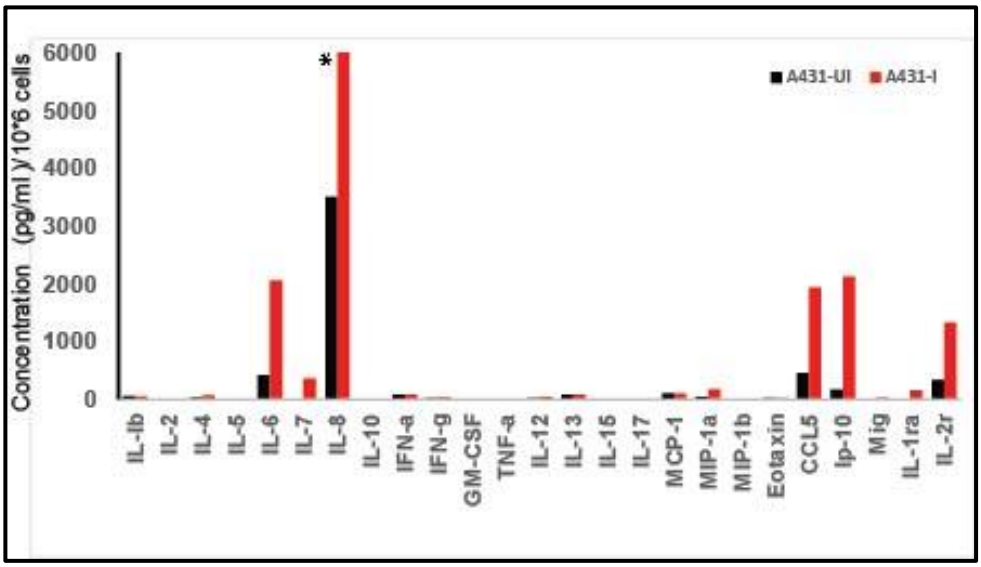

Figure 56: Multiplex detection immunoassay for A431 SIP-1 stable inducible squamous cell carcinoma EMT model.

Equal number of cells were seeded and cultured for 3 days. The supernatants from A431-UI and A431-I cells were collected after 3 days. The test samples, control samples and standards were incubated with different beads attached to various chemokine or cytokine capture antibodies overnight. The beads were analysed with a luminex detection system to measure the concentration of the soluble factors. A431-UI (un-induced DLD-SIP1 cells), A431-I (induced DLD-SIP1 cells). * More than 6000 pg/ml.

In conclusion, the increase level of CCL5 in the induced DLD-SIP1 cells is in agreement with the R&D arrays finding. The sharp decrease of IL-8 in DLD-SIP1 cells after induction is also in align with our R&D arrays result. However, the opposite result was obtained from A31-SIP1 cells. Indeed, up-regulation of IL-8 has been repeatedly reported to promote metastasis in CRC [560-563], and that contrary finding for DLD-SIP1 CRC EMT model could be an isolated finding for CRC. For this reason, at this stage, IL-8 will not be investigated any further and CCL5 be the focus of further investigation.

4.2.3.3 Further validation of CCL5 induction in SIP1 inducible models and in CRC cell lines.

4.2.3.3.1 CCL5 expression in DLD-SIP1 CRC EMT model

CCL5 was found repeatedly up-regulated upon SIP1 induction in the R&D arrays as well as multiplex immunoassay. Other validated techniques including WB, mRNA analysis and IF techniques were used to validate the intracellular amount of CCL5, whilst ELISA was used to confirm the extracellular expression.

CCL5 mRNA was also found up-regulated upon SIP1 induction in the DLD-SIP1 cells compared to the induced ones**; see figure 57**. WB showed that the intracellular protein is equally expressed in both induced and non-induced DLD-SIP1 cells; **see figure 57**. This might indicate that the WB technique is not an appropriate way to detect the intracellular CCL5 protein. IF was therefore used.

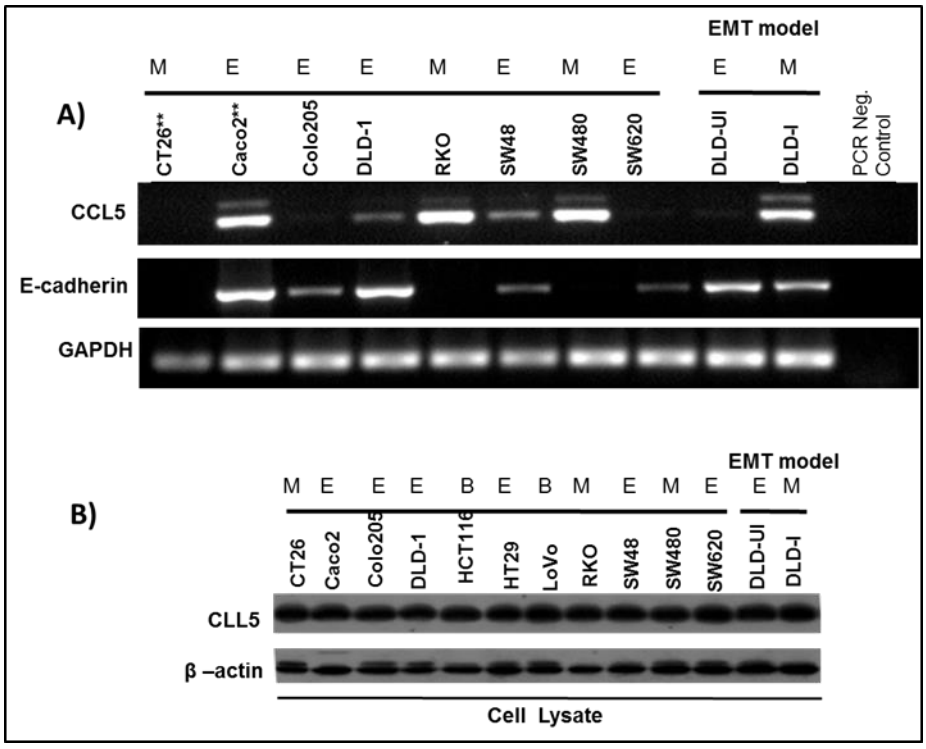

Figure 57: Expression of CCL5 in a panel of CRC cell lines and the DLD SIP-1 inducible CRC EMT model

A) RT-PCR of CCL5 in a panel of CRC cell lines and the DLD SIP-1 inducible CRC EMT model. B) Protein level of CCL5 chemokines in a panel of CRC cell lines and DLD SIP-1 stably induced CRC-EMT model. The figure is a representative demonstration of at least 3 independent results. ** CT26 and Caco2 were miss-loaded when identifying CCL5; CT26 cells have more CCL5 than Caco2cells.

IF staining also showed up-regulation of CCL5 in DLD-SIP1 cells upon induction. The IF staining also showed that CCL5 protein accumulates in the cytoplasm, and not the nucleus; **see figure 58**.

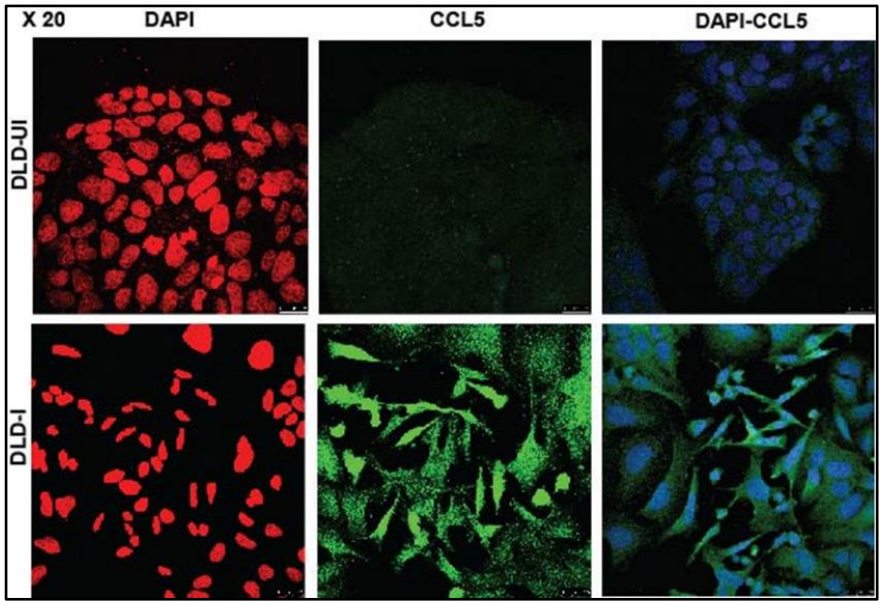

Figure 58: Spatial intracellular CCL5 expression was analysed using immunofluorescence and confocal microscopy in DLD SIP-1 CRC EMT model.

DLD-SIP1 cells were induced for 3 days with 2 µg/ml doxycycline. DLD-I cells showed high CCL5 expression compared to the un-induced ones. CCL5 was detected using a CCL5 antibody followed by green- (Alexa 488) conjugated secondary antibody. DAPI counterstain was used to detect the nuclei. The figure is a representative demonstration of at least 2 independent results. DLD-UI (un-induced DLD-SIP1 cells) DLD-I (induced DLD-SIP1 cells).

ELISA results indicated that the abundant secretion of CCL5 was 2.6-times greater in the induced DLD compared to the un-induced cells with a *p* value of 0.001. The A431-SIP1 model was also used to investigate the level of secreted CCL5 before and after SIP1 induction. Similarly, CCL5 was ~ 8-times greater in A431-induced cells compared to A431 un-induced cells with *p* value of 0.004. Of note, as SIP1 induction changes cell cycle properties of DLD-SIP1 and A431-SIP1 cells, cells were therefore counted at the time of supernatant collection and the level of CCL5 was normalised pg/one million cells; **see figure 59 .**

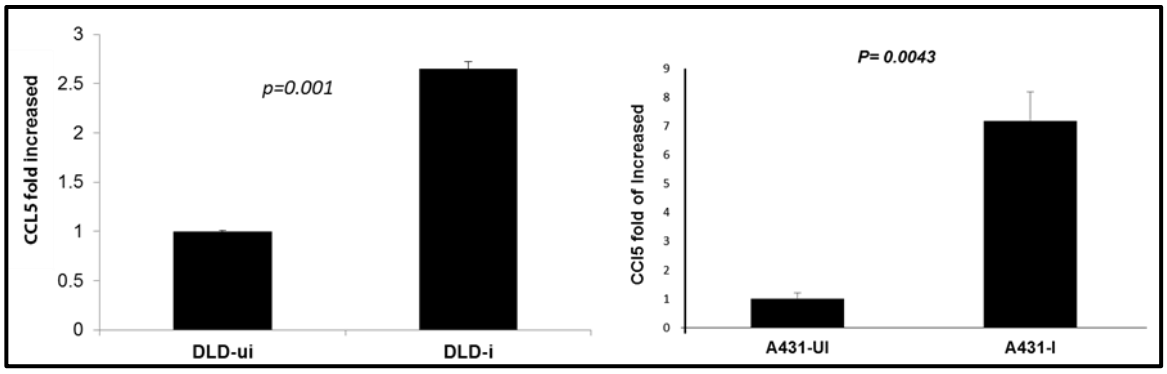

Figure 59: Human CCL5 was detected by sandwich ELISA in the supernatant of DLD SIP-1 and A431-SIP1 cells.

DLD-I and A431-I cells were induced for 3 days using 2 µg/ml doxycycline, and the supernatants were collected to analyse the abundance of secreted CCL5 by ELISA. The wells of a 96 plate were coated overnight at room temperature with 1.0 µg/ml mouse anti-human CCL5 capture antibody. A three-fold serial dilution of the highest standard (2000 pg/ml), and diluted cell line supernatants were used. A detection antibody at a 20 ng/ml working concentration was followed by diluted streptavidin-conjugated-HRP (1:1000) and Substrate Solution (1:1 H_2O_2: Tetramethylbenzidine). The optical density was determined using a microplate reader at 450 nm with the wavelength correction at 570 nm. The readings were taken every 5 min intervals for 40 min. The results were normalised by the cell number to measure the average secretion of CCL5 per million cells. The figure is a representative result of 3 independent experiments. DLD-UI (DLD-un-induced), DLD-I (DLD induced).

4.2.3.3.2 CCL5 expression in a selected cohort of CRC cell Lines

To generalise our finding for CCL5, Caco2, Colo205, DLD-1, SW48 epithelial cell lines, SW620 intermediate epithelial cells and CT26, RKO, SW480 mesenchymal cell lines were chosen. The EMT status of these cell lines was investigated in chapter 3. Both RT-PCR and WB investigated the intracellular level of CCL5 in the chosen panel, whereas ELISA was used to examine the extracellular expression.

Interestingly, CCL5 mRNA was observed to be up-regulated more in the mesenchymal cell lines (CT26, RKO, and SW480) as compared to the epithelial ones; **see figure 57.** Similar to the DLD-SIP1 EMT CRC model, CCL5 was found widely distributed in all 12 CRC cell lines, which could, again suggest that WB is not the appropriate technique to investigate CCL5; **see figure 57.**

ELISA showed that CCL5 concentration in the supernatants of the epithelial cell lines ranged between 28-186 pg/ml, whereas it varied from 440-990 pg/ml in the mesenchymal ones. As a result, the average concentration of secreted CCL5 is statistically significant between the epithelial group (107.6 ± 30 pg/ml) and the mesenchymal group (639.7 ± 175 pg/ml) with a *p* value of 0.0075; **see figure 60.**

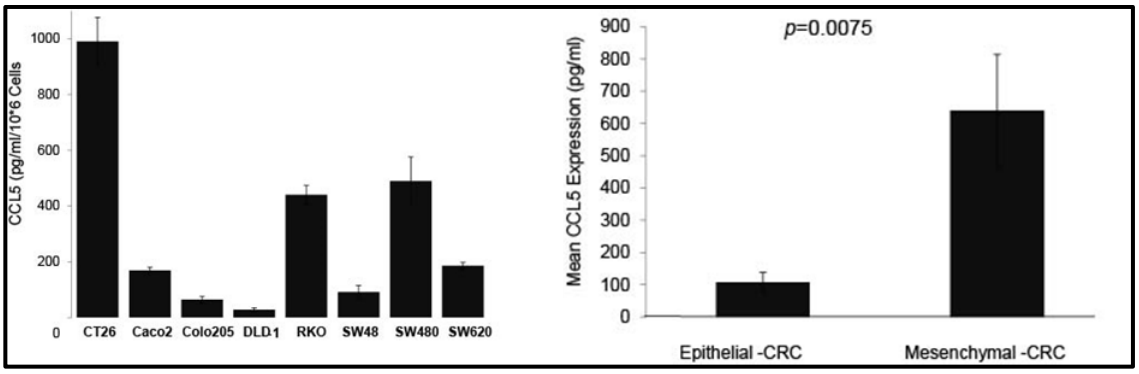

Figure 60: Human CCL5 was detected by sandwich ELISA in the supernatants of five chosen epithelial or intermediate epithelial CRC cell lines and three mesenchymal CRC cell lines.

The figure shows a statistically significant difference in CCL5 expression between epithelial and mesenchymal CRC cells. The results were normalised by the cell number to detect the average CCL5 secretion per 1 million cells. The figure is a representative result of three experiments.

4.2.4 The final candidate

CCL5 was reproducibly shown to change in SIP1-inducible EMT models as well as present in mesenchymal CRC cells. IL-8 down-regulation upon induction of SIP1 did not agree with A431-SIP1 inducible model, and also a conflict finding of IL-8 up -regulation in CRC has also been frequently reported. CXLC5 was only expressed in DLD-1 cells but no other CRC cell line, and MDK exhibited no significant difference between the epithelial and the mesenchymal EMT groups. Consequently, CCL5 met the selective criteria that were established at the start of this chapter and for that, it is chosen for further study.

4.3 Discussion

Patients with invasive cancer or the presence of distant metastasis have an immunosuppressed phenotype and thus a poor prognosis [220, 230, 332, 354]. In addition, metastasis and a poor prognosis have been associated with altered secretion of chemokines which in turn can reduce any anti-tumour response [184, 386, 564]. However, the role of EMT in altering the secretion of chemokines and thus enhancing metastasis and evading immune destruction has been not widely studied in cancer, particularly in CRC. Thus, I hypothesized that EMT and the anti-tumour response may be linked via altered secretion of soluble factors by metastatic cells in favour of an immune-compromised tumour microenvironment.

To test our hypothesis, the intracellular and extracellular expression of 67 human chemokines and cytokines were investigated using a defined CRC-EMT model; see figure 53. To our knowledge, this is the first study characterising the expression of a large number of cytokines and chemokines using DLD-SIP1 CRC-EMT model.

Technically, the R&D systems arrays worked as expected. The reference control spots showed the same pixel densities in the un-induced and induced DLD-SIP1 samples. Importantly, similar findings were obtained for chemokines which were present in both cytokine and chemokine arrays. For example, CCL5 is spotted in the chemokine and cytokine arrays and it was up-regulated in both. Similar results were also observed for CXCL7, CXCL4 chemokines and IL-1α cytokine in the two cellular compartments. The major findings are the significant increases in CCL5 and the sharp decrease in IL-8 in both arrays and in the two cellular compartments. Other interesting findings from the arrays were the remarkable increase of extracellular MDK and the remarkable decrease of the intracellular CXCL5. All these findings indicate that the arrays have a high sensitivity and accuracy.

To select a soluble factor for future studies, I established a 2 tier selection criteria. Briefly, I aimed to narrow down to 4 soluble factors using tier 1 criteria, analyse it further using tier 2 criteria and select only 1 soluble factor as the main focus of my thesis.

Tier 1:

- Chemokines and cytokines will be equally assessed but chemokines will be given priority because there are less studied as compared to cytokines. This is necessary for the novelty aspect of the project.
- They should be significantly increased or decreased, both in the cell and in the cell supernatant.
- There should be a significant correlation in the literature in relation to cancer/ metastasis with minimal mechanistic investigation.

Tier 2:

- The change in expression should be validated by more than one applicable technique (ELISA, multiplex, etc.) and give similar results.
  The expression change (increase/decrease) should be valid in the CRC panel of cell lines. The final candidate should have no conflicting results between mesenchymal and epithelial groups.

As a result, the following chemokines were chosen; CCL5, IL-8, MDK and CXCL5 as they fulfilled the tier1 criteria. From assessing tier 2 criteria a candidate was selected to test the project hypothesis.

Up-regulation of IL-8 was repeatedly reported to promote metastasis in CRC [560-563]. In addition, up regulation of IL-8 was implicated in modulating the tumour microenvironment via the EMT programme [442, 444]. However, expression of IL-8 in DLD-SIP1 CRC-EMT model showed the opposite; I observed a strong down-regulation of IL-8 during SIP1-induced CRC EMT. Using a squamous cell cancer model of SIP1 induced EMT (A431), I investigated changes in cytokine/chemokine expression using a multiplex beads immunoassay. In this screening, it was found that IL-8 was up regulated upon SIP1 induction; **see figure 56.** For these reasons, I concluded that the secretion of IL-8 cannot be directly regulated by SIP1, and thus I excluded it from the study.

Although increased levels of MDK have been widely reported in the literature, it has been scarcely studied in CRC and EMT fields [403, 565, 566]. The sharp increase in expression determined by the R and D system arrays was only at the extracellular compartment. The intracellular MDK was investigated further by mRNA and IF, and a significant increase was observed in the induced DLD-SIP1 cells compare to un-induced cells; **see figure 54.** The mRNA and the intracellular protein level of the CRC panel gave inconclusive results, and no significant finding between the mesenchymal and the epithelial groups was observed; **see figure 53**. For that, I did not focus on MDK.

CXCL5 was not significantly different between the epithelial and the mesenchymal groups; there was no detectable amount of the protein or mRNA levels in the CRC panel apart from DLD-1 cell line and DLD-SIP1 CRC EMT model**; see figure 53.** Thus, the decrease of CXCL5 in induced DLD-SIP1 cells is an isolated, not general phenomenon. In addition to this, although our findings of decreased CXCL5 were supported by other authors, a controversial observation related to CXCL5 expression in cancer was reported as well [567, 568]. More specifically, CXCL5 was reported to be highly expressed in CRC [569, 570]. Furthermore, human CXCL5 has a very high structural homology to human CXCL6 [571], which would make it difficult to differentiate the biological action between them or reach the level of *in vivo* experiments. Having considering all the aforementioned reasons, I left CXCL5 out of our study.

CCL5 results successfully met our selective criteria. In both arrays, the extracellular and the intracellular proteins were sharply increased in the induced DLD-SIP1 cells compared

to the un-induced cells. Human CCL5 ELISA, beads immunoassay and RT-PCR confirmed our arrays findings for DLD-SIP1 CRC-EMT and A431-SIP1 squamous cancer EMT models; **see figure 57.** IF results also asserting a significant increase of CCL5 in the induced DLD-SIP1 cells, and it showed, that CCL5 is localised to the cytoplasm; **see figure 58.**

To investigate further, the intracellular and the extracellular expression of CCL5 was checked in our CRC panel using WB, RT-PCR, and human CCL5 ELISA, respectively; **see figure 57.** RT-PCR showed that the *CCL5* gene is transcribed more in the metastatic cells compared to the epithelial once; **see figure 57**.Accordingly, the ELISA result showed that translation and secretion of CCL5 is much more in the mesenchymal cells (CT26, RKO and SW480) compared to the epithelial ones (p value =0.0075); **see figure 60.**

Indeed, CCL5 has been implicated as a poor prognostic factor in predicting disease-free survival [462, 572-578]. However, there is a discrepancy about the source of CCL5. Few reports indicated that CCL5 is secreted more by MSCs and the direct contact of these cells to cancer cells enhanced their migration and invasion and thus metastasis [307, 308, 579, 580]. Furthermore, activated CTLs, DCs and other immune cells infiltrating into the tumour stroma were also reported to be a source of CCL5 [581, 582]. Others reported that CCL5 is directly produced by the tumour cells themselves and this can enhance their metastasis [433, 462, 572, 578]. In our opinion, both tumour cells and the stroma could coordinate the level of both paracrine and autocrine signalling of CCL5 to enhance tumour immunosuppression, invasion and metastasis.

Our findings differentiate specifically which tumour cells secrete more CCL5. CCL5 is secreted more by the mesenchymal (metastatic) tumour cells, which were found in chapter 3 to express ZEB1 or ZEB2. In fact, other scientists have supported our findings of CCL5 up-regulation in the mesenchymal cells indirectly. It was found that CCL5 is expressed more at the invasive front of CRC primary tumours, and that cancer cells at the invasive front are more metastatic, display signs of EMT and can predict poor patient survival [523, 524]. Another piece of evidence is that, a stem like subpopulation within ovarian cancer expresses (CD133+) and a stem-like subpopulation within breast cancer expresses (CD44+, CD24-) were found to have to have high CCL5 expression [583-585]. It has been previously determined that one of the important signs of cells undergoing EMT is that they acquire stemness features including resistance to apoptosis, self-renewing and the ability to differentiate [284]. Furthermore, Kao *et al*., detected that MDA-MB-231, Hs578T and SUM-159 breast cell lines, which showed fibronectin, vimentin, and MMP2 mesenchymal

markers, were found to have a high level of CCL5 [586]. Taken together, the novelty of our CCL5 findings is that, we determined which tumour CRC cells secrete more CCL5 in the context of EMT.

As a conclusion of the chapter, CCL5 was the only chemokine which met our selective criteria. It is therefore the candidate to be chosen for further investigation to address our initial hypothesis.

In the next two chapters, CCL5 will be studied in more detail following two main objectives:

- The mechanistic role of ZEB1/2 EMT in activating CCL5 in CRC **(Chapter 5).**
- The molecular basis of immune infiltration as a result of CCL5 up-regulation in the context of EMT in CRC **(Chapter 6).**

Chapter 5: The Mechanistic Role of ZEB1/2 EMT in Activating CCL5 in CRC

5.1 Introduction

CCL5 is the candidate that was chosen from the previous chapter, with a set of selective criteria in order to test the hypothesis of the project. Indeed, an observation from the previous chapter is that CCL5 is more highly expressed after induction of the *SIP1* gene in DLD-SIP-1 and A431-SIP1 cells, and in the mesenchymal CRC cell lines expressing SIP1 or ZEB1. In fact, in the third chapter, I found that ZEB1/2 were the EMT regulatory markers that help to differentiate EMT status in the CRC panel. As mentioned, ZEB1/2 have been strongly implicated in CRC metastasis and are associated with poor patient survival [217, 523].Therefore, I have proposed that CCL5 might be up-regulated upon induction of ZEB1/2 in carcinoma cells making EMT and metastasis possible by escaping immune destruction. In fact, TWIST and SNAIL have been implicated in up regulating IL-8 and CCL2 in CRC and breast cancer [357, 442, 457, 587], but little has been studied in the context of EMT-mediated chemokine production in CRC. Whilst there are two recent reports linking CCL5 up-regulation to EMT [580, 588], none show direct evidence that ZEB1/2 up-regulate CCL5 expression. We think our project is novel in respect to understanding the role of ZEB1/2 in driving CCL5 expression, and in highlight the benefit of CCL5-targeted cancer therapy.

Before conducting the chapter objectives, it is worth introducing CCL5 briefly with respect to cancer and the mechanism of its regulation.

5.1.1 C-C chemokine ligand 5 (CCL5) in cancer

C-C chemokine ligand 5 (CCL5) is a member of the 'CC' subfamily of chemokines. It is also known as RANTES (Regulated upon Activation, Normal T cell Expressed and presumably Secreted), as it was originally identified as a product of activated T cells [589]. Human CCL5 protein is 91aa (8-10 KDa) and exhibits approximately 85% homology with mouse Ccl5 [590]. The activity of CCL5 is mediated via binding to CCR1, CCR3 and CCR5. Among these receptors, CCR5 is considered the main receptor for CCL5 and the major co-receptor for HIV [388, 431].

CCL5 plays an active role in recruiting various kinds of immune cells such as T cells, macrophages and eosinophils into sites of inflammation [591]. It also contributes to maturation and proliferation of normal T cells, dendritic cells and natural killer cells [592-594]. Recent research indicates that CCL5 has an important role in the progression and metastasis of many solid tumours such as melanoma, breast cancer, gastric cancer, colon cancer, ovarian cancer and prostate cancer [572, 574, 576, 595-597].

5.1.1.1 **Expression of CCL5 in human specimens**

CCL5 up-regulation in human tissue, plasma, serum is associated with anti-tumour responses and cancer progression. CCL5 can promote T cell infiltration into the surrounding stroma which assists in tumour rejection [598-605]. On the other hand, over-expression of CCL5 is positively associated with malignant transformation in breast cancer at primary tumour sites, regional lymph nodes and metastatic sites compared to normal epithelial cells, ductal epithelial cells and benign tumours [578]. More specifically, a tissue microarray analysis of 2,254 human breast cancer tissues reveals that CCL5 and its receptor CCR5 are highly expressed in the HER2 positive genetic subtype of breast cancer compared to non-cancerous breast samples [433]. Similarly, Erreni *et.al.,* observed that CCL5 is expressed predominantly at the invasive front of primary colorectal cancers[576]. Cambien *et.al.* Found that metastatic liver and pulmonary resection pieces from CRC exhibited the highest levels of CCL5 compared to the primary tumour and healthy tissues [462]. In addition, plasma/serum CCL5 levels were higher in patients with cancers compared to healthy individuals and in relapsed patients with metastases compared with patients in remission [573, 606-610]. These findings are in agreement with the dual function of chemokines in cancer in promoting both tumour rejection and cancer progression in the late stages of disease [386].

5.1.1.2 **Regulation of CCL5 expression**

The underlying mechanism by which CCL5 contributes to tumour biology is not clear. Up-regulation of CCL5 can both promote anti-tumour response and immune-suppression. T cell and NK cell infiltration into the TME is also implicated in helping tumour rejection [598-605]. Similarly, a recent CRC study indicated that MSI patients have more active adaptive immune responses (comprising CD3+, CD8+, CD45RO+ and T-bet+ T lymphocytes) compared to Microsatellite stable (MSS) patients. The presence of these immune cells was associated with high expression of CCL5, CXCL10, and CXCL9 and

recruitment of Th1 and memory CD45RO+ T cells to the TME which could be a good prognostic indication for MSI CRC subtype [599].

In contrary, various reports observed that CCL5 is able to induce immune tolerance in the tumour microenvironment by recruiting CCR5+ Tregs, Th2 cells and inducing CD8+ T cells to commit apoptosis [611-613]. In addition, CCL5 has been implicated in promoting triple-negative mammary tumour progression by maintaining the immunosuppressive capacity of human CD11b (+)/Gr-1(+) MSDCs [614]. Furthermore, the secretion of CCL5 by cancer cells themselves or recruitment of TAMs, can stimulate angiogenesis and metastasis by secreting angiogenesis factors such as MMPs, IL-8 and VEGF [588, 615-617]. Moreover, up-regulation of CCL5 is implicated in enhancing tumour cell migration via high nuclear β-catenin localisation in breast cancer [618] and through increased phosphorylation of MEK/ERK and PI3K/AKT, which in turn up-regulate $\alpha V\beta 3$ integrin expression and activate NF-κB [575, 619]. Authors also identified that CCL5 signalling can promote tumour cell migration and invasion by MMP-9 and MMP2 over-expression through activation of PI3K/Akt, MEK/ERK, JAK2-STAT3 signalling pathways and the downstream molecule NF-κB [308, 577, 583, 620, 621]. Moreover, Murooka *et al*., pointed out that CCL5 signalling can enhance tumour cell proliferation by inducing the mTOR pathway [592]. However, Karnoub *et al.,* found that CCL5 does not promote proliferation and survival of breast cancer cell lines, instead it significantly enhances invasion in lung metastasis [307]. Recently, Long *et al.,* proposed the previously reported CSLCs as a source of CCL5 that can activate the non-CSLCs via binding to non-CSLCs CCR1/3/5. This in turn activates NF-κB signalling and hence migration and invasion of ovarian cancer cells [585]. From all these studies, it can be suggested that targeting CCL5 signalling may be a potential opportunity for therapy in various type of cancers. However, further elucidation of the role of CCL5 signalling in immunosuppression and cancer progression is still needed.

5.1.1.3 **Regulation of CCL5 in the context of EMT**

Although many studies indicate the importance of CCL5 in cancer, there have been few researchers studying CCL5 in the context of EMT. In fact there are only 7 studies describing the role of EMT in the positive regulation of CCL5/RANTES in cancer and *vice versa*. Of these, only one focused on CRC, whilst others included one head and neck cancer, two prostate cancers, one ovarian cancer, one breast cancer and one chondrosarcoma; **see figure 61.**

In prostate cancer, Barnett *et al.*, pinpointed that over-expression of SNAIL via reactive oxygen species (ROS) induces EMT and as a result activates CCL5 over-expression [622]. In addition, Luo and colleagues reported that MSCs mediated up-regulation of CCL5 in prostate cancer, increasing stem cell populations, leading to the up-regulation of several molecules including ZEB1, CD133 and MMP9 [580]. The ovarian cancer study showed that the paracrine action of CCL5 (over-expressed by CD133+ CSLC ovarian cancer cells) on the neighbouring non-CSLCs CCR1/3/5 activates NF-κB signalling pathway thereby activating EMT, and thus invasion and metastasis of non-CSLCs [585]. The breast cancer study suggested that the coordinated expression of CCL2 & CCL5 and TNFα & IL-1β in breast cancer enhances EMT, disease progression and metastasis. However, TNF-α and IL-1β in particular led to EMT [623]. The CRC study found that the secretion of abundant CCL5 by tumour-associated dendritic cells (TADCs) upon SNAIL over-expression, contributes by enhancing migration, invasion, and inducing EMT via non-coding RNA 'Metastasis-Associated Lung Adenocarcinoma Transcript 1' (MALAT-1) [582]. The head and neck study by Hsu *et al*., showed that acetylation of SNAIL by CREB binding protein (CBP) at lysine 146 and lysine 187 activated several genes including TNF-α, CCL2 and CCL5 through which TAMs were recruited and could modulate the TME [509]. The chondrosarcoma study showed that up-regulation CCL5 leads to down-regulation of miR-200b, which is negatively correlated with ZEB expression, the main contributor in inducing EMT, resulting in up-regulation of VEGF-dependent angiogenesis through PI3K/AKT signalling [588]. Indeed, investigating and understanding the role of the EMT programme in regulating CCL5 or the role of CCL5 in inducing EMT would be novel and beneficial for targeted CRC therapy.

5.1.1.4 **CCL5 in cancer therapy**

Different compounds have been utilised to block the activity of the CCL5-CCR5 axis in cancer. The small molecule Maraviroc, an FDA-approved drug for the treatment of CCR5-trophic HIV infection, has shown a promising effect in reducing formation of pulmonary metastasis by basal breast tumour cells *in vivo* [433], and in preventing hepatocellular carcinoma development in a mouse model [461]. TAK-779, a small molecular weight quaternary ammonium derivative, is another CCR5 antagonist which has been found to diminish Treg infiltration and reduce tumour cell proliferation in a pancreatic carcinoma model *in vivo* [612].

Figure 61: A systematic review of EMT and CCL5 in cancer.

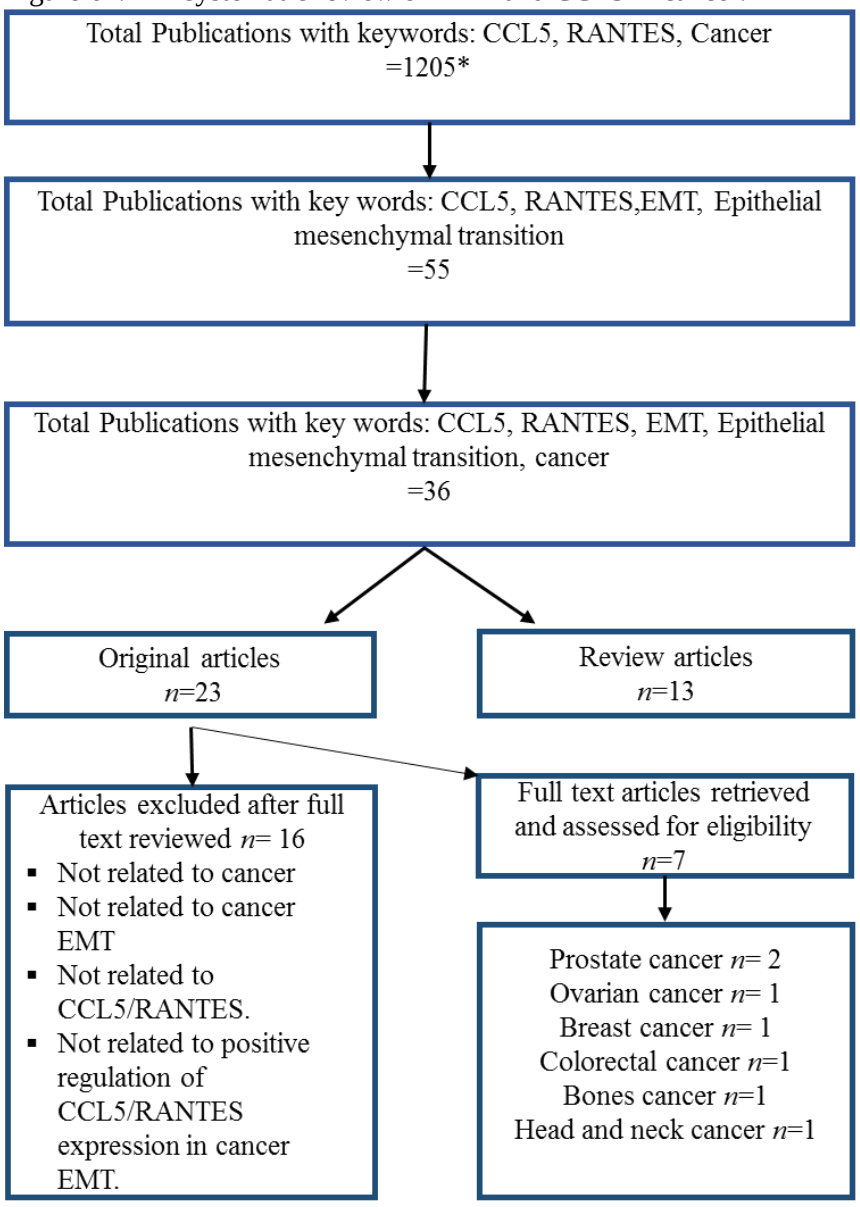

*Total publications from all databases provided by University of Southampton http://library.soton.ac.uk/medicine/databases
Including Web of science, PubMed, Scopus, Medline Ovid, EMBASE.

However, in colorectal cancer Cambien *et al.*, found that this molecule could only inhibit liver metastasis if PDGFRβ is blocked before TAK-779 treatment [462]. Recently, a novel pyridine quaternary alkaloid isolated from *Aniba sp*. (Anibamine) has been reported to bind and inhibit CCR5. Anibamine was observed to suppress adhesion, invasion and proliferation of highly metastatic M12 prostate cancer cells and OVCAR-3 ovarian cancer cells without causing any significant cytotoxicity [624, 625]. In addition to these molecules, inhibition of CCL5 by a neutralisation antibody in breast cancer showed a reduction of metastasis, MSC, TAM and MDSC infiltration [307, 614, 616]. Overall, targeting CCL5/CCR5 may have a great therapeutic potential in cancer therapy.

5.2 The aim

The mechanism of ZEB1/2, as EMT inducing transcription factors, in activating CCL5 transcription in CRC will be examined. In order to investigate this:

- In *silico* analysis of the *CCL5* promoter will be performed for ZEB1/2 binding motifs (E-boxes)
- The *CCL5* promoter will be cloned into a reporter plasmid (pGL3 basic).
- Luciferase assays will be undertaken in a selection of naturally epithelial or mesenchymal CRC cell lines and in the SIP1 induced EMT models to investigate if SIP1 (ZEB2) or ZEB1 can up-regulate CCL5.
- Chromatin Immunoprecipitation (ChIP) assays will be performed to show whether up regulation of CCL5 is direct upon SIP1 binding or not.

5.3 Results

5.3.1 Analysing and cloning the *CCL5* promoter

5.3.1.1 Analysing CCL5 promoter for ZEB1/2 E-boxes

In order to study the mechanistic influence of ZEB1/2 proteins in activating CCL5 transcription, ZEB1/2 binding motifs (E-boxes binding sites) were studied using the TFBIND program. Two strong ZEB1/2 binding sites (with 90% confidence) were

identified. The first one is CACCTC, and the second one is CACGTG which is located in first exon; **see figure 62 and figure 65.**

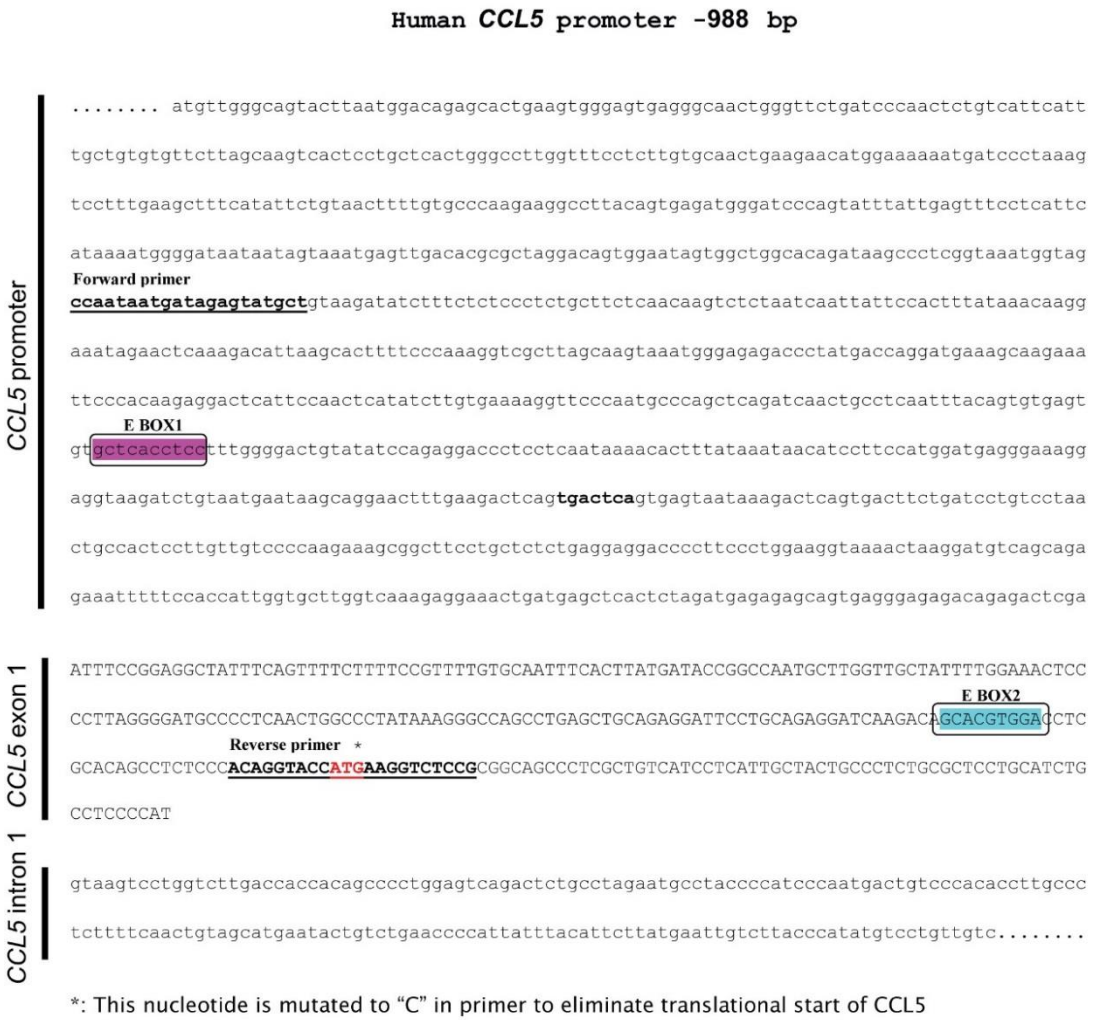

Figure 62: The sequence of the cloned region of the *CCL5* promoter (including a part of the first exon).

The sequence shows potential ZEB1/2 motif sites (E-box1 and E-box2), and the PCR primers that were used to amplify the promoter from human genomic DNA. Restriction enzyme sites (*Mlu I* and *Xho I*) were added to the designed primers in order to clone the intended DNA fragment into the pGL3 vector.

5.3.1.2 **Cloning of the *CCL5* promoter**

As we found two potential sites for ZEB binding we intended to clone a 988 bp fragment of the *CCL5* promoter and a part of the first exon. Before proceeding with cloning, the candidate genomic DNA fragment was analysed for restriction enzyme binding sites using the web cutter programme. In order to ligate the promoter into pGL3 plasmid, the forward primer was designed to have a *Mlu I* restriction site, whereas the reverse primer was designed to have an *Xho I* restriction site. In addition, the reverse primers were chosen to

be within the proposed start codon (ATG) site. However, the start codon was mutated in order to eliminate translational start of CCL5 which would create a bias when the luciferase assay is performed; **see figure 62 and figure 65.**

By following the steps for the *CCL5* promoter **in figure 63**, the *CCL5* promoter was first amplified with KOD polymerase, extracted from the gel, cut with *Mlu I* and *Xho I* along with pGL3 plasmid. The cut vector and insert were loaded on a 1% gel along with the uncut pGL3 plasmid to check the efficiency of digestion; the cut pGL3 is higher in size compared to the un-cut supercoiled pGL3. Afterwards, the cut DNA fragments (vector insert) were ligated using Takara ligation system (Clontech). The new constructed pGL3 *CCL5* promoter plasmid was transformed immediately into α-select silver competent cells. The transformed bacteria were spread onto LB agar plates with 100 µg/ml Ampicillin and grown overnight. Subsequently, six colonies were chosen to investigate the success of *CCL5* promoter cloning using colony PCR. Out of the six clones, only one was found at the right size (~988 bp). The colony was then propagated overnight in LB medium containing 100 µg/ml Ampicillin, and mini-preped the next day. Before sending the mini-preped plasmid to sequencing, the presence of insert was validated by performing a restriction digestion using *Mlu I* and *Xho I*. The excised fragment was found at the right size of *CCL5* promoter amplicon (~988 bp). The nucleic acid sequencing was done by using the pGL3 reverse primer, and the resulted sequence was checked for any mutations using the BLAST programme. No mutations were found (**see appendix figure 84, 85 and 86**). Finally, the bacteria containing the constructed plasmid was cultured further in 125ml LB medium with 100 µg/ml Ampicillin to obtain a larger quantity of the pGL3 *CCL5* promoter construct. The resulting maxi-prep was checked one more time by digesting with *Mlu I* and Xho I, and again the insert was detected at ~988 bp.

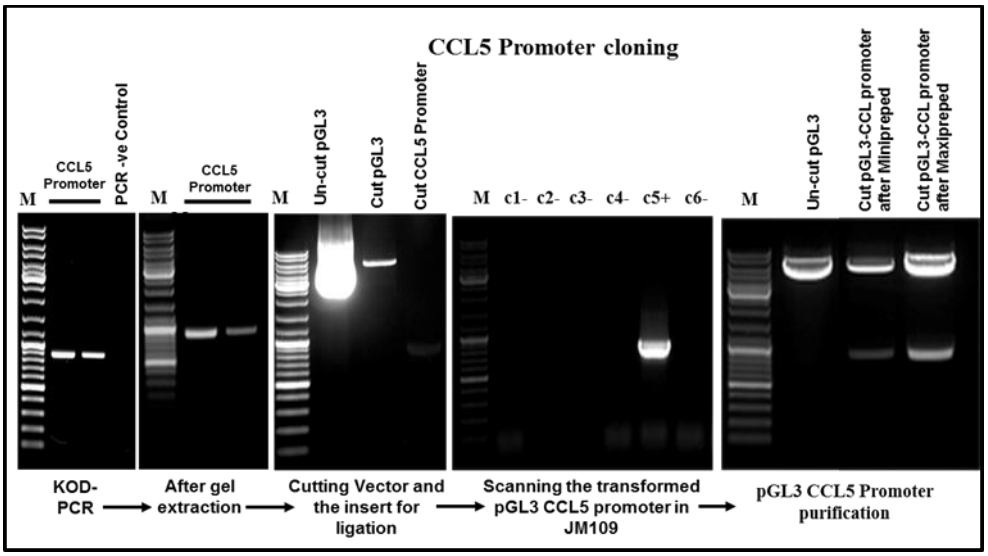

Figure 63: Illustration of the steps used to clone the *CCL5* promoter into pGL3.

Briefly, the *CCL5* promoter including a part of the first exon was amplified from human genomic DNA using KOD polymerase, and then extracted using an extraction kit. The extracted *CCL5* promoter was cut with *Mlu I* and *Xho I* and ligated into the pGL3 plasmid and transformed into JM109 competent bacteria. After overnight incubation, 6 colonies were picked and analysed for the presence of the insert by performing colony PCR. Only one colony out of six was positive (C5). C5, was cultured overnight in LB medium containing 100µg µg/ml Ampicillin, and then purified by miniprep. The authenticity of the colony was validated for the presence of the promoter by using the same restriction enzymes that were added to the designed *CCL5* promoter PCR primers (*Mlu I* and *Xho I*). The insert was successfully separated from pGL3 vector, and *CCL5* promoter was observed at the same amplicon size (988 bp). C5 was also sequenced (Source Bioscience Life technology) which showed an identical sequence of the intended cloned region for the *CCL5* promoter.

5.3.2 Luciferase assay for the *CCL5* Promoter

A luciferase assay was used to investigate the effect of ZEB1/2 as drivers of the pGL3 CCL5 promoter reporter. To do that, SIP1 was induced in DLD-SIP1 and A431-SIP1 models for 3 days and used as a positive source for SIP1 as driver. On the other hand, SW480 and RKO cells, which were found to have moderate to high levels of ZEB1 protein (**see figure 64**), were used as a positive source for the ZEB1 reporter. The SW620 cell line, which was found in chapter 3 to have negligible amounts of ZEB1protein, was included in the study in order to compare results to SW480 cells. In this project, SW620 and SW480 cells were considered as a CRC EMT model as they both originated from primary and secondary tumours of the same CRC patient, and SW480 cells appeared more mesenchymal than SW620. On the other hand, DLD-1 cells were used as negative source for both SIP1 and ZEB1, and its output signals were used to calculate the percentage of increase in the signals of the chosen cell lines.

Figure 64 is a representative figure for three standardised luciferase experiments (each in triplicate). SW480 and RKO with a high level of ZEB1 driver, and DLD-I and A431-1 with a high level of SIP1 driver showed a remarkable effect on activating the *CCL5* promoter with ~ 5, 10, 5 and 9-fold increase compare to DLD-1 cells, respectively. Whereas, SW620, DLD-UI and A431-UI cells had an insignificant effect on the promoter with 115 % ±9, 121 % ±14 and 104 % ± 21 activity compare to 100 % ± 5 for DLD-1 cells, correspondingly.

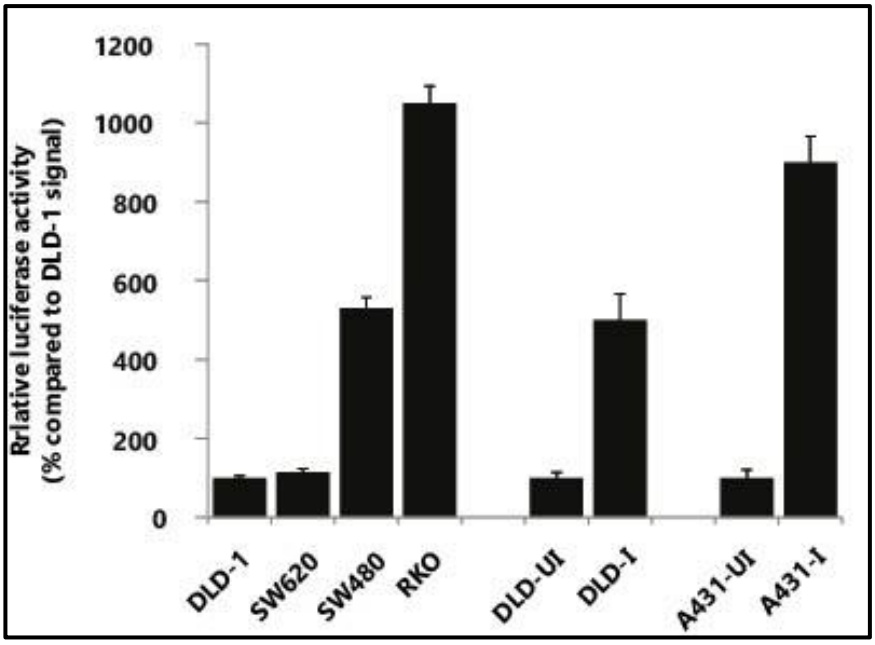

Figure 64: Relative luciferase activity of *CCL5* promoter in a panel of CRC cell lines.

DLD-SIP1 and A431-SIP1 cells were induced for 3 days using doxycycline prior to use. pGL3 or pGL3 *CCL5* promoter and Renilla luciferase plasmid were transfected into DLD-1, SW620, SW480, and RKO as well as in DLD-SIP1 and A431-SIP1 cells using the Lipofectamine protocol. The luciferase activity obtained from *firefly* (FF) and *Renilla* (RN) was calculated as a ratio FF: RN. The relative luciferase activity of the *CCL5* promoter (presented in the figure as a percentage) in DLD-1 epithelial cells that showed no SIP1 or ZEB2 expression in our EMT CRC panel, was used to compare the relative luciferase activity of the *CCL5* promoter in all the other examined CRC cells. The luciferase activity was observed more in the mesenchymal cells expressing SIP1 or ZEB1 proteins (SW480, RKO and DLD-I and A431-I cells) compared to the epithelial (DLD-UI, A431-UI cells) and the intermediate epithelial (SW620). DLD-UI (un-induced DLD-SIP1 cells), DLD-I (induced DLD-SIP1 cells), A431-UI (un-induced A431-SIP1 cells), A431-I (induced A431-SIP1 cells). The figures are a representative demonstration of at least 3 independent results.

5.3.2.1 Luciferase Assay for the *CCL5* Promoter with Mutated ZEB1/2 E-Boxes

In order to see if ZEB1/2 are binding to E-boxes on the *CCL5* promoter and activating *CCL5* transcription, Site-Directed Mutagenesis (SDM) was performed for the *CCL5* promoter ZEB1/2 E-box 1 (gctCACCTCctt mutated to gctAAAATCctt) and *CCL5*

promoter ZEB1/2 E-box 2 (cagCACGTGgac mutated to cagAAAAAGgac) or for both; **see figure 65.**

Figure 66, 67 and 68 illustrate the effects of the E-box1 mutation (E1m), the E-box 2 mutation (E2m) or E-box1 and 2 mutations (E1m + E2m) on the binding affinity of SIP1 protein in A431-SIP1 and DLD-SIP1 EMT-CRC model, and the binding affinity of ZEB1 protein in SW480 and SW620 cells.

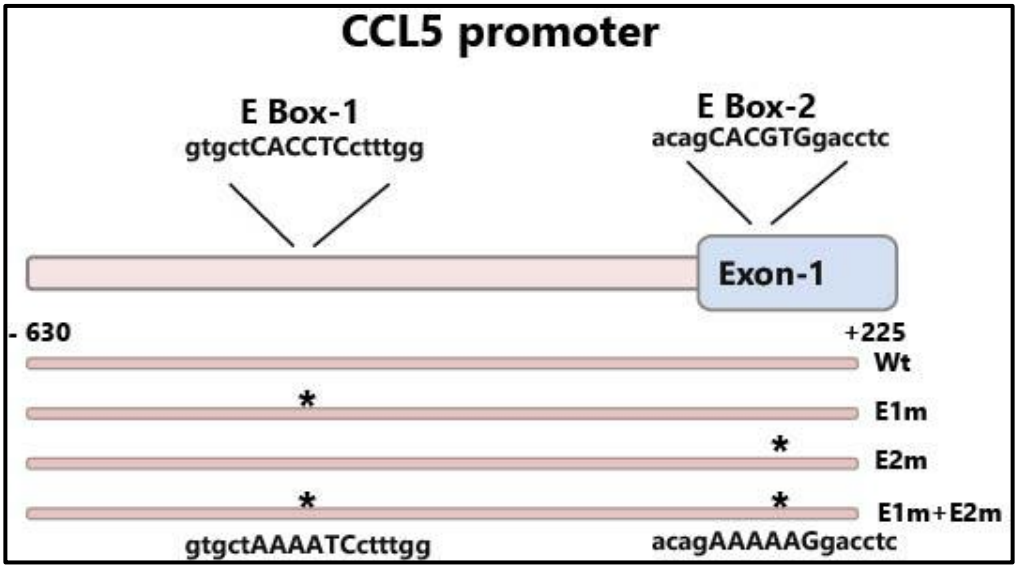

Figure 65: An illustration of *CCL5* promoter with SIP1/ZEB2 motif sites with or without mutation.

The illustration shows the length of the promoter including the first exon and the SIP1/ZEB1 binding sites within the region. The SIP1/ZEB2 motif sites were mutated individually at E-box1 (E1m) or E-box1 (E2m) or at the two binding sites (E1m+E2m) using the site directed mutagenesis protocol.

Consistently, up-regulation of *CCL5* promoter was seen in DLD-I cells (~ 5 folds increase compared to DLD-UI cells), A431-I cells (~ 5 folds increase compared to A431-UI cells) and SW480 cells (~ 3 folds higher compared to SW620 cells). Noticeably, a meaningful down-regulation of the promoter was seen with E1m, E2m and E1m + E2m in all the examined cells. However, the strongest effect was with E2m, as the combination of E1m and E2m was slightly stronger compared to E2m alone; see figure **66, 67, 68.**

The reduction of luciferase activity associated with SDM in DLD-UI and A431-UI cells was not significant. It was about 20-40 % down-regulation compared to ~ 300-400 % reduction in DLD-I and A431-I. On the other hand, both SW480 and SW620 cells showed

a similar amount of decrease in *CCL5* promoter activity when the E-Boxes were mutated (by ~ 40-80 %) compared to the wildtype promoter; **see figure 66 and 67, 68.**

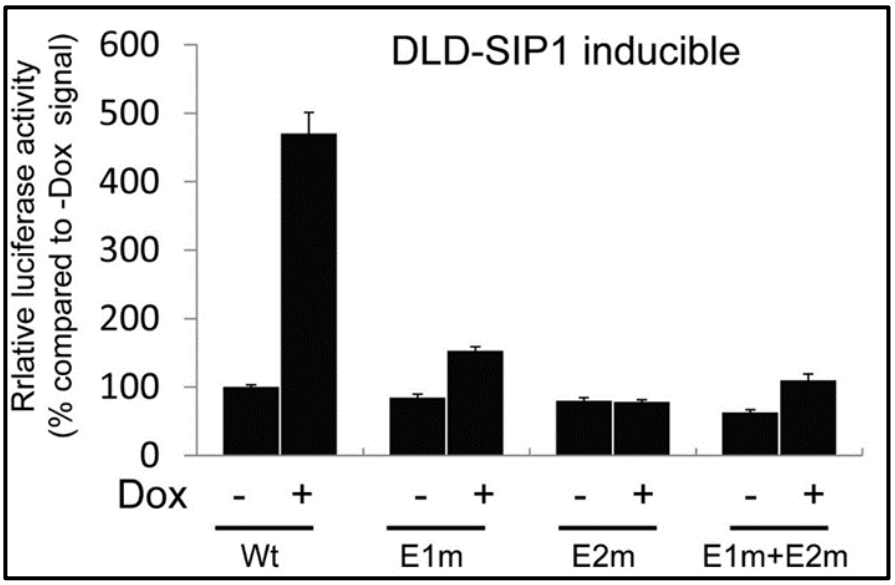

Figure 66: The relative luciferase activity of the *CCL5* promoter with or without SIP1/ZEB1motif sites mutations in DLD-SIP1 CRC EMT model.

DLD-SIP1 cells were induced for 3 days using doxycycline prior to use. pGL3 or pGL3 *CCL5* promoter or pGL3 *CCL5* promoter with SIP1/ZEB1 E-box1 mutation (E1m) or pGL3 *CCL5* promoter with SIP1/ZEB1 E-box2 mutation (E2m) or pGL3 *CCL5* promoter with SIP1/ZEB1 E-box1 and E-box2 mutations (E1m+E2m) were transfected into DLD-UI and DLD-I cells. 5ng of Renilla luciferase plasmid was also transfected along with the other plasmids using Lipofectamine protocol. The luciferase activity obtained from *firefly* (FF) and *Renilla* (RN) was calculated as a ratio FF: RN. The relative luciferase activity of the wild-type *CCL5* promoter in DLD-UI and DLD-I cells (presented as a percentage in the figure) were used to compare the relative luciferase activity in DLD-UI and DLD-I cells with the mutated *CCL5* promoters (E1m, E2m or E1m+E2m). DLD-UI cells showed no difference in the relative luciferase activity of *CCL5* promoter with or without the mutations. On the other hand, induced DLD-SIP1cells transfected with E1m, E2m or E1m+E2m *CCL5* promoters showed a radical reduction of the relative luciferase activity compared to DLD-I cells with the wild-type *CCL5* promoter. The results conclude that SIP1 is involved in activating the *CCL5* promoter. DLD-UI (un-induced DLD-SIP1 cells), DLD-I (induced DLD-SIP1 cells). The figures are a representative demonstration of at least 3 independent results.

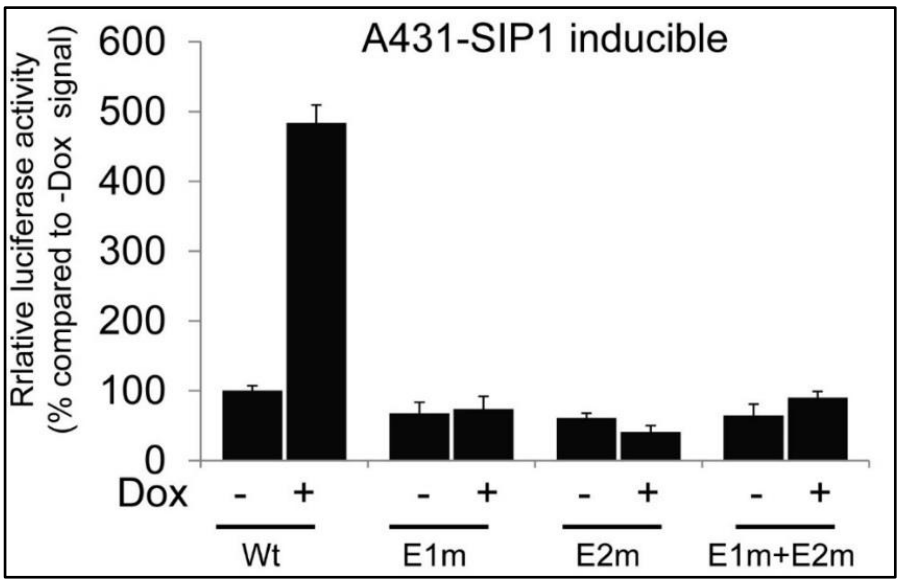

Figure 67: The relative luciferase activity of the *CCL5* promoter with or without SIP1/ZEB1motif sites mutations in A431-SIP1 squamous cell carcinoma EMT model.

A431-SIP1 cells were induced for 3 days using doxycycline prior to use. pGL3 or pGL3 *CCL5* wild-type promoter or pGL3 *CCL5* promoter with SIP1/ZEB1 E-box1 mutation (E1m) or pGL3 *CCL5* promoter with SIP1/ZEB1 E-box2 mutation (E2m) or pGL3 *CCL5* promoter with both SIP1/ZEB1 E-box1 and E-box2 mutations (E1m+E2m) were transfected into A431-UI and A431-I cells. 5ng Renilla luciferase plasmid was transfected along with the other transfected plasmids using the Lipofectamine protocol. The luciferase activity obtained from *firefly* (FF) and *Renilla* (RN) was calculated as a ratio FF: RN. The relative luciferase activity of the *CCL5* wild-type promoter in A431-UI or A431-I was used to compare the relative luciferase activity in A431-UI or A431-I cells with the mutated *CCL5* promoters (E1m, E2m or E1m+E2m). A431-UI cells showed no difference in the relative luciferase activity with or without mutations in the *CCL5* promoter. On the other hand, A431-I cells transfected with E1m, E2m or E1m+E2m *CCL5* promoter showed a remarkable reduction in the relative luciferase activity compared to A431-I cells with wild type *CCL5* promoter. The results conclude that SIP1 may therefore be involved in activating the *CCL5* promoter. A431-UI (un-induced A431-SIP1 cells), A431-I (induced A431-SIP1 cells). The figures are a representative demonstration of at least 3 independent results.

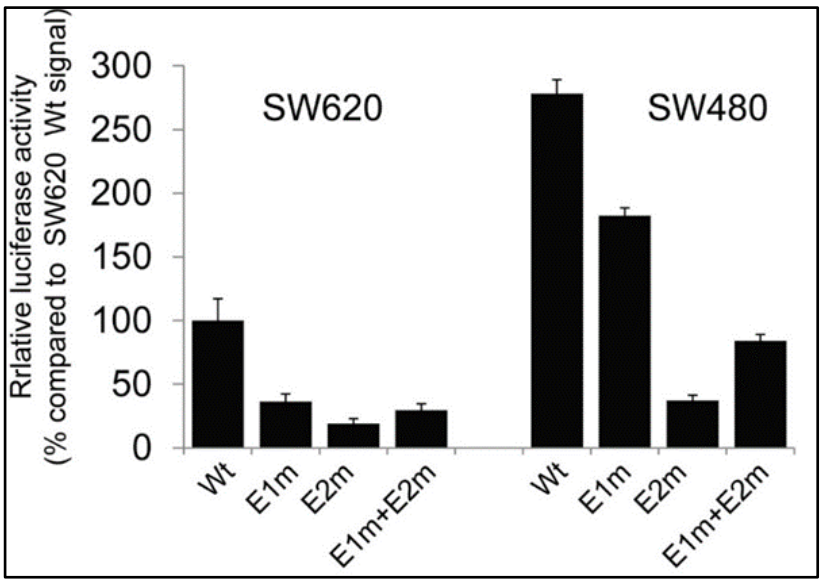

Figure 68: The Relative luciferase activity of the *CCL5* promoter with or without SIP1/ZEB1motif sites mutations in SW620 and SW480 cells.

pGL3 or pGL3 CCL5 promoter (wild-type promoter) or pGL3 CCL5 promoter with SIP1/ZEB1 E-box1 mutation (E1m) or pGL3 CCL5 promoter with SIP1/ZEB1 E-box2 mutation (E2m) or pGL3 CCL5 promoter with SIP1/ZEB1 E-box1 and E-box2 mutations (E1m+E2m) were transfected into SW620 and SW480 cells. 5ng of Renilla luciferase plasmid was also transfected into the cells along with the other plasmids using the Lipofectamine protocol. The luciferase activity obtained from firefly (FF) and Renilla (RN) was calculated as a ratio FF: RN.
The relative luciferase activity of the wild-type CCL5 promoter (presented as a percentage in the figure) in SW620 cells was used to compare the relative luciferase activity in the SW620 cells with the mutated *CCL5* promoters (E1m, E2m or E1m+E2m). SW620 cells (expressing low-no ZEB1) showed a reduction in the relative luciferase activity compared to SW620 cells with the wild-type *CCL5* promoter.
The relative luciferase activity of the wild-type CCL5 promoter (presented as a percentage in the figure) in SW480 cells was used to compare the relative luciferase activity in the SW480 cells with the mutated *CCL5* promoters (E1m, E2m or E1m+E2m). SW480 cells (expressing high levels of ZEB1) showed a significant reduction in the relative luciferase activity compared to SW480 cells with the wild-type CCL5 promoter
The results conclude that ZEB1 may be involved in activating the *CCL5* promoter. The figures are a representative demonstration of at least 3 independent results.

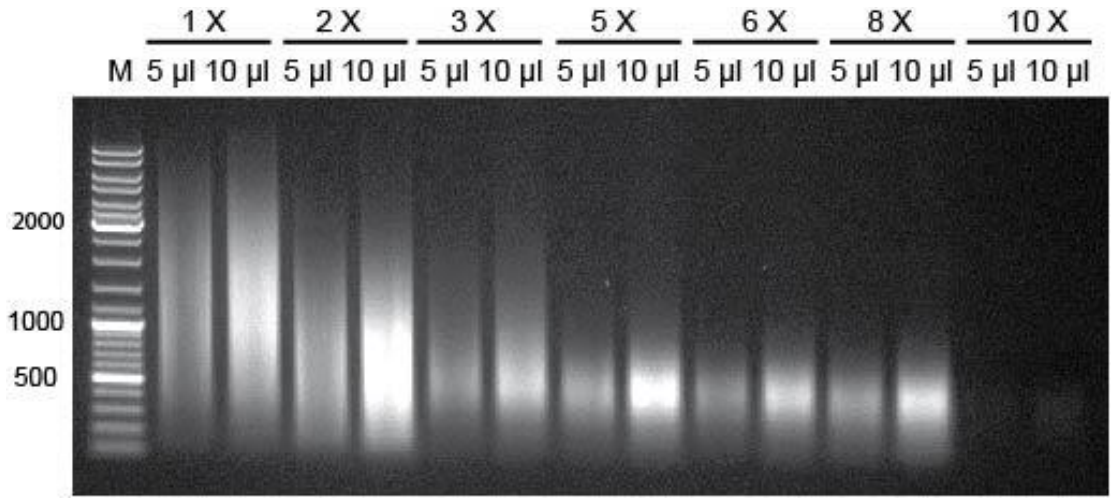

Figure 69: Shearing size of DNA from DLD-SIP1 cells using a different number of pulses.

The recommended chromatin size (200-1500 bp) was assessed in DLD-SIP1 cells prior to use in ChIP using a different set of pulses, ranging from (1x to 10x) at 1.0 energy output. Different amounts (5 and 10 µl) of each sheared condition was loaded onto a 1% agarose gels. The size of the sheared chromatin declined gradually with more pulses. The best chromatin shearing condition for DLD-SIP1 cells is between 3 and 5 pulses (the DNA size is ≤ 1500 bp). ChIP (chromatin immunoprecipitation assay)

In order to further validate the shearing efficiency, different genomic DNA amplicons at ~ 800 bp, ~ 1200 bp and ~ 1480 bp were checked; see **figure 70.** Our findings suggest that ~ 800 bp the amplicon can be detected even after 10 pulses of sonication. On the other hand, the 1200 bp DNA amplification is undetectable at 8 pulses, and the 1480 bp amplicon disappears after 5 pulses. From there, it can be concluded that the best sonication condition for DLD-SIP1 cells, with fragments of chromatin between 200-1500 bp, is at five pulses of 20 second each, with a 30 second rest on ice between each pulse at 1.0 setting as power output.

After validating the best chromatin shearing condition for DLD-SIP-1 cells, the cells were induced for 3 days with doxycycline. Both induced and un- induced DLD-SIP cells were fixed to preserve the binding of chromatin and associated proteins with DNA. Cells were then harvested, lysed and nuclei then collected and the chromatin sheared with five pulses. Before proceeding with the immunoprecipitation (IP) step, DLD-UI and DLD-I fragmented inputs were checked further for their sizes; see **figure 71**. The inputs fractionated were all at the recommended range of ~200-1500 bp. Also, loading of 50 ng of DLD-UI and DLD-I input DNA showed that the sheared DNA was suitable to amplify 147 bp, 800 bp and 1200bp.The amplicon at 1400 bp was weakly amplified. The amplicon at 2400 bp was undetectable. From these results it can be concluded that the range of the

sheared chromatin of DLD-UI and DLD-I were acceptable (≥ 200 bp and ≤ 1500 bp), and the chromatin was ready to proceed to IP stage.

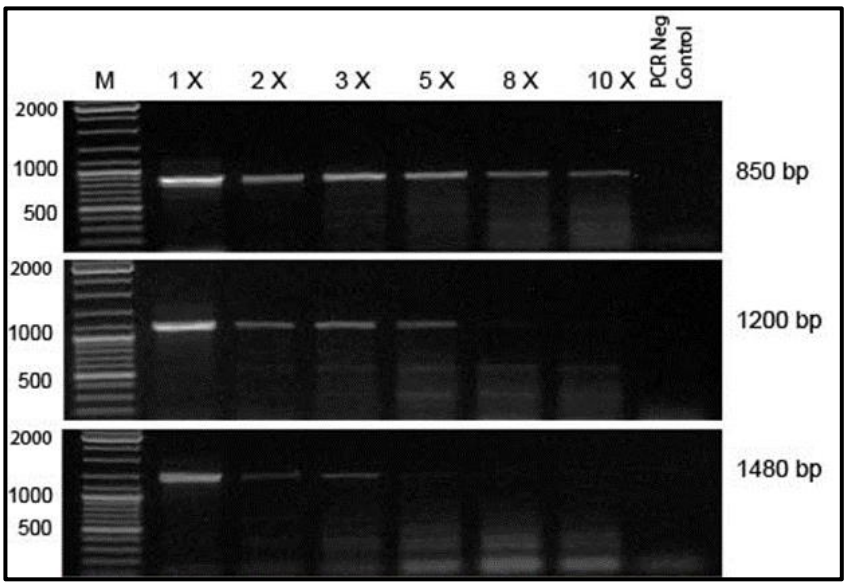

Figure 70: Further validation of chosen shearing condition (5 pulses) for DLD-SIP1 cells using PCR.

Various pair of primers with well-known DNA amplicon sizes (~850 bp, 1200 bp and 1480 bp) along with the chromatins (templates) that were obtained from different pulses and Taq polymerase were mixed to perform PCR. The PCR products were loaded on a 1% agarose gel. The 800 bp amplicons was observed with > 5 pulses. The 1200bp amplicons disappeared sharply after 5 pulses, whereas the 1480 bp amplicons disappeared after 3 pulses. As the recommended size to proceed with ChIP is no more than 1500 bp, 5 pulses was chosen as an optimised shearing condition for DLD-SIP1 cells. ChIP (chromatin immunoprecipitation assay); M (DNA ladder).

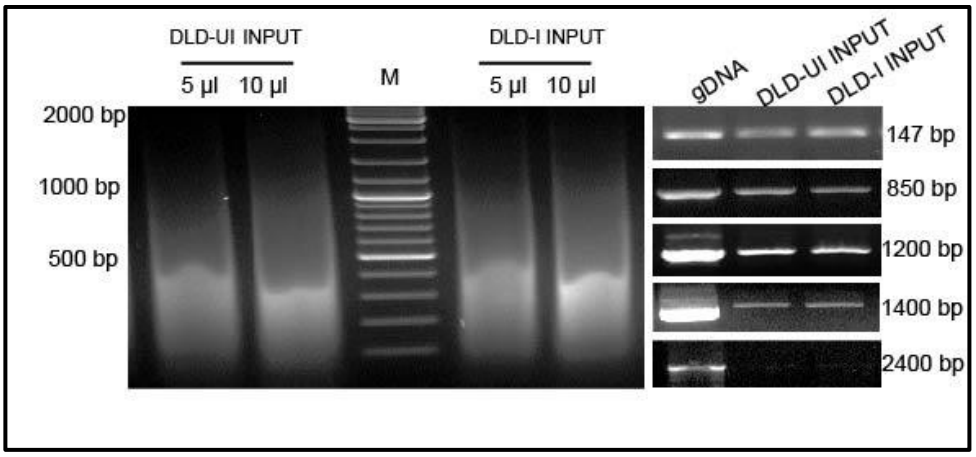

Figure 71: Validation of DLD-UI and DLD-I inputs before proceeding with immunoprecipitation (IP).

DLD-SIP1 cells were treated with 2 µg/ml doxycycline for 3 days prior to use for ChIP. DLD-UI and DLD-I inputs were checked for their shearing sizes by loading a different amount (5 and 10 µl) from each input on a 1% agarose gel. The chromatin shearing was observed to range within the recommended chromatin size for ChIP (200-1500 bp) in both DLD-UI and DLD-I. The sizes of the inputs were validated further by PCR using various pair of primers with well-known DNA amplicon sizes (~ 147 bp, 850 bp, 1200 bp, 1480 bp and 2400 bp). The PCR products were loaded in 1% agarose gel. The PCR results indicated that the size of the inputs were within the recommended range (>200 bp and < 1500 bp) and the sheared chromatins were ready to use for IP. DLD-UI (un-induced DLD-SIP1 cells); DLD-I (induced DLD-SIP1 cells); ChIP (chromatin immunoprecipitation assay); M (DLD ladder).

As SIP1 is myc-tagged, a ChIP validated Myc antibody was used to check the presence of exogenous SIP1 on the *CCL5* promoter. In addition, negative control (matching IgG) and positive control (RNA polymerase II) antibodies were included. In order to analyse the final product, PCR was performed with primers for *GAPDH* (provided with the kit), *CDH1* and human *plakophilin 2* (*PKP2*) gene promoters, as reported previously [216]. Primers for *CCL5* promoter ZEB1/2 E-BOX1 and *CCL5* promoter ZEB1/2 E-Box 2 were designed by us; **see Table 8.**

The PCR results **in figure 72** showed that there was equal loading of DLD-UI and DLD-I DNA inputs for each investigated promoter. In addition, the negative IgG control and the RNA polymerase II-positive control antibody successfully worked with all the investigated promoters. The negative control showed no or a very weak signal with all the promoters. In addition, the positive control showed a positive binding in both DLD-UI and DLD-I but at different levels. The dissimilarity amount of positivity between DLD-UI and DLD-I depends on activation of transcription of *GAPDH, CDH1, PKP2* or *CCL5* genes. In general, RNA polymerase II showed equal binding with *GAPDH* promoter in DLD-UI and DLD-I as GAPDH expression does not change during EMT, while SIP1 binding was less to *CDH1* and *PKP2* gene promoters in DLD-I cells compared to DLD-UI. In contrast,

RNA polymerase II binds more to the *CCL5* promoter ZEB1/2 E-box 2 in DLD-I in comparison to DLD-UI. Our results showed that SIP1 binds to E-cadherin, *PKP* and *CCL5* promoters, but not to the *GAPDH* promoter, in DLD-I compared to DLD-UI cells. Due to technical difficulties we could not detect the *CCL5* promoter ZEB1/2 E-box 1 amplicon.

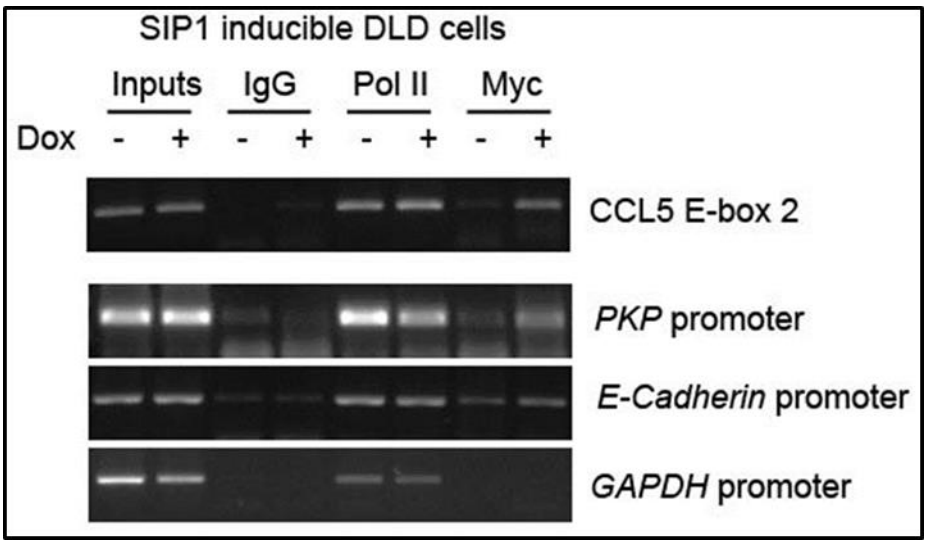

Figure 72: Validation of DLD-UI and DLD-I inputs before proceeding with immunoprecipitation (IP).

DLD-SIP1 cells were treated with 2 µg/ml doxycycline for 3 days prior to use for ChIP. DLD-UI and DLD-I inputs were checked for their shearing sizes by loading a different amount (5 and 10 µl) from each input on a 1% agarose gel. The chromatin shearing was observed to range within the recommended chromatin size for ChIP (200-1500 bp) in both DLD-UI and DLD-I. The sizes of the inputs were validated further by PCR using various pair of primers with well-known DNA amplicon sizes (~ 147 bp, 850 bp, 1200 bp, 1480 bp and 2400 bp). The PCR products were loaded on a 1% agarose gel. The PCR results indicated that the size of the inputs were within the recommended range (>200 bp and < 1500 bp) and the sheared chromatins were ready to use for IP. DLD-UI (un-induced DLD-SIP1 cells); DLD-I (induced DLD-SIP1 cells); ChIP (chromatin immunoprecipitation assay); M (DLD ladder).

5.4 Discussion

At the transcriptional level, the *CCL5* promoter was reported to have binding sites for SIP1, activator protein 1 (AP1), NF-κB and C/EBP transcription factors, which up-regulate its expression [626-629]. However, none of these transcription factors have been studied in the context of cancer for *CCL5* promoter, apart from NF-kB [630].

Despite the importance of *CCL5* and EMT-inducing transcription factors (SNAIL, TWIST, and ZEB) in predicting poor cancer survival, the interaction between them has rarely been studied; **see section 5.1.1.3 and figure 61.** In fact, identification of EMT-inducing

transcription factors binding to the *CCL5* promoter and therefore dissecting pathways controlling its expression is critical for targeted therapies.

In chapter 3, we observed that ZEB1/2 are the main EMT inducers in stratifying our CRC panel in terms of EMT status. **In chapter 4**, we concluded that CCL5 is over-expressed in SIP1-induced EMT models as well as naturally metastatic (mesenchymal) CRC cells. From there, we proposed that ZEB1/2 EMT inducers, directly or indirectly, up-regulate the expression of CCL5. Before conducting any further experiment, we searched the literature and found no direct evidence for our proposal. From searching, it was found that up-regulation of CCL5 positively regulates expression of ZEB1 [580], and negatively regulates miR-200b [588]; mir-200 has frequently been reported to have a negative feedback with ZEB1/2 expression [250]. In addition, it was also reported that up-regulation of CCL5 causes β-catenin localization to the nucleus[618], and activation of NF-kB expression[575]; β-catenin and NF-kB molecules were also correlated with ZEB1 or ZEB2 expression [175, 631]. However, none of the searched reports showed a relationship between ZEB1/2 and *CCL5* expression at the transcriptional level. For this reason, is the focus of this chapter was to analyse the *CCL5* promoter for the presence of E-boxes and then clone these into the pGL3 plasmid. Luciferase and ChIP techniques were used to identify the target.

ZEB1 and ZEB 2 (SIP1) proteins are conserved with a high sequence homology. Both contain two separate clusters of zinc fingers, one at the N-terminus and one at the C-terminus. Both of the two-handed zinc fingers bind independently with a high affinity to a targeted gene promoter in order to obtain optimal suppression or activation. One of the well conserved binding site sequence for ZEB1/2 is CAC(C)T(C) [132]. We found the same binding site in the *CCL5* promoter using the TFBIND program with 90% confidence. The first one is CACCTC and the second one is CACGTG; **see figure 62 and 65**. In fact, ZEB1/2 were reported to interact physically with *Xenopus Xbra2*, and human *α4-integrin, CDH1, cyclin D1, Plakophilin* 2 (*PKP*), *connexin26, ZO3, and p53* family member gene promoters to regulate their gene transcription [132, 214, 216, 482, 632, 633].These genes are involved in cell differentiation, physiological development as well as in facilitating metastases and thus EMT.

The CCL5 promoter was successfully cloned into the pGL3 basic vector; **see figure 63**. The pGL3 plasmid was used as it is one of the most commonly used plasmids for such assays. pGL3 has a *firefly* luciferase gene that is driven by the intended promoter.

Consequently, it produces a signal proportional to the activity of the inserted promoter upon its interaction with the driver protein/s.

The pGL3 *CCL5* promoter was transfected into DLD-1 cells (negative for SIP1 or ZEB1), into DLD-SIP1 and A431-SIP1 models (a positive source for SIP1as driver), and into SW480, and RKO (a positive source for ZEB1 protein as driver). Although SW620 is not a representative source of either SIP1 or ZEB1, we decided to include it in our selective panel for our luciferase assay in order to compare it with SW480 cells. In fact, we considered SW480 and SW620 as a good model to study the influence of EMT and MET. The output signals were used to calculate the fold of increase in the signals of the chosen cell lines compared to DLD-1. SW480, RKO, induced DLD-SIP1 and induced A431-SIP1 gave a 5-10-fold increase compared to DLD-1.Whereas, SW620, un-induced DLD-SIP1 and un-induced A431-SIP1 cells gave a signal near to the negative internal control of DLD-1 cells. From the results, we confirmed that both SIP1 and ZEB1 could contribute to the activation of the *CCL5* promoter; **see figure 64.** However, whether or not SIP1 and ZEB1 bind directly to the promoter was not clear. To investigate that, the identified E-boxes were mutated individually or together using the SDM procedure. We did base substitution or miss matched mutation by replacing more than 2 bases with Adenine; E1m (gctCACCTCctt mutated to gctAAAATCctt), Em2 (cagCACGTGgac mutated to cagAAAAAGgac); **see figure 65.** In fact, the designed mutations were performed and validated previously, which gave maximum inactivation of the analysed promoter [482]. Apart from RKO, the same cell lines were transfected again with either the pGL3 *CCL5* promoter or the pGL3 *CCL5* promoter with E1m or E2m or E1m+E2m. All the cell lines harbouring SIP1or ZEB1 proteins (induced DLD-SIP1, induced A431-SIP1, and SW480 cells), and transfected with the mutated promoter showed a reduction of the promoter activity compared to the signal produced by the corresponding cells with the wild type promoter; **see figure 66, 67 and 68.** On the other hand, un-induced DLD-SIP1 and A431-SIP1 cells showed no statistically significant change in promoter activity with or without the mutated *CCL5* promoter. Of note, SW620 showed some reduction of the promoter activity upon its transfection with the mutated promoter compared to cells with the wild type promoter. Although, we observed no ZEB1 for SW20 by WB, this does not eliminate the fact it could have a negligible amount of ZEB1 protein. In fact, in chapter 3, SW620 was described as a metastable cell line showing both mesenchymal and epithelial markers. We also noted that the cell lines with the protein drivers showed more inhibition of the luciferase signal with E2m (CACAGTG) compared to E1m (CACCTG), which could suggest that the E2m binding site is a stronger binding site for the zinc finger cluster of

ZEB1/2. In addition, it was seen that the promoter activity increased slightly when mutations in both E-boxes were present. Nonetheless, none of these observations can fail to highlight the importance of the E1m site for ZEB1/2-binding. Indeed, the presence of the two binding sites is important for the two-handed zinc fingers in ZEB1/2 in order to show maximum activation or repression of the targeted gene [132]. However, it could suggest that the presence of other binding sites exist for ZEB1/2 at the distal site of the promoter or even in the coding or other non-coding regions of the gene, as it was previously reported for some genes and for some other transcription factors [634]. From all of these finding, it can be proposed that SIP1 and ZEB1 have a direct effect on CCL5 in metastatic cells.

To confirm further that SIP1 is physically localised to CCL5 promoter we performed ChIP. DLD-SIP1 inducible model was used as a model for this experiment. The same model was previously used to study the mechanism of action for SIP1 on the cyclin D1 promoter, E-cadherin promoter and other promoters related to cell–cell junctions [216, 632]. Induction of SIP1 was observed to bind directly to *E-cadherin, PKP*, *ZO-3*, and the *Connexin26* promoter repressing gene transcription [216]. Form that, we intended to use same *E-cadherin* and *PKP* promoter primers as a positive control for positive SIP1 binding sites along with our designed primers for the *CCL5* promoter ZEB1/2 E-box1 and ZEB1/2 E-box2.The chromatin size for DLD-SIP1 cells was successfully optimized at the recommended size (between 200-1500 bp); more than 1500 bp would be non-efficient for pulling down the intended antibodies and less than 200bp might cause over degradation related to decreased PCR yield; **see figure 69, 70 and 71**. The Myc tag antibody was the one used to detect exogenous SIP1 at the promoters. Anti-IgG negative control antibody and anti-RNA polymerase II positive control antibody were used along with myc-tag antibody in order to avoid misinterpretation of the results due to non-specific binding of myc-tagged antibody. Thus, the combined results helped the interpretation of the *CCL5* promoter findings because RNA polymerase II is present on actively transcribed promoters, including GAPH and E-cadherin (in epithelial cells). The *GAPDH* promoter was used along with *E-cadherin*, *PKP* and the *CCL5* promoter to analyse the binding affinity of the negative IgG and the positive RNA-polymerase and myc-tag antibodies. The *GAPDH* promoter was previously studied for RNA polymerase II-binding [635]. In the immunoprecipitation step of ChIP, a bridge IgM antibody was used along with RNA-polymerase II and myc-tag antibodies in order to enrich their binding affinity to protein G beads, and thus improve the yield of the immune-precipitated chromatin. The value of the bridging antibody in ChIP has previously been studied [636].

Semi-Qualitative PCR was used to validate the ChIP results; **see figure 72**. The inputs, which represent the amount of chromatin in each sample before immunoprecipitation, showed an equal yield for all the amplified promoter regions in both un-induced and induced DLD-SIP1 chromatin. The negative control (mouse IgG) showed no or a minor signal in both the un-induced and induced DLD-SIP1 cells. The supplier also reported the presence of a slight background, which means a weak band is not due to contamination. RNA-polymerase II showed an equal amount of binding for *GAPDH* promoter. As the amount of transcription and translation for GAPDH should be equal in the used cells, the results can be used as another good indication that the chromatin amount between the two samples is equal. The *E-cadherin* and *PKP* promoters were shown to be repressed by a myc-tagged SIP1 antibody, causing reduced levels of gene transcription with RNA-polymerase II in the induced cells compare to the induced ones. The repression of *E-cadherin* and *PKP* promoters by SIP1 were validated by the increased signal in the induced chromatin, in agreement with the previous reports which also indicated that our assay worked accurately [216]. The *CCL5* promoter showed up-regulation of transcription with RNA-polymerase II and a clear localisation of SIP1 to the E-box2. The transcriptional activation for the *CCL5* promoter for CCL5 is in agreement with our luciferase results for DLD-SIP1 cells. Unfortunately, the E-box1 result could not be obtained due to non-specific binding of the designed primers. In fact, many PCR conditions with different annealing and extension temperatures and times were tried, but no condition gave a sharp band at the specific amplicon size. Designing other primers and analysing this region in more detail will be necessary. The primers have already been designed, ordered and received from the manufacturer; however, due to time limitations toward the thesis submission deadline, the primers have not been tried yet.

From the ChIP and luciferase findings, it can be confidently concluded that SIP1 directly binds to the *CCL5* promoter activating gene transcription. This is an original and novel finding.

Chapter 6: The Molecular Basis of Immune Infiltration as a Result of a Metastasis Program in CRC

6.1 Introduction

The presence of CCL5 in the serum of cancer patients or the expression of CCL5 as detected by IHC have been proposed as a negative prognostic marker [433, 462, 578, 610]. A key study also identified CCL5 as a chemokine secreted by mesenchymal stem cells that are recruited to primary breast cancers. The exposure of breast cancer cells to CCL5 facilitated metastasis [307], but no mechanism e.g. whether CCL5 can induce EMT or the immune-deficient microenvironment allowed cancer cells to escape immunity and metastasize, has been identified. These results suggest that CCL5 is necessary for metastasis. Our findings suggest that, in addition to mesenchymal stem cells, CCL5 can also be abundantly secreted by cancer cells undergoing EMT. In order to investigate whether CCL5 can induce EMT and therefore metastasis or EMT-induced CCL5 expression can alter immune infiltration in CRC to favour an immuno-deficient microenvironment; we first intended to investigate whether CCL5 contributes to EMT and therefore metastasis by generating a CCL5 over-expressing CRC cell line, checking its EMT properties, and performing *in vivo* experiments.

6.2 The aims

- Create a CCL5 over-expressing CRC cell line and characterise its properties in relation to EMT and CCL5 expression.
- Investigate whether the CCL5 secreted by this cell line is functional using chemotaxis assays.
- Performing *in vivo* experiments to define if the presence of CCL5 can induce metastasis using immuno-deficient mice.
- Investigate if activation of EMT by SIP1 is correlated with CCL5 and certain types of immune filtrate using a tissue microarray of human CRC patients.
- Create a syngeneic CRC CCL5 knock -down cell line.

- Investigate if CCL5 knock-down alters the immune microenvironment using syngeneic animal models.
- Perform functional assay (e.g. chemotaxis or T-cell differentiation/activation) using CCL5 as an immune regulator.

6.3 Results

6.3.1 Generating CCL5 over-expressing DLD-1 cells

6.3.1.1 Cloning of the *CCL5* coding region

In order to generate a stable transfected cell line over-expressing CCL5, and thus to perform functional studies, I intended to clone human *CCL5* for eukaryotic expression; **see figure 73.** The *CCL5* open reading frame was amplified from induced DLD-SIP1 cDNA using KOD polymerase; a cell line that showed a high level of CCL5. The amplified band was extracted, purified, and ligated directly into pcDNA3.1 TOPO plasmid, and then transformed into α-select silver competent cells. The transformed bacteria were spread onto LB agar plates with 100 µg/ml Ampicillin and grown overnight. Five colonies were chosen to investigate the success of CCL5 cloning using colony PCR. Four of the five colonies were positive for CCL5 ligation. The positive colonies were propagated overnight in LB medium with 100 µg/ml Ampicillin and mini-preped next day. As TOPO cloning facilitates blunt end ligation, the direction of CCL5 within the plasmid was checked by PCR using a CCL5 specific forward (from the insert) primer and V5-tag specific reverse (from vector) primer before sending it to sequencing. Among the five purified CCL5 pcDNA3.1 plasmids, only two were found to have the right orientation (colony 1 and 4). One positive colony with the correctly-orientated insert and containing no mutations was cultured in 125ml LB medium with 100 µg/ml Ampicillin, maxi-preped in order to have large quantities of pcDNA3.1 CCL5; **see figure 73.**

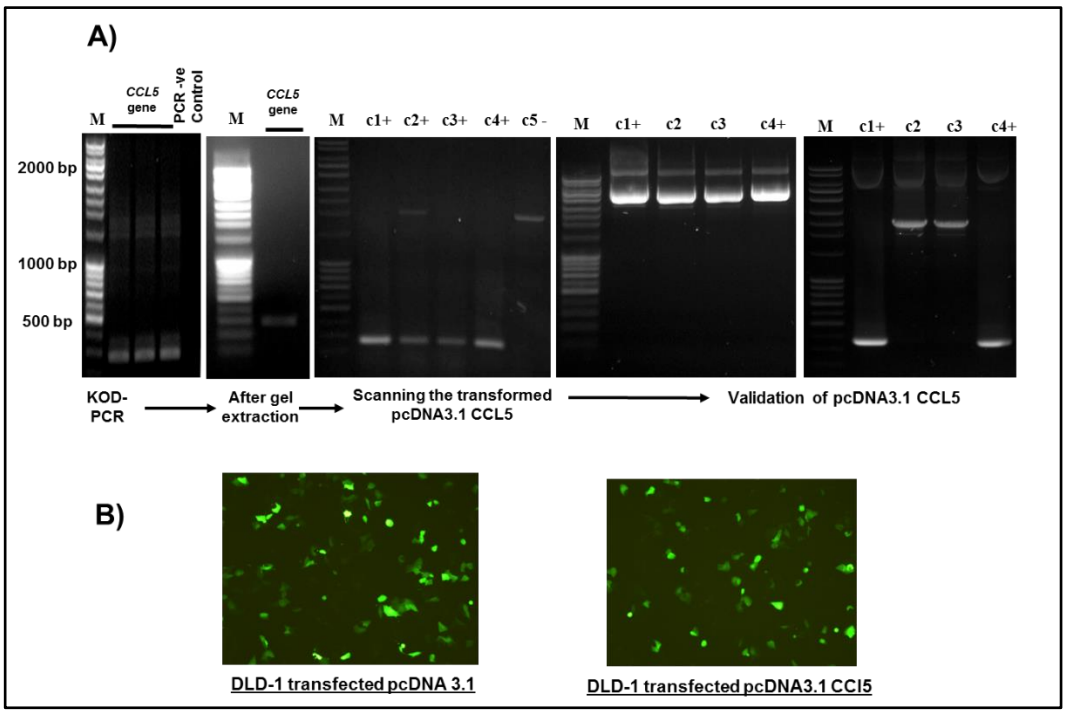

Figure 73: A) Steps of CCL5 cloning.

The *CCL5* open reading frame was amplified using KOD polymerase and extracted using gel extraction kit. The extracted CCL5 was cloned into pcDNA3.1-TOPO plasmid using topoisomerase-based ligation and transformed into JM109 competent bacteria. After overnight incubation, 5 colonies were picked up and the insert gene was analysed for its presence by colony PCR. Four colonies out of five were identified positive (C1, C2, C3, C4). C1, C2, C3 and C4 were cultured overnight in LB medium containing 100µg µg/ml ampicillin, and then purified by mini-prep. The direction of CCL5 was validated by PCR using the V5 reverse primer (from the vector) and CCL5 specific forward primer. (From the insert) Only C1 and C4 had the correct CCL5 orientation. To validate C1 and C4 further, they were sequenced (Source Bioscience Life technology).
B) An equal number of DLD-1 cells/well (wild type) were transfected using pEGFP with pcDNA3.1 or pcDNA3.1 CCL5 using Lipofectamine LTX™. The efficiency was checked by observing pEGFP expression using a fluorescent microscope. M (DNA ladder), A (DNA band), c (colony), GFP (green fluorescent protein).

In order to validate the cloning, DLD-1 cells, that secrete a low level of CCL5 (30 pg/ml± 7), were transfected with pcDNA3.1 CCL5 + pEGFP plasmids. The results showed that CCL5 transfection was successful, and transfected cells had a six-fold increase in CCL5 expression compared to the cells transfected with pcDNA3.1 + pEGFP plasmids; **see figure 74**.

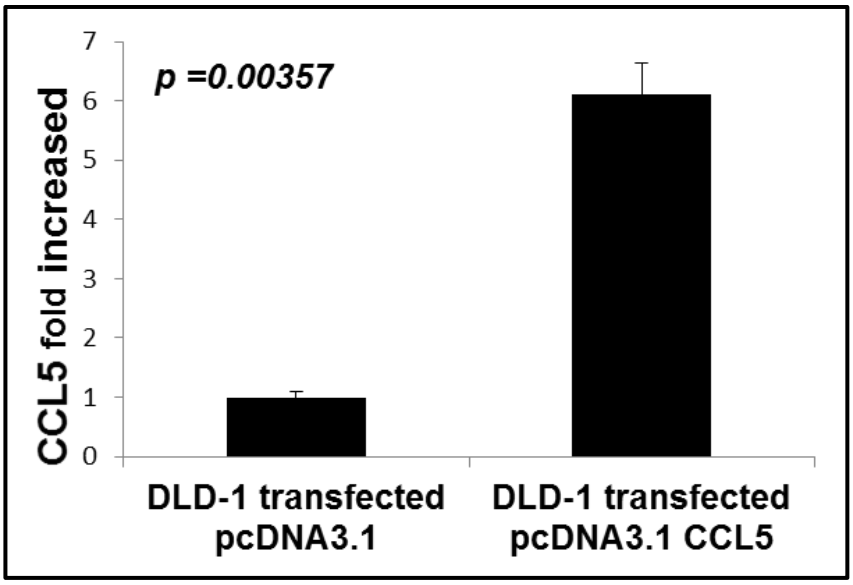

Figure 74: The abundance of secreted CCL5 in DLD-1 transfected cells with pcDNA3.1 or pcDNA3.1-CCL5 was detected using a human CCL5 sandwich ELISA.

The DLD-1 pcDNA3.1 CCL5 cells showed more than a six-fold increase in CCL5 expression compared to the negative control DLD-1 pcDNA3.1 cells. The figure is a representative result of *n*=3; all gave similar results.

6.3.1.2 **Stable Transfection of pcDNA3.1 CCL5 into DLD-1 Cells**

Among all the epithelial CRC cell lines with low CCL5 level, DLD-1 was chosen to create stable CCL5 expression (29 ± 7 pg/ml). The successfully cloned pcDNA3.1 CCL5 plasmid **(see section 6.3.1.1)** and neomycin (G418) antibiotic were used to achieve this goal. Neomycin was chosen because the pcDNA3.1 construct contains a neomycin resistance gene. Before transfecting pcDNA3.1-CCL5 plasmid to DLD1 cells, a kill curve was performed to optimize the amount of neomycin necessary for the selection of positive DLD-1 cells harbouring the CCL5 plasmid. To achieve this, DLD-1 cells (40 % confluent) were seeded in duplicate and treated with a gradually increasing concentration of neomycin, from 0 to 1000 µg/ml. The antibiotic toxicity was determined visually every 2-3 days over a period of one week. The optimal dose was defined as maximum cell death over one week with the lowest dose. From there, the minimal visual toxicity after 7 days was observed at ≤ 200 µg/ml, whereas at 300 and 400 µg/ml the cells were at the maximum death point after 7days. In contrast, visual toxicity of cells at concentrations ≥ 500 µg/ml was evident in the first 2-3 days. Given this, the optimal Neomycin dose was selected at 300 µg/ml.

After determining the optimal Neomycin dose, DLD-1 cells were seeded and at ~60% confluency were transfected with pcDNA3.1 CCL5 or control plasmid using

Lipofectamine; for more details of the Lipofectamine procedure please see **section 2.9.1**. Two days after transfection, 300 µg Neomycin was added. Every 3 days, the cells were examined and the media was replaced with complete DMEM with 300 µg/ml Neomycin. The cells which had undergone Neomycin selection were left to grow for two more weeks. The resulted mixed clones were further diluted at a density of 80 cell/10 ml and seeded in 100 µl to each well of a 96 well plates to obtain single cell clones. The clones were expanded gradually until they reach 90% confluency in 6 well plates. At this point, the supernatants from clones were collected, and the cells were trypsined, counted and CCL5 ELISA was performed. Consequently, cells were propagated in a 75 cm^2 flask with one half frozen and the other half collected to examine E-cadherin expression and the intracellular expression of CCL5.

A total of 22 clones from CCL5 and 25 clones from control vectors were obtained after Neomycin selection and examined. Extracellular CCL5 levels were detected by ELISA; please **refer to section 2.7.2** for the detailed procedure. Supernatants from DLD-1 cells without transfection, from control plasmid clones and DLD-1 cells with a transient transfection with pcDNA3.1 or pcDNA3.1 CCL5 were included in the study as positive and negative controls for CCL5 expression in order to validate the ELISA results for the 22 clones. Repeatedly and as seen previously, DLD-1 pcDNA3.1-CCL5 cells had a 7-fold increase of CCL5 compare to DLD-1 and DLD-1 pcDNA3.1 cells; **see figure 75.** From these controls, the cut-off value for the positive CCL5 level was set at ≥ 200 pg/ml. As a result, the ELISA result classified the clones into 3 groups:

A- Negative clones for CCL5 expression when the level is ≤ 200 pg/ml, which includes clone 1, 2, 6, 7, 8, 9, 17, 19 and 21. **(see figure 75)**

B- Low-moderate CCL5-expressing clones when the level is ≥ 200 and ≤1000 pg/ml, including clones 3, 5, 10, 14, 16, 18 and 20 in this group. **(see figure 75)**

C- Positive clones with high CCL5 expression when the level is ≥ 1000 pg/ml, which included clones 4, 11, 12, 13, 15 and 22 in this group**. (see figure 75)**

The clones obtained using the control plasmid expressed low levels of CCL5 similar to group A. As we obtained low-negative clones from CCL5-plasmid selection we continued and used these clones instead of control plasmid clones.

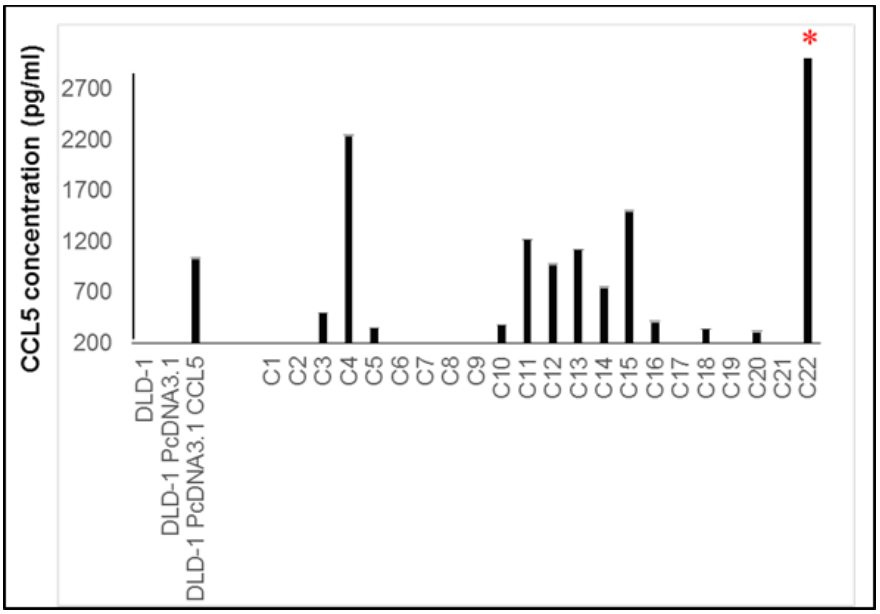

Figure 75: ELISA screening for the secreted level of CCL5 in twenty-two DLD-CCL5 clones.

Twenty-two clones were generated from DLD-1 cells stably transfected with pcDNA3.1 CCL5. DLD-1 cells and DLD-1 cells with the transient pcDNA 3.1 or pcDNA3.1 CCL5 were included as internal positive and negative controls for the performed human CCL5 sandwich ELISA. The cut-off value was set at 200 pg/ml according to the control results. Subsequently, three groups were established. Negative CCL5 clones (≤ 200pg/ml), low-moderate CCL5 clones (200-1000 pg/ml), and high CCL5 clones (≥ 1000 pg/ml). The results were normalised by the cell number to measure the average secretion of CCL5 per million cells. The figure is a representative result of n=2. * The result for clone 22 is (8740 pg/ml).

6.3.1.3 **Choosing a DLD-1 stable Clone**

From the 22 listed clones, one negative clone (clone 17; 30 pg/ml ± 9), one positive clone with low-moderate CCL5 expression (clone 16; 410 pg/ml ± 5), two positive clones with high CCL5 expression (clone 4; 2240 ± 10) and a clone with very high CCL5 expression (clone 22; 8740 pg/ml ± 23) were chosen. Their morphological appearance was examined, and the abundance of E-cadherin and CCL5 were investigated by WB in order to choose the best clones to proceed with the animal study; **see figure 76**. From the WB it can be seen that all clones have various levels of E-cadherin. Clone 4 has the highest expression of E-cadherin while clone 22 has the lowest expression. Clone 16 and 17 have similar levels of E-cadherin. Based on the morphological analysis by light microscopy, it appeared that clone 4 and clone 17 were the ones resembling the parental DLD-1 cells. On the other hand, clone 22 looked epithelial but invasive as the cells on the periphery of islands had filopodia-like structures. Clone 16 epithelial islands were intact but the size of the cells were larger than the parental DLD-1 cells; **see figure 76**. For the reasons that **1-** the most mesenchymal CRC cell line in our panel (CT26 cells) produced around 990 pg/ml CCL5, and **2-** different clones have different E-cadherin levels we selected clones 17 (CCL5

negative) and 4 (CCL5 high) for further studies. These clones express similar abundance of E-cadherin and the positive clone (Clones 4) produces physiological levels of CCL5, comparable to CT26; **see figure 75 and 76.**

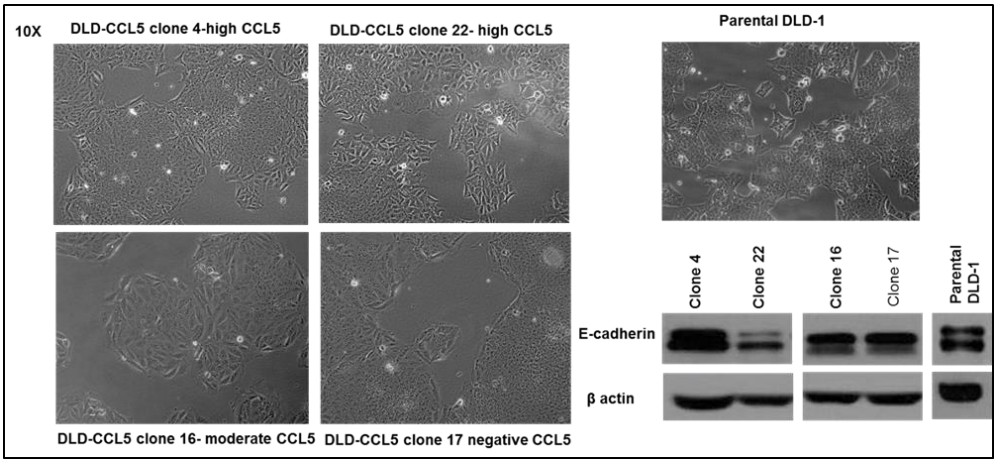

Figure 76: Validation of morphology and E-cadherin levels in the chosen DLD-CCL5 clones. The morphological changes were investigated as compared to the parental DLD-1 cells. Clone 22- showed an invasive but epithelial morphology, clone 16 showed intact morphology but the size of the cells were larger than the parental DLD-1 cells. Clone 4 and clone 17 showed a morphology similar to the parental DLD-1 cells. E-cadherin was expressed in all the clones but much less in clone 22 compared to the parental DLD-1 cells and the other clones.

6.3.2 Validation of CCL5 produced by DLD-1-stably transfected cells

6.3.2.1 **Flow cytometry analysis for CCR5 (CCL5 Ligand Receptor)**

It is well known that chemokines serve as attractants for cell types possessing their corresponding receptor. In that regard, CCL5 chemo-attracts cells harbouring CCR5, CCR3 or CCR1 [388, 431]. In order to investigate if CCL5 secreted from positive clones are functional or not we performed a screening of our CRC cell line panel for surface CCR5 expression**.**

Isotype IgG negative control and CCR5 APC antibodies were used to analyse CCR5 expression by flow-cytometry in DLD-1, HCT116, DLD-UI, DLD-I, SW480 and SW620 cells. Around 10,000 events using Forward Scatter (FSC) versus Side Scatter (SSC) were collected to mark live cells and CCR5 expression was detected using the APC channel. The results were displayed on a logarithmic scale in a FSC vs. FL4 (APC channel) histograms. The positive and negative results were defined by the shift compared to the isotype negative control. The assay was repeated twice *(n*= 2) in order to validate the results.

The results are summarized in **figure 77**. In essence, the isotype IgG negative control gave similar results in all cell lines with a mean range from 45.94 to 64.07 Mean Fluorescence intensity (MFI). CCR5 histograms all shifted considerably to the right in comparison to isotype IgG negative control histograms, which mean that all the cell lines expressed CCR5. However, the expression was at a range of levels. Induced DLD-SIP1 metastatic cells expressed more CCR5 (MFI of 225.88 with 83.71 CV) compared to un-induced DLD-SIP1 epithelial cells (MFI of 186.31 with 87.82 CV). In addition, SW480 mesenchymal cells had more CCR5 expression (MFI of 217.73 with 99.23 CV) compared to the intermediate epithelial SW620 cells (MFI of 128 with 74.76 CV). DLD-1 epithelial cells expressed CCR5 receptor at (MFI of 146 with 76.06 CV), whereas HCT116 intermediate mesenchymal had CCR5 receptor at (MFI of 160 with 68.86 CV). By closely analysing these results, it can be seen that the mesenchymal (DLD-I and SW480 cells) and intermediate mesenchymal cells (HCT116 cells) express more CCR5 compared to epithelial (DLD-UI and DLD-1 cells) and intermediate epithelial cells (SW620 cells) with 153 ± 29.7 *vs* 201 ± 35.9, respectively (p=0.14)

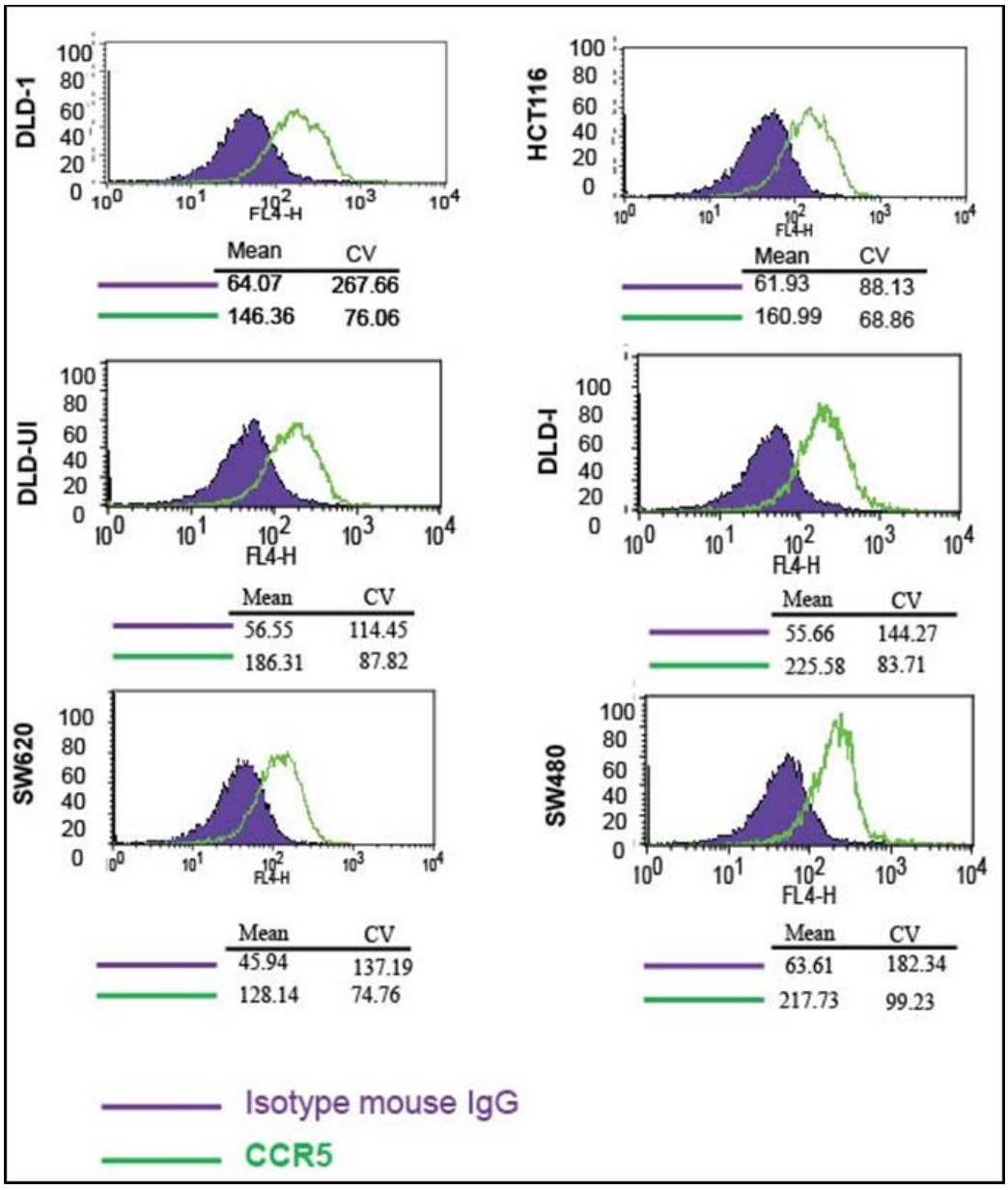

Figure 77: CCR5 expression in a panel of CRC cell lines and in the DLD-SIP1 CRC EMT model. DLD-I cells were induced for 3 days using 2 µg/ml doxycycline. 2 million cells from each cell line were treated with either isotype IgG negative control or APC-conjugated CCR5 antibody, and analysed by flow-cytometry. CCR5 expression was detected using the FL4 channel. The results were displayed on a logarithmic scale in a FSC vs. FL4 (APC channel) histograms. The positive and negative results were defined by the shift compared to the isotype negative control. The assay was repeated twice (n= 2), with similar results. All the CRC cells express CCR5, but SW480 and DLD-I cells express highest among all.

6.3.2.2 **Transwell Invasion Assay**

Before conducting any further experiments with the DLD-1 CCL5 clones, the functional activity of the secreted CCL5 was measured as a function of chemoattraction towards cells harbouring its receptor (CCR5).

The SW480 cell line which was found to have the highest level of CCR5 (**see figure77)** , was therefore chosen to assess its migration toward serum-free DMEM, DMEM with 10% serum, and the supernatant from clone 17 (CCL5 expression (30 pg/ml ± 9) or supernatant from clone 22 (8740 pg/ml ± 23) representing low and high CCL5 expression, respectively. Also, the migration of SW480 cells was assessed with DMEM containing 5000 pg/ml recombinant CCL5 or clone 22 supernatant containing 0.12 µg /ml CCL5 neutralising antibody in order to inactivate CCL5 in the unbound form. The migrated SW480 cells were stained with DAPI and examined by a dark field fluorescent microscope attached to a camera. The ImageJ program and a nucleus-counting macro [634] was used to count the number of cells in each picture. Of note, the assay were repeated five times (*n*=5) in order to get a conclusive result.

Final representative figures were illustrated **in figures 78 and 79.** From these figures, it can be seen that SW480 cells migrated less toward DMEM (150 cells ±20) with or without 10 % serum (190 cells ± 27). On the other hand, the cells migrated strongly towards the supernatant from clone 22 (1510 cells ± 92) compared to supernatant from clone 17 (403 cells ± 59). The migration of the cells that were incubated with DMEM containing recombinant CCL5, was enhanced by ~ 360% (702 cells ±100) compared to DMEM with 10% serum (190 cells ± 27)., and it is approximately 50 % of the number of migrated cells toward the clone 22 supernatant (1500 cells ± 92). In contrast, when cells were incubated with clone 22 supernatant containing CCL5 neutralising antibody, an 80% reduction in the number of migrated cells was observed (312 cells ± 45) compared to the migrated cells toward the clone 22 supernatant (1500 cells ± 92). Interestingly, this reduction in the cell number is close to the number of cells obtained from clone 17 (403 cells ± 59).

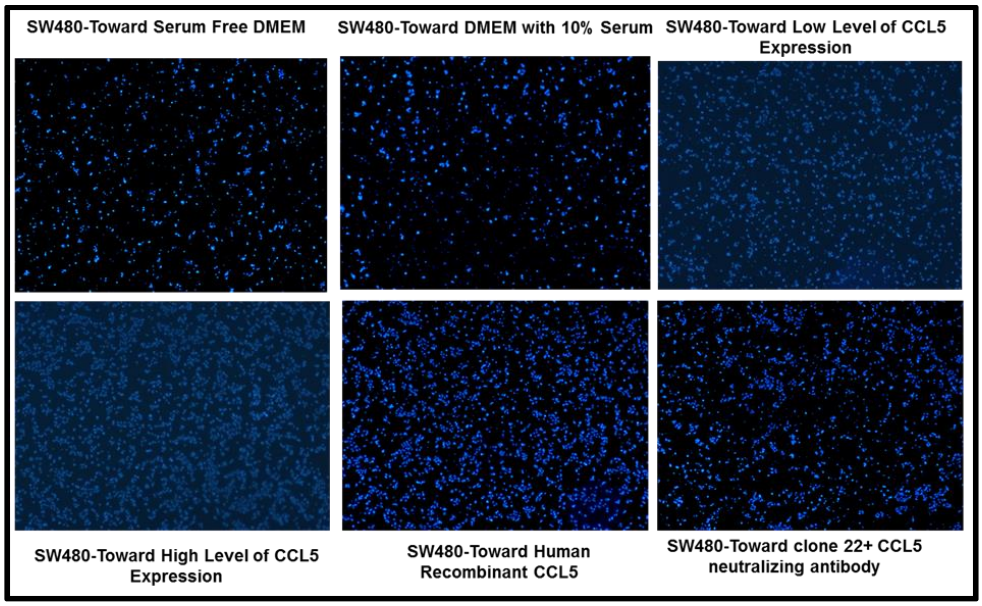

Figure 78: SW480 cells chosen to validate the functional activity of CCL5 obtained from the stably transfected DLD cells.

The migrated cells were stained by DAPI, and examined by a fluorescent microscope using UV light. The number of migrated cells from each condition were counted using image J.

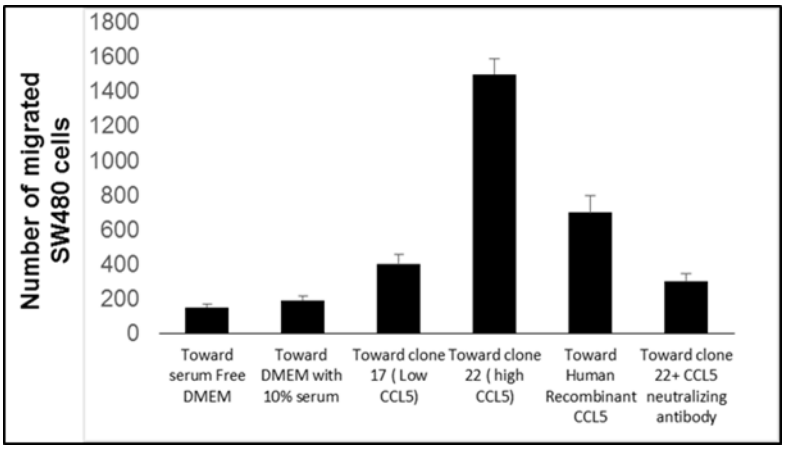

Figure 79: A bar chart illustrating the number of migrated SW480 cells in each individual condition.

SW480 cells migrated more toward clone 22 (high CCL5) and recombinant CCL5 conditions compared to clone 17 (negative CCL5), DMEM, serum-free DMEM or clone 22 containing the CCL5 neutralising antibody.

6.3.3 *In vivo* studies

In the previous section, we validated that the DLD-CCL5 clones express various levels of CCL5 and the secreted CCL5 produced a functional effect as a chemoattractant. To investigate if CCL5 solely contributes to metastasis, as proposed by Weinberg and colleagues [307], we intended to inject DLD-CCL5 clones into mice. To exclude the

contribution of immune infiltrate we used a SCID mice that lacks functional B and T-cells. One week before conducting the animal studies, clone 4 with high CCL5 expression and clone 17 with very low CCL5 expression were defrosted. The E-cadherin protein expression and the morphological appearance were examined two days before injection into the mice.

This time, supernatants from DLD-1, DLD-UI and DLD-I cells were used as internal controls to validate CCL5 ELISA results on that day of the assay. In agreement with the previous results, CCL5 was found 3 times more in DLD-I compared to DLD-UI and DLD-1 cells; **see figure 59.** Clone 4, which was seen to have high expression CCL5 (2240 ±123), gave approximately the same figure (1943 pg/ml ±102). Clone 17 which was observed to have low CCL5 (30 pg/ml ± 9), registered 123 pg/ml ± 20; **see figure 80.**

Similarly, E-cadherin expression level and the morphological phenotype of both clones were relatively similar to the morphology and amount of E-cadherin in the parent DLD-1 cells**; see figure 80.**

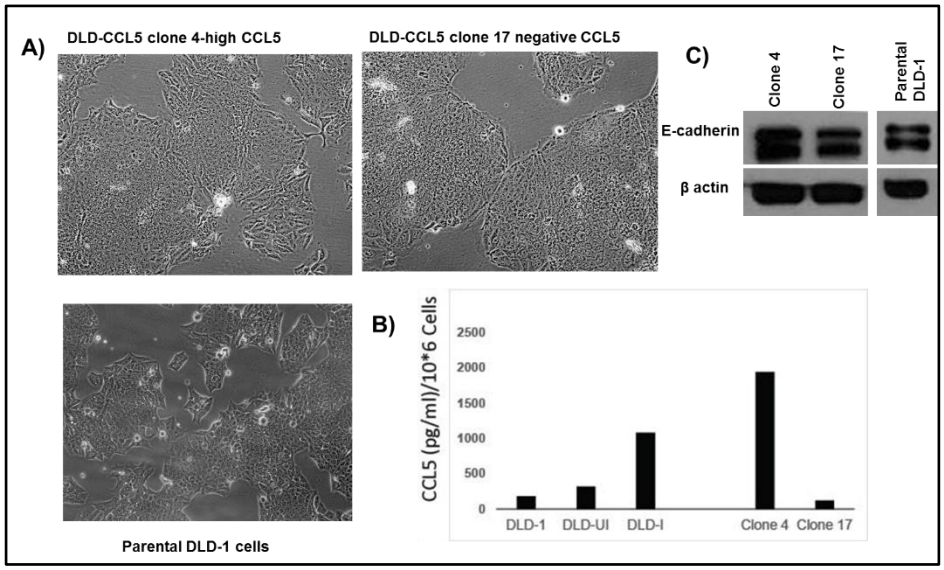

Figure 80: Validation of clone 4 (high CCL5) and clone 17 (negative CCL5) before proceeding with the animal experiment.

A) The cell morphology of clone 4 and clone 17 and parental DLD-1 cells. Both clones showed similar morphology compared to parental DLD-1 cells.
B) The secreted abundance of CCL5 in clone 4 and clone 17 as well as in parental DLD-1 and DLD-SIP1cells (internal positive and negative CCL5 controls) using human CCL5 ELISA. The figure showed that the level of CCL5 in clone 4 is much more than in clone 17 or parental DLD-1 cells.
C) The expression level of E-cadherin in clone 4, clone 17 and parental DLD-1 cells by WB. Both clones have E-cadherin levels similar to parental DLD-1 cells.

6.3.3.1 **Orthotropic CRC model with controlled CCL5 expression**

DLD cells are epithelial by definition and in terms of cellular characteristics, they are therefore not metastatic. However, like other epithelial carcinoma cells they may undergo EMT if they are exposed to the correct extracellular signals. This cell line was shown to produce sizeable tumours when injected subcutaneously but no distant metastasis was observed [497]. This can be due to the lack of correct environmental signals produced in the colon microenvironment. To study if local CCL5 would facilitate metastasis we planned to perform *in vivo* studies. To allow settling of DLD-CCL5 clones at the correct physiological environment we planned to inject cells into the caecum. Non-metastatic (epithelial) CRC cell lines were shown to metastasise when injected into the caecum [637]. This would allow DLD cells to potentially develop metastasis if higher CCL5 exposure would activate metastasis, similar to that described in breast cancer by Weinberg and colleagues [307]. In that article the source of CCL5 was mesenchymal stem cells (MSCs) whereas we have shown that metastatic cancer cells can also produce CCL5.

We have chosen NOD/SCID mice for this experiment. As NOD/SCID mice have no B or T cells, this model will also allow us to dissect whether CCL5 has any direct role in activating metastasis pathways or immune infiltration in TME modulated by CCL5 expression by facilitating metastasis.

Therefore, we injected 2 x 10^6 cells (of DLD-CCL5 clone 4 or clone 17) orthotropically, into the ceacum of SCID mice (5 animals in each group). The tumours were left to develop for 12 weeks and animals were euthanised before any cancer-related side effects were observed. Ceacums (primary CRC) and livers (potential site of metastases) were harvested and the carcasses were investigated carefully for the presence of visible metastases elsewhere in other distant organs. The tumours in ceacum were palpable but no metastasis was visibly observed on the livers. Histopathological examination, comprised of multiple sections, of ceacums from low- or high-CCL5 expressing tumours showed no difference in size of primary tumours (**see figure 81**). Multiple depth sectioning and histopathological examination of livers also showed no detectable metastasis**; see figure 82.** These results suggest that CCL5 expression in the CRC TME is not sufficient to induce metastasis.

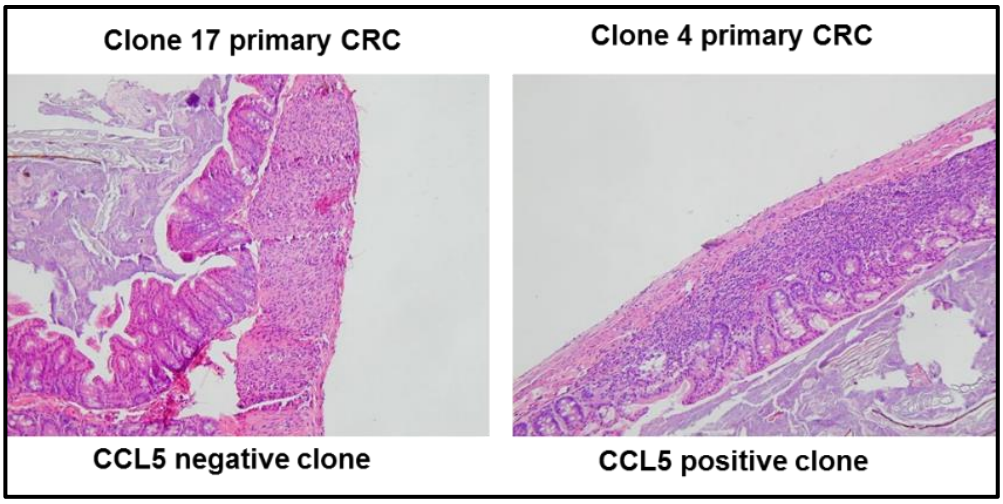

Figure 81: Examining the presence of cancer formed by DLD cells expressing CCL5 or not in the Ceacum.

2 x 10^6 cells from DLD-CCL5 clone 17 or DLD-CCL5 clone 4 were injected into SCID mice. The tumours were left to develop for 12 weeks. There was no difference in size of the formed primary tumours, and the IHC H&E staining showed no sign of invasion in either clones.

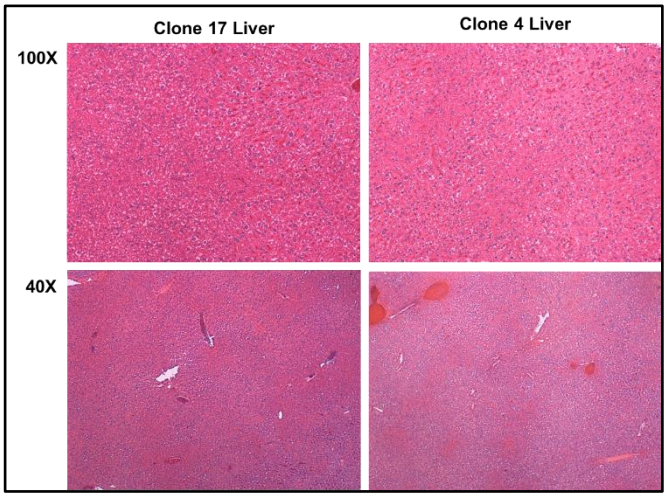

Figure 82: Haematoxylin and eosin (H&E) staining for the livers (potential site of metastases) from the orthothpically injected SCID mice with clone 4 or clone 17.

Pathological examination of the livers showed no detectable metastasis.

6.3.4 SIP1 expression linked with immune infiltrate

Our results from the previous section suggest that CCL5 produced within the TME is not sufficient to induce metastasis of an epithelial CRC cell line. Additionally we also observed that the highest CCL5 expressing clone (DLD-clone 22) is still epithelial and expresses E-cadherin. We therefore hypothesized that CCL5 in the local TME creates an immune-privileged environment to allow metastatic carcinoma cells to evade immunity and metastasise successfully. This hypothesis creates a direct link with the expression of an EMT-inducing transcription factor (SIP1) and the presence of a different set of immune

cells in metastatic and non-metastatic tumours. This is because CCL5 is a major chemokine regulating chemo-attraction of many kinds of lymphocytes including, but not limited to cytotoxic T-cells and regulatory T cells [611, 638]. To investigate if there is any association of SIP1with different T cell subpopulations in primary CRC we performed an immunohistochemistry-based screening for CD3 (pan T cell marker), CD4 (T helper cell), CD8 (cytotoxic T-cell) and FoxP3 (T reg cells) expressing T cell subpopulations in a cohort of patients with known SIP1 status. Another PhD student (Mr. Rahul Sreekumar) of my supervisor has previously shown that SIP1 expression predicts poor prognosis, reduced cancer-specific survival and disease-free survival in a cohort of consecutive CRC patients, all of which were operated on in the Southampton General Hospital (SGH) between July 2007 and October 2008 (*n*=75). All patients have at least 5 year follow up. We therefore chose this cohort as our sample (referred to as CRC cohort ABC).

6.3.4.1 **Tumour micro array (TMA) generation:**

Following recommendations of a pathologist (Dr. Karwan Moutasim) we intended to create a TMA from the blocks of the CRC cohort ABC. This has allowed us to reduce the costs of IHC as well as analysing each sample from multiple points (3X3 mm cores from non-necrotic tumour and 3X3 mm cores from the invasive front). To create the TMA, I obtained patient numbers for CRC cohort ABC, obtained an unprocessed tumour block and had them all cut and H & E (haematoxylin and eosin)- stained. Dr. Moutasim has marked the aforementioned regions from each block using H & E stained sections and SGH histopathology unit has created TMAs, placing material from 25 patients (6 cores from each patient=150 cores) in a block. Each block has been named as A, B or C, hence the name CRC cohort ABC, representing all 75 patients.

After that, sections of CRC cohort ABC has been cut and stained for CD3, CD4, CD8 and FoxP3 antibodies. All antibodies are routinely used in the diagnostic pathology lab of SGH so are therefore optimised for diagnostic purposes.

Our initial results showed that the staining has worked to a high standard and we had a variety of staining ranging from strongly positive to negative. However, due to the time limitations of pathologists, we could not score all the sections although we are intending to include this data in our future publications; **see figure 83**.

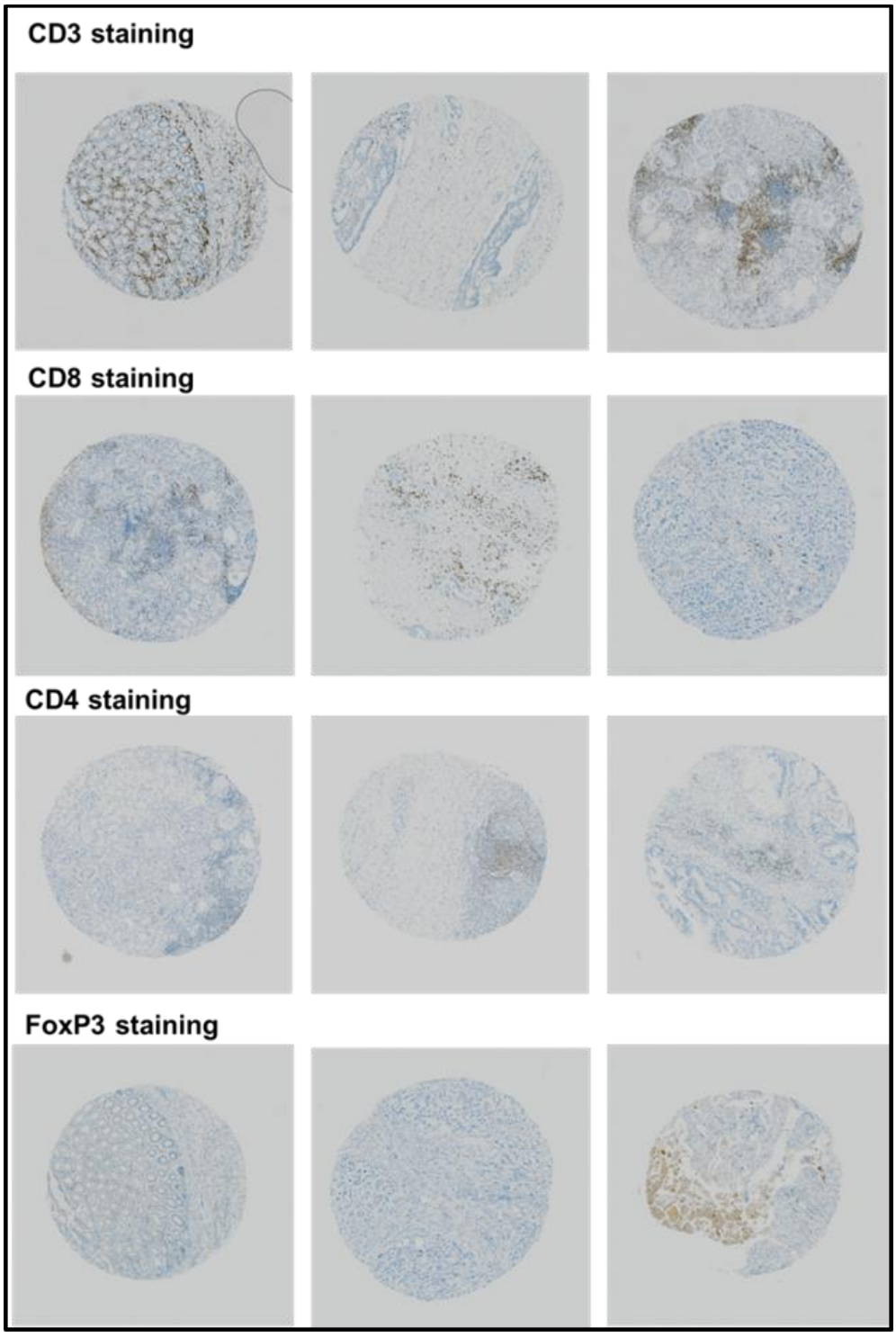

Figure 83: A representation of 3 different patterns of staining for each antibody used in this study.

Tissue blocks from a CRC cohort (75 patients) were collected. Depending on SIP1 status, the blocks were grouped into A, B or C. Each individual block was marked, by our departmental pathologist (Dr. Karwan Moutasim), for 3 potential invasion sites and 3 tumour cores using H&E staining. The histopathology lab created TMAs according to the designed plan. Each TMA slide from each group was stained with various surface markers for T cells, including CD3 (T cells pan marker), CD4 (T helper cells surface marker), CD8 (T cytotoxic surface marker) and FoxP3 (T reg marker). However, due to time limitation toward thesis submission we could not score the TMAs. Our initial results showed that the staining has worked at a high standard and we had a variety of staining ranging from strongly positive to negative. CCL5 is planned to be stained as well in our cohort in order to link the expression to T-cell infiltration.

6.4 Discussion

Karnoub *et al.*, found that CCL5 is up regulated via direct contact to mesenchymal stem cells (MCSs), and the over-expression of CCL5 in breast cancer cell lines does not promote proliferation and survival, instead it significantly enhances invasion and lung metastasis [307]. The author's findings suggest that CCL5 is necessary for metastasis. However, in immune-competent conditions and the human context, whether CCL5 induces EMT or generates an immune-deficient microenvironment allowing cancer cells to escape immunity and metastasise, is not clear. In fact, our findings from chapter 4 indicated that, in addition to mesenchymal stem cells, CCL5 is abundantly expressed by cancer cells undergoing EMT. Moreover, we found that ZEB1/2 can directly up-regulate CCL5 in cancer cells. Whether the amount of CCL5 secreted by MSCs or metastatic cancer cells differ is not addressed. However, it is quite likely that large tumours contain more metastatic cells than MSCs therefore the major source of CCL5 in the tumour should be ZEB1/2 expressing CRC cells. On the other hand, juxtacrine signalling between cancer cells and MSCs accompanied with abundant CCL5 in TME may be responsible for enhanced metastasis as observed by Weinberg and colleagues [307].

Moreover, many authors propose that CCL5 over-expression can predict poor survival and accumulates strongly at the invasive and metastatic front [433, 462, 578]. Also, CCL5 over-expression need was reported to modulate TME in favour of tumour growth, survival, migration, invasion and metastasis via recruiting CCR5+ Tregs, Th2, MSDCs, TAMs and inducing CD8+ T cells to die via apoptosis [611, 612] [614]. Despite the importance of all the aforementioned studies, few reports published have highlighted the role of CCL5 in EMT or *vice vers*a [622] [588] [585]; **see figure 61.** More importantly, a link between EMT, CCL5 and cancer favouring the TME has barely been studied especially in the context of CRC with direct links to ZEB1/2. Recently, a novel study performed by Hsu *et al*., showed that acetylation of SNAIL by CBP at lysine 146 and lysine 187 activated several genes including TNF-α, CCL2 and CCL5 by which TAMs recruited, and thus modulate TME which resulted in enhancing metastasis [509]. Again no mechanism, e.g. whether secreted factors induce EMT or metastatic cells evade immune response by modulating TME, has been proposed.

Beside our *in vitro* findings for the mechanistic role of ZEB1/2 in activating CCL5 expression **(chapter5),** the *in vivo* functional studies were planned to investigate whether

CCL5 can induce EMT and therefore metastasis by itself or that the presence of immunosuppressive TME is a must for metastasis in CRC.

Firstly, to investigate whether CCL5 contributes to EMT and therefore metastasis, a CCL5 over-expressing CRC cell line was generated by cloning CCL5 into pcDNA3.1 and transfecting it into DLD-1 cells. DLD-1 cells were chosen as it harbours a negligible amount of CCL5 (30 pg/ml± 7) and is a non-metastatic cell line [497]. All of these selective criteria are important in order to avoid any future complication with the interpretation. Neomycin was the drug used to determine the optimal kill curve for DLD-1 cells as well as to generate the clones. This drug was chosen because the pcDNA3.1 construct contains the Neomycin resistance gene, and it is frequently used in our group to generate cell lines over-expressing transgenes. The optimal dose concentration for DLD-1 was found to be 300 µg/ml in which we observed maximum cell death with the lowest concentration over a one-week period. Twenty two clones were collected and analysed, along with wild type DLD-1 cells, for their CCL5 level by ELISA as well as for their E-cadherin by WB. From the ELISA results, the cut-off value was established at 200 pg/ml due to the level of CCL5 in the wild type DLD-1 cells. From there, we classified the 22 clones into 3 groups: negative CCL5-expressing clones (<200pg/ml), low to moderate CCL5-expressing clones (≥ 200 and ≤1000 pg/ml) and high CCL5-expressing clones (≥ 1000 pg/ml). From this classification, clones 4, 16, 17 and 22 was selected; one negative clone (clone 17; 30 pg/ml ± 9), one with moderate CCL5 expression (clone 16; 410 pg/ml ± 5), two positive clones with high CCL5 expression (clone 4; 2240 ± 10) and one clone with very high CCL5 expression (clone 22; 8740 pg/ml ± 23) were chosen for further study; **see figure 75.**

The selected clones were examined for their morphological appearance and E-cadherin expression in order to choose the most appropriate clones to proceed with the animal study; **see figure 76**. From there, clone 22 was excluded from the study because, despite being epithelial, it showed quite an "invasive" appearance, which was reflected in its lower E-cadherin levels. Although clone 22 can be good to use in animal studies, it may cause misinterpretation of the metastasis ability associated with CCL5. Clone 16 expressed a mediocre amount of CCL5 and displayed intact epithelial islands with relatively abundant E-cadherin but the cells were larger than the parental DLD-1 cells, and for that, we did not choose it. Clone 4 and clone 17 showed a morphological appearance and E-cadherin level similar to parental DLD-1 cells despite clone 4 having very high levels of CCL5. For that,

Clones 4 and 17 were chosen to assess whether CCL5 alone can induce EMT and therefore metastasis.

Before injecting clones 17 and 4 into the NOD/SCID mice, functional CCL5 production from these cells was evaluated by migration assay toward the CCL5 receptor (CCR5); see **figures 77.** Although it is well established that CCL5 can also bind to CCR3 and CCR1 as well, CCR5 is considered the main receptor for CCL5. After analysing a selected panel of CRC cell lines (DLD-1, HCT116, SW620, SW480, DLD-UI and DLD-I) for CCR5 by flow-cytometry, SW480 cells were chosen. SW480 and DLD-SIP1 cells were shown to have the highest level of CCR5 among the cell lines tested. SW480 but not DLD-SIP1 cells were chosen for the migration assay because it is easy to grow and there is no need to use doxycycline that was used to induce DLD-SIP1 cells for 3 days. In addition, these cells are mesenchymal, and therefore they are very motile. Interestingly, I noticed that the cells described in chapter 3 as mesenchymal or intermediate mesenchymal express more CCR5 compared to epithelial and intermediate epithelial cells with 153 ± 29.7 vs 201 ± 35.9, respectively (p=0.14). Assessing CCR5 expression in a larger CRC cell line panel or patient cohort and linking this to EMT status would be fruitful. In fact, high expression of CCR5 in cancer has been reported to serve as a poor prognostic marker [424, 639].

The migration of SW480 cells to various culture conditions were conducted including free-serum, DMEM with 10 % serum, supernatant of clone 16 (negative CCL5 expression), supernatant of clone 22 (positive for CCL5 expression), DMEM with recombinant CCL5 or clone 22 supernatant with a CCL5-neutralising antibody. DMEM with or without serum were included to exclude any migration background caused by the serum or the medium. In order to validate that the migration toward CCL5 is specific to recombinant CCL5, a neutralising antibody against CCL5 was included. The results indicate that CCL5 in the stable transfected cell line is functional and valid for any further experiments, as we observed more migration toward clone 22 and recombinant CCL5 culture conditions compared to the other conditions and it is inhibited by a CCL5 neutralising antibody; see **figure 78, 79.**

NOD/SCID mice were chosen as the mouse strain in order to exclude the interference of immune infiltrate to the primary tumour. Before injecting the positive and the negative clones into the SCID mice, the clones were assessed, again, for their CCL5 expression as well as for their visual morphology and E-cadherin abundance; **see figure 80.** The reasons behind re-assessing the clones were to ensure that the clones had not lost their CCL5 and E-cadherin expression levels. In addition, we wanted to make sure that they did not acquire

any morphological changes over the period of their cell culture. This assessment would increase the accuracy of our main aim and the final interpretation of the results. Repeatedly, the results showed no change in the morphology or the level of CCL5 and E-cadherin, therefore validating their use for the animal experiments. The IHC results indicated that there was no evidence of distant metastasis. As preliminary data, this might pinpoint that the presence of CCL5 alone in the TME is not sufficient to induce metastasis**;** **see figure 81**. The presence of other soluble factors IL-1β, TNF-α and CCL2 could be essential to coordinate with CCL5 to trigger EMT, and thus metastasis [623]. However, in our group we observed that orthotropically injecting induced DLD-SIP1 but not un-induced DLD-SIP1 cells to mice causes distant metastasis to the peritoneal cavity and liver. In this project, we observed that cells also over-express CCL5 after SIP1-induction. This data could direct us to say that the presence of SIP1 by cancer cells is sufficient for metastasis in an immune-deficient TME. In my opinion, it is beneficial to knock down CCL5 in the induced DLD-SIP1 cells and inject them to nude mice as well as knock down CCL5 in the mesenchymal mouse CT26 cells and inject it into immune-competent mice to study the immune infiltration changes in the TME associated with the presence of SIP1.

In order to assess that CCL5 up-regulation changes the immune cell infiltration of the tumour microenvironment in a favour of metastasis in CRC, TMA was done for 75 CRC samples with known SIP1 status. The SIP1 status was done by our group, the findings indicated that patients expressing SIP1 have a poor prognosis, and SIP1 is a good marker to predict metastasis (Sreekumar *et al*, in preparation). Three tumour cores and 3 invasive fronts from each block were punched and placed in paraffin as a TMA slide. The slides were stained individually with specific markers for T lymphocyte markers, previously reported in cancer including CD3+, CD4+, CD8+, and Treg [352, 354, 611].The staining and the scanning of the slide were achieved. However due to time restrictions towards the submission deadline for this thesis, we could not analyse the findings and investigate with the association of SIP1 and the T cell infiltrate. Of note, we will be performing CCL5 staining to attain a direct link between SIP1 and CCL5.

Chapter 7: Conclusion and Future Directions

7.1 Study objective and aims

The objective of this study was to identify the soluble factor which changed its expression most significantly during SIP1-induced EMT, and link it with a reduced anti-tumour response.

To achieve this objective, the following aims were defined:

- Characterise the EMT status of a panel of CRC cell lines and a CRC-EMT model.
- General screening of large numbers of human cytokines and chemokines and associate them with EMT status.
- Investigate the mechanism how this chemokine is over-expressed during EMT.
- Study the mechanistic role of the chosen soluble factor in CRC EMT.
- Study the functional role of the chosen soluble factor in relation to immune infiltration in CRC EMT.

7.2 Summary of the project findings

The results of this project were summarised in 4 chapters:

Chapter 3: EMT status in CRC.

Chapter 4: EMT-driven cytokine/chemokine expression in CRC.

Chapter 5: The mechanistic role of ZEB1/2 EMT in activating the chosen soluble factor in CRC.

Chapter 6: The molecular basis of immune infiltration as a result of a metastasis programme in CRC.

In chapter 3, EMT status was assessed in 12 cell lines and a stable inducible model of CRC-EMT, DLD-SIP1. I believe this is first time such a large-scale study has been conducted. Our microscopy, western blotting, RT-PCR and IF data concluded in classifying the 12 cell lines into three separate classes:

A- An epithelial cell category, which includes AAC1, Caco2, Colo205, DLD-1, HT29 and SW48 cell lines.
B- A mesenchymal cell category, which includes CT26, RKO, and SW480 cell lines.
C- An intermediate cell category, which includes HCT116, LoVo, SW620 cell lines.

In my transfer viva, the examiner advised me to further characterise the metastable or the intermediate cells, which exhibit both mesenchymal and epithelial features. In the literature, this phenotype has been described and suggested to add a spectrum of heterogeneity instead of only presenting the two extreme ends of the EMT process, and could increase the potential advantage of a more targeted therapy[128]. Cell plasticity was investigated by IF staining for E-cadherin, vimentin, F-actin and P-cadherin. Although, P-cadherin was suggested as a good biomarker to differentiate these cells [130], I could not obtain good results with it either due to problems with the antibody or because P-Cadherin is not a marker of the metastable phenotype in CRC unlike it was shown for breast cancer. Nonetheless, from the various methods we used to characterise EMT status, we are confident to conclude that the metastable cell lines should be sub-classified as:

- SW620 is an intermediate/metastable epithelial cell line (more positive for epithelial features)
- HCT116 and LoVo are intermediate/metastable mesenchymal cell lines (more positive for mesenchymal features)

We also concluded that the DLD-SIP1 stable inducible model is a very good model to investigate the role of what drives EMT. SW480 and SW620 could be considered as a second EMT model because they represent epithelial and mesenchymal properties as they were obtained from the same patient. SNAIL was seen in all CRC cell lines and it would be beneficial to study the mechanism and the function of it in CRC; this is possibly related to transformation rather than EMT. ZEB1/2 are the major regulators of EMT in CRC as they were only found in the mesenchymal cell lines. The CT26 mouse cell line is the most mesenchymal among our CRC cell line panel, and that could be due to the simultaneous expression of multiple EMT transcriptional inducible factors such as SIP1, TWIST and SLUG.

In chapter 4, a large number of chemokines and cytokines (n= 67) were screened using DLD-SIP1 cells; see **figure 51 and 52**. Selective criteria were defined to identify the most reliably-induced chemokine, and from that CCL5 was chosen. CCL5 was found to be sharply increased in induced DLD-SIP1cells. This result was confirmed repeatedly by RT-

PCR, ELISA assay and multiplex immunoassay and also using another SIP1 induced EMT model (A431-SIP1 cells); see **figures 55, 56, 58 and 59**. The CRC panel was then investigated for CCL5 mRNA and protein expression by RT-PCR and ELISA, respectively; see **figures 57 and 60.** These results concluded that mesenchymal cells produce more CCL5 compared to epithelial ones. The novelty of our finding is that CCL5 is secreted more by the metastatic mesenchymal cancer cells, in addition to MSCs or tumour stroma [307, 579]. The relative contribution of each source and their relevance are yet to be determined.

From both chapter 3 and 4 we suggest that ZEB1/2 could be the drivers of CCL5 expression in CRC. In chapter 5, we studied the potential binding sites of ZEB1/2 at the *CCL5* promoter by transfecting the pGL3-CCL5 promoter into CRC cells harbouring either ZEB1 or ZEB2 (SIP1) proteins. Luciferase and ChIP were performed to carry out this goal. These results concluded that ZEB1/2 could be contributors in up-regulating CCL5 directly, and this is an original finding.

In chapter 6, we planned to study whether CCL5 can induce metastasis or EMT-induced CCL5 expression can alter immune infiltration in CRC to favour an immune-deficient microenvironment.

Firstly, to investigate whether CCL5 contributes to EMT and therefore metastasis, we generated DLD-1 cells over-expressing CCL5 and injected these cells orthotropically into SCID mice in order to exclude the interference of immune-infiltration. Histopathological examination suggested the increased abundance of CCL5 did not enhance metastasis in mice lacking T and B cells. This means CCL5 alone is not capable of inducing metastasis in CRC.

A TMA of 75 sections from CRCs with known SIP1 status were stained for markers to detect all T cells (CD3+ pan marker), T helper cells (CD3+ CD4+), cytotoxic T cells (CD3+, CD8+) or T-reg cells (CD3+, Foxp3+). The array and the staining were done but due to restrictions in time, pathological analysis of the finding was not conducted.

7.3 Future directions:

- We are confident that the EMT status for all the CRC cell lines used has been characterised. However, we could not validate the recently recommended marker in breast cancer to differentiate the intermediate EMT phenotype (P-cadherin). It could be beneficial to repeat these experiments with another P-cadherin antibody and using validated metastable breast cancer cell lines as positive controls to determine the importance of this recommended marker for intermediate cells in CRC.
- We found that ZEB1/2 directly up-regulate CCL5 expression using luciferase reporter and ChIP assays. However, due to problems with primers, the ZEB1/2 E-box1 in the *CCL5* promoter could not be assessed in the ChIP assay. It would be useful to design other set of primers covering this region and repeat the PCR using the chromatin we obtained. In addition, by analysing the whole *CCL5* promoter and the coding and non-coding regions of the gene, we determined the presence of other strong E-boxes. It would be beneficial to investigate them for their importance as other sites for ZEB1/2 using the SIP1-bound chromatin obtained.
- In chapter 6 we managed to investigate whether CCL5 can cause metastasis without the interference of immune-cells using SCID mice. However, due to time restrictions toward the submission deadline we could not investigate if CCL5 expression can alter immune infiltration; particularly T cells in CRC, thus promoting tumour growth and metastasis. To further investigate this and to complete the project, the following should be carried out:

  - The chemo-attractant function of CCL5 on different immune cells should be examined. PBMCs from normal individuals can be collected and used for Transwell invasion and migration assays along with supernatants from stable DLD-CCL5 cells. The control for this experiment to ensure that the migrated immune cells are attracted because of CCL5 will be supernatant from cells treated with a CCL5-neutralising antibody. We will analyse the migration of immune cells by flow cytometry using various surface markers of immune cells such as CD3 (pan T cell marker), CD4 (T helper cell marker), CD8 (T cytotoxic marker) and CD19 (B cell marker). This will clarify which lymphocytes will be specifically attracted to tumours with CCL5-expressing metastatic cells.

- A TMA of 75 sections CRC samples with known SIP1 status were stained with cytotoxic T cells (CD3+, CD8+), T helper cells (CD3+, CD4+) or T-reg cells (CD3+, Foxp3+). Pathological analysis of the TMAs slides should be carried out. We should also include CCL5 staining to validate the over-expression of CCL5 in CRC and the association of SIP1 and CCL5 expression.
- We will need to generate a stable CCL5-knock down in the murine CT26 cells using shRNA and then inject these cells into immune-competent mice. Then, we can examine the immune infiltration by IHC using various markers for fibroblasts, MSCs and immune cells. A key readout of this experiment is assessing the metastatic potential of CT26 cells with or without CCL5. This experiment is a follow up of the orthotopic DLD model and will tell us whether CCL5 is directly regulating the survival of metastatic cells by altering the TME. The T-cells infiltrating CT26 tumours should also be investigated qualitatively and quantitatively.

Appendices

Table 12: The list of chemokines in the R&D chemokine array.

Coordinate	Analyte/Control	Alternate Nomenclature
A1, A2, A19, A20	Reference Spots	-----
B3, B4	6Ckine	CCL21
B5, B6	CCL28	MEC
B7, B8	CXCL16	SRPSOX
B9, B10	Chemerin	TIG-2
B11, B12	ENA-78	CXCL5
B13, B14	Eotaxin-3	CCL26
B15, B16	Fractalkine	CX3CL1
B17, B18	GROα	CXCL1
C3, C4	HCC-1	CCL14
C5, C6	I-309	CCL1
C7, C8	IL-8	CXCL8
C9, C10	IL-16	LCF
C11, C12	IP-10	CXCL10
C13, C14	I-TAC	CXCL11
C15, C16	Lymphotactin	XCL1
C17, C18	MCP-1	CCL2
D3, D4	MCP-3	CCL7
D5, D6	MDC	CCL22
D7, D8	Midkine	-----
D9, D10	MIG	CXCL9
D11, D12	MIP-1α/β	CCL3, CCL4
D13, D14	MIP-1δ	CCL15
D15, D16	MIP-3α	CCL20
D17, D18	MIP-3β	CCL19
E3, E4	NAP-2	CXCL7
E5, E6	PARC	CCL18
E7, E8	PF4	CXCL4
E9, E10	RANTES	CCL5
E11, E12	SDF-1	CXCL12
E13, E14	TARC	CCL17
E15, E16	VCC-1	CXCL17
F3, F4	Fibrinogen (Sample Control)	-----
F5, F6	gp130 (Sample Control)	IL6ST, CD130
F7, F8	Transferrin R (Sample Control)	TfR, CD71
F9, F10	Negative Control	-----
G1, G2	Reference Spots	-----

Table 13 The list of cytokines in the R&D systems cytokines array.

Coordinate	Target/Control	Alternate Nomenclature
A1, A2	Reference Spot	-----
A3, A4	C5/C5a	Complement Component 5/5a
A5, A6	CD40 Ligand	CD154
A7, A8	G-CSF	CSFβ, CSF-3
A9, A10	GM-CSF	CSFα, CSF-2
A11, A12	GROα	CXCL1
A13, A14	I-309	CCL1
A15, A16	sICAM-1	CD54
A17, A18	IFN-γ	Type II IFN
A19, A20	Reference Spot	-----
B3, B4	IL-1α	IL-1F1
B5, B6	IL-1β	IL-1F2
B7, B8	IL-1ra	IL-1F3
B9, B10	IL-2	-----
B11, B12	IL-4	-----
B13, B14	IL-5	-----
B15, B16	IL-6	-----
B17, B18	IL-8	CXCL8
C3, C4	IL-10	-----
C5, C6	IL-12 p70	-----
C7, C8	IL-13	-----
C9, C10	IL-16	LCF
C11, C12	IL-17	-----
C13, C14	IL-17E	-----
C15, C16	IL-23	-----
C17, C18	IL-27	-----
D3, D4	IL-32α	-----
D5, D6	IP-10	CXCL10
D7, D8	I-TAC	CXCL11
D9, D10	MCP-1	CCL2
D11, D12	MIF	GIF, DER6
D13, D14	MIP-1α	CCL3
D15, D16	MIP-1β	CCL4
D17, D18	Serpin E1	PAI-1
E1, E2	Reference Spot	-----
E3, E4	RANTES	CCL5
E5, E6	SDF-1	CXCL12
E7, E8	TNF-α	TNFSF1A
E9, E10	sTREM-1	-----

```
Query  144    CCAATAATGATAGAGTATGCTGTAAGATATCTTTCTCTCCNTCTGCTTCTCAACAAGTCT  203
              ||||||||||||||||||||||||||||||||||||||| ||||||||||||||||||||
Sbjct  45820  CCAATAATGATAGAGTATGCTGTAAGATATCTTTCTCTCCCTCTGCTTCTCAACAAGTCT  45761

Query  204    CTAATCAATTATTCCACTTTATAAACAAGGAAATAGAACTCAAAGACATTAAGCACTTTT  263
              ||||||||||||||||||||||||||||||||||||||||||||||||||||||||||||
Sbjct  45760  CTAATCAATTATTCCACTTTATAAACAAGGAAATAGAACTCAAAGACATTAAGCACTTTT  45701

Query  264    CCCAAAGGTCGCTTAGCAAGTAAATGGGAGAGACCCTATGACCAGGATGAAAGCAAGAAA  323
              ||||||||||||||||||||||||||||||||||||||||||||||||||||||||||||
Sbjct  45700  CCCAAAGGTCGCTTAGCAAGTAAATGGGAGAGACCCTATGACCAGGATGAAAGCAAGAAA  45641

Query  324    TTCCCACAAGAGGACTCATTCCAACTCATATCTTGTGAAAAGGTTCCCAATGCCCAGCTC  383
              ||||||||||||||||||||||||||||||||||||||||||||||||||||||||||||
Sbjct  45640  TTCCCACAAGAGGACTCATTCCAACTCATATCTTGTGAAAAGGTTCCCAATGCCCAGCTC  45581

Query  384    AGATCAACTGCCTCAATTTACAGTGTGAGTGTGCTAAAATCCTTTGGGGACTGTATATCC  443
              |||||||||||||||||||||||||||||||| |  ||||||||||||||||||||||
Sbjct  45580  AGATCAACTGCCTCAATTTACAGTGTGAGTGTGCTCACCTCCTTTGGGGACTGTATATCC  45521

Query  444    AGAGGACCCTCCTCAATAAAACACTTTATAAATAACATCCTTCCATGGATGAGGGAAAGG  503
              ||||||||||||||||||||||||||||||||||||||||||||||||||||||||||||
Sbjct  45520  AGAGGACCCTCCTCAATAAAACACTTTATAAATAACATCCTTCCATGGATGAGGGAAAGG  45461gct

Query  504    AGGTAAGATCTGTAATGAATAAGCAGGAACTTTGAAGACTCAGTGACTCAGTGAGTAATA  563
              |||||||||||||||||||||||||||||||| ||||||||||||||||||||||||||||
Sbjct  45460  AGGTAAGATCTGTAATGAATAAGCAGGAACTTTGAAGACTCAGTGACTCAGTGAGTAATA  45401

Query  564    AAGACTCAGTGACTTCTGATCCTGTCCTAACTGCCACTCCTTGTTGTCCCCAAGAAAGCG  623
              ||||||||||||||||||||||||||||||||||||||||||||||||||||||||||||
Sbjct  45400  AAGACTCAGTGACTTCTGATCCTGTCCTAACTGCCACTCCTTGTTGTCCCCAAGAAAGCG  45341

Query  624    GCTTCCTGCTCTCTGAGGAGGACCCCTTCCCTGGAAGGTAAAACTAAGGATGTCAGCAGA  683
              ||||||||||||||||||||||||||||||||||||||||||||||||||||||||||||
Sbjct  45340  GCTTCCTGCTCTCTGAGGAGGACCCCTTCCCTGGAAGGTAAAACTAAGGATGTCAGCAGA  45281

Query  684    GAAATTTTTCCACCATTGGTGCTTGGTCAAAGAGGAAACTGATGAGCTCACTCTAGATGA  743
              ||||||||||||||||||||||||||||||||||||||||||||||||||||||||||||
Sbjct  45280  GAAATTTTTCCACCATTGGTGCTTGGTCAAAGAGGAAACTGATGAGCTCACTCTAGATGA  45221

Query  744    GAGAGCAGTGAGGGAGAGACAGAGACTCGAATTTCCGGAGGCTATTTCAGTTTTCTTTTC  803
              ||||||||||||||||||||||||||||||||||||||||||||||||||||||||||||
Sbjct  45220  GAGAGCAGTGAGGGAGAGACAGAGACTCGAATTTCCGGAGGCTATTTCAGTTTTCTTTTC  45161

Query  804    CGTTTTGTGCAATTTCACTTATGATACCGGCCAATGCTTGGTTGCTATTTTGGAAACTCC  863
              ||||||||||||||||||||||||||||||||||||||||||||||||||||||||||||
Sbjct  45160  CGTTTTGTGCAATTTCACTTATGATACCGGCCAATGCTTGGTTGCTATTTTGGAAACTCC  45101

Query  864    CCTTAGGGGATGCCCCTCAACTGGCCCTATAAAGGGCCAGCCTGAGCTGCAGAGGATTCC  923
              ||||||||||||||||||||||||||||||||||||||||||||||||||||||||||||
Sbjct  45100  CCTTAGGGGATGCCCCTCAACTGGCCCTATAAAGGGCCAGCCTGAGCTGCAGAGGATTCC  45041

Query  924    TGCAGAGGATCAAGACAGCACGTGGACCTCGCACAGCCTCTCCCACAGGTACCATCAAGG  983
              |||||||||||||||||||||||||||||||||||||||||||||||||||||| ||||
Sbjct  45040  TGCAGAGGATCAAGACAGCACGTGGACCTCGCACAGCCTCTCCCACAGGTACCATGAAGG  44981

Query  984    TCTCCGC  990
              |||||||
Sbjct  44980  TCTCCGC  44974
```

Figure 84: DNA sequence of the mutated CCL5 *promoter* ZEB2BOX2 (top line) aligned with wild-type *CCL5* promoter sequence (bottom line) using the BLAST program

```
Query  225    CCAATAATGATAGAGTATGCTGTAAGATATCTTTCTCTCCNTCTGCTTCTCAACAAGTCT  284
              ||||||||||||||||||||||||||||||||||||||| ||||||||||||||||||
Sbjct  45820  CCAATAATGATAGAGTATGCTGTAAGATATCTTTCTCTCCCTCTGCTTCTCAACAAGTCT  45761

Query  285    CTAATCAATTATTNCACTTTATAAACAAGGAAATAGAACTCAAAGACATTAAGCACTTTT  344
              |||||||||||||| ||||||||||||||||||||||||||||||||||||||||||||
Sbjct  45760  CTAATCAATTATTCCACTTTATAAACAAGGAAATAGAACTCAAAGACATTAAGCACTTTT  45701

Query  345    CCCAAAGGTCGCTTAGCAAGTAAATGGGAGAGACCCTATGACCAGGATGAAAGCAAGAAA  404
              ||||||||||||||||||||||||||||||||||||||||||||||||||||||||||||
Sbjct  45700  CCCAAAGGTCGCTTAGCAAGTAAATGGGAGAGACCCTATGACCAGGATGAAAGCAAGAAA  45641

Query  405    TTCCCACAAGAGGACTCATTCCAACTCATATCTTGTGAAAAGGTTCCCAATGCCCAGCTC  464
              ||||||||||||||||||||||||||||||||||||||||||||||||||||||||||||
Sbjct  45640  TTCCCACAAGAGGACTCATTCCAACTCATATCTTGTGAAAAGGTTCCCAATGCCCAGCTC  45581

Query  465    AGATCAACTGCCTCAATTTACAGTGTGAGTGTGCTCACCTCCTTTGGGGACTGTATATCC  524
              ||||||||||||||||||||||||||||||||||||||||||||||||||||||||||||
Sbjct  45580  AGATCAACTGCCTCAATTTACAGTGTGAGTGTGCTCACCTCCTTTGGGGACTGTATATCC  45521

Query  525    AGAGGACCCTCCTCAATAAAACACTTTATAAATAACATCCTTCCATGGATGAGGGAAAGG  584
              ||||||||||||||||||||||||||||||||||||||||||||||||||||||||||||
Sbjct  45520  AGAGGACCCTCCTCAATAAAACACTTTATAAATAACATCCTTCCATGGATGAGGGAAAGG  45461

Query  585    AGGTAAGATCTGTAATGAATAAGCAGGAACTTCGAAGACTCAGTGACTCAGTGAGTAATA  644
              |||||||||||||||||||||||||||||| ||||||||||||||||||||||||||||
Sbjct  45460  AGGTAAGATCTGTAATGAATAAGCAGGAACTTTGAAGACTCAGTGACTCAGTGAGTAATA  45401

Query  645    AAGACTCAGTGACTTCTGATCCTGTCCTAACTGCCACTCCTTGTTGTCCCCAAGAAAGCG  704
              ||||||||||||||||||||||||||||||||||||||||||||||||||||||||||||
Sbjct  45400  AAGACTCAGTGACTTCTGATCCTGTCCTAACTGCCACTCCTTGTTGTCCCCAAGAAAGCG  45341

Query  705    GCTTCCTGCTCTCTGAGGAGGACCCCTTCCCTGGAAGGTAAAACTAAGGATGTCAGCAGA  764
              ||||||||||||||||||||||||||||||||||||||||||||||||||||||||||||
Sbjct  45340  GCTTCCTGCTCTCTGAGGAGGACCCCTTCCCTGGAAGGTAAAACTAAGGATGTCAGCAGA  45281

Query  765    GAAATTTTTCCACCATTGGTGCTTGGTCAAAGAGGAAACTGATGAGCTCACTCTAGATGA  824
              ||||||||||||||||||||||||||||||||||||||||||||||||||||||||||||
Sbjct  45280  GAAATTTTTCCACCATTGGTGCTTGGTCAAAGAGGAAACTGATGAGCTCACTCTAGATGA  45221

Query  825    GAGAGCAGTGAGGGAGAGACAGAGACTCGAATTTCCGGAGGCTATTTCAGTTTTCTTTTC  884
              ||||||||||||||||||||||||||||||||||||||||||||||||||||||||||||
Sbjct  45220  GAGAGCAGTGAGGGAGAGACAGAGACTCGAATTTCCGGAGGCTATTTCAGTTTTCTTTTC  45161

Query  885    CGTTTTGTGCAATTTCACTTATGATACCGGCCAATGCTTGGTTGCTATTTTGGAAACTCC  944
              ||||||||||||||||||||||||||||||||||||||||||||||||||||||||||||
Sbjct  45160  CGTTTTGTGCAATTTCACTTATGATACCGGCCAATGCTTGGTTGCTATTTTGGAAACTCC  45101

Query  945    CCTTAGGGGATGCCCCTCAACTGGCCCTATAAAGGGCCAGCCTGAGCTGCAGAGGATTCC  1004
              ||||||||||||||||||||||||||||||||||||||||||||||||||||||||||||
Sbjct  45100  CCTTAGGGGATGCCCCTCAACTGGCCCTATAAAGGGCCAGCCTGAGCTGCAGAGGATTCC  45041

Query  1005   TGCAGAGGATCAAGACAGAAAAAGGACCTCGCACAGCCTCTCCCACAGGTACCATCAAGG  1064
              |||||||||||||||||  |    |||||||||||||||||||||||||||||| ||||
Sbjct  45040  TGCAGAGGATCAAGACAGCACGTGGACCTCGCACAGCCTCTCCCACAGGTACCATGAAGG  44981

Query  1065   TCTCCGC  1071
              |||||||
Sbjct  44980  TCTCCGC  44974
```

Figure 85: DNA sequence of the mutated *CCL5* promoter ZEB2 BOX2 (top line) aligned with wild-type *CCL5* promoter sequence (bottom line) using the BLAST program

```
Query  265    CCCAAAGGTCGCTTAGCAAGTAAATGGGAGAGACCCTATGACCAGGATGAAAGCAAGAAA  324
              ||||||||||||||||||||||||||||||||||||||||||||||||||||||||||||
Sbjct  45700  CCCAAAGGTCGCTTAGCAAGTAAATGGGAGAGACCCTATGACCAGGATGAAAGCAAGAAA  45641

Query  325    TTCCCACAAGAGGACTCATTCCAACTCATATCTTGTGAAAAGGTTCCCAATGCCCAGCTC  384
              ||||||||||||||||||||||||||||||||||||||||||||||||||||||||||||
Sbjct  45640  TTCCCACAAGAGGACTCATTCCAACTCATATCTTGTGAAAAGGTTCCCAATGCCCAGCTC  45581

Query  385    AGATCAACTGCCTCAATTTACAGTGTGAGTGTGCTAAAATCCTTTGGGGACTGTATATCC  444
              |||||||||||||||||||||||||||||||| |  ||||||||||||||||||||||
Sbjct  45580  AGATCAACTGCCTCAATTTACAGTGTGAGTGTGCTCACCTCCTTTGGGGACTGTATATCC  45521

Query  445    AGAGGACCCTCCTCAATAAAACACTTTATAAATAACATCCTTCCATGGATGAGGGAAAGG  504
              ||||||||||||||||||||||||||||||||||||||||||||||||||||||||||||
Sbjct  45520  AGAGGACCCTCCTCAATAAAACACTTTATAAATAACATCCTTCCATGGATGAGGGAAAGG  45461

Query  505    AGGTAAGATCTGTAATGAATAAGCAGGAACTTCGAAGACTCAGTGACTCAGTGAGTAATA  564
              |||||||||||||||||||||||||||||| ||||||||||||||||||||||||||||
Sbjct  45460  AGGTAAGATCTGTAATGAATAAGCAGGAACTTTGAAGACTCAGTGACTCAGTGAGTAATA  45401

Query  565    AAGACTCAGTGACTTCTGATCCTGTCCTAACTGCCACTCCTTGTTGTCCCCAAGAAAGCG  624
              ||||||||||||||||||||||||||||||||||||||||||||||||||||||||||||
Sbjct  45400  AAGACTCAGTGACTTCTGATCCTGTCCTAACTGCCACTCCTTGTTGTCCCCAAGAAAGCG  45341

Query  625    GCTTCCTGCTCTCTGAGGAGGACCCCTTCCCTGGAAGGTAAAACTAAGGATGTCAGCAGA  684
              ||||||||||||||||||||||||||||||||||||||||||||||||||||||||||||
Sbjct  45340  GCTTCCTGCTCTCTGAGGAGGACCCCTTCCCTGGAAGGTAAAACTAAGGATGTCAGCAGA  45281

Query  685    GAAATTTTTCCACCATTGGTGCTTGGTCAAAGAGGAAACTGATGAGCTCACTCTAGATGA  744
              ||||||||||||||||||||||||||||||||||||||||||||||||||||||||||||
Sbjct  45280  GAAATTTTTCCACCATTGGTGCTTGGTCAAAGAGGAAACTGATGAGCTCACTCTAGATGA  45221

Query  745    GAGAGCAGTGAGGGAGAGACAGAGACTCGAATTTCCGGAGGCTATTTCAGTTTTCTTTTC  804
              ||||||||||||||||||||||||||||||||||||||||||||||||||||||||||||
Sbjct  45220  GAGAGCAGTGAGGGAGAGACAGAGACTCGAATTTCCGGAGGCTATTTCAGTTTTCTTTTC  45161

Query  805    CGTTTTGTGCAATTTCACTTATGATACCGGCCAATGCTTGGTTGCTATTTTGGAAACTCC  864
              ||||||||||||||||||||||||||||||||||||||||||||||||||||||||||||
Sbjct  45160  CGTTTTGTGCAATTTCACTTATGATACCGGCCAATGCTTGGTTGCTATTTTGGAAACTCC  45101

Query  865    CCTTAGGGGATGCCCCTCAACTGGCCCTATAAAGGGCCAGCCTGAGCTGCAGAGGATTCC  924
              ||||||||||||||||||||||||||||||||||||||||||||||||||||||||||||
Sbjct  45100  CCTTAGGGGATGCCCCTCAACTGGCCCTATAAAGGGCCAGCCTGAGCTGCAGAGGATTCC  45041

Query  925    TGCAGAGGATCAAGACAGAAAAAGGACCTCGCACAGCCTCTCCCACAGGTACCATCAAGG  984
              |||||||||||||||||  |   |||||||||||||||||||||||||||||| ||||
Sbjct  45040  TGCAGAGGATCAAGACAGCACGTGGACCTCGCACAGCCTCTCCCACAGGTACCATGAAGG  44981

Query  985    TCTCCGC  991
              |||||||
Sbjct 44980    TCTCCGC 44974
```

Figure 86: DNA sequence of the mutated *CCL5* promoter ZEB2BOX1 and ZEB2BOX2 (top line) aligned with wild-type *CCL5* promoter sequence (bottom line) using the BLAST program.

List of References

1. Hanahan, D. and R.A. Weinberg, *The hallmarks of cancer.* Cell, 2000. **100**(1): p. 57-70.
2. Hanahan, D. and R.A. Weinberg, *Hallmarks of cancer: the next generation.* Cell, 2011. **144**(5): p. 646-74.
3. Thiery, J.P., et al., *Epithelial-mesenchymal transitions in development and disease.* Cell, 2009. **139**(5): p. 871-90.
4. Sanchez-Tillo, E., et al., *EMT-activating transcription factors in cancer: beyond EMT and tumor invasiveness.* Cell Mol Life Sci, 2012. **69**(20): p. 3429-56.
5. Graham, T.R., et al., *Insulin-like growth factor-I-dependent up-regulation of ZEB1 drives epithelial-to-mesenchymal transition in human prostate cancer cells.* Cancer Res, 2008. **68**(7): p. 2479-88.
6. Lo, H.W., et al., *Epidermal growth factor receptor cooperates with signal transducer and activator of transcription 3 to induce epithelial-mesenchymal transition in cancer cells via up-regulation of TWIST gene expression.* Cancer Res, 2007. **67**(19): p. 9066-76.
7. McCormack, N. and S. O'Dea, *Regulation of epithelial to mesenchymal transition by bone morphogenetic proteins.* Cell Signal, 2013. **25**(12): p. 2856-62.
8. Espinoza, I. and L. Miele, *Deadly crosstalk: Notch signaling at the intersection of EMT and cancer stem cells.* Cancer Lett, 2013. **341**(1): p. 41-5.
9. Katoh, Y. and M. Katoh, *FGFR2-related pathogenesis and FGFR2-targeted therapeutics (Review).* Int J Mol Med, 2009. **23**(3): p. 307-11.
10. Taipale, J. and P.A. Beachy, *The Hedgehog and Wnt signalling pathways in cancer.* Nature, 2001. **411**(6835): p. 349-54.
11. Heldin, C.H., M. Vanlandewijck, and A. Moustakas, *Regulation of EMT by TGFbeta in cancer.* FEBS Lett, 2012. **586**(14): p. 1959-70.
12. Gonzalez, D.M. and D. Medici, *Signaling mechanisms of the epithelial-mesenchymal transition.* Sci Signal, 2014. **7**(344): p. re8.
13. Moustakas, A., S. Souchelnytskyi, and C.H. Heldin, *Smad regulation in TGF-beta signal transduction.* J Cell Sci, 2001. **114**(Pt 24): p. 4359-69.
14. Arora, K. and R. Warrior, *A new Smurf in the village.* Dev Cell, 2001. **1**(4): p. 441-2.
15. Massague, J., *How cells read TGF-beta signals.* Nat Rev Mol Cell Biol, 2000. **1**(3): p. 169-78.
16. Rosenzweig, B.L., et al., *Cloning and characterization of a human type II receptor for bone morphogenetic proteins.* Proc Natl Acad Sci U S A, 1995. **92**(17): p. 7632-6.
17. Hoodless, P.A., et al., *MADR1, a MAD-related protein that functions in BMP2 signaling pathways.* Cell, 1996. **85**(4): p. 489-500.

18. Derynck, R. and Y.E. Zhang, *Smad-dependent and Smad-independent pathways in TGF-beta family signalling.* Nature, 2003. **425**(6958): p. 577-84.
19. Massague, J., *TGFbeta in Cancer.* Cell, 2008. **134**(2): p. 215-30.
20. Pardali, K. and A. Moustakas, *Actions of TGF-beta as tumor suppressor and pro-metastatic factor in human cancer.* Biochim Biophys Acta, 2007. **1775**(1): p. 21-62.
21. Jechlinger, M., et al., *Autocrine PDGFR signaling promotes mammary cancer metastasis.* J Clin Invest, 2006. **116**(6): p. 1561-70.
22. Kim, H.J., et al., *Constitutively active type I insulin-like growth factor receptor causes transformation and xenograft growth of immortalized mammary epithelial cells and is accompanied by an epithelial-to-mesenchymal transition mediated by NF-kappaB and snail.* Mol Cell Biol, 2007. **27**(8): p. 3165-75.
23. Murillo, M.M., et al., *Involvement of EGF receptor and c-Src in the survival signals induced by TGF-beta1 in hepatocytes.* Oncogene, 2005. **24**(28): p. 4580-7.
24. Lemmon, M.A. and J. Schlessinger, *Cell signaling by receptor tyrosine kinases.* Cell, 2010. **141**(7): p. 1117-34.
25. Irie, H.Y., et al., *Distinct roles of Akt1 and Akt2 in regulating cell migration and epithelial-mesenchymal transition.* J Cell Biol, 2005. **171**(6): p. 1023-34.
26. Engelman, J.A., J. Luo, and L.C. Cantley, *The evolution of phosphatidylinositol 3-kinases as regulators of growth and metabolism.* Nat Rev Genet, 2006. **7**(8): p. 606-19.
27. Vanhaesebroeck, B., et al., *The emerging mechanisms of isoform-specific PI3K signalling.* Nat Rev Mol Cell Biol, 2010. **11**(5): p. 329-41.
28. Liu, P., et al., *Targeting the phosphoinositide 3-kinase pathway in cancer.* Nat Rev Drug Discov, 2009. **8**(8): p. 627-44.
29. Khan, K.H., et al., *Targeting the PI3K-AKT-mTOR signaling network in cancer.* Chin J Cancer, 2013. **32**(5): p. 253-65.
30. Engelman, J.A., *Targeting PI3K signalling in cancer: opportunities, challenges and limitations.* Nat Rev Cancer, 2009. **9**(8): p. 550-62.
31. Kang, J.S., C. Liu, and R. Derynck, *New regulatory mechanisms of TGF-beta receptor function.* Trends Cell Biol, 2009. **19**(8): p. 385-94.
32. Yue, J. and K.M. Mulder, *Activation of the mitogen-activated protein kinase pathway by transforming growth factor-beta.* Methods Mol Biol, 2000. **142**: p. 125-31.
33. Yoon, S. and R. Seger, *The extracellular signal-regulated kinase: multiple substrates regulate diverse cellular functions.* Growth Factors, 2006. **24**(1): p. 21-44.
34. Samatar, A.A. and P.I. Poulikakos, *Targeting RAS-ERK signalling in cancer: promises and challenges.* Nat Rev Drug Discov, 2014. **13**(12): p. 928-42.

35. Yamashita, M., et al., *TRAF6 mediates Smad-independent activation of JNK and p38 by TGF-beta.* Mol Cell, 2008. **31**(6): p. 918-24.
36. Cuadrado, A. and A.R. Nebreda, *Mechanisms and functions of p38 MAPK signalling.* Biochem J, 2010. **429**(3): p. 403-17.
37. Han, J. and P. Sun, *The pathways to tumor suppression via route p38.* Trends Biochem Sci, 2007. **32**(8): p. 364-71.
38. Wagner, E.F. and A.R. Nebreda, *Signal integration by JNK and p38 MAPK pathways in cancer development.* Nat Rev Cancer, 2009. **9**(8): p. 537-49.
39. del Barco Barrantes, I. and A.R. Nebreda, *Roles of p38 MAPKs in invasion and metastasis.* Biochem Soc Trans, 2012. **40**(1): p. 79-84.
40. Fodde, R. and T. Brabletz, *Wnt/beta-catenin signaling in cancer stemness and malignant behavior.* Curr Opin Cell Biol, 2007. **19**(2): p. 150-8.
41. Jamieson, C., M. Sharma, and B.R. Henderson, *Targeting the beta-catenin nuclear transport pathway in cancer.* Semin Cancer Biol, 2014. **27**: p. 20-9.
42. Polakis, P., *Wnt signaling in cancer.* Cold Spring Harb Perspect Biol, 2012. **4**(5).
43. Sawa, H. and H.C. Korswagen, *Wnt signaling in C. elegans.* WormBook, 2013: p. 1-30.
44. Vousden, K.H. and D.P. Lane, *p53 in health and disease.* Nat Rev Mol Cell Biol, 2007. **8**(4): p. 275-83.
45. Smith, J., et al., *The ATM-Chk2 and ATR-Chk1 pathways in DNA damage signaling and cancer.* Adv Cancer Res, 2010. **108**: p. 73-112.
46. Harris, S.L. and A.J. Levine, *The p53 pathway: positive and negative feedback loops.* Oncogene, 2005. **24**(17): p. 2899-908.
47. Beckerman, R. and C. Prives, *Transcriptional regulation by p53.* Cold Spring Harb Perspect Biol, 2010. **2**(8): p. a000935.
48. Wade, M., Y.V. Wang, and G.M. Wahl, *The p53 orchestra: Mdm2 and Mdmx set the tone.* Trends Cell Biol, 2010. **20**(5): p. 299-309.
49. Kubbutat, M.H., S.N. Jones, and K.H. Vousden, *Regulation of p53 stability by Mdm2.* Nature, 1997. **387**(6630): p. 299-303.
50. Haupt, Y., et al., *Mdm2 promotes the rapid degradation of p53.* Nature, 1997. **387**(6630): p. 296-9.
51. Li, X.L., et al., *P53 mutations in colorectal cancer - molecular pathogenesis and pharmacological reactivation.* World J Gastroenterol, 2015. **21**(1): p. 84-93.
52. Meek, D.W., *Regulation of the p53 response and its relationship to cancer.* Biochem J, 2015. **469**(3): p. 325-46.
53. Brown, C.J., et al., *Awakening guardian angels: drugging the p53 pathway.* Nat Rev Cancer, 2009. **9**(12): p. 862-73.
54. Ferlay, J., D.M. Parkin, and E. Steliarova-Foucher, *Estimates of cancer incidence and mortality in Europe in 2008.* Eur J Cancer, 2010. **46**(4): p. 765-81.

55. UK, C.R., *Bowel cancer incidence statistics*

56. Jass, J.R., *Classification of colorectal cancer based on correlation of clinical, morphological and molecular features.* Histopathology, 2007. **50**(1): p. 113-30.
57. Zauber, A.G., et al., *Colonoscopic polypectomy and long-term prevention of colorectal-cancer deaths.* N Engl J Med, 2012. **366**(8): p. 687-96.
58. Stryker, S.J., et al., *Natural history of untreated colonic polyps.* Gastroenterology, 1987. **93**(5): p. 1009-13.
59. Pino, M.S. and D.C. Chung, *The chromosomal instability pathway in colon cancer.* Gastroenterology, 2010. **138**(6): p. 2059-72.
60. Davies, R.J., R. Miller, and N. Coleman, *Colorectal cancer screening: prospects for molecular stool analysis.* Nat Rev Cancer, 2005. **5**(3): p. 199-209.
61. Davis, N.C. and R.C. Newland, *Terminology and classification of colorectal adenocarcinoma: the Australian clinico-pathological staging system.* Aust N Z J Surg, 1983. **53**(3): p. 211-21.
62. Edge, S.B. and C.C. Compton, *The American Joint Committee on Cancer: the 7th edition of the AJCC cancer staging manual and the future of TNM.* Ann Surg Oncol, 2010. **17**(6): p. 1471-4.
63. Ueno, H., et al., *Optimal colorectal cancer staging criteria in TNM classification.* J Clin Oncol, 2012. **30**(13): p. 1519-26.
64. Cunningham, D., et al., *Colorectal cancer.* Lancet, 2010. **375**(9719): p. 1030-47.
65. Parkin, D.M., *1. The fraction of cancer attributable to lifestyle and environmental factors in the UK in 2010.* Br J Cancer, 2011. **105 Suppl 2**: p. S2-5.
66. Eaden, J.A., K.R. Abrams, and J.F. Mayberry, *The risk of colorectal cancer in ulcerative colitis: a meta-analysis.* Gut, 2001. **48**(4): p. 526-35.
67. Gala, M. and D.C. Chung, *Hereditary colon cancer syndromes.* Semin Oncol, 2011. **38**(4): p. 490-9.
68. Miyaki, M., et al., *Characteristics of somatic mutation of the adenomatous polyposis coli gene in colorectal tumors.* Cancer Res, 1994. **54**(11): p. 3011-20.
69. Fearon, E.R., et al., *Interleukin-2 production by tumor cells bypasses T helper function in the generation of an antitumor response.* Cell, 1990. **60**(3): p. 397-403.
70. Chung, D.C., *The genetic basis of colorectal cancer: insights into critical pathways of tumorigenesis.* Gastroenterology, 2000. **119**(3): p. 854-65.
71. Powell, S.M., et al., *APC mutations occur early during colorectal tumorigenesis.* Nature, 1992. **359**(6392): p. 235-7.

72. Kinzler, K.W. and B. Vogelstein, *Lessons from hereditary colorectal cancer.* Cell, 1996. **87**(2): p. 159-70.
73. Fearon, E.R., *Molecular genetics of colorectal cancer.* Annu Rev Pathol, 2011. **6**: p. 479-507.
74. Segditsas, S. and I. Tomlinson, *Colorectal cancer and genetic alterations in the Wnt pathway.* Oncogene, 2006. **25**(57): p. 7531-7.
75. Arber, N., et al., *Activation of c-K-ras mutations in human gastrointestinal tumors.* Gastroenterology, 2000. **118**(6): p. 1045-50.
76. Tsao, J. and D. Shibata, *Further evidence that one of the earliest alterations in colorectal carcinogenesis involves APC.* Am J Pathol, 1994. **145**(3): p. 531-4.
77. Vousden, K.H. and C. Prives, *Blinded by the Light: The Growing Complexity of p53.* Cell, 2009. **137**(3): p. 413-31.
78. Muller, P.A. and K.H. Vousden, *p53 mutations in cancer.* Nat Cell Biol, 2013. **15**(1): p. 2-8.
79. Vogelstein, B., et al., *Genetic alterations during colorectal-tumor development.* N Engl J Med, 1988. **319**(9): p. 525-32.
80. Shibata, D., et al., *Genomic instability in repeated sequences is an early somatic event in colorectal tumorigenesis that persists after transformation.* Nat Genet, 1994. **6**(3): p. 273-81.
81. Vilar, E. and S.B. Gruber, *Microsatellite instability in colorectal cancer-the stable evidence.* Nat Rev Clin Oncol, 2010. **7**(3): p. 153-62.
82. Cancer Research UK, *Bowel cancer screening*
83. Lindholm, E., H. Brevinge, and E. Haglind, *Survival benefit in a randomized clinical trial of faecal occult blood screening for colorectal cancer.* Br J Surg, 2008. **95**(8): p. 1029-36.
84. Atkin, W.S., et al., *Once-only flexible sigmoidoscopy screening in prevention of colorectal cancer: a multicentre randomised controlled trial.* Lancet, 2010. **375**(9726): p. 1624-33.
85. Newcomb, P.A., et al., *Long-term efficacy of sigmoidoscopy in the reduction of colorectal cancer incidence.* J Natl Cancer Inst, 2003. **95**(8): p. 622-5.
86. Diehl, F., et al., *Analysis of mutations in DNA isolated from plasma and stool of colorectal cancer patients.* Gastroenterology, 2008. **135**(2): p. 489-98.
87. Manfredi, S., et al., *Incidence and patterns of recurrence after resection for cure of colonic cancer in a well defined population.* Br J Surg, 2006. **93**(9): p. 1115-22.
88. Cummings, L.C., J.D. Payes, and G.S. Cooper, *Survival after hepatic resection in metastatic colorectal cancer: a population-based study.* Cancer, 2007. **109**(4): p. 718-26.
89. Taniguchi, H., et al., *Comparison in survival between hepatic metastases of gastric and colorectal cancers.* Hepatogastroenterology, 1997. **44**(15): p. 897-900.

90. Pedersen, I.K., et al., *Resection of liver metastases from colorectal cancer. Indications and results.* Dis Colon Rectum, 1994. **37**(11): p. 1078-82.
91. Edwards, M.S., et al., *A systematic review of treatment guidelines for metastatic colorectal cancer.* Colorectal Dis, 2012. **14**(2): p. e31-47.
92. Peeters, M. and T. Price, *Biologic therapies in the metastatic colorectal cancer treatment continuum--applying current evidence to clinical practice.* Cancer Treat Rev, 2012. **38**(5): p. 397-406.
93. Luu, C., et al., *Targeted therapies in colorectal cancer: surgical considerations.* J Gastrointest Oncol, 2013. **4**(3): p. 328-36.
94. Clarke, J.M. and H.I. Hurwitz, *Targeted inhibition of VEGF receptor 2: an update on ramucirumab.* Expert Opin Biol Ther, 2013. **13**(8): p. 1187-96.
95. Yap, T.A., et al., *First-in-man clinical trial of the oral pan-AKT inhibitor MK-2206 in patients with advanced solid tumors.* J Clin Oncol, 2011. **29**(35): p. 4688-95.
96. An, H.J., et al., *Adjuvant chemotherapy with or without pelvic radiotherapy after simultaneous surgical resection of rectal cancer with liver metastases: analysis of prognosis and patterns of recurrence.* Int J Radiat Oncol Biol Phys, 2012. **84**(1): p. 73-80.
97. Valastyan, S. and R.A. Weinberg, *Tumor metastasis: molecular insights and evolving paradigms.* Cell, 2011. **147**(2): p. 275-92.
98. Fidler, I.J., *The pathogenesis of cancer metastasis: the 'seed and soil' hypothesis revisited.* Nat Rev Cancer, 2003. **3**(6): p. 453-8.
99. Poste, G. and I.J. Fidler, *The pathogenesis of cancer metastasis.* Nature, 1980. **283**(5743): p. 139-46.
100. Friedl, P. and K. Wolf, *Tumour-cell invasion and migration: diversity and escape mechanisms.* Nat Rev Cancer, 2003. **3**(5): p. 362-74.
101. Tsai, J.H. and J. Yang, *Epithelial-mesenchymal plasticity in carcinoma metastasis.* Genes Dev, 2013. **27**(20): p. 2192-206.
102. Talmadge, J.E. and I.J. Fidler, *AACR centennial series: the biology of cancer metastasis: historical perspective.* Cancer Res, 2010. **70**(14): p. 5649-69.
103. Husemann, Y., et al., *Systemic spread is an early step in breast cancer.* Cancer Cell, 2008. **13**(1): p. 58-68.
104. Yoo, P.S., et al., *Liver resection for metastatic colorectal cancer in the age of neoadjuvant chemotherapy and bevacizumab.* Clin Colorectal Cancer, 2006. **6**(3): p. 202-7.
105. Gupta, G.P. and J. Massague, *Cancer metastasis: building a framework.* Cell, 2006. **127**(4): p. 679-95.
106. Steeg, P.S., *Metastasis suppressors alter the signal transduction of cancer cells.* Nat Rev Cancer, 2003. **3**(1): p. 55-63.
107. Hay, E.D., *An overview of epithelio-mesenchymal transformation.* Acta Anat (Basel), 1995. **154**(1): p. 8-20.

108. LaGamba, D., A. Nawshad, and E.D. Hay, *Microarray analysis of gene expression during epithelial-mesenchymal transformation.* Dev Dyn, 2005. **234**(1): p. 132-42.
109. Greenburg, G. and E.D. Hay, *Epithelia suspended in collagen gels can lose polarity and express characteristics of migrating mesenchymal cells.* J Cell Biol, 1982. **95**(1): p. 333-9.
110. Zeisberg, M. and E.G. Neilson, *Biomarkers for epithelial-mesenchymal transitions.* J Clin Invest, 2009. **119**(6): p. 1429-37.
111. Kalluri, R. and R.A. Weinberg, *The basics of epithelial-mesenchymal transition.* J Clin Invest, 2009. **119**(6): p. 1420-8.
112. Perez-Moreno, M., C. Jamora, and E. Fuchs, *Sticky business: orchestrating cellular signals at adherens junctions.* Cell, 2003. **112**(4): p. 535-48.
113. Kirschner, N. and J.M. Brandner, *Barriers and more: functions of tight junction proteins in the skin.* Ann N Y Acad Sci, 2012. **1257**: p. 158-66.
114. D'Hondt, C., et al., *Regulation of connexin- and pannexin-based channels by post-translational modifications.* Biol Cell, 2013.
115. Alberts, B., *Molecular biology of the cell*. 5th ed. 2008, New York ; Abingdon: Garland Science. xxxiii, 1268, [90] p.
116. Tarin, D. and C.B. Croft, *Ultrastructural features of wound healing in mouse skin.* J Anat, 1969. **105**(Pt 1): p. 189-90.
117. Kalluri, R. and M. Zeisberg, *Fibroblasts in cancer.* Nat Rev Cancer, 2006. **6**(5): p. 392-401.
118. Tomasek, J.J., et al., *Myofibroblasts and mechano-regulation of connective tissue remodelling.* Nat Rev Mol Cell Biol, 2002. **3**(5): p. 349-63.
119. Simian, M., et al., *The interplay of matrix metalloproteinases, morphogens and growth factors is necessary for branching of mammary epithelial cells.* Development, 2001. **128**(16): p. 3117-31.
120. Hay, E.D., *The mesenchymal cell, its role in the embryo, and the remarkable signaling mechanisms that create it.* Dev Dyn, 2005. **233**(3): p. 706-20.
121. Kalluri, R., *EMT: when epithelial cells decide to become mesenchymal-like cells.* J Clin Invest, 2009. **119**(6): p. 1417-9.
122. Lee, J.M., et al., *The epithelial-mesenchymal transition: new insights in signaling, development, and disease.* J Cell Biol, 2006. **172**(7): p. 973-81.
123. Jordan, N.V., G.L. Johnson, and A.N. Abell, *Tracking the intermediate stages of epithelial-mesenchymal transition in epithelial stem cells and cancer.* Cell Cycle, 2011. **10**(17): p. 2865-73.
124. Chao, Y., et al., *Partial mesenchymal to epithelial reverting transition in breast and prostate cancer metastases.* Cancer Microenviron, 2012. **5**(1): p. 19-28.

125. Futterman, M.A., A.J. Garcia, and E.A. Zamir, *Evidence for partial epithelial-to-mesenchymal transition (pEMT) and recruitment of motile blastoderm edge cells during avian epiboly.* Dev Dyn, 2011. **240**(6): p. 1502-11.
126. Jolly, M.K., et al., *Implications of the Hybrid Epithelial/Mesenchymal Phenotype in Metastasis.* Front Oncol, 2015. **5**: p. 155.
127. Grande, M.T., et al., *Snail1-induced partial epithelial-to-mesenchymal transition drives renal fibrosis in mice and can be targeted to reverse established disease.* Nat Med, 2015. **21**(9): p. 989-97.
128. Huang, R.Y., et al., *An EMT spectrum defines an anoikis-resistant and spheroidogenic intermediate mesenchymal state that is sensitive to e-cadherin restoration by a src-kinase inhibitor, saracatinib (AZD0530).* Cell Death Dis, 2013. **4**: p. e915.
129. Sarrio, D., et al., *Epithelial and mesenchymal subpopulations within normal basal breast cell lines exhibit distinct stem cell/progenitor properties.* Stem Cells, 2012. **30**(2): p. 292-303.
130. Ribeiro, A.S. and J. Paredes, *P-Cadherin Linking Breast Cancer Stem Cells and Invasion: A Promising Marker to Identify an "Intermediate/Metastable" EMT State.* Front Oncol, 2014. **4**: p. 371.
131. Perl, A.K., et al., *A causal role for E-cadherin in the transition from adenoma to carcinoma.* Nature, 1998. **392**(6672): p. 190-3.
132. Comijn, J., et al., *The two-handed E box binding zinc finger protein SIP1 downregulates E-cadherin and induces invasion.* Mol Cell, 2001. **7**(6): p. 1267-78.
133. Wells, A., C. Yates, and C.R. Shepard, *E-cadherin as an indicator of mesenchymal to epithelial reverting transitions during the metastatic seeding of disseminated carcinomas.* Clin Exp Metastasis, 2008. **25**(6): p. 621-8.
134. Chao, Y.L., C.R. Shepard, and A. Wells, *Breast carcinoma cells re-express E-cadherin during mesenchymal to epithelial reverting transition.* Mol Cancer, 2010. **9**: p. 179.
135. Chao, Y., et al., *Hepatocyte induced re-expression of E-cadherin in breast and prostate cancer cells increases chemoresistance.* Clin Exp Metastasis, 2012. **29**(1): p. 39-50.
136. Wendt, M.K., et al., *Down-regulation of epithelial cadherin is required to initiate metastatic outgrowth of breast cancer.* Mol Biol Cell, 2011. **22**(14): p. 2423-35.
137. Stevenson, B.R., et al., *Identification of ZO-1: a high molecular weight polypeptide associated with the tight junction (zonula occludens) in a variety of epithelia.* J Cell Biol, 1986. **103**(3): p. 755-66.
138. Van Itallie, C.M., et al., *ZO-1 stabilizes the tight junction solute barrier through coupling to the perijunctional cytoskeleton.* Mol Biol Cell, 2009. **20**(17): p. 3930-40.

139. Anderson, J.M., et al., *Characterization of ZO-1, a protein component of the tight junction from mouse liver and Madin-Darby canine kidney cells.* J Cell Biol, 1988. **106**(4): p. 1141-9.
140. Lahsnig, C., et al., *ILEI requires oncogenic Ras for the epithelial to mesenchymal transition of hepatocytes and liver carcinoma progression.* Oncogene, 2009. **28**(5): p. 638-50.
141. Shinto, O., et al., *Inhibitory effect of a TGFbeta receptor type-I inhibitor, Ki26894, on invasiveness of scirrhous gastric cancer cells.* Br J Cancer, 2010. **102**(5): p. 844-51.
142. Soini, Y., *Tight junctions in lung cancer and lung metastasis: a review.* Int J Clin Exp Pathol, 2012. **5**(2): p. 126-36.
143. Wang, H., et al., *Epithelial-mesenchymal transition (EMT) induced by TNF-alpha requires AKT/GSK-3beta-mediated stabilization of snail in colorectal cancer.* PLoS One, 2013. **8**(2): p. e56664.
144. Hynes, R.O., *Integrins: versatility, modulation, and signaling in cell adhesion.* Cell, 1992. **69**(1): p. 11-25.
145. Bates, R.C., et al., *Transcriptional activation of integrin beta6 during the epithelial-mesenchymal transition defines a novel prognostic indicator of aggressive colon carcinoma.* J Clin Invest, 2005. **115**(2): p. 339-47.
146. Bates, R.C. and A.M. Mercurio, *The epithelial-mesenchymal transition (EMT) and colorectal cancer progression.* Cancer Biol Ther, 2005. **4**(4): p. 365-70.
147. Strutz, F., et al., *Identification and characterization of a fibroblast marker: FSP1.* J Cell Biol, 1995. **130**(2): p. 393-405.
148. Ebralidze, A., et al., *Isolation and characterization of a gene specifically expressed in different metastatic cells and whose deduced gene product has a high degree of homology to a Ca2+-binding protein family.* Genes Dev, 1989. **3**(7): p. 1086-93.
149. Okada, H., et al., *Early role of Fsp1 in epithelial-mesenchymal transformation.* Am J Physiol, 1997. **273**(4 Pt 2): p. F563-74.
150. Xue, C., et al., *The gatekeeper effect of epithelial-mesenchymal transition regulates the frequency of breast cancer metastasis.* Cancer Res, 2003. **63**(12): p. 3386-94.
151. Dellagi, K., et al., *Alteration of vimentin intermediate filament expression during differentiation of human hemopoietic cells.* EMBO J, 1983. **2**(9): p. 1509-14.
152. Cochard, P. and D. Paulin, *Initial expression of neurofilaments and vimentin in the central and peripheral nervous system of the mouse embryo in vivo.* J Neurosci, 1984. **4**(8): p. 2080-94.
153. Satelli, A. and S. Li, *Vimentin in cancer and its potential as a molecular target for cancer therapy.* Cell Mol Life Sci, 2011. **68**(18): p. 3033-46.
154. Raymond, W.A. and A.S. Leong, *Vimentin--a new prognostic parameter in breast carcinoma?* J Pathol, 1989. **158**(2): p. 107-14.

155. Reis-Filho, J.S., *Re: Korsching et al. The origin of vimentin expression in invasive breast cancer: epithelial-mesenchymal transition, myoepithelial histogenesis or histogenesis from progenitor cells with bilinear differentiation potential? J Pathol 2005; 206: 451-457.* J Pathol, 2005. **207**(3): p. 367-9; author reply 370-1.
156. Sethi, S., et al., *Molecular signature of epithelial-mesenchymal transition (EMT) in human prostate cancer bone metastasis.* Am J Transl Res, 2010. **3**(1): p. 90-9.
157. Hu, L., et al., *Association of Vimentin overexpression and hepatocellular carcinoma metastasis.* Oncogene, 2004. **23**(1): p. 298-302.
158. Al-Saad, S., et al., *The prognostic impact of NF-kappaB p105, vimentin, E-cadherin and Par6 expression in epithelial and stromal compartment in non-small-cell lung cancer.* Br J Cancer, 2008. **99**(9): p. 1476-83.
159. Thiery, J.P., *Epithelial-mesenchymal transitions in tumour progression.* Nat Rev Cancer, 2002. **2**(6): p. 442-54.
160. Hinz, B. and G. Gabbiani, *Mechanisms of force generation and transmission by myofibroblasts.* Curr Opin Biotechnol, 2003. **14**(5): p. 538-46.
161. Wang, J., R. Zohar, and C.A. McCulloch, *Multiple roles of alpha-smooth muscle actin in mechanotransduction.* Exp Cell Res, 2006. **312**(3): p. 205-14.
162. Theriault, B.L., et al., *BMP4 induces EMT and Rho GTPase activation in human ovarian cancer cells.* Carcinogenesis, 2007. **28**(6): p. 1153-62.
163. Rees, J.R., et al., *In vivo and in vitro evidence for transforming growth factor-beta1-mediated epithelial to mesenchymal transition in esophageal adenocarcinoma.* Cancer Res, 2006. **66**(19): p. 9583-90.
164. Karagiannis, G.S., et al., *Enrichment map profiling of the cancer invasion front suggests regulation of colorectal cancer progression by the bone morphogenetic protein antagonist, gremlin-1.* Mol Oncol, 2013. **7**(4): p. 826-39.
165. Qian, Y.R., et al., *Angiotensin-converting enzyme 2 attenuates the metastasis of non-small cell lung cancer through inhibition of epithelial-mesenchymal transition.* Oncol Rep, 2013. **29**(6): p. 2408-14.
166. Park, J. and J.E. Schwarzbauer, *Mammary epithelial cell interactions with fibronectin stimulate epithelial-mesenchymal transition.* Oncogene, 2013.
167. Sarrio, D., et al., *Epithelial-mesenchymal transition in breast cancer relates to the basal-like phenotype.* Cancer Res, 2008. **68**(4): p. 989-97.
168. Valenta, T., G. Hausmann, and K. Basler, *The many faces and functions of beta-catenin.* EMBO J, 2012. **31**(12): p. 2714-36.
169. Gavert, N. and A. Ben-Ze'ev, *beta-Catenin signaling in biological control and cancer.* J Cell Biochem, 2007. **102**(4): p. 820-8.

170. Heuberger, J. and W. Birchmeier, *Interplay of cadherin-mediated cell adhesion and canonical Wnt signaling.* Cold Spring Harb Perspect Biol, 2010. **2**(2): p. a002915.
171. Medici, D., E.D. Hay, and D.A. Goodenough, *Cooperation between snail and LEF-1 transcription factors is essential for TGF-beta1-induced epithelial-mesenchymal transition.* Mol Biol Cell, 2006. **17**(4): p. 1871-9.
172. Brabletz, T., et al., *Nuclear overexpression of the oncoprotein beta-catenin in colorectal cancer is localized predominantly at the invasion front.* Pathol Res Pract, 1998. **194**(10): p. 701-4.
173. Ansieau, S., et al., *TWISTing an embryonic transcription factor into an oncoprotein.* Oncogene, 2010. **29**(22): p. 3173-84.
174. Conacci-Sorrell, M., et al., *Autoregulation of E-cadherin expression by cadherin-cadherin interactions: the roles of beta-catenin signaling, Slug, and MAPK.* J Cell Biol, 2003. **163**(4): p. 847-57.
175. Sanchez-Tillo, E., et al., *beta-catenin/TCF4 complex induces the epithelial-to-mesenchymal transition (EMT)-activator ZEB1 to regulate tumor invasiveness.* Proc Natl Acad Sci U S A, 2011. **108**(48): p. 19204-9.
176. Pan, X., R.P. Hobbs, and P.A. Coulombe, *The expanding significance of keratin intermediate filaments in normal and diseased epithelia.* Curr Opin Cell Biol, 2013. **25**(1): p. 47-56.
177. Haines, R.L. and E.B. Lane, *Keratins and disease at a glance.* J Cell Sci, 2012. **125**(Pt 17): p. 3923-8.
178. Homberg, M. and T.M. Magin, *Beyond expectations: novel insights into epidermal keratin function and regulation.* Int Rev Cell Mol Biol, 2014. **311**: p. 265-306.
179. Toivola, D.M., et al., *Keratins in health and disease.* Curr Opin Cell Biol, 2015. **32**: p. 73-81.
180. Fuchs, E. and H. Green, *Changes in keratin gene expression during terminal differentiation of the keratinocyte.* Cell, 1980. **19**(4): p. 1033-42.
181. Khan, F.M., et al., *Keratin 19 demonstration of canal of Hering loss in primary biliary cirrhosis: "minimal change PBC"?* Hepatology, 2013. **57**(2): p. 700-7.
182. Bayrak, R., S. Yenidunya, and H. Haltas, *Cytokeratin 7 and cytokeratin 20 expression in colorectal adenocarcinomas.* Pathol Res Pract, 2011. **207**(3): p. 156-60.
183. Gurzu, S. and I. Jung, *Aberrant pattern of the cytokeratin 7/cytokeratin 20 immunophenotype in colorectal adenocarcinomas with BRAF mutations.* Pathol Res Pract, 2012. **208**(3): p. 163-6.
184. Yamagishi, H., et al., *Aberrant cytokeratin expression as a possible prognostic predictor in poorly differentiated colorectal carcinoma.* J Gastroenterol Hepatol, 2013. **28**(12): p. 1815-22.

185. Fortier, A.M., E. Asselin, and M. Cadrin, *Keratin 8 and 18 loss in epithelial cancer cells increases collective cell migration and cisplatin sensitivity through claudin1 up-regulation.* J Biol Chem, 2013. **288**(16): p. 11555-71.
186. Dominguez, R. and K.C. Holmes, *Actin structure and function.* Annu Rev Biophys, 2011. **40**: p. 169-86.
187. O'Connell, C.B., M.J. Tyska, and M.S. Mooseker, *Myosin at work: motor adaptations for a variety of cellular functions.* Biochim Biophys Acta, 2007. **1773**(5): p. 615-30.
188. Tsujita, K. and T. Itoh, *Phosphoinositides in the regulation of actin cortex and cell migration.* Biochim Biophys Acta, 2015. **1851**(6): p. 824-31.
189. Jaffe, A.B. and A. Hall, *Rho GTPases: biochemistry and biology.* Annu Rev Cell Dev Biol, 2005. **21**: p. 247-69.
190. Steffen, A., et al., *Filopodia formation in the absence of functional WAVE- and Arp2/3-complexes.* Mol Biol Cell, 2006. **17**(6): p. 2581-91.
191. Wang, W., R. Eddy, and J. Condeelis, *The cofilin pathway in breast cancer invasion and metastasis.* Nat Rev Cancer, 2007. **7**(6): p. 429-40.
192. Frugtniet, B., W.G. Jiang, and T.A. Martin, *Role of the WASP and WAVE family proteins in breast cancer invasion and metastasis.* Breast Cancer (Dove Med Press), 2015. **7**: p. 99-109.
193. Wang, W., et al., *The activity status of cofilin is directly related to invasion, intravasation, and metastasis of mammary tumors.* J Cell Biol, 2006. **173**(3): p. 395-404.
194. Gross, S.R., *Actin binding proteins: their ups and downs in metastatic life.* Cell Adh Migr, 2013. **7**(2): p. 199-213.
195. Li, A., et al., *Fascin is regulated by slug, promotes progression of pancreatic cancer in mice, and is associated with patient outcomes.* Gastroenterology, 2014. **146**(5): p. 1386-96.e1-17.
196. Aokage, K., et al., *Dynamic molecular changes associated with epithelial-mesenchymal transition and subsequent mesenchymal-epithelial transition in the early phase of metastatic tumor formation.* Int J Cancer, 2011. **128**(7): p. 1585-95.
197. Chiquet-Ehrismann, R. and R.P. Tucker, *Tenascins and the importance of adhesion modulation.* Cold Spring Harb Perspect Biol, 2011. **3**(5).
198. Sun, X.J., et al., *The EDA-containing cellular fibronectin induces epithelial mesenchymal transition in lung cancer cells through integrin alpha9beta1-mediated activation of PI3-K /Akt and Erk1/2.* Carcinogenesis, 2013.
199. Cheng, J.C. and P.C. Leung, *Type I collagen down-regulates E-cadherin expression by increasing PI3KCA in cancer cells.* Cancer Lett, 2011. **304**(2): p. 107-16.
200. Espinosa Neira, R. and E.P. Salazar, *Native type IV collagen induces an epithelial to mesenchymal transition-like process in mammary*

epithelial cells MCF10A. Int J Biochem Cell Biol, 2012. **44**(12): p. 2194-203.
201. Colognato, H. and P.D. Yurchenco, *Form and function: the laminin family of heterotrimers.* Dev Dyn, 2000. **218**(2): p. 213-34.
202. Giannelli, G., et al., *Laminin-5 with transforming growth factor-beta1 induces epithelial to mesenchymal transition in hepatocellular carcinoma.* Gastroenterology, 2005. **129**(5): p. 1375-83.
203. Carpenter, P.M., et al., *Motility induction in breast carcinoma by mammary epithelial laminin 332 (laminin 5).* Mol Cancer Res, 2009. **7**(4): p. 462-75.
204. Carpenter, P.M., et al., *Laminin 5 expression in metaplastic breast carcinomas.* Am J Surg Pathol, 2008. **32**(3): p. 345-53.
205. Hamasaki, H., et al., *Expression of laminin 5-gamma2 chain in cutaneous squamous cell carcinoma and its role in tumour invasion.* Br J Cancer, 2011. **105**(6): p. 824-32.
206. Marinkovich, M.P., *Tumour microenvironment: laminin 332 in squamous-cell carcinoma.* Nat Rev Cancer, 2007. **7**(5): p. 370-80.
207. Gasparoni, A., et al., *Prognostic value of differential expression of Laminin-5 gamma2 in oral squamous cell carcinomas: correlation with survival.* Oncol Rep, 2007. **18**(4): p. 793-800.
208. Nawshad, A. and E.D. Hay, *TGFbeta3 signaling activates transcription of the LEF1 gene to induce epithelial mesenchymal transformation during mouse palate development.* J Cell Biol, 2003. **163**(6): p. 1291-301.
209. Yang, J., et al., *Twist, a master regulator of morphogenesis, plays an essential role in tumor metastasis.* Cell, 2004. **117**(7): p. 927-39.
210. Batlle, E., et al., *The transcription factor snail is a repressor of E-cadherin gene expression in epithelial tumour cells.* Nat Cell Biol, 2000. **2**(2): p. 84-9.
211. Aigner, K., et al., *The transcription factor ZEB1 (deltaEF1) promotes tumour cell dedifferentiation by repressing master regulators of epithelial polarity.* Oncogene, 2007. **26**(49): p. 6979-88.
212. Gheldof, A., et al., *Evolutionary functional analysis and molecular regulation of the ZEB transcription factors.* Cell Mol Life Sci, 2012. **69**(15): p. 2527-41.
213. Wakamatsu, N., et al., *Mutations in SIP1, encoding Smad interacting protein-1, cause a form of Hirschsprung disease.* Nat Genet, 2001. **27**(4): p. 369-70.
214. Eger, A., et al., *DeltaEF1 is a transcriptional repressor of E-cadherin and regulates epithelial plasticity in breast cancer cells.* Oncogene, 2005. **24**(14): p. 2375-85.
215. Spaderna, S., et al., *The transcriptional repressor ZEB1 promotes metastasis and loss of cell polarity in cancer.* Cancer Res, 2008. **68**(2): p. 537-44.

216. Vandewalle, C., et al., *SIP1/ZEB2 induces EMT by repressing genes of different epithelial cell-cell junctions.* Nucleic Acids Res, 2005. **33**(20): p. 6566-78.
217. Vandewalle, C., F. Van Roy, and G. Berx, *The role of the ZEB family of transcription factors in development and disease.* Cell Mol Life Sci, 2009. **66**(5): p. 773-87.
218. Bindels, S., et al., *Regulation of vimentin by SIP1 in human epithelial breast tumor cells.* Oncogene, 2006. **25**(36): p. 4975-85.
219. Tatari, M.N., et al., *ZEB2-transgene expression in the epidermis compromises the integrity of the epidermal barrier through the repression of different tight junction proteins.* Cell Mol Life Sci, 2014. **71**(18): p. 3599-609.
220. Sayan, A.E., et al., *SIP1 protein protects cells from DNA damage-induced apoptosis and has independent prognostic value in bladder cancer.* Proc Natl Acad Sci U S A, 2009. **106**(35): p. 14884-9.
221. Okugawa, Y., et al., *Clinical significance of Zinc finger E-box Binding homeobox 1 (ZEB1) in human gastric cancer.* J Surg Oncol, 2012. **106**(3): p. 280-5.
222. Cai, M.Y., et al., *Overexpression of ZEB2 in peritumoral liver tissue correlates with favorable survival after curative resection of hepatocellular carcinoma.* PLoS One, 2012. **7**(2): p. e32838.
223. Kurahara, H., et al., *Epithelial-mesenchymal transition and mesenchymal-epithelial transition via regulation of ZEB-1 and ZEB-2 expression in pancreatic cancer.* J Surg Oncol, 2012. **105**(7): p. 655-61.
224. Hajra, K.M., D.Y. Chen, and E.R. Fearon, *The SLUG zinc-finger protein represses E-cadherin in breast cancer.* Cancer Res, 2002. **62**(6): p. 1613-8.
225. Zhou, B.P., et al., *Dual regulation of Snail by GSK-3beta-mediated phosphorylation in control of epithelial-mesenchymal transition.* Nat Cell Biol, 2004. **6**(10): p. 931-40.
226. Yook, J.I., et al., *A Wnt-Axin2-GSK3beta cascade regulates Snail1 activity in breast cancer cells.* Nat Cell Biol, 2006. **8**(12): p. 1398-406.
227. Thuault, S., et al., *HMGA2 and Smads co-regulate SNAIL1 expression during induction of epithelial-to-mesenchymal transition.* J Biol Chem, 2008. **283**(48): p. 33437-46.
228. Merikallio, H., et al., *Snail promotes an invasive phenotype in lung carcinoma.* Respir Res, 2012. **13**: p. 104.
229. Shioiri, M., et al., *Slug expression is an independent prognostic parameter for poor survival in colorectal carcinoma patients.* Br J Cancer, 2006. **94**(12): p. 1816-22.
230. Shin, N.R., et al., *Overexpression of Snail is associated with lymph node metastasis and poor prognosis in patients with gastric cancer.* BMC Cancer, 2012. **12**: p. 521.

231. Kosaka, T., et al., *Expression of snail in upper urinary tract urothelial carcinoma: prognostic significance and implications for tumor invasion.* Clin Cancer Res, 2010. **16**(23): p. 5814-23.
232. Blechschmidt, K., et al., *The E-cadherin repressor Snail is associated with lower overall survival of ovarian cancer patients.* Br J Cancer, 2008. **98**(2): p. 489-95.
233. Moody, S.E., et al., *The transcriptional repressor Snail promotes mammary tumor recurrence.* Cancer Cell, 2005. **8**(3): p. 197-209.
234. Uchikado, Y., et al., *Slug Expression in the E-cadherin preserved tumors is related to prognosis in patients with esophageal squamous cell carcinoma.* Clin Cancer Res, 2005. **11**(3): p. 1174-80.
235. Sugimachi, K., et al., *Transcriptional repressor snail and progression of human hepatocellular carcinoma.* Clin Cancer Res, 2003. **9**(7): p. 2657-64.
236. Franco, H.L., et al., *Redundant or separate entities?--roles of Twist1 and Twist2 as molecular switches during gene transcription.* Nucleic Acids Res, 2011. **39**(4): p. 1177-86.
237. Alexander, N.R., et al., *N-cadherin gene expression in prostate carcinoma is modulated by integrin-dependent nuclear translocation of Twist1.* Cancer Res, 2006. **66**(7): p. 3365-9.
238. Casas, E., et al., *Snail2 is an essential mediator of Twist1-induced epithelial mesenchymal transition and metastasis.* Cancer Res, 2011. **71**(1): p. 245-54.
239. Niu, R.F., et al., *Up-regulation of Twist induces angiogenesis and correlates with metastasis in hepatocellular carcinoma.* J Exp Clin Cancer Res, 2007. **26**(3): p. 385-94.
240. Yang, M.H., et al., *Direct regulation of TWIST by HIF-1alpha promotes metastasis.* Nat Cell Biol, 2008. **10**(3): p. 295-305.
241. Tran, D.D., et al., *Temporal and spatial cooperation of Snail1 and Twist1 during epithelial-mesenchymal transition predicts for human breast cancer recurrence.* Mol Cancer Res, 2011. **9**(12): p. 1644-57.
242. Terauchi, M., et al., *Possible involvement of TWIST in enhanced peritoneal metastasis of epithelial ovarian carcinoma.* Clin Exp Metastasis, 2007. **24**(5): p. 329-39.
243. Song, L.B., et al., *The clinical significance of twist expression in nasopharyngeal carcinoma.* Cancer Lett, 2006. **242**(2): p. 258-65.
244. Sasaki, K., et al., *Significance of Twist expression and its association with E-cadherin in esophageal squamous cell carcinoma.* J Exp Clin Cancer Res, 2009. **28**: p. 158.
245. Xie, F., K. Li, and X. Ouyang, *Twist, an independent prognostic marker for predicting distant metastasis and survival rates of esophageal squamous cell carcinoma patients.* Clin Exp Metastasis, 2009. **26**(8): p. 1025-32.

246. Kajiyama, H., et al., *Twist expression predicts poor clinical outcome of patients with clear cell carcinoma of the ovary.* Oncology, 2006. **71**(5-6): p. 394-401.
247. Kim, K., Z. Lu, and E.D. Hay, *Direct evidence for a role of beta-catenin/LEF-1 signaling pathway in induction of EMT.* Cell Biol Int, 2002. **26**(5): p. 463-76.
248. Nawshad, A., et al., *TGFbeta3 inhibits E-cadherin gene expression in palate medial-edge epithelial cells through a Smad2-Smad4-LEF1 transcription complex.* J Cell Sci, 2007. **120**(Pt 9): p. 1646-53.
249. Lamouille, S., et al., *Regulation of epithelial-mesenchymal and mesenchymal-epithelial transitions by microRNAs.* Curr Opin Cell Biol, 2013. **25**(2): p. 200-7.
250. Brabletz, S. and T. Brabletz, *The ZEB/miR-200 feedback loop--a motor of cellular plasticity in development and cancer?* EMBO Rep, 2010. **11**(9): p. 670-7.
251. Bracken, C.P., et al., *A double-negative feedback loop between ZEB1-SIP1 and the microRNA-200 family regulates epithelial-mesenchymal transition.* Cancer Res, 2008. **68**(19): p. 7846-54.
252. Park, S.M., et al., *The miR-200 family determines the epithelial phenotype of cancer cells by targeting the E-cadherin repressors ZEB1 and ZEB2.* Genes Dev, 2008. **22**(7): p. 894-907.
253. Ru, P., et al., *miRNA-29b suppresses prostate cancer metastasis by regulating epithelial-mesenchymal transition signaling.* Mol Cancer Ther, 2012. **11**(5): p. 1166-73.
254. Lindsey, S. and S.A. Langhans, *Crosstalk of Oncogenic Signaling Pathways during Epithelial-Mesenchymal Transition.* Front Oncol, 2014. **4**: p. 358.
255. Reinhold, W.C., et al., *Multifactorial regulation of E-cadherin expression: an integrative study.* Mol Cancer Ther, 2010. **9**(1): p. 1-16.
256. Wels, C., et al., *Transcriptional activation of ZEB1 by Slug leads to cooperative regulation of the epithelial-mesenchymal transition-like phenotype in melanoma.* J Invest Dermatol, 2011. **131**(9): p. 1877-85.
257. Dave, N., et al., *Functional cooperation between Snail1 and twist in the regulation of ZEB1 expression during epithelial to mesenchymal transition.* J Biol Chem, 2011. **286**(14): p. 12024-32.
258. Solnica-Krezel, L., *Conserved patterns of cell movements during vertebrate gastrulation.* Curr Biol, 2005. **15**(6): p. R213-28.
259. Tucker, R.P., *Neural crest cells: a model for invasive behavior.* Int J Biochem Cell Biol, 2004. **36**(2): p. 173-7.
260. Mercado-Pimentel, M.E. and R.B. Runyan, *Multiple transforming growth factor-beta isoforms and receptors function during epithelial-mesenchymal cell transformation in the embryonic heart.* Cells Tissues Organs, 2007. **185**(1-3): p. 146-56.

261. Ciruna, B. and J. Rossant, *FGF signaling regulates mesoderm cell fate specification and morphogenetic movement at the primitive streak.* Dev Cell, 2001. **1**(1): p. 37-49.
262. Micalizzi, D.S., S.M. Farabaugh, and H.L. Ford, *Epithelial-mesenchymal transition in cancer: parallels between normal development and tumor progression.* J Mammary Gland Biol Neoplasia, 2010. **15**(2): p. 117-34.
263. Cheung, M., et al., *The transcriptional control of trunk neural crest induction, survival, and delamination.* Dev Cell, 2005. **8**(2): p. 179-92.
264. Skromne, I. and C.D. Stern, *Interactions between Wnt and Vg1 signalling pathways initiate primitive streak formation in the chick embryo.* Development, 2001. **128**(15): p. 2915-27.
265. Sanchez-Martin, M., et al., *Deletion of the SLUG (SNAI2) gene results in human piebaldism.* Am J Med Genet A, 2003. **122A**(2): p. 125-32.
266. Perez-Mancera, P.A., et al., *SLUG in cancer development.* Oncogene, 2005. **24**(19): p. 3073-82.
267. Sanchez-Martin, M., et al., *SLUG (SNAI2) deletions in patients with Waardenburg disease.* Hum Mol Genet, 2002. **11**(25): p. 3231-6.
268. Inai, K., et al., *BMP-2 induces cell migration and periostin expression during atrioventricular valvulogenesis.* Dev Biol, 2008. **315**(2): p. 383-96.
269. Liebner, S., et al., *Beta-catenin is required for endothelial-mesenchymal transformation during heart cushion development in the mouse.* J Cell Biol, 2004. **166**(3): p. 359-67.
270. Azhar, M., et al., *Transforming growth factor beta in cardiovascular development and function.* Cytokine Growth Factor Rev, 2003. **14**(5): p. 391-407.
271. Romano, L.A. and R.B. Runyan, *Slug is an essential target of TGFbeta2 signaling in the developing chicken heart.* Dev Biol, 2000. **223**(1): p. 91-102.
272. Scanlon, C.S., et al., *Biomarkers of epithelial-mesenchymal transition in squamous cell carcinoma.* J Dent Res, 2013. **92**(2): p. 114-21.
273. Strutz, F., et al., *Role of basic fibroblast growth factor-2 in epithelial-mesenchymal transformation.* Kidney Int, 2002. **61**(5): p. 1714-28.
274. Iwano, M., et al., *Evidence that fibroblasts derive from epithelium during tissue fibrosis.* J Clin Invest, 2002. **110**(3): p. 341-50.
275. Boutet, A., et al., *Snail activation disrupts tissue homeostasis and induces fibrosis in the adult kidney.* EMBO J, 2006. **25**(23): p. 5603-13.
276. Rastaldi, M.P., et al., *Epithelial-mesenchymal transition of tubular epithelial cells in human renal biopsies.* Kidney Int, 2002. **62**(1): p. 137-46.
277. Bataille, F., et al., *Evidence for a role of epithelial mesenchymal transition during pathogenesis of fistulae in Crohn's disease.* Inflamm Bowel Dis, 2008. **14**(11): p. 1514-27.

278. Brabletz, T., et al., *Variable beta-catenin expression in colorectal cancers indicates tumor progression driven by the tumor environment.* Proc Natl Acad Sci U S A, 2001. **98**(18): p. 10356-61.
279. Nieto, M.A., *The ins and outs of the epithelial to mesenchymal transition in health and disease.* Annu Rev Cell Dev Biol, 2011. **27**: p. 347-76.
280. Yilmaz, M. and G. Christofori, *EMT, the cytoskeleton, and cancer cell invasion.* Cancer Metastasis Rev, 2009. **28**(1-2): p. 15-33.
281. Huber, M.A., N. Kraut, and H. Beug, *Molecular requirements for epithelial-mesenchymal transition during tumor progression.* Curr Opin Cell Biol, 2005. **17**(5): p. 548-58.
282. Grunert, S., M. Jechlinger, and H. Beug, *Diverse cellular and molecular mechanisms contribute to epithelial plasticity and metastasis.* Nat Rev Mol Cell Biol, 2003. **4**(8): p. 657-65.
283. Larue, L. and A. Bellacosa, *Epithelial-mesenchymal transition in development and cancer: role of phosphatidylinositol 3' kinase/AKT pathways.* Oncogene, 2005. **24**(50): p. 7443-54.
284. Mani, S.A., et al., *The epithelial-mesenchymal transition generates cells with properties of stem cells.* Cell, 2008. **133**(4): p. 704-15.
285. Kudo-Saito, C., et al., *Cancer metastasis is accelerated through immunosuppression during Snail-induced EMT of cancer cells.* Cancer Cell, 2009. **15**(3): p. 195-206.
286. Spano, D. and M. Zollo, *Tumor microenvironment: a main actor in the metastasis process.* Clin Exp Metastasis, 2012. **29**(4): p. 381-95.
287. Catalano, V., et al., *Tumor and its microenvironment: a synergistic interplay.* Semin Cancer Biol, 2013. **23**(6 Pt B): p. 522-32.
288. Whiteside, T.L., *The tumor microenvironment and its role in promoting tumor growth.* Oncogene, 2008. **27**(45): p. 5904-12.
289. Watnick, R.S., *The role of the tumor microenvironment in regulating angiogenesis.* Cold Spring Harb Perspect Med, 2012. **2**(12): p. a006676.
290. Funasaka, T. and A. Raz, *The role of autocrine motility factor in tumor and tumor microenvironment.* Cancer Metastasis Rev, 2007. **26**(3-4): p. 725-35.
291. Lin, Q. and Z. Yun, *Impact of the hypoxic tumor microenvironment on the regulation of cancer stem cell characteristics.* Cancer Biol Ther, 2010. **9**(12): p. 949-56.
292. Tredan, O., et al., *Drug resistance and the solid tumor microenvironment.* J Natl Cancer Inst, 2007. **99**(19): p. 1441-54.
293. Lee, E., N.B. Pandey, and A.S. Popel, *Crosstalk between cancer cells and blood endothelial and lymphatic endothelial cells in tumour and organ microenvironment.* Expert Rev Mol Med, 2015. **17**: p. e3.
294. Bhome, R., et al., *A top-down view of the tumor microenvironment: structure, cells and signaling.* Front Cell Dev Biol, 2015. **3**: p. 33.

295. Upreti, M., A. Jyoti, and P. Sethi, *Tumor microenvironment and nanotherapeutics.* Transl Cancer Res, 2013. **2**(4): p. 309-319.
296. Marsh, T., K. Pietras, and S.S. McAllister, *Fibroblasts as architects of cancer pathogenesis.* Biochim Biophys Acta, 2013. **1832**(7): p. 1070-8.
297. Orimo, A., et al., *Stromal fibroblasts present in invasive human breast carcinomas promote tumor growth and angiogenesis through elevated SDF-1/CXCL12 secretion.* Cell, 2005. **121**(3): p. 335-48.
298. Kikuchi, Y., et al., *Periostin is expressed in pericryptal fibroblasts and cancer-associated fibroblasts in the colon.* J Histochem Cytochem, 2008. **56**(8): p. 753-64.
299. De Wever, O., et al., *Tenascin-C and SF/HGF produced by myofibroblasts in vitro provide convergent pro-invasive signals to human colon cancer cells through RhoA and Rac.* Faseb j, 2004. **18**(9): p. 1016-8.
300. Allen, E., I.B. Walters, and D. Hanahan, *Brivanib, a dual FGF/VEGF inhibitor, is active both first and second line against mouse pancreatic neuroendocrine tumors developing adaptive/evasive resistance to VEGF inhibition.* Clin Cancer Res, 2011. **17**(16): p. 5299-310.
301. Yu, Y., et al., *Cancer-associated fibroblasts induce epithelial-mesenchymal transition of breast cancer cells through paracrine TGF-beta signalling.* Br J Cancer, 2014. **110**(3): p. 724-32.
302. Zhou, B., et al., *A role for cancer-associated fibroblasts in inducing the epithelial-to-mesenchymal transition in human tongue squamous cell carcinoma.* J Oral Pathol Med, 2014. **43**(8): p. 585-92.
303. Giannoni, E., et al., *Reciprocal activation of prostate cancer cells and cancer-associated fibroblasts stimulates epithelial-mesenchymal transition and cancer stemness.* Cancer Res, 2010. **70**(17): p. 6945-56.
304. Dominici, M., et al., *Minimal criteria for defining multipotent mesenchymal stromal cells. The International Society for Cellular Therapy position statement.* Cytotherapy, 2006. **8**(4): p. 315-7.
305. Quante, M., et al., *Bone marrow-derived myofibroblasts contribute to the mesenchymal stem cell niche and promote tumor growth.* Cancer Cell, 2011. **19**(2): p. 257-72.
306. Mishra, P.J., et al., *Carcinoma-associated fibroblast-like differentiation of human mesenchymal stem cells.* Cancer Res, 2008. **68**(11): p. 4331-9.
307. Karnoub, A.E., et al., *Mesenchymal stem cells within tumour stroma promote breast cancer metastasis.* Nature, 2007. **449**(7162): p. 557-63.
308. Bai, H., et al., *CCL5 secreted from bone marrow stromal cells stimulates the migration and invasion of Huh7 hepatocellular carcinoma cells via the PI3K-Akt pathway.* Int J Oncol, 2014. **45**(1): p. 333-43.
309. Ljujic, B., et al., *Human mesenchymal stem cells creating an immunosuppressive environment and promote breast cancer in mice.* Sci Rep, 2013. **3**: p. 2298.

310. Martin, F.T., et al., *Potential role of mesenchymal stem cells (MSCs) in the breast tumour microenvironment: stimulation of epithelial to mesenchymal transition (EMT).* Breast Cancer Res Treat, 2010. **124**(2): p. 317-26.
311. Samples, J., M. Willis, and N. Klauber-Demore, *Targeting angiogenesis and the tumor microenvironment.* Surg Oncol Clin N Am, 2013. **22**(4): p. 629-39.
312. Li, T., et al., *Molecular regulation of lymphangiogenesis in development and tumor microenvironment.* Cancer Microenviron, 2012. **5**(3): p. 249-60.
313. Butler, J.M., H. Kobayashi, and S. Rafii, *Instructive role of the vascular niche in promoting tumour growth and tissue repair by angiocrine factors.* Nat Rev Cancer, 2010. **10**(2): p. 138-46.
314. Alitalo, K., *The lymphatic vasculature in disease.* Nat Med, 2011. **17**(11): p. 1371-80.
315. Ferrara, N., *VEGF and the quest for tumour angiogenesis factors.* Nat Rev Cancer, 2002. **2**(10): p. 795-803.
316. Folkman, J., *Tumor angiogenesis: therapeutic implications.* N Engl J Med, 1971. **285**(21): p. 1182-6.
317. Wong, B.W., et al., *Emerging novel functions of the oxygen-sensing prolyl hydroxylase domain enzymes.* Trends Biochem Sci, 2013. **38**(1): p. 3-11.
318. Tang, N., et al., *Loss of HIF-1alpha in endothelial cells disrupts a hypoxia-driven VEGF autocrine loop necessary for tumorigenesis.* Cancer Cell, 2004. **6**(5): p. 485-95.
319. Skuli, N., et al., *Endothelial deletion of hypoxia-inducible factor-2alpha (HIF-2alpha) alters vascular function and tumor angiogenesis.* Blood, 2009. **114**(2): p. 469-77.
320. Branco-Price, C., et al., *Endothelial cell HIF-1alpha and HIF-2alpha differentially regulate metastatic success.* Cancer Cell, 2012. **21**(1): p. 52-65.
321. Ning, Q., et al., *Vascular endothelial growth factor receptor-1 activation promotes migration and invasion of breast cancer cells through epithelial-mesenchymal transition.* PLoS One, 2013. **8**(6): p. e65217.
322. Zhang, Z., et al., *Endothelial cell-secreted EGF induces epithelial to mesenchymal transition and endows head and neck cancer cells with stem-like phenotype.* Cancer Res, 2014. **74**(10): p. 2869-81.
323. Cao, Y., *Opinion: emerging mechanisms of tumour lymphangiogenesis and lymphatic metastasis.* Nat Rev Cancer, 2005. **5**(9): p. 735-43.
324. Kesler, C.T., et al., *Lymphatic vessels in health and disease.* Wiley Interdiscip Rev Syst Biol Med, 2013. **5**(1): p. 111-24.
325. Tammela, T. and K. Alitalo, *Lymphangiogenesis: Molecular mechanisms and future promise.* Cell, 2010. **140**(4): p. 460-76.

326. Vesely, M.D., et al., *Natural innate and adaptive immunity to cancer.* Annu Rev Immunol, 2011. **29**: p. 235-71.
327. Whiteside, T.L., *Inhibiting the inhibitors: evaluating agents targeting cancer immunosuppression.* Expert Opin Biol Ther, 2010. **10**(7): p. 1019-35.
328. Lippitz, B.E., *Cytokine patterns in patients with cancer: a systematic review.* Lancet Oncol, 2013. **14**(6): p. e218-28.
329. Grivennikov, S.I., F.R. Greten, and M. Karin, *Immunity, inflammation, and cancer.* Cell, 2010. **140**(6): p. 883-99.
330. Noy, R. and J.W. Pollard, *Tumor-associated macrophages: from mechanisms to therapy.* Immunity, 2014. **41**(1): p. 49-61.
331. Mantovani, A., et al., *Macrophage polarization: tumor-associated macrophages as a paradigm for polarized M2 mononuclear phagocytes.* Trends Immunol, 2002. **23**(11): p. 549-55.
332. Sica, A., et al., *Tumour-associated macrophages are a distinct M2 polarised population promoting tumour progression: potential targets of anti-cancer therapy.* Eur J Cancer, 2006. **42**(6): p. 717-27.
333. Liu, J., et al., *Tumor-associated macrophages recruit CCR6+ regulatory T cells and promote the development of colorectal cancer via enhancing CCL20 production in mice.* PLoS One, 2011. **6**(4): p. e19495.
334. Daurkin, I., et al., *Tumor-associated macrophages mediate immunosuppression in the renal cancer microenvironment by activating the 15-lipoxygenase-2 pathway.* Cancer Res, 2011. **71**(20): p. 6400-9.
335. Chen, P., et al., *Tumor-associated macrophages promote angiogenesis and melanoma growth via adrenomedullin in a paracrine and autocrine manner.* Clin Cancer Res, 2011. **17**(23): p. 7230-9.
336. Bonde, A.K., et al., *Intratumoral macrophages contribute to epithelial-mesenchymal transition in solid tumors.* BMC Cancer, 2012. **12**: p. 35.
337. Gabrilovich, D.I., et al., *The terminology issue for myeloid-derived suppressor cells.* Cancer Res, 2007. **67**(1): p. 425; author reply 426.
338. Yang, L., et al., *Abrogation of TGF beta signaling in mammary carcinomas recruits Gr-1+CD11b+ myeloid cells that promote metastasis.* Cancer Cell, 2008. **13**(1): p. 23-35.
339. Simpson, K.D., D.J. Templeton, and J.V. Cross, *Macrophage migration inhibitory factor promotes tumor growth and metastasis by inducing myeloid-derived suppressor cells in the tumor microenvironment.* J Immunol, 2012. **189**(12): p. 5533-40.
340. Toh, B., et al., *Mesenchymal transition and dissemination of cancer cells is driven by myeloid-derived suppressor cells infiltrating the primary tumor.* PLoS Biol, 2011. **9**(9): p. e1001162.
341. Knutson, K.L. and M.L. Disis, *Tumor antigen-specific T helper cells in cancer immunity and immunotherapy.* Cancer Immunol Immunother, 2005. **54**(8): p. 721-8.

342. Ossendorp, F., et al., *Importance of CD4(+) T helper cell responses in tumor immunity.* Immunol Lett, 2000. **74**(1): p. 75-9.
343. Wilke, C.M., et al., *Th17 cells in cancer: help or hindrance?* Carcinogenesis, 2011. **32**(5): p. 643-9.
344. Surman, D.R., et al., *Cutting edge: CD4+ T cell control of CD8+ T cell reactivity to a model tumor antigen.* J Immunol, 2000. **164**(2): p. 562-5.
345. Tsung, K., et al., *Macrophages as effector cells in interleukin 12-induced T cell-dependent tumor rejection.* Cancer Res, 2002. **62**(17): p. 5069-75.
346. Tatsumi, T., et al., *Disease stage variation in CD4+ and CD8+ T-cell reactivity to the receptor tyrosine kinase EphA2 in patients with renal cell carcinoma.* Cancer Res, 2003. **63**(15): p. 4481-9.
347. Fridman, W.H., et al., *The immune contexture in human tumours: impact on clinical outcome.* Nat Rev Cancer, 2012. **12**(4): p. 298-306.
348. Chae, W.J., et al., *Ablation of IL-17A abrogates progression of spontaneous intestinal tumorigenesis.* Proc Natl Acad Sci U S A, 2010. **107**(12): p. 5540-4.
349. Facciabene, A., G.T. Motz, and G. Coukos, *T-regulatory cells: key players in tumor immune escape and angiogenesis.* Cancer Res, 2012. **72**(9): p. 2162-71.
350. Gao, Q., et al., *Intratumoral balance of regulatory and cytotoxic T cells is associated with prognosis of hepatocellular carcinoma after resection.* J Clin Oncol, 2007. **25**(18): p. 2586-93.
351. Bates, G.J., et al., *Quantification of regulatory T cells enables the identification of high-risk breast cancer patients and those at risk of late relapse.* J Clin Oncol, 2006. **24**(34): p. 5373-80.
352. Tao, H., et al., *Prognostic potential of FOXP3 expression in non-small cell lung cancer cells combined with tumor-infiltrating regulatory T cells.* Lung Cancer, 2012. **75**(1): p. 95-101.
353. Miracco, C., et al., *Utility of tumour-infiltrating CD25+FOXP3+ regulatory T cell evaluation in predicting local recurrence in vertical growth phase cutaneous melanoma.* Oncol Rep, 2007. **18**(5): p. 1115-22.
354. Salama, P., et al., *Tumor-infiltrating FOXP3+ T regulatory cells show strong prognostic significance in colorectal cancer.* J Clin Oncol, 2009. **27**(2): p. 186-92.
355. Rech, A.J., et al., *CD25 blockade depletes and selectively reprograms regulatory T cells in concert with immunotherapy in cancer patients.* Sci Transl Med, 2012. **4**(134): p. 134ra62.
356. Ohmura, Y., et al., *Combinations of tumor-specific CD8+ CTLs and anti-CD25 mAb provide improved immunotherapy.* Oncol Rep, 2008. **19**(5): p. 1265-70.
357. Kudo-Saito, C., et al., *CCL2 is critical for immunosuppression to promote cancer metastasis.* Clin Exp Metastasis, 2013. **30**(4): p. 393-405.

358. Maher, J. and E.T. Davies, *Targeting cytotoxic T lymphocytes for cancer immunotherapy.* Br J Cancer, 2004. **91**(5): p. 817-21.
359. Matsushita, H., et al., *Cytotoxic T lymphocytes block tumor growth both by lytic activity and IFNgamma-dependent cell-cycle arrest.* Cancer Immunol Res, 2015. **3**(1): p. 26-36.
360. Qin, Z., et al., *A critical requirement of interferon gamma-mediated angiostasis for tumor rejection by CD8+ T cells.* Cancer Res, 2003. **63**(14): p. 4095-100.
361. Seo, A.N., et al., *Tumour-infiltrating CD8+ lymphocytes as an independent predictive factor for pathological complete response to primary systemic therapy in breast cancer.* Br J Cancer, 2013. **109**(10): p. 2705-13.
362. Zlobec, I. and A. Lugli, *Invasive front of colorectal cancer: dynamic interface of pro-/anti-tumor factors.* World J Gastroenterol, 2009. **15**(47): p. 5898-906.
363. Lugli, A., et al., *CD8+ lymphocytes/ tumour-budding index: an independent prognostic factor representing a 'pro-/anti-tumour' approach to tumour host interaction in colorectal cancer.* Br J Cancer, 2009. **101**(8): p. 1382-92.
364. Akalay, I., et al., *Epithelial-to-mesenchymal transition and autophagy induction in breast carcinoma promote escape from T-cell-mediated lysis.* Cancer Res, 2013. **73**(8): p. 2418-27.
365. Sprent, J., *Antigen-presenting cells. Professionals and amateurs.* Curr Biol, 1995. **5**(10): p. 1095-7.
366. Chaux, P., et al., *Tumor-infiltrating dendritic cells are defective in their antigen-presenting function and inducible B7 expression in rats.* Int J Cancer, 1997. **72**(4): p. 619-24.
367. Engelhardt, J.J., et al., *Marginating dendritic cells of the tumor microenvironment cross-present tumor antigens and stably engage tumor-specific T cells.* Cancer Cell, 2012. **21**(3): p. 402-17.
368. Bharadwaj, U., et al., *Elevated interleukin-6 and G-CSF in human pancreatic cancer cell conditioned medium suppress dendritic cell differentiation and activation.* Cancer Res, 2007. **67**(11): p. 5479-88.
369. Menetrier-Caux, C., et al., *Inhibition of the differentiation of dendritic cells from CD34(+) progenitors by tumor cells: role of interleukin-6 and macrophage colony-stimulating factor.* Blood, 1998. **92**(12): p. 4778-91.
370. Almand, B., et al., *Increased production of immature myeloid cells in cancer patients: a mechanism of immunosuppression in cancer.* J Immunol, 2001. **166**(1): p. 678-89.
371. Cortez-Retamozo, V., et al., *Origins of tumor-associated macrophages and neutrophils.* Proc Natl Acad Sci U S A, 2012. **109**(7): p. 2491-6.
372. Eguizabal, C., et al., *Natural killer cells for cancer immunotherapy: pluripotent stem cells-derived NK cells as an immunotherapeutic perspective.* Front Immunol, 2014. **5**: p. 439.

373. Marcus, A., et al., *Recognition of tumors by the innate immune system and natural killer cells.* Adv Immunol, 2014. **122**: p. 91-128.
374. Karre, K., et al., *Selective rejection of H-2-deficient lymphoma variants suggests alternative immune defence strategy.* Nature, 1986. **319**(6055): p. 675-8.
375. Lieberman, J., *The ABCs of granule-mediated cytotoxicity: new weapons in the arsenal.* Nat Rev Immunol, 2003. **3**(5): p. 361-70.
376. Bauer, S., et al., *Activation of NK cells and T cells by NKG2D, a receptor for stress-inducible MICA.* Science, 1999. **285**(5428): p. 727-9.
377. Imai, K., et al., *Natural cytotoxic activity of peripheral-blood lymphocytes and cancer incidence: an 11-year follow-up study of a general population.* Lancet, 2000. **356**(9244): p. 1795-9.
378. Wu, J. and L.L. Lanier, *Natural killer cells and cancer.* Adv Cancer Res, 2003. **90**: p. 127-56.
379. Coca, S., et al., *The prognostic significance of intratumoral natural killer cells in patients with colorectal carcinoma.* Cancer, 1997. **79**(12): p. 2320-8.
380. Ishigami, S., et al., *Prognostic value of intratumoral natural killer cells in gastric carcinoma.* Cancer, 2000. **88**(3): p. 577-83.
381. Villegas, F.R., et al., *Prognostic significance of tumor infiltrating natural killer cells subset CD57 in patients with squamous cell lung cancer.* Lung Cancer, 2002. **35**(1): p. 23-8.
382. Sconocchia, G., et al., *NK cells and T cells cooperate during the clinical course of colorectal cancer.* Oncoimmunology, 2014. **3**(8): p. e952197.
383. Wilson, E.B., et al., *Human tumour immune evasion via TGF-beta blocks NK cell activation but not survival allowing therapeutic restoration of anti-tumour activity.* PLoS One, 2011. **6**(9): p. e22842.
384. Lopez-Soto, A., et al., *Regulation of NKG2D signaling during the epithelial-to-mesenchymal transition.* Oncoimmunology, 2013. **2**(9): p. e25820.
385. Ames, E. and W.J. Murphy, *Advantages and clinical applications of natural killer cells in cancer immunotherapy.* Cancer Immunol Immunother, 2014. **63**(1): p. 21-8.
386. Balkwill, F.R., *The chemokine system and cancer.* J Pathol, 2012. **226**(2): p. 148-57.
387. Le, Y., et al., *Chemokines and chemokine receptors: their manifold roles in homeostasis and disease.* Cell Mol Immunol, 2004. **1**(2): p. 95-104.
388. Allen, S.J., S.E. Crown, and T.M. Handel, *Chemokine: receptor structure, interactions, and antagonism.* Annu Rev Immunol, 2007. **25**: p. 787-820.

389. Crump, M.P., et al., *Solution structure of eotaxin, a chemokine that selectively recruits eosinophils in allergic inflammation.* J Biol Chem, 1998. **273**(35): p. 22471-9.
390. Baldwin, E.T., et al., *Crystal structure of interleukin 8: symbiosis of NMR and crystallography.* Proc Natl Acad Sci U S A, 1991. **88**(2): p. 502-6.
391. Zlotnik, A. and O. Yoshie, *The chemokine superfamily revisited.* Immunity, 2012. **36**(5): p. 705-16.
392. Proost, P., et al., *Amino-terminal truncation of chemokines by CD26/dipeptidyl-peptidase IV. Conversion of RANTES into a potent inhibitor of monocyte chemotaxis and HIV-1-infection.* J Biol Chem, 1998. **273**(13): p. 7222-7.
393. Mortier, A., J. Van Damme, and P. Proost, *Regulation of chemokine activity by posttranslational modification.* Pharmacol Ther, 2008. **120**(2): p. 197-217.
394. Nguyen, L.T. and H.J. Vogel, *Structural perspectives on antimicrobial chemokines.* Front Immunol, 2012. **3**: p. 384.
395. Proudfoot, A.E., *The biological relevance of chemokine-proteoglycan interactions.* Biochem Soc Trans, 2006. **34**(Pt 3): p. 422-6.
396. Handel, T.M., et al., *Regulation of protein function by glycosaminoglycans--as exemplified by chemokines.* Annu Rev Biochem, 2005. **74**: p. 385-410.
397. Salanga, C.L. and T.M. Handel, *Chemokine oligomerization and interactions with receptors and glycosaminoglycans: the role of structural dynamics in function.* Exp Cell Res, 2011. **317**(5): p. 590-601.
398. Czaplewski, L.G., et al., *Identification of amino acid residues critical for aggregation of human CC chemokines macrophage inflammatory protein (MIP)-1alpha, MIP-1beta, and RANTES. Characterization of active disaggregated chemokine variants.* J Biol Chem, 1999. **274**(23): p. 16077-84.
399. Proudfoot, A.E., et al., *Glycosaminoglycan binding and oligomerization are essential for the in vivo activity of certain chemokines.* Proc Natl Acad Sci U S A, 2003. **100**(4): p. 1885-90.
400. Moser, B., et al., *Chemokines: multiple levels of leukocyte migration control.* Trends Immunol, 2004. **25**(2): p. 75-84.
401. Nomiyama, H., N. Osada, and O. Yoshie, *The evolution of mammalian chemokine genes.* Cytokine Growth Factor Rev, 2010. **21**(4): p. 253-62.
402. Vandercappellen, J., J. Van Damme, and S. Struyf, *The role of CXC chemokines and their receptors in cancer.* Cancer Lett, 2008. **267**(2): p. 226-44.
403. Zhu, W.W., et al., *Evaluation of midkine as a diagnostic serum biomarker in hepatocellular carcinoma.* Clin Cancer Res, 2013. **19**(14): p. 3944-54.

404. Palczewski, K., et al., *Crystal structure of rhodopsin: A G protein-coupled receptor.* Science, 2000. **289**(5480): p. 739-45.
405. Cherezov, V., et al., *High-resolution crystal structure of an engineered human beta2-adrenergic G protein-coupled receptor.* Science, 2007. **318**(5854): p. 1258-65.
406. Wu, B., et al., *Structures of the CXCR4 chemokine GPCR with small-molecule and cyclic peptide antagonists.* Science, 2010. **330**(6007): p. 1066-71.
407. Park, S.H., et al., *Structure of the chemokine receptor CXCR1 in phospholipid bilayers.* Nature, 2012. **491**(7426): p. 779-83.
408. Katritch, V., V. Cherezov, and R.C. Stevens, *Diversity and modularity of G protein-coupled receptor structures.* Trends Pharmacol Sci, 2012. **33**(1): p. 17-27.
409. Lagane, B., et al., *Mutation of the DRY motif reveals different structural requirements for the CC chemokine receptor 5-mediated signaling and receptor endocytosis.* Mol Pharmacol, 2005. **67**(6): p. 1966-76.
410. Baggiolini, M., *Chemokines in pathology and medicine.* J Intern Med, 2001. **250**(2): p. 91-104.
411. Haematology, A.o.G.a.C.i.O.a., *CCR2 (chemokine (C-C motif) receptor 2).* 2016.
412. Davenport, A.P., et al., *International Union of Basic and Clinical Pharmacology. LXXXVIII. G protein-coupled receptor list: recommendations for new pairings with cognate ligands.* Pharmacol Rev, 2013. **65**(3): p. 967-86.
413. Ulvmar, M.H., E. Hub, and A. Rot, *Atypical chemokine receptors.* Exp Cell Res, 2011. **317**(5): p. 556-68.
414. Wilson, S., G. Wilkinson, and G. Milligan, *The CXCR1 and CXCR2 receptors form constitutive homo- and heterodimers selectively and with equal apparent affinities.* J Biol Chem, 2005. **280**(31): p. 28663-74.
415. Bayburt, T.H., et al., *Monomeric rhodopsin is sufficient for normal rhodopsin kinase (GRK1) phosphorylation and arrestin-1 binding.* J Biol Chem, 2011. **286**(2): p. 1420-8.
416. Nomiyama, H., N. Osada, and O. Yoshie, *A family tree of vertebrate chemokine receptors for a unified nomenclature.* Dev Comp Immunol, 2011. **35**(7): p. 705-15.
417. Zlotnik, A., O. Yoshie, and H. Nomiyama, *The chemokine and chemokine receptor superfamilies and their molecular evolution.* Genome Biol, 2006. **7**(12): p. 243.
418. Murphy, P.M., et al., *International union of pharmacology. XXII. Nomenclature for chemokine receptors.* Pharmacol Rev, 2000. **52**(1): p. 145-76.

419. Nomiyama, H., N. Osada, and O. Yoshie, *Systematic classification of vertebrate chemokines based on conserved synteny and evolutionary history.* Genes Cells, 2013. **18**(1): p. 1-16.
420. Rot, A. and U.H. von Andrian, *Chemokines in innate and adaptive host defense: basic chemokinese grammar for immune cells.* Annu Rev Immunol, 2004. **22**: p. 891-928.
421. Raman, D., T. Sobolik-Delmaire, and A. Richmond, *Chemokines in health and disease.* Exp Cell Res, 2011. **317**(5): p. 575-89.
422. Barnes, P.J., *Mediators of chronic obstructive pulmonary disease.* Pharmacol Rev, 2004. **56**(4): p. 515-48.
423. Distler, J.H. and O. Distler, *Inflammation: Microparticles and their roles in inflammatory arthritides.* Nat Rev Rheumatol, 2010. **6**(7): p. 385-6.
424. Gilliam, B.L., D.J. Riedel, and R.R. Redfield, *Clinical use of CCR5 inhibitors in HIV and beyond.* J Transl Med, 2011. **9 Suppl 1**: p. S9.
425. Hannan, N.J., et al., *The chemokines, CX3CL1, CCL14, and CCL4, promote human trophoblast migration at the feto-maternal interface.* Biol Reprod, 2006. **74**(5): p. 896-904.
426. Zaja-Milatovic, S. and A. Richmond, *CXC chemokines and their receptors: a case for a significant biological role in cutaneous wound healing.* Histol Histopathol, 2008. **23**(11): p. 1399-407.
427. Kakinuma, T. and S.T. Hwang, *Chemokines, chemokine receptors, and cancer metastasis.* J Leukoc Biol, 2006. **79**(4): p. 639-51.
428. Granot, Z., et al., *Tumor entrained neutrophils inhibit seeding in the premetastatic lung.* Cancer Cell, 2011. **20**(3): p. 300-14.
429. Gu-Trantien, C., et al., *CD4(+) follicular helper T cell infiltration predicts breast cancer survival.* J Clin Invest, 2013. **123**(7): p. 2873-92.
430. Qian, B.Z., et al., *CCL2 recruits inflammatory monocytes to facilitate breast-tumour metastasis.* Nature, 2011. **475**(7355): p. 222-5.
431. Aldinucci, D. and A. Colombatti, *The Inflammatory Chemokine CCL5 and Cancer Progression.* Mediators Inflamm, 2014. **2014**: p. 292376.
432. Bates, R.C., M.J. DeLeo, 3rd, and A.M. Mercurio, *The epithelial-mesenchymal transition of colon carcinoma involves expression of IL-8 and CXCR-1-mediated chemotaxis.* Exp Cell Res, 2004. **299**(2): p. 315-24.
433. Velasco-Velazquez, M. and R.G. Pestell, *The CCL5/CCR5 axis promotes metastasis in basal breast cancer.* Oncoimmunology, 2013. **2**(4): p. e23660.
434. Muller, A., et al., *Involvement of chemokine receptors in breast cancer metastasis.* Nature, 2001. **410**(6824): p. 50-6.
435. Murakami, T., et al., *Expression of CXC chemokine receptor-4 enhances the pulmonary metastatic potential of murine B16 melanoma cells.* Cancer Res, 2002. **62**(24): p. 7328-34.
436. Kang, Y., et al., *A multigenic program mediating breast cancer metastasis to bone.* Cancer Cell, 2003. **3**(6): p. 537-49.

437. Wendel, C., et al., *CXCR4/CXCL12 participate in extravasation of metastasizing breast cancer cells within the liver in a rat model.* PLoS One, 2012. **7**(1): p. e30046.
438. Wiley, H.E., et al., *Expression of CC chemokine receptor-7 and regional lymph node metastasis of B16 murine melanoma.* J Natl Cancer Inst, 2001. **93**(21): p. 1638-43.
439. Ma, H., et al., *CCR7 enhances TGF-beta1-induced epithelial-mesenchymal transition and is associated with lymph node metastasis and poor overall survival in gastric cancer.* Oncotarget, 2015. **6**(27): p. 24348-60.
440. Li, A., et al., *IL-8 directly enhanced endothelial cell survival, proliferation, and matrix metalloproteinases production and regulated angiogenesis.* J Immunol, 2003. **170**(6): p. 3369-76.
441. Gabellini, C., et al., *Functional activity of CXCL8 receptors, CXCR1 and CXCR2, on human malignant melanoma progression.* Eur J Cancer, 2009. **45**(14): p. 2618-27.
442. Hwang, W.L., et al., *SNAIL regulates interleukin-8 expression, stem cell-like activity, and tumorigenicity of human colorectal carcinoma cells.* Gastroenterology, 2011. **141**(1): p. 279-91, 291 e1-5.
443. Li, X.J., et al., *As an independent unfavorable prognostic factor, IL-8 promotes metastasis of nasopharyngeal carcinoma through induction of epithelial-mesenchymal transition and activation of AKT signaling.* Carcinogenesis, 2012. **33**(7): p. 1302-9.
444. Fernando, R.I., et al., *IL-8 signaling plays a critical role in the epithelial-mesenchymal transition of human carcinoma cells.* Cancer Res, 2011. **71**(15): p. 5296-306.
445. Fu, X.T., et al., *Macrophage-secreted IL-8 induces epithelial-mesenchymal transition in hepatocellular carcinoma cells by activating the JAK2/STAT3/Snail pathway.* Int J Oncol, 2015. **46**(2): p. 587-96.
446. Palena, C., D.H. Hamilton, and R.I. Fernando, *Influence of IL-8 on the epithelial-mesenchymal transition and the tumor microenvironment.* Future Oncol, 2012. **8**(6): p. 713-22.
447. Cheng, X.S., et al., *CCL20 and CXCL8 synergize to promote progression and poor survival outcome in patients with colorectal cancer by collaborative induction of the epithelial-mesenchymal transition.* Cancer Lett, 2014.
448. Hou, K.Z., Z.Q. Fu, and H. Gong, *Chemokine ligand 20 enhances progression of hepatocellular carcinoma via epithelial-mesenchymal transition.* World J Gastroenterol, 2015. **21**(2): p. 475-83.
449. Bertran, E., et al., *Overactivation of the TGF-beta pathway confers a mesenchymal-like phenotype and CXCR4-dependent migratory properties to liver tumor cells.* Hepatology, 2013. **58**(6): p. 2032-44.
450. Bertran, E., et al., *Role of CXCR4/SDF-1 alpha in the migratory phenotype of hepatoma cells that have undergone epithelial-*

mesenchymal transition in response to the transforming growth factor-beta. Cell Signal, 2009. **21**(11): p. 1595-606.
451. Yao, C., et al., *CXCL12/CXCR4 Axis Upregulates Twist to Induce EMT in Human Glioblastoma.* Mol Neurobiol, 2015.
452. Zhang, S.S., et al., *CD133(+)CXCR4(+) colon cancer cells exhibit metastatic potential and predict poor prognosis of patients.* BMC Med, 2012. **10**: p. 85.
453. Li, X., et al., *SDF-1/CXCR4 signaling induces pancreatic cancer cell invasion and epithelial-mesenchymal transition in vitro through non-canonical activation of Hedgehog pathway.* Cancer Lett, 2012. **322**(2): p. 169-76.
454. Sobolik, T., et al., *CXCR4 drives the metastatic phenotype in breast cancer through induction of CXCR2 and activation of MEK and PI3K pathways.* Mol Biol Cell, 2014. **25**(5): p. 566-82.
455. Ploenes, T., et al., *CC-chemokine ligand 18 induces epithelial to mesenchymal transition in lung cancer A549 cells and elevates the invasive potential.* PLoS One, 2013. **8**(1): p. e53068.
456. Meng, F., et al., *CCL18 promotes epithelial-mesenchymal transition, invasion and migration of pancreatic cancer cells in pancreatic ductal adenocarcinoma.* Int J Oncol, 2015. **46**(3): p. 1109-20.
457. Low-Marchelli, J.M., et al., *Twist1 induces CCL2 and recruits macrophages to promote angiogenesis.* Cancer Res, 2013. **73**(2): p. 662-71.
458. Xia, L., et al., *Forkhead box Q1 promotes hepatocellular carcinoma metastasis by transactivating ZEB2 and VersicanV1 expression.* Hepatology, 2014. **59**(3): p. 958-73.
459. Liles, W.C., et al., *Mobilization of hematopoietic progenitor cells in healthy volunteers by AMD3100, a CXCR4 antagonist.* Blood, 2003. **102**(8): p. 2728-30.
460. Broxmeyer, H.E., et al., *Rapid mobilization of murine and human hematopoietic stem and progenitor cells with AMD3100, a CXCR4 antagonist.* J Exp Med, 2005. **201**(8): p. 1307-18.
461. Ochoa-Callejero, L., et al., *Maraviroc, a CCR5 antagonist, prevents development of hepatocellular carcinoma in a mouse model.* PLoS One, 2013. **8**(1): p. e53992.
462. Cambien, B., et al., *CCL5 neutralization restricts cancer growth and potentiates the targeting of PDGFRbeta in colorectal carcinoma.* PLoS One, 2011. **6**(12): p. e28842.
463. Cho, K.S., et al., *Inhibition of tumor growth and histopathological changes following treatment with a chemokine receptor CXCR4 antagonist in a prostate cancer xenograft model.* Oncol Lett, 2013. **6**(4): p. 933-938.
464. Guleng, B., et al., *Blockade of the stromal cell-derived factor-1/CXCR4 axis attenuates in vivo tumor growth by inhibiting angiogenesis in a*

vascular endothelial growth factor-independent manner. Cancer Res, 2005. **65**(13): p. 5864-71.
465. Loberg, R.D., et al., *Targeting CCL2 with systemic delivery of neutralizing antibodies induces prostate cancer tumor regression in vivo.* Cancer Res, 2007. **67**(19): p. 9417-24.
466. Sugiyama, D., et al., *Anti-CCR4 mAb selectively depletes effector-type FoxP3+CD4+ regulatory T cells, evoking antitumor immune responses in humans.* Proc Natl Acad Sci U S A, 2013. **110**(44): p. 17945-50.
467. Borsig, L., et al., *Inflammatory chemokines and metastasis-tracing the accessory.* Oncogene, 2013.
468. Schall, T.J. and A.E. Proudfoot, *Overcoming hurdles in developing successful drugs targeting chemokine receptors.* Nat Rev Immunol, 2011. **11**(5): p. 355-63.
469. Leinco Technologies. *General Western Blot Protocol, Diagram 2: Illustration of Detection in Westren Blots*. 2016
470. Maniatis, T., *Molecular cloning : a laboratory manual / T.Maniatis, E.F. Fritsch, J. Sambrook.* . 1982.
471. Abcam, *Direct vs indirect immunofluorescence.* 1998-2016.
472. brand, R.D.s.a.b., *Proteome Profiler™ Antibody Arrays.* 2016.
473. brand, R.D.s.a.b., *Luminex Assay Principle.* 2016.
474. EIAab, *ELISA: Direct and Indirect "Sandwich" ELISA General Protocols.* 2016.
475. The New Zealand Biotechnology Learning Hub, *DNA cloning.* 2007.
476. Thermo Fisher Scientific Inc, *pcDNA™3.1 Directional TOPO® Expression Kit.* 2015.
477. Services, I.C.P., *Novel hybrid promoter and recombinant vector comprising the same WO 2012074277 A2.*
478. Ibidi, *Transfection.* 2016.
479. Díaz, M., et al., *Application of flow cytometry to industrial microbial bioprocesses.* Biochemical Engineering Journal, 2010. **48**(3): p. 385-407.
480. GmbH, B., *Haptotaxis Assays.* 2016.
481. Technologies, A., *QuikChange II Site-Directed Mutagenesis Kits - Details & Specifications.* 2016.
482. Remacle, J.E., et al., *New mode of DNA binding of multi-zinc finger transcription factors: deltaEF1 family members bind with two hands to two target sites.* Embo j, 1999. **18**(18): p. 5073-84.
483. Smale, S.T., *Luciferase assay.* Cold Spring Harb Protoc, 2010. **2010**(5): p. pdb.prot5421.
484. Jiwaji, M., et al., *The Renilla luciferase gene as a reference gene for normalization of gene expression in transiently transfected cells.* BMC Mol Biol, 2010. **11**: p. 103.
485. Yoshihiro Ohmiya, *APPLICATIONS OF BIOLUMINESCENCE. Cell Based Assays and Imaging.* Biomedical Research Institute. National Institute of Advanced Industrial Science and Technology (AIST).

486. Promega Corporation, *Dual-Luciferase® Reporter Assay.* 2003-2009.
487. Active motif, *ChIP-IT® High Sensitivity.* 2016.
488. Kampf, C., et al., *Production of tissue microarrays, immunohistochemistry staining and digitalization within the human protein atlas.* J Vis Exp, 2012(63).
489. Abnova Corporation, *ProteoScreen® - Tissue Microarray Expression Profiling.* 2016.
490. Acloque, H., et al., *Epithelial-mesenchymal transitions: the importance of changing cell state in development and disease.* J Clin Invest, 2009. **119**(6): p. 1438-49.
491. Thiery, J.P. and J.P. Sleeman, *Complex networks orchestrate epithelial-mesenchymal transitions.* Nat Rev Mol Cell Biol, 2006. **7**(2): p. 131-42.
492. Medici, D., E.D. Hay, and B.R. Olsen, *Snail and Slug promote epithelial-mesenchymal transition through beta-catenin-T-cell factor-4-dependent expression of transforming growth factor-beta3.* Mol Biol Cell, 2008. **19**(11): p. 4875-87.
493. Schmalhofer, O., S. Brabletz, and T. Brabletz, *E-cadherin, beta-catenin, and ZEB1 in malignant progression of cancer.* Cancer Metastasis Rev, 2009. **28**(1-2): p. 151-66.
494. Williams, A.C., S.J. Harper, and C. Paraskeva, *Neoplastic transformation of a human colonic epithelial cell line: in vitro evidence for the adenoma to carcinoma sequence.* Cancer Res, 1990. **50**(15): p. 4724-30.
495. Wang, M., et al., *Active immunotherapy of cancer with a nonreplicating recombinant fowlpox virus encoding a model tumor-associated antigen.* J Immunol, 1995. **154**(9): p. 4685-92.
496. Fogh, J., J.M. Fogh, and T. Orfeo, *One hundred and twenty-seven cultured human tumor cell lines producing tumors in nude mice.* J Natl Cancer Inst, 1977. **59**(1): p. 221-6.
497. Trainer, D.L., et al., *Biological characterization and oncogene expression in human colorectal carcinoma cell lines.* Int J Cancer, 1988. **41**(2): p. 287-96.
498. Semple, T.U., et al., *Tumor and lymphoid cell lines from a patient with carcinoma of the colon for a cytotoxicity model.* Cancer Res, 1978. **38**(5): p. 1345-55.
499. Tibbetts, L.M., et al., *Chemotherapy of cell-line-derived human colon carcinomas in mice immunosuppressed with antithymocyte serum.* Cancer, 1977. **40**(5 Suppl): p. 2651-9.
500. Dexter, D.L., J.A. Barbosa, and P. Calabresi, *N,N-dimethylformamide-induced alteration of cell culture characteristics and loss of tumorigenicity in cultured human colon carcinoma cells.* Cancer Res, 1979. **39**(3): p. 1020-5.
501. Brattain, M.G., et al., *Heterogeneity of malignant cells from a human colonic carcinoma.* Cancer Res, 1981. **41**(5): p. 1751-6.

502. Drewinko, B., et al., *Establishment of a human carcinoembryonic antigen-producing colon adenocarcinoma cell line.* Cancer Res, 1976. **36**(2 Pt 1): p. 467-75.
503. Boyd, D., et al., *Alterations of the biological characteristics of a colon carcinoma cell line by colon-derived substrata material.* Cancer Res, 1988. **48**(10): p. 2825-31.
504. Leibovitz, A., et al., *Classification of human colorectal adenocarcinoma cell lines.* Cancer Res, 1976. **36**(12): p. 4562-9.
505. Lelbovitz, A., et al., *Detection and analysis of a glucose 6-phosphate dehydrogenase phenotype B cell line contamination.* J Natl Cancer Inst, 1979. **63**(3): p. 635-45.
506. Kroepil, F., et al., *Down-regulation of CDH1 is associated with expression of SNAI1 in colorectal adenomas.* PLoS One, 2012. **7**(9): p. e46665.
507. Kaler, P., L. Augenlicht, and L. Klampfer, *Activating mutations in beta-catenin in colon cancer cells alter their interaction with macrophages; the role of snail.* PLoS One, 2012. **7**(9): p. e45462.
508. Kaler, P., et al., *Tumor associated macrophages protect colon cancer cells from TRAIL-induced apoptosis through IL-1beta-dependent stabilization of Snail in tumor cells.* PLoS One, 2010. **5**(7): p. e11700.
509. Hsu, D.S., et al., *Acetylation of snail modulates the cytokinome of cancer cells to enhance the recruitment of macrophages.* Cancer Cell, 2014. **26**(4): p. 534-48.
510. Itoh, M., et al., *The 220-kD protein colocalizing with cadherins in non-epithelial cells is identical to ZO-1, a tight junction-associated protein in epithelial cells: cDNA cloning and immunoelectron microscopy.* J Cell Biol, 1993. **121**(3): p. 491-502.
511. Gottardi, C.J., et al., *The junction-associated protein, zonula occludens-1, localizes to the nucleus before the maturation and during the remodeling of cell-cell contacts.* Proc Natl Acad Sci U S A, 1996. **93**(20): p. 10779-84.
512. Morris, A.P., et al., *Junctional Adhesion Molecules (JAMs) are differentially expressed in fibroblasts and co-localize with ZO-1 to adherens-like junctions.* Cell Commun Adhes, 2006. **13**(4): p. 233-47.
513. Reichert, M., T. Muller, and W. Hunziker, *The PDZ domains of zonula occludens-1 induce an epithelial to mesenchymal transition of Madin-Darby canine kidney I cells. Evidence for a role of beta-catenin/Tcf/Lef signaling.* J Biol Chem, 2000. **275**(13): p. 9492-500.
514. Bauer, H., et al., *The dual role of zonula occludens (ZO) proteins.* J Biomed Biotechnol, 2010. **2010**: p. 402593.
515. Brattain, M.G., et al., *Establishment of mouse colonic carcinoma cell lines with different metastatic properties.* Cancer Res, 1980. **40**(7): p. 2142-6.
516. Kang, M.H., et al., *Inhibition of PI3 kinase/Akt pathway is required for BMP2-induced EMT and invasion.* Oncol Rep, 2009. **22**(3): p. 525-34.

517. Liu, Y.N., et al., *MiR-1 and miR-200 inhibit EMT via Slug-dependent and tumorigenesis via Slug-independent mechanisms.* Oncogene, 2013. **32**(3): p. 296-306.
518. Schlegel, N., et al., *Desmoglein 2-mediated adhesion is required for intestinal epithelial barrier integrity.* Am J Physiol Gastrointest Liver Physiol, 2010. **298**(5): p. G774-83.
519. Hwang, S., et al., *E-cadherin is critical for collective sheet migration and is regulated by the chemokine CXCL12 protein during restitution.* J Biol Chem, 2012. **287**(26): p. 22227-40.
520. Hamada, K., et al., *Liver metastasis models of colon cancer for evaluation of drug efficacy using NOD/Shi-scid IL2Rgammanull (NOG) mice.* Int J Oncol, 2008. **32**(1): p. 153-9.
521. de Vries, J.E., et al., *In vivo and in vitro invasion in relation to phenotypic characteristics of human colorectal carcinoma cells.* Br J Cancer, 1995. **71**(2): p. 271-7.
522. Ghoul, A., et al., *Epithelial-to-mesenchymal transition and resistance to ingenol 3-angelate, a novel protein kinase C modulator, in colon cancer cells.* Cancer Res, 2009. **69**(10): p. 4260-9.
523. Kahlert, C., et al., *Overexpression of ZEB2 at the invasion front of colorectal cancer is an independent prognostic marker and regulates tumor invasion in vitro.* Clin Cancer Res, 2011. **17**(24): p. 7654-63.
524. Paterson, E.L., et al., *Down-regulation of the miRNA-200 family at the invasive front of colorectal cancers with degraded basement membrane indicates EMT is involved in cancer progression.* Neoplasia, 2013. **15**(2): p. 180-91.
525. Celesti, G., et al., *Presence of Twist1-Positive Neoplastic Cells in the Stroma of Chromosome-Unstable Colorectal Tumors.* Gastroenterology, 2013.
526. Liang, Y.J., et al., *MiR-124 targets Slug to regulate epithelial-mesenchymal transition and metastasis of breast cancer.* Carcinogenesis, 2013. **34**(3): p. 713-22.
527. Kuo, T.C., et al., *Angiopoietin-like protein 1 suppresses SLUG to inhibit cancer cell motility.* J Clin Invest, 2013. **123**(3): p. 1082-95.
528. Kawai, K., et al., *A new in vivo model to analyze hepatic metastasis of the human colon cancer cell line HCT116 in NOD/Shi-scid/IL-2Rgamma(null) (NOG) mice by (18)F-FDG PET/CT.* Oncol Rep, 2013. **29**(2): p. 464-8.
529. Kimball, P.M. and M.G. Brattain, *Isolation of a cellular subpopulation from a human colonic carcinoma cell line.* Cancer Res, 1980. **40**(5): p. 1574-9.
530. Sakuma, K., M. Aoki, and R. Kannagi, *Transcription factors c-Myc and CDX2 mediate E-selectin ligand expression in colon cancer cells undergoing EGF/bFGF-induced epithelial-mesenchymal transition.* Proc Natl Acad Sci U S A, 2012. **109**(20): p. 7776-81.

531. Yang, A.D., et al., *Chronic oxaliplatin resistance induces epithelial-to-mesenchymal transition in colorectal cancer cell lines.* Clin Cancer Res, 2006. **12**(14 Pt 1): p. 4147-53.
532. Aho, S., et al., *Characterization of the ubinuclein protein as a new member of the nuclear and adhesion complex components (NACos).* Biol Cell, 2009. **101**(6): p. 319-34.
533. Mertens, C., C. Kuhn, and W.W. Franke, *Plakophilins 2a and 2b: constitutive proteins of dual location in the karyoplasm and the desmosomal plaque.* J Cell Biol, 1996. **135**(4): p. 1009-25.
534. Zuo, Y., et al., *Novel roles of liver sinusoidal endothelial cell lectin in colon carcinoma cell adhesion, migration and in-vivo metastasis to the liver.* Gut, 2013. **62**(8): p. 1169-78.
535. Xiong, H., et al., *Roles of STAT3 and ZEB1 proteins in E-cadherin down-regulation and human colorectal cancer epithelial-mesenchymal transition.* J Biol Chem, 2012. **287**(8): p. 5819-32.
536. Breen, E., G. Steele, Jr., and A.M. Mercurio, *Role of the E-cadherin/alpha-catenin complex in modulating cell-cell and cell-matrix adhesive properties of invasive colon carcinoma cells.* Ann Surg Oncol, 1995. **2**(5): p. 378-85.
537. McCombs, W.B., 3rd, et al., *Morphologic and immunologic studies of a human colon tumor cell line (SW-48).* Cancer, 1976. **38**(6): p. 2316-27.
538. Ireton, R.C., et al., *A novel role for p120 catenin in E-cadherin function.* J Cell Biol, 2002. **159**(3): p. 465-76.
539. Hewitt, R.E., et al., *Validation of a model of colon cancer progression.* J Pathol, 2000. **192**(4): p. 446-54.
540. Haga, C.L. and D.G. Phinney, *MicroRNAs in the imprinted DLK1-DIO3 region repress the epithelial-to-mesenchymal transition by targeting the TWIST1 protein signaling network.* J Biol Chem, 2012. **287**(51): p. 42695-707.
541. Maher, M.T., et al., *Beta-catenin phosphorylated at serine 45 is spatially uncoupled from beta-catenin phosphorylated in the GSK3 domain: implications for signaling.* PLoS One, 2010. **5**(4): p. e10184.
542. Lee, C.C., et al., *TCF12 protein functions as transcriptional repressor of E-cadherin, and its overexpression is correlated with metastasis of colorectal cancer.* J Biol Chem, 2012. **287**(4): p. 2798-809.
543. Han, X., et al., *Silencing SOX2 induced mesenchymal-epithelial transition and its expression predicts liver and lymph node metastasis of CRC patients.* PLoS One, 2012. **7**(8): p. e41335.
544. Li, Y., et al., *FMNL2 enhances invasion of colorectal carcinoma by inducing epithelial-mesenchymal transition.* Mol Cancer Res, 2010. **8**(12): p. 1579-90.
545. Singh, A.B., et al., *Claudin-1 up-regulates the repressor ZEB-1 to inhibit E-cadherin expression in colon cancer cells.* Gastroenterology, 2011. **141**(6): p. 2140-53.

546. de Toledo, M., et al., *Cooperative anti-invasive effect of Cdc42/Rac1 activation and ROCK inhibition in SW620 colorectal cancer cells with elevated blebbing activity.* PLoS One, 2012. **7**(11): p. e48344.
547. Chen, M.L., L.S. Liang, and X.K. Wang, *miR-200c inhibits invasion and migration in human colon cancer cells SW480/620 by targeting ZEB1.* Clin Exp Metastasis, 2012. **29**(5): p. 457-69.
548. Yuan, K., et al., *Decreased Levels of miR-224 and the Passenger Strand of miR-221 Increase MBD2, Suppressing Maspin and Promoting Tumor Growth and Metastasis in Mice.* Gastroenterology, 2013.
549. Kowalski, P.J., M.A. Rubin, and C.G. Kleer, *E-cadherin expression in primary carcinomas of the breast and its distant metastases.* Breast Cancer Res, 2003. **5**(6): p. R217-22.
550. Gunasinghe, N.P., et al., *Mesenchymal-epithelial transition (MET) as a mechanism for metastatic colonisation in breast cancer.* Cancer Metastasis Rev, 2012. **31**(3-4): p. 469-78.
551. Kubens, B.S. and K.S. Zanker, *Differences in the migration capacity of primary human colon carcinoma cells (SW480) and their lymph node metastatic derivatives (SW620).* Cancer Lett, 1998. **131**(1): p. 55-64.
552. Chung, B.M., J.D. Rotty, and P.A. Coulombe, *Networking galore: intermediate filaments and cell migration.* Curr Opin Cell Biol, 2013. **25**(5): p. 600-12.
553. Kwan, R., K. Looi, and M.B. Omary, *Absence of keratins 8 and 18 in rodent epithelial cell lines associates with keratin gene mutation and DNA methylation: Cell line selective effects on cell invasion.* Exp Cell Res, 2015. **335**(1): p. 12-22.
554. Yamaguchi, H. and J. Condeelis, *Regulation of the actin cytoskeleton in cancer cell migration and invasion.* Biochim Biophys Acta, 2007. **1773**(5): p. 642-52.
555. Stevenson, R.P., D. Veltman, and L.M. Machesky, *Actin-bundling proteins in cancer progression at a glance.* J Cell Sci, 2012. **125**(Pt 5): p. 1073-9.
556. Schoumacher, M., et al., *Actin, microtubules, and vimentin intermediate filaments cooperate for elongation of invadopodia.* J Cell Biol, 2010. **189**(3): p. 541-56.
557. Palmieri, V., et al., *Mechanical and structural comparison between primary tumor and lymph node metastasis cells in colorectal cancer.* Soft Matter, 2015. **11**(28): p. 5719-26.
558. Yaal-Hahoshen, N., et al., *The chemokine CCL5 as a potential prognostic factor predicting disease progression in stage II breast cancer patients.* Clin Cancer Res, 2006. **12**(15): p. 4474-80.
559. Curiel, T.J., et al., *Specific recruitment of regulatory T cells in ovarian carcinoma fosters immune privilege and predicts reduced survival.* Nat Med, 2004. **10**(9): p. 942-9.

560. Biasi, F., et al., *Progressive increase of matrix metalloprotease-9 and interleukin-8 serum levels during carcinogenic process in human colorectal tract.* PLoS One, 2012. **7**(7): p. e41839.
561. Yan, Z., et al., *Identification of candidate colon cancer biomarkers by applying a random forest approach on microarray data.* Oncol Rep, 2012. **28**(3): p. 1036-42.
562. Lee, Y.S., et al., *Interleukin-8 and its receptor CXCR2 in the tumour microenvironment promote colon cancer growth, progression and metastasis.* Br J Cancer, 2012. **106**(11): p. 1833-41.
563. Doll, D., et al., *Differential expression of the chemokines GRO-2, GRO-3, and interleukin-8 in colon cancer and their impact on metastatic disease and survival.* Int J Colorectal Dis, 2010. **25**(5): p. 573-81.
564. Reis, S.T., et al., *Increased expression of MMP-9 and IL-8 are correlated with poor prognosis of Bladder Cancer.* BMC Urol, 2012. **12**: p. 18.
565. Huang, Y., et al., *Midkine induces epithelial-mesenchymal transition through Notch2/Jak2-Stat3 signaling in human keratinocytes.* Cell Cycle, 2008. **7**(11): p. 1613-22.
566. Rawnaq, T., et al., *The Multifunctional Growth Factor Midkine Promotes Proliferation and Migration in Pancreatic Cancer.* Mol Cancer Res, 2014.
567. Speetjens, F.M., et al., *Disrupted expression of CXCL5 in colorectal cancer is associated with rapid tumor formation in rats and poor prognosis in patients.* Clin Cancer Res, 2008. **14**(8): p. 2276-84.
568. Keates, S., et al., *Enterocytes are the primary source of the chemokine ENA-78 in normal colon and ulcerative colitis.* Am J Physiol, 1997. **273**(1 Pt 1): p. G75-82.
569. Kawamura, M., et al., *CXCL5, a promoter of cell proliferation, migration and invasion, is a novel serum prognostic marker in patients with colorectal cancer.* Eur J Cancer, 2012. **48**(14): p. 2244-51.
570. Rubie, C., et al., *ELR+ CXC chemokine expression in benign and malignant colorectal conditions.* BMC Cancer, 2008. **8**: p. 178.
571. Wuyts, A., et al., *Biochemical and biological characterization of neutrophil chemotactic protein, a novel rabbit CXC chemokine from alveolar macrophages.* Biochemistry, 2000. **39**(47): p. 14549-57.
572. Mrowietz, U., et al., *The chemokine RANTES is secreted by human melanoma cells and is associated with enhanced tumour formation in nude mice.* Br J Cancer, 1999. **79**(7-8): p. 1025-31.
573. Niwa, Y., et al., *Correlation of tissue and plasma RANTES levels with disease course in patients with breast or cervical cancer.* Clin Cancer Res, 2001. **7**(2): p. 285-9.
574. Vaday, G.G., et al., *Expression of CCL5 (RANTES) and CCR5 in prostate cancer.* Prostate, 2006. **66**(2): p. 124-34.

575. Huang, C.Y., et al., *CCL5 increases lung cancer migration via PI3K, Akt and NF-kappaB pathways.* Biochem Pharmacol, 2009. **77**(5): p. 794-803.
576. Erreni, M., et al., *Expression of chemokines and chemokine receptors in human colon cancer.* Methods Enzymol, 2009. **460**: p. 105-21.
577. Horst, D., et al., *Invasion associated up-regulation of nuclear factor kappaB target genes in colorectal cancer.* Cancer, 2009. **115**(21): p. 4946-58.
578. Luboshits, G., et al., *Elevated expression of the CC chemokine regulated on activation, normal T cell expressed and secreted (RANTES) in advanced breast carcinoma.* Cancer Res, 1999. **59**(18): p. 4681-7.
579. Makinoshima, H. and M. Dezawa, *Pancreatic cancer cells activate CCL5 expression in mesenchymal stromal cells through the insulin-like growth factor-I pathway.* FEBS Lett, 2009. **583**(22): p. 3697-703.
580. Luo, J., et al., *Infiltrating bone marrow mesenchymal stem cells increase prostate cancer stem cell population and metastatic ability via secreting cytokines to suppress androgen receptor signaling.* Oncogene, 2014. **33**(21): p. 2768-78.
581. Negus, R.P., et al., *Quantitative assessment of the leukocyte infiltrate in ovarian cancer and its relationship to the expression of C-C chemokines.* Am J Pathol, 1997. **150**(5): p. 1723-34.
582. Kan, J.Y., et al., *Chemokine (C-C Motif) Ligand 5 is Involved in Tumor-Associated Dendritic Cell-Mediated Colon Cancer Progression Through Non-Coding RNA MALAT-1.* J Cell Physiol, 2015. **230**(8): p. 1883-94.
583. Long, H., et al., *Autocrine CCL5 signaling promotes invasion and migration of CD133+ ovarian cancer stem-like cells via NF-kappaB-mediated MMP-9 upregulation.* Stem Cells, 2012. **30**(10): p. 2309-19.
584. Zhang, Y., et al., *Role of CCL5 in invasion, proliferation and proportion of CD44+/CD24- phenotype of MCF-7 cells and correlation of CCL5 and CCR5 expression with breast cancer progression.* Oncol Rep, 2009. **21**(4): p. 1113-21.
585. Long, H., et al., *CD133+ ovarian cancer stem-like cells promote non-stem cancer cell metastasis via CCL5 induced epithelial-mesenchymal transition.* Oncotarget, 2015. **6**(8): p. 5846-59.
586. Kao, J., et al., *Molecular profiling of breast cancer cell lines defines relevant tumor models and provides a resource for cancer gene discovery.* PLoS One, 2009. **4**(7): p. e6146.
587. Li, S., et al., *TWIST1 associates with NF-kappaB subunit RELA via carboxyl-terminal WR domain to promote cell autonomous invasion through IL8 production.* BMC Biol, 2012. **10**: p. 73.
588. Liu, G.T., et al., *CCL5 promotes VEGF-dependent angiogenesis by down-regulating miR-200b through PI3K/Akt signaling pathway in human chondrosarcoma cells.* Oncotarget, 2014. **5**(21): p. 10718-31.

589. Schall, T.J., et al., *A human T cell-specific molecule is a member of a new gene family.* J Immunol, 1988. **141**(3): p. 1018-25.
590. Schall, T.J., N.J. Simpson, and J.Y. Mak, *Molecular cloning and expression of the murine RANTES cytokine: structural and functional conservation between mouse and man.* Eur J Immunol, 1992. **22**(6): p. 1477-81.
591. Katsounas, A., J.F. Schlaak, and R.A. Lempicki, *CCL5: a double-edged sword in host defense against the hepatitis C virus.* Int Rev Immunol, 2011. **30**(5-6): p. 366-78.
592. Sallusto, F., et al., *Rapid and coordinated switch in chemokine receptor expression during dendritic cell maturation.* Eur J Immunol, 1998. **28**(9): p. 2760-9.
593. Schall, T.J., et al., *Selective attraction of monocytes and T lymphocytes of the memory phenotype by cytokine RANTES.* Nature, 1990. **347**(6294): p. 669-71.
594. Maghazachi, A.A., *Role of chemokines in the biology of natural killer cells.* Curr Top Microbiol Immunol, 2010. **341**: p. 37-58.
595. Bieche, I., et al., *Molecular profiling of inflammatory breast cancer: identification of a poor-prognosis gene expression signature.* Clin Cancer Res, 2004. **10**(20): p. 6789-95.
596. Cao, Z., et al., *Role of RANTES and its receptor in gastric cancer metastasis.* J Huazhong Univ Sci Technolog Med Sci, 2011. **31**(3): p. 342-7.
597. Milliken, D., et al., *Analysis of chemokines and chemokine receptor expression in ovarian cancer ascites.* Clin Cancer Res, 2002. **8**(4): p. 1108-14.
598. Zumwalt, T.J., et al., *Active secretion of CXCL10 and CCL5 from colorectal cancer microenvironments associates with GranzymeB+ CD8+ T-cell infiltration.* Oncotarget, 2015. **6**(5): p. 2981-91.
599. Boissiere-Michot, F., et al., *Characterization of an adaptive immune response in microsatellite-instable colorectal cancer.* Oncoimmunology, 2014. **3**: p. e29256.
600. Lavergne, E., et al., *Intratumoral CC chemokine ligand 5 overexpression delays tumor growth and increases tumor cell infiltration.* J Immunol, 2004. **173**(6): p. 3755-62.
601. Gonzalez-Martin, A., et al., *Maximal T cell-mediated antitumor responses rely upon CCR5 expression in both CD4(+) and CD8(+) T cells.* Cancer Res, 2011. **71**(16): p. 5455-66.
602. Chew, V., et al., *Chemokine-driven lymphocyte infiltration: an early intratumoural event determining long-term survival in resectable hepatocellular carcinoma.* Gut, 2012. **61**(3): p. 427-38.
603. Hong, M., et al., *Chemotherapy induces intratumoral expression of chemokines in cutaneous melanoma, favoring T-cell infiltration and tumor control.* Cancer Res, 2011. **71**(22): p. 6997-7009.

604. Musha, H., et al., *Selective infiltration of CCR5(+)CXCR3(+) T lymphocytes in human colorectal carcinoma.* Int J Cancer, 2005. **116**(6): p. 949-56.
605. Liu, J., et al., *Local production of the chemokines CCL5 and CXCL10 attracts CD8+ T lymphocytes into esophageal squamous cell carcinoma.* Oncotarget, 2015. **6**(28): p. 24978-89.
606. Dehqanzada, Z.A., et al., *Assessing serum cytokine profiles in breast cancer patients receiving a HER2/neu vaccine using Luminex technology.* Oncol Rep, 2007. **17**(3): p. 687-94.
607. Tsukishiro, S., et al., *Elevated serum RANTES levels in patients with ovarian cancer correlate with the extent of the disorder.* Gynecol Oncol, 2006. **102**(3): p. 542-5.
608. Kim, H.K., et al., *Elevated levels of circulating platelet microparticles, VEGF, IL-6 and RANTES in patients with gastric cancer: possible role of a metastasis predictor.* Eur J Cancer, 2003. **39**(2): p. 184-91.
609. Sadeghi, M., et al., *Serum levels of chemokines CCL4 and CCL5 in cirrhotic patients indicate the presence of hepatocellular carcinoma.* Br J Cancer, 2015. **113**(5): p. 756-62.
610. Sima, A.R., et al., *Serum chemokine ligand 5 (CCL5/RANTES) level might be utilized as a predictive marker of tumor behavior and disease prognosis in patients with gastric adenocarcinoma.* J Gastrointest Cancer, 2014. **45**(4): p. 476-80.
611. Chang, L.Y., et al., *Tumor-derived chemokine CCL5 enhances TGF-beta-mediated killing of CD8(+) T cells in colon cancer by T-regulatory cells.* Cancer Res, 2012. **72**(5): p. 1092-102.
612. Tan, M.C., et al., *Disruption of CCR5-dependent homing of regulatory T cells inhibits tumor growth in a murine model of pancreatic cancer.* J Immunol, 2009. **182**(3): p. 1746-55.
613. Serrels, A., et al., *Nuclear FAK controls chemokine transcription, Tregs, and evasion of anti-tumor immunity.* Cell, 2015. **163**(1): p. 160-73.
614. Zhang, Y., et al., *A novel role of hematopoietic CCL5 in promoting triple-negative mammary tumor progression by regulating generation of myeloid-derived suppressor cells.* Cell Res, 2013. **23**(3): p. 394-408.
615. Azenshtein, E., et al., *The angiogenic factors CXCL8 and VEGF in breast cancer: regulation by an array of pro-malignancy factors.* Cancer Lett, 2005. **217**(1): p. 73-86.
616. Svensson, S., et al., *CCL2 and CCL5 Are Novel Therapeutic Targets for Estrogen-Dependent Breast Cancer.* Clin Cancer Res, 2015. **21**(16): p. 3794-805.
617. Wang, S.W., et al., *CCL5/CCR5 axis induces vascular endothelial growth factor-mediated tumor angiogenesis in human osteosarcoma microenvironment.* Carcinogenesis, 2015. **36**(1): p. 104-14.

618. Yasuhara, R., et al., *The beta-catenin signaling pathway induces aggressive potential in breast cancer by up-regulating the chemokine CCL5.* Exp Cell Res, 2015. **338**(1): p. 22-31.
619. Wang, S.W., et al., *CCL5 and CCR5 interaction promotes cell motility in human osteosarcoma.* PLoS One, 2012. **7**(4): p. e35101.
620. Kim, J.E., et al., *LYR71, a derivative of trimeric resveratrol, inhibits tumorigenesis by blocking STAT3-mediated matrix metalloproteinase 9 expression.* Exp Mol Med, 2008. **40**(5): p. 514-22.
621. Kato, T., et al., *CCR1/CCL5 interaction promotes invasion of taxane-resistant PC3 prostate cancer cells by increasing secretion of MMPs 2/9 and by activating ERK and Rac signaling.* Cytokine, 2013. **64**(1): p. 251-7.
622. Barnett, P., et al., *Snail-mediated regulation of reactive oxygen species in ARCaP human prostate cancer cells.* Biochem Biophys Res Commun, 2011. **404**(1): p. 34-9.
623. Soria, G., et al., *Inflammatory mediators in breast cancer: coordinated expression of TNFalpha & IL-1beta with CCL2 & CCL5 and effects on epithelial-to-mesenchymal transition.* BMC Cancer, 2011. **11**: p. 130.
624. Zhang, X., et al., *Anibamine, a natural product CCR5 antagonist, as a novel lead for the development of anti-prostate cancer agents.* Bioorg Med Chem Lett, 2010. **20**(15): p. 4627-30.
625. Zhang, Y., et al., *The potential role of anibamine, a natural product CCR5 antagonist, and its analogues as leads toward development of anti-ovarian cancer agents.* Bioorg Med Chem Lett, 2012. **22**(15): p. 5093-7.
626. Pocock, J., et al., *Differential activation of NF-kappa B, AP-1, and C/EBP in endotoxin-tolerant rats: mechanisms for in vivo regulation of glomerular RANTES/CCL5 expression.* J Immunol, 2003. **170**(12): p. 6280-91.
627. Moriuchi, H., M. Moriuchi, and A.S. Fauci, *Nuclear factor-kappa B potently up-regulates the promoter activity of RANTES, a chemokine that blocks HIV infection.* J Immunol, 1997. **158**(7): p. 3483-91.
628. Kumar, D., et al., *JNK MAPK pathway regulates constitutive transcription of CCL5 by human NK cells through SP1.* J Immunol, 2009. **182**(2): p. 1011-20.
629. Fessele, S., et al., *Molecular and in silico characterization of a promoter module and C/EBP element that mediate LPS-induced RANTES/CCL5 expression in monocytic cells.* FASEB J, 2001. **15**(3): p. 577-9.
630. Lv, D., et al., *CCL5 as a potential immunotherapeutic target in triple-negative breast cancer.* Cell Mol Immunol, 2013. **10**(4): p. 303-10.
631. Chua, H.L., et al., *NF-kappaB represses E-cadherin expression and enhances epithelial to mesenchymal transition of mammary epithelial cells: potential involvement of ZEB-1 and ZEB-2.* Oncogene, 2007. **26**(5): p. 711-24.

632. Mejlvang, J., et al., *Direct repression of cyclin D1 by SIP1 attenuates cell cycle progression in cells undergoing an epithelial mesenchymal transition.* Mol Biol Cell, 2007. **18**(11): p. 4615-24.
633. Fontemaggi, G., et al., *deltaEF1 repressor controls selectively p53 family members during differentiation.* Oncogene, 2005. **24**(49): p. 7273-80.
634. Sayan, A.E., et al., *Fra-1 controls motility of bladder cancer cells via transcriptional upregulation of the receptor tyrosine kinase AXL.* Oncogene, 2012. **31**(12): p. 1493-503.
635. Morris, D.P., G.A. Michelotti, and D.A. Schwinn, *Evidence that phosphorylation of the RNA polymerase II carboxyl-terminal repeats is similar in yeast and humans.* J Biol Chem, 2005. **280**(36): p. 31368-77.
636. Active motif, *Bridging Antibody for Mouse IgG.* 2016.
637. Zhang, L., et al., *miR-153 supports colorectal cancer progression via pleiotropic effects that enhance invasion and chemotherapeutic resistance.* Cancer Res, 2013. **73**(21): p. 6435-47.
638. Ben-Baruch, A., *The Tumor-Promoting Flow of Cells Into, Within and Out of the Tumor Site: Regulation by the Inflammatory Axis of TNFalpha and Chemokines.* Cancer Microenviron, 2012. **5**(2): p. 151-64.
639. Manes, S., et al., *CCR5 expression influences the progression of human breast cancer in a p53-dependent manner.* J Exp Med, 2003. **198**(9): p. 1381-9.